

THESIS

UNIVERSITE DE PAU ET DES PAYS DE L'ADOUR - EBERHARD KARLS UNIVERSITÄT TÜBINGEN

Defended on December 9th, 2015 by

Hasina Harimino RAMANITRA

Submitted in fulfilment of the requirements for the degree of

Doctor of Philosophy

in Physical-Chemistry at

UNIVERSITÉ DE PAU ET DES PAYS DE L'ADOUR

and

EBERHARD KARLS UNIVERSITÄT TÜBINGEN

Incorporation of fullerene into polymers for photovoltaic applications

*Incorporation du fullerène dans des polymères pour
applications dans le photovoltaïque*

Advisors: Dr. Roger C. HIORNS, Prof. Thomas CHASSÉ

Co-advisors: Dr. Christine DAGRON-LARTIGAU, Dr. Heiko PEISERT

JURY

Prof. Pietrick HUDHOMME

Prof. Laurence VIGNAU

Dr. Hans-Joachim EGELHAAF

Dr. Francesco GIACALONE

Rapporteur

Rapporteur

Examineur

Examineur



Incorporation of fullerene into polymers for photovoltaic applications

Dissertation

der Mathematisch-Naturwissenschaftlichen Fakultät
der Eberhard Karls Universität Tübingen
zur Erlangung des Grades eines
Doktors der Naturwissenschaften
(Dr. rer. nat.)

vorgelegt von

M.S.c Hasina Harimino RAMANITRA
Antananarive, Madagascar

Tübingen

2015

Gedruckt mit Genehmigung der Mathematisch-Naturwissenschaftlichen Fakultät der
Eberhard Karls Universität Tübingen.

Tag der mündlichen Qualifikation:

09.12.2015

Dekan:

Prof. Dr. Wolfgang Rosenstiel

1. Berichterstatter:

Prof. Dr. Thomas Chassé

2. Berichterstatter:

Dr. Roger C. Hiorns

*Alla mia famiglia e
a Laurent*

No man is an island,
Entire of itself,
Every man is a piece of the continent,
A part of the main.
If a clod be washed away by the sea,
Europe is the less.
As well as if a promontory were.
As well as if a manor of thy friend's
Or of thine own were:
Any man's death diminishes me,
Because I am involved in mankind,
And therefore never send to know for whom the bell tolls;
It tolls for thee.

(John Donne)

Acknowledgment

I would like to thank all the people who helped me during my PhD studies. Without their help, support and advices, I would not have been able to reach this important goal. In particular, I would like to thank Dr. Roger Hiorns and Prof. Thomas Chassé, my supervisors, who guided me in my research. My sincere gratitude goes to Dr. Heiko Peisert, for all the help he has given to me and for the great patience he has demonstrated. A big thank goes also to Dr. Christine Dagrón-Lartigau for the advices and the support she has given to me and to Dr. Khoukh Abdel, whose advices in NMR technique were extremely helpful.

Aurélien and Alberto, thank you for have being such great lab-mates and flat-mates.

I do not even find the right words to thank Dr. Mélanie Pedeutour (mamma) for just being herself:
THANK YOU MEL!

I would also like to thank my family.

Mamma, papa, Mbola, grazie per tutto l'amore e il sostegno che mi avete dato nel corso degli anni. Non so come esprimervi la mia gratitudine per tutto quello che avete fatto per me. Spero che consideriate questo mio traguardo anche vostro e che questo vi renda orgogliosi di tutto il lavoro che avete compiuto. Grazie!

Laurent, Sabine, Jean-Luc, merci pour tout le soutien et les petites attentions que vous m'avez montré. Je vous suis reconnaissante pour tout le temps que vous m'avez dédié, tous les voyages que vous avez faits pour et avec moi et surtout, merci pour avoir été présents pour moi.

Finally yet importantly, I would like to thank the friends and colleagues. Those who I have met during these years at ESTABLIS meetings, at the EPCP, at the Institut für Physikalische und Theoretische Chemie., we have shared a lot of adventures, time and thoughts. Thank you all for have being always so nice and helpful. Those who I have met during my undergraduated studies and that are still as helpful and amazing as always. Thank you all guys!

Abstract

Photovoltaic technology (PV) makes it possible to directly convert sunlight into electricity and it is seen as a very promising solution to the current energy crisis. Although the PV market is dominated by inorganic-based devices, those systems present high production costs and deployment issues that limit their application. Polymer-based organic solar cells (OPVs) are promising sources of renewable energy due to their facile, low cost production, and formable nature. Due to its electronic properties and high electron mobility, small molecule fullerene (C_{60}) derivatives are widely used in large scale OPVs. However the morphological properties of C_{60} derivatives decrease device stability as C_{60} easily undergoes self-aggregation during OPV use. The processibility of C_{60} can be improved by incorporating it into a polymer. These systems are already described in literature but have in general a multistage synthesis that could affect the electronic properties of C_{60} as well as give insoluble products due to reticulative reactions.

The objective of the work here presented was to prepare innovative polymers based on C_{60} for photovoltaic and electronic devices using reliable, well-known C_{60} chemistry.

At the University of Pau (EPCP Lab), after the syntheses of small molecules to be used as co-monomers, two synthetic routes were used in order to obtain main- chain oligo- and polyfullerenes. The first route is based on the atom transfer radical addition polymerization (ATRAP), which has already been used for the preparation of main-chain polyfullerenes. With this method, soluble compounds with various molecular weights were prepared. The second route was discovered in this work and exploits a well-known fullerene chemistry to prepare soluble polyfullerenes with reasonably high molecular weights. Preliminary studies to understand the effect of the reaction parameters (reagents, reagents concentration, temperature, time and solvent) and the kinetics of the polymerisation were performed. Material characterisations were carried out via GPC chromatography, NMR spectroscopy, and UV-visible and IR spectroscopies. Thermal analyses (TGA and DSC) were also run to complete the characterisations. Both C_{60} and its derivative, [6,6]-phenyl- C_{61} -butyric acid methyl ester (PCBM), have been exploited as monomers in the reactions.

A nine-month (cotutelle) stay at Tübingen University, Germany, permitted a study of the synthesized materials by means of XPS and UPS spectroscopies. The aim of these studies was to obtain a better understanding of the energy levels pictures of the oligo- and polyfullerenes. Thin films of the compounds were deposited on different substrates via solution processes (doctor

blade or spin coating) to obtain *ex-situ* samples for characterisation.

Samples of polyfullerene-containing active layers were prepared during a short stay (1 week) at BELECTRIC OPV GmbH, Nuremberg (Germany), and analysed by optical microscopy and AFM microscopy during thermal-degradation studies at Tübingen University. These studies were completed thanks to collaborations with researchers at BELECTRIC OPV GmbH, who have incorporated the compounds into devices and performed complementary and comparable experiments. As general trends, the compounds are found to improve the stability of the devices upon thermal stresses.

Résumé

La technologie photovoltaïque (PV) permet de convertir directement la lumière du soleil en électricité et elle est considérée une solution très prometteuse à la crise de l'énergie. Bien que le marché du PV soit actuellement dominé par des dispositifs à base de minéraux, ces systèmes présentent des coûts de production élevés et de nombreux problèmes environnementaux. Ces aspects limitent leur application. Les cellules solaires organiques à base de polymères (OPV) sont de prometteuses sources d'énergie renouvelable en raison de leur faible coût de production et grâce à leur nature déformable. En raison de ses propriétés électroniques et de la haute mobilité d'électrons, de petites molécules dérivées du fullerène C_{60} sont largement utilisées dans la production OPV à grande échelle. Toutefois, les propriétés morphologiques des dérivés du C_{60} diminuent la stabilité des dispositifs. En effet, le C_{60} subit facilement le phénomène d'auto-agrégation lors de l'utilisation de la cellule. L'aptitude au traitement du C_{60} peut être améliorée en l'incorporant dans un polymère. Ces systèmes sont déjà décrits dans la littérature, mais reposent en général sur une synthèse en plusieurs étapes qui pourraient affecter les propriétés électroniques du C_{60} ainsi que donner des produits insolubles en raison de la réaction de réticulation.

L'objectif de ce travail est de préparer des polymères innovants basés sur le fullerène (C_{60}) pour les dispositifs photovoltaïques et électroniques, à l'aide d'une chimie du C_{60} bien connue et en se basant sur des procédés fiables.

À l'Université de Pau (au sein de l'équipe EPCP), après les synthèses de petites molécules qui ont été utilisées en tant que co-monomères, deux différentes voies de synthèse ont été exploitées afin d'obtenir oligo- et polyfullerènes contenant le C_{60} dans leur chaîne principale. La première voie exploitée, est basée sur la réaction « Atom Transfer Radical Addition Polymerisation » (ATRAP), qui a déjà été utilisée pour la préparation de main-chain polyfullerènes. Avec cette méthode, des composés très solubles ayant des poids moléculaires variables ont été préparés. La deuxième voie a été découverte dans ce travail de thèse et exploite une chimie du C_{60} bien connue pour obtenir des « main-chain » polyfullerènes qui présentent un haut poids moléculaire et qui sont bien solubles dans les solvants courants. Des études préliminaires ont été effectuées dans le but de comprendre les effets des paramètres de réaction (réactifs, leur concentration, température, temps de réaction et solvants) et la cinétique de la polymérisation. Les matériaux ont été caractérisés par chromatographie d'exclusion stérique,

SEC, spectroscopie RMN, et à travers spectroscopie UV-vis et IR. Des analyses thermiques (TGA et DSC) complètent les caractérisations. Le fullerène C₆₀, ainsi que son dérivé, [6,6] -phényl-C61-butérique ester méthylique d'acide (PCBM), ont été exploités en tant que monomères dans les réactions de polymérisation.

Un séjour de neuf mois (cotutelle) à l'université de Tübingen, en Allemagne, a permis d'étudier les matériaux synthétisés par spectroscopies XPS et UPS. Le but de ces études était d'obtenir une meilleure compréhension des niveaux énergétiques des oligo- et polyfullerènes. Des couches minces de composés ont été déposées sur différents substrats par des procédés en solution (doctor blade ou spin coating) pour obtenir des échantillons *ex-situ* pour les analyses.

Des échantillons de couches actives contenant des polyfullerène ont également été préparés lors d'un court séjour (une semaine) à BELECTRIC OPV GmbH, Nuremberg (Allemagne). Les échantillons ont été analysés par microscopie optique et microscopie AFM dans le cadre d'une étude sur la stabilité thermique de la couche active à l'Université de Tübingen. Ces études ont été réalisées aussi grâce à la collaboration avec des chercheurs de BELECTRIC OPV GmbH, qui ont intégré les composés dans des dispositifs et réalisé des expériences complémentaires et comparables. Comme tendances générales, les composés améliorent la stabilité des dispositifs quand les derniers sont soumis à un stress thermique.

Abstract- German

Da durch Photovoltaik (PV) Sonnenlicht direkt in Elektrizität umgewandelt werden kann, ist diese Technologie sehr vielversprechend für die Lösung der gegenwärtigen Energiekrise. Der PV Markt ist durch anorganische Solarzellen dominiert, obwohl hohe Produktionskosten und ein Aufwand für Entwicklungen die Anwendung dieser Systeme limitiert. Eine auf Polymeren basierte, organische Photovoltaik (OPV) zeichnet sich im Gegensatz dazu durch eine einfache und preiswerte Produktion, sowie durch hohe Flexibilität aus und stellt deshalb eine vielversprechende erneuerbare Energiequelle dar. Fulleren(C_{60})- Derivate sind aufgrund der elektronischen Eigenschaften und der hohen Mobilität für Elektronen in großflächigen OPV Anwendungen weit verbreitet. Die morphologischen Eigenschaften der Fulleren(C_{60})- Derivate führen jedoch zu einer Aggregation dieser Moleküle und somit zu einer geringen Stabilität der Bauelemente. Die Verarbeitbarkeit von C_{60} kann jedoch durch Einbindung in polymere Strukturen verbessert werden. Solche Verbindungen wurden bereits in der Literatur beschrieben, sie werden generell in einer mehrstufigen Synthese hergestellt, die die elektronischen Eigenschaften von C_{60} verändert und auch zu unlöslichen Produkten durch Vernetzungsreaktionen führen kann.

Das Ziel der vorliegenden Arbeit ist die Präparation von innovativen, C_{60} basierten Polymeren für photovoltaische und andere elektronische Bauelemente unter Anwendung einer zuverlässigen, bereits bekannten Fullerenchemie.

An der Universität Pau (EPCP Lab) wurden zunächst die kleineren Moleküle synthetisiert, die als Comonomere verwendet wurden. Um Hauptketten Oligo- und Polyfullerene herzustellen, wurden zwei Synthesewege verfolgt. Der erste Weg basiert auf der Atom Transfer Radical Additionspolymerisation (ATRAP) – eine Route die für die Synthese von Hauptketten-Polyfullerene bekannt ist. Mit dieser Methode wurden lösliche Verbindungen mit unterschiedlichem Molekulargewicht hergestellt. Der zweite Syntheseweg wird in dieser Arbeit erstmalig vorgestellt, unter Nutzung der bekannten Fullerenchemie werden Polyfullerene mit vergleichsweise hohem Molekulargewicht synthetisiert. Vorbereitende Studien wurden durchgeführt, um Reaktionsparameter (Reagenzien und deren Konzentration, Temperatur, Lösungsmittel und Reaktionsdauer) und die Kinetik der Polymerisation zu verstehen. Die Reaktionsprodukte wurden mit Gel-Permeations-Chromatographie (GPC), NMR Spektroskopie sowie UV/vis und IR Spektroskopie charakterisiert. Zusätzlich wurden thermogravimetrische

Analyse (TGA) und dynamische Differenzkalorimetrie (differential scanning calorimetry, DSC) angewandt. Sowohl C60, als auch das C60 Derivat [6,6]-phenyl-C61-butyric acid methyl ester (PCBM) wurden als Monomere in den Polymerisationsreaktionen verwandt.

In einem neunmonatigen Co-tutelle Aufenthalt an der Eberhard-Karls-Universität Tübingen (Deutschland) wurden die synthetisierten Materialien mittels Photoemission (XPS und UPS) untersucht. Das Ziel dieser Untersuchungen war insbesondere, die Lage der Energieniveaus in Oligo- und Polyfullerenen besser zu verstehen. Dafür wurden *ex-situ* dünne Filme dieser Verbindungen auf unterschiedlichen Substraten aus Lösungen hergestellt („doctor blade casting“ oder „Spin-coating“).

Proben der Polyfulleren-haltigen aktiven Schichten in Bauelementen wurden während eines Kurzaufenthaltes von einer Woche bei der BELECTRIC OPV GmbH (Nürnberg, Deutschland) hergestellt. Nachfolgend wurde deren thermische Degradation an der Eberhard-Karls-Universität Tübingen mit optischer Mikroskopie sowie AFM untersucht. Diese Studien wurden durch vergleichbare und komplementäre Untersuchungen in Kooperation mit Mitarbeitern der BELECTRIC OPV GmbH ergänzt, wobei diese Verbindungen in Bauelemente inkorporiert wurden. Generell wurde festgestellt, dass diese Verbindungen die thermische Stabilität der Bauelemente erhöhen.

Table of contents

Introduction	3
1 Fullerene and its application to organic photovoltaics.....	3
1.1 Buckminsterfullerene.....	3
1.1.1 C ₆₀ chemistry	5
1.1.1.1 Cycloadditions on C ₆₀	7
<i>Cyclopropanation</i>	7
<i>Diels-Alder cycloaddition</i>	9
<i>Addition of azomethine ylides (Prato chemistry)</i>	11
1.1.1.2 Nucleophilic additions.....	12
1.1.1.3 Radical functionalization.....	14
1.1.1.4 Endohedral fullerenes	14
1.2 Organic photovoltaics.....	16
1.2.1 Operating principles and device architecture	19
1.2.2 Influence of the nanoscale morphology	24
1.2.3 Device characterizations	27
1.2.4 Device stability.....	30
1.2.5 Materials for the active layer	32
1.2.5.1 Donor material.....	34
1.2.5.2 Acceptor materials.....	38
1.2.6 Material Characterizations.....	43
1.2.6.1 Photoemission spectroscopy, XPS and UPS	43
1.2.6.2 Working principle	43
1.2.6.3 Information from data	45
1.2.6.4 Integer charge-transfer model.....	47
1.3 The role of fullerenes in organic photovoltaics	50
1.3.1 Fullerene acceptors	50
1.3.2 Fullerene interlayers	53
1.3.3 Fullerene additives	53
1.3.4 Fullerene as donor materials	55
1.4 Polyfullerenes	56

1.4.1	Polyfullerenes: introduction.....	56
1.4.1.1	All-carbon polyfullerenes	57
1.4.1.2	Organometallic polyfullerenes	57
1.4.1.3	Crosslinked polyfullerenes	57
1.4.1.4	End-capped polymers	58
1.4.1.5	Star-shaped polymers	59
1.4.1.6	C ₆₀ -dendrimers	60
1.4.1.7	Main-chain polymers.....	62
1.4.1.8	Side-chain polymers.....	68
1.4.1.9	Double-cable polymers	69
1.4.1.10	C ₆₀ -supramolecular polymers	69
1.4.2	Polyfullerenes in organic photovoltaics	70
2	Synthesis and characterization of novel polyfullerenes.....	75
2.1	Syntheses of the comonomers.....	78
2.2	Synthesis and Characterisation of PolyPCBMs	80
2.2.1	Size-exclusion chromatography (SEC).....	81
2.2.2	Nuclear magnetic resonance (NMR)	87
2.2.3	Thermogravimetric analysis (TGA)	91
2.2.4	Differential scanning calorimetry (DSC).....	93
2.2.5	UV-visible optical spectroscopy	95
2.2.6	X-ray photoemission spectroscopy.....	96
2.2.7	Matrix Assisted Laser Desorption/Ionization - time-of-flight mass spectrometry (MALDI-TOF)	99
2.3	Synthesis and characterization of poly-C ₆₀ -pyrrolidine.....	103
2.3.1	Size-exclusion chromatography (SEC).....	105
2.3.2	Kinetics.....	107
2.3.3	Nuclear magnetic resonance (NMR)	112
2.3.4	FTIR characterization.....	119
2.3.5	Thermogravimetric analysis (TGA)	120
2.3.6	Differential scanning calorimetry (DSC).....	121
2.3.7	UV-visible optical spectroscopy	122
2.3.8	X-ray photoemission spectroscopy.....	124
2.3.8.1	Substrates	125

	<i>ITO-coated glass with PEI as surface modifier</i>	125
	<i>ITO-coated glasses with different surface cleaning methods</i>	126
	<i>Au layer co-evaporated on Si wafer</i>	131
	2.3.8.2 Energy level alignment on different substrates	133
3	Application of polyfullerenes in organic solar cells	141
3.1	PolyPCBM acceptors in OPV devices	144
3.1.1	Organic solar cells based on polyPCBM:P3HT blends.....	144
3.1.2	Device thermal stability.....	147
3.1.3	Low band gap: polyPCBM solar cells	149
3.2	Polyfulleropyrrolidines-based organic solar cells	151
3.2.1	Polyfulleropyrrolidine as an acceptor	152
3.2.2	Polyfulleropyrrolidine as an interlayer.....	153
3.2.3	Polyfulleropyrrolidine as an additive.....	155
3.2.4	Device thermal stability.....	158
3.3	Comparison between polyPCBM and PPCs.....	160
4	Thermal degradation study on thin films	167
4.1	Accelerated thermal degradation study on P3HT:PCBM based films with and without polyfullerene additive	169
4.1.1	Study of the film morphology evolution via UV-visible spectroscopy.....	169
4.1.2	Study of the film morphology evolution via optical microscopy	171
4.2	Investigating the use of poly(fulleropyrrolidine) additive in KP115:PCBM based BHJ blends	174
4.2.1	Evolution of BHJ morphology with thermal stress using optical microscopy	174
4.2.2	Evolution of BHJ morphology with thermal stress using UV-visible spectroscopy	179
4.3	Impact of the film quality on the morphological degradation behaviour	181
5	Experimental section	185
5.1	Experimental conditions	185
5.2	Synthetic protocols and NMR analysis of comonomers.....	187
	1,4-Bis(octyloxy)benzene (2a)	187
	1,4-Bis(dodecyloxy)benzene (2b)	188
	2,5-Bis(bromomethyl)-1,4-bis(octyloxy)benzene (3a)	190
	1,4-Bis(bromomethyl)-2,5-bis(dodecyloxy)benzene (3b)	192
	2,5-Bis(octyloxy)terephthaldehyde (5a)	194

2,5-Bis(dodecyloxy)terephthaldehyde (5b).....	195
5.3 Synthesis and NMR spectra of oligo- and poly-PCBM	197
Synthesis of polyPCBM_A.....	197
Synthesis of polyPCBM_F	199
5.4 Synthesis and characterization of poly(fulleropyrrolidines)	202
Synthesis of PPC1	202
Synthesis of PPC2	204
Synthesis of PPC3	204
Synthesis of PPC4	206
Synthesis of PPC5	208
Synthesis of PPC6	210
5.5 Device fabrication and characterization.....	213
Conclusions	215
Conclusions	219
Appendix A : Modelling and UV-visible characterisation.....	I
Appendix B: UV-visible spectroscopy of P3HT:PCBM and P3HT:poly(fulleropyrrolidines)HHR63.....	VII
Appendix C: Summary.....	IX
Appendix D: Résumé détaillé.....	XV
Appendix E: Summary – German	XXIII

List of abbreviations

A: acceptor material

ATRA: atom transfer radical addition

ATRAP: atom transfer radical addition polymerization

ATRP: atom transfer polymerization

BHJ: bulk heterojunction

D: donor material

D-C: double cable

DFT - Density Functional Theory

DOSY: diffusion-ordered NMR spectroscopy

DSC: differential scanning calorimetry

DSSCs: dye sensitized solar cells

EKUT - Eberhard-Karls Tübingen Universität

EPCP: Equipe de Physique et Chimie des Polymères

EQE: external quantum efficiency

ESL: electron-selective layer

ESR: electron spin resonance spectroscopy

ESTABLIS - Ensuring Stability in Organic Solar Cells

ETL: electron transporting layer

FF: fill factor

FT-IR: Fourier-transform infrared spectroscopy

HOMO: highest occupied molecular orbital

HPLC: high pressure liquid chromatography

HSQC: Heteronuclear single quantum coherence spectroscopy

HTL: hole transporting layer

ICT: integer charge transfer

IPR: isolated pentagon rule

IPREM : Institut des Sciences Analytiques et de Physico-Chimie pour l'Environnement et les Matériaux

LBG: low bang gap

LUMO: lowest unoccupied molecular orbital

MALDI-TOF: matrix-assisted laser desorption/ionization time-of-flight

MP: maximum power

MW: microwave

NMR: nuclear magnetic resonance

OFET: organic field-effect transistor

OLED: organic light-emitting diode

OPV: organic photovoltaic

OSC: organic solar cell

PCBM: phenyl-C₆₁-butyric acid methyl ester

PCE: power conversion efficiency

PES: photoemission spectroscopy

PHJ: planar heterojunction

PL: photoluminescence

PV: photovoltaic

ROS: reactive oxygen species

RP: shunt resistance

RS: series resistance

SACAP: sterically controlled azomethine ylide cycloaddition polymerization

SEC: size exclusion chromatography

STC: science & training committee

TGA: thermogravimetric analysis

UHV: ultra-high vacuum

UPPA: Université de Pau et des Pays de l'Adour

UPS: ultraviolet photoemission spectroscopy

UV: ultraviolet

VBM: valence band maximum

XPS: X-ray photoemission spectroscopy

Preamble

During a conference in Seattle, I found myself looking at the audience and ask them “why did I made my life challenging?”. The aim was of course to introduce the very attracting properties of organic solar cells and the challenges encountered in this field. In particular the challenges encountered when working on fullerene-based n-type materials. However that question was much more for me. It was a real question. It was a question I have asked myself so many times. But I was almost at the end of my PhD life and I now had the answer for that question. I did made the last years challenging, the years of “I will stay longer in the lab”, “sorry I have a deadline, and it was yesterday”, “this weekend I have a date with the spectrometer in the lab, do you want to join?” or even better “these data make no sense, I have lost the last 2 months”. Even though, I did it because it was worth it.

First of all, now I can prepare my luggage for a week-stay to the other corner of the world in less than 10 min. More important, I have had the opportunity to work in different places and laboratories, e.g. at IPREM/EPCP in Pau (France), at Aston university (UK), and at the Institute of Physical and Theoretical Chemistry - Division of Condensed Matter in Tübingen (Germany), and I had the opportunity to meet and to collaborate with good friends and great scientists.

Beside the scientific aspect, this thesis have also been a great opportunity for self-development. I had the opportunity to improve my language skills, to gain skills in outreach, communication and project management, and networking. It also gives me the opportunity to improve my teaching skills as I had the chance to participate to the university teaching activity as laboratory teaching assistant and as master student co-supervisor. This has been a great opportunity that has brought incredible enrichment in my professional and personal life.

About this thesis

This thesis is a part of the Region Aquitaine project FULLINC and the European Project ESTABLIS. The main objective of the project was to prepare innovative materials based on fullerene for photovoltaic and electronic devices using well-known and reliable routes.

The materials have been used in Establis' OPVs. The ESTABLIS project has been created with the aim to provide different approaches to avoid organic solar cells performance loss caused by degradation over an extended period of time, see 10 to 15 years.

This thesis is a cotutelle between the Université de Pau et des Pays de l'Adour (UPPA), in France, and Eberhard Karls Universität Tübingen (EKTU), in Germany. A one-month secondment at Aston University, UK, to develop organic synthetic techniques has also been spent.

Some parts of this thesis have already been presented during national and international conferences. Part of the work will be published in a joint patent between Merck, CNRS, UPPA and Belectric OPV GmbH. More publications and the details for the oral and poster presentations will be found at the beginning of the appropriate section.

Structure of the work

The thesis comprises five parts: (1) A general introduction to the scientific topics addressed in the dissertation. (2) A report on the synthesis of novel fullerene-based materials with discussions on the obtained results. (3) A chapter reporting the applications of the synthesized materials into organic solar cells. (4) A chapter where thermal degradation study on active layer blends containing the novel materials is addressed. (5) An experimental section where experimental protocols and conditions as well as experimental results are collected.

A concluding section summarizing the principal outcomes of this study, is found at the end of the manuscript.

Finally, appendices to the individual chapters are proposed.

The work in this thesis has received funding from European Union Seventh Framework Program (FP7/2011) under grant agreement no. 290022.

Introduction

1 Fullerene and its application to organic photovoltaics

Fullerenes are a family of large all-carbon cage molecules. The lowest molecular weight structure of this family with some stability in ambient condition is C_{36} .^[1] The most abundant and stable form of fullerene is buckminster fullerene (C_{60}) first discovered in 1985 by Kroto, Heath, O'Brien, Curl and Smalley^[2] during experiments on the mechanism of formation of long-chain carbon molecules in interstellar space and circumstellar shells. Thanks to their discovery Kroto, Curl and Smalley were awarded the Nobel Prize in Chemistry in 1996. The production of C_{60} on milligram scale, by resistive heating of graphite, was first reported by Krätschmer, Lamb, Fostiropoulos and Huffman in 1990.^[3] This was the breakthrough that permitted the rapid development in the characterization and functionalization of this material, which due to its properties is widely studied in numerous scientific disciplines, ranging from solar cells^[4] to medicine.^[5]

1.1 Buckminsterfullerene

Fullerene (C_{60}), also called buckminster fullerene after the architect Buckminster Fuller who designed geodesic domes in the 1960s, is an aromatic, highly symmetric (I_h) molecule with 120 possible symmetrical operations. It has the shape of a truncated icosahedron, similar to a football (**Figure 1**), in which the carbon nuclei reside on a sphere of about 0.7 nm. This molecule presents a 4 Å diameter cavity inside. The physical properties of C_{60} are shown in **Table 1**.^[6]

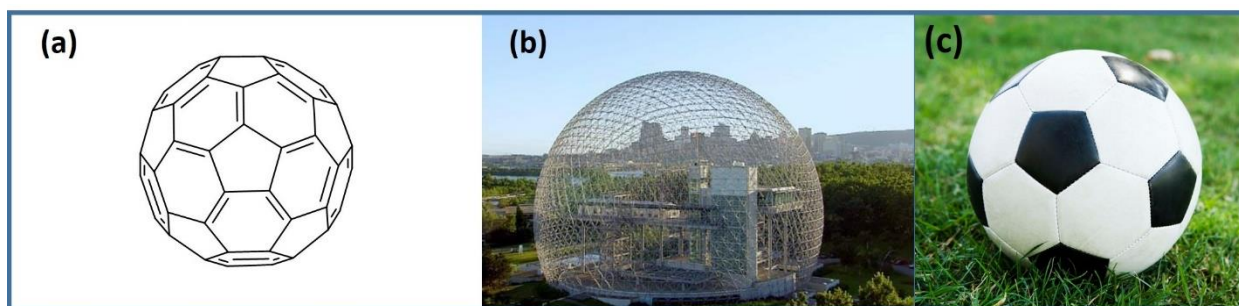


Figure 1 : (a) Buckminster fullerene, (b) Montreal Biosphere by Buckminster Fuller, 1967 and (c) a football.

Property	
Aspect	Black solid
Odor	Odorless
Chemical formula	C ₆₀
Molecular weight	720.65 g mol ⁻¹
Density	1.7 to 1.9 g cm ⁻¹
Standard heat of formation	9.08 kcal mol ⁻¹
Index of refraction	2.2 (600nm)
Boiling point	Sublimes at 800K
Resistivity	1014 Ohms m ⁻¹
Crystal form	Hexagonal cubic
Optical band gap	1.68 Ev
Vapour pressure	5×10 ⁻⁶ torr (r.t.) - 8×10 ⁻⁴ torr (800K)

Table 1: Physical properties of C₆₀.

C₆₀ obeys Euler's theorem as it presents 12 pentagonal faces and 20 hexagonal faces. As hexagons are added to attain the higher fullerenes, or removed in case of the lower fullerenes, the molecule loses its roundness and stability. C₆₀ is the smallest fullerene to obey also the isolated pentagon rule (IPR) which predicts that the fullerene structure in which all the pentagons are isolated are more stable than those with adjacent pentagons.[7] The presence of pentagonal faces results in an anisotropic electron distribution on the cage and this is reflected in the presence of two types of bond sets, namely hexagon-pentagon (6:5) bonds and hexagon-hexagon (6:6) bonds.[8] The 6:6 bonds are short (1.391 Å) with a significant π -electron density while the 6:5 bonds are longer (1.455 Å) and constitute electron-poor regions. In C₆₀ hexagon structures the electronic delocalization is not as in a benzene ring; C₆₀ is not an aromatic structure according to the common rules for aromaticity. All the carbons in the structure are equivalent as confirmed by the ¹³C NMR spectrum of C₆₀ in benzene-*d*₆ where a single peak is present at 143.29 (Figure 2).[9]



Figure 2: 125 MHz NMR spectrum after 1024 scans (28 min) of a C₆₀-C₇₀ mixture saturated in C₆D₆ as the only solvent. Signal to noise ratio 16: 1. C₆₀ exhibits one ¹³C NMR resonance at δ 143.29 (image reproduced from ref.9).

As mentioned above, the pentagonal faces permit the spherical structure of the molecule, imposing a substantial curvature of the surface and a strong pyramidalization of the individual tri-conjugate carbon atoms.[10]

1.1.1 C₆₀ chemistry

The pyramidalization of fullerene carbon atoms is a source of strain in the fullerene geometry and affects the molecule's reactivity; the relief of strain is primarily responsible for fullerene reactivity. In general, fullerenes are insoluble or sparingly soluble in most common organic solvents.[11–14]The solubilities of C₆₀ in some of the most commonly used solvents are listed in **Table 2**.

Solvent	Solubility (25 °C) mg/mL
n-hexane	0.043
cyclohexane	0.036
dichloromethane	0.26
chloroform	0.16
dibromoethane	0.50
methanol	0.000
acetone	0.001
benzene	1.7
toluene	2.8
xylene	5.2
1,2,4-trimethylbenzene[8]	17.9
chlorobenzene	7.2
1,2-dichlorobenzene	27
1-methylnaphthalene	33
carbon disulfide	7.9
tetrahydrofuran	0.000

Table 2: Solubility of C₆₀ in some of the most commonly used solvents.[12]

The low solubility makes C_{60} difficult to handle. It is well-known that this problem can be in part solved by the chemical functionalization of this carbon allotrope. Considering the great interest for fullerene in a wide range of applications, which go from bio-medical to organo-electronic applications, the chemistry of this small molecule has been well investigated since its discovery.

Despite its relative stability, fullerene C_{60} undergoes many reactions. Its chemical reactivity is typical of an electron deficient olefin and can be reduced by up to 6 electrons. The reaction type can be of different nature but since fullerene does not contain hydrogen atoms that can be substituted, it does not undergo the common reactions for aromatic systems. For example, aromatic substitution reactions are not applicable to C_{60} . Some general reactions that occurs with fullerene C_{60} are schematically reported in **Figure 3**.

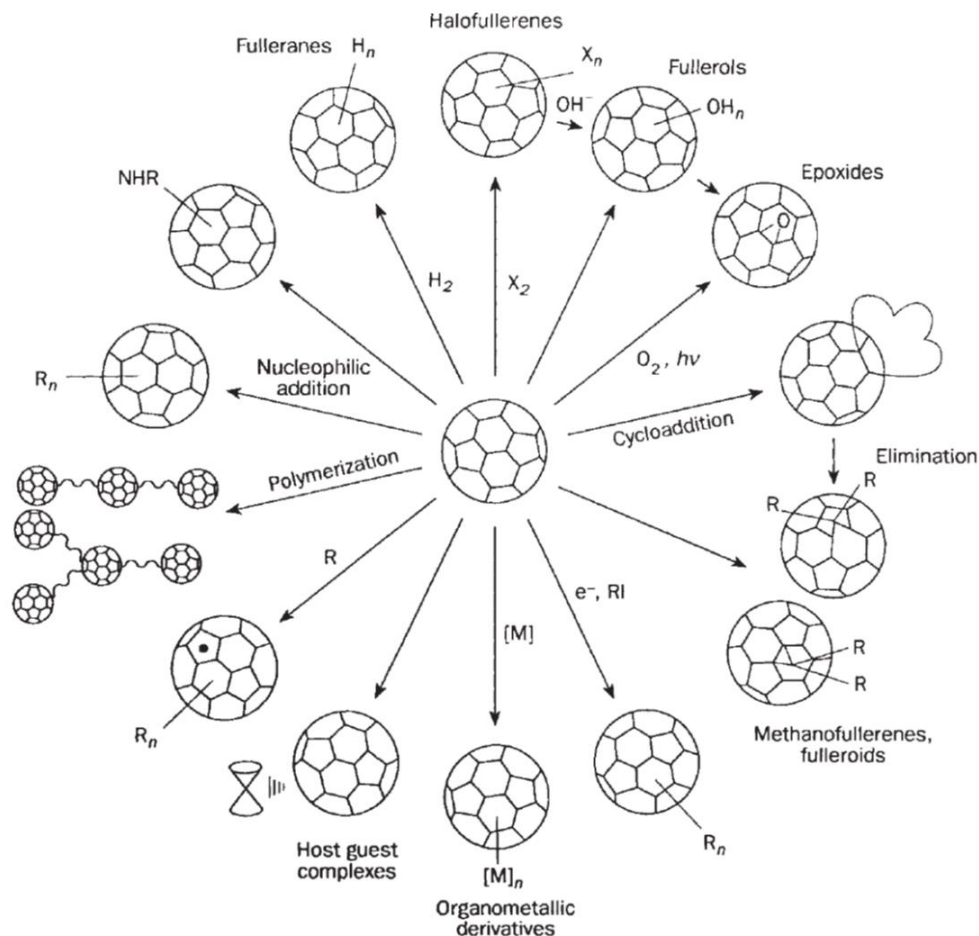


Figure 3: Some general reaction of C_{60} . Image reproduced from ref.15.

Chemical modifications on C_{60} can result in single or multiple attacks on the cage and usually take place at the 6:6 bonds. In the case of single-additions, the reactions can be classified into categories based on the nature of the obtained structure. With relations to the shape built on a 6:6 ring junction of the C_{60} there can be: (a) open structure, (b) three-membered ring, (c) four-membered ring, (d) five-membered ring and (e) six-membered ring as reported in literature **(Figure 4)**.^[16]

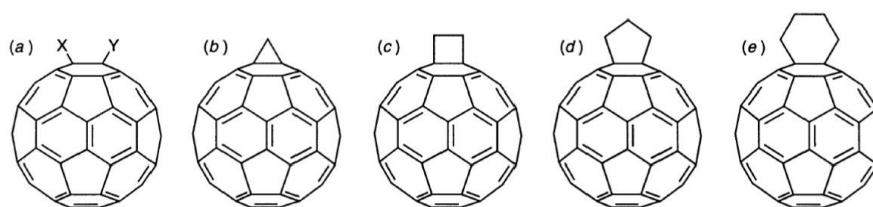


Figure 4: Geometrical shapes built onto a 6,6 ring junction of C_{60} : (a) open; (b) three-membered ring; (c) four-membered ring; (d) five-membered ring and (e) six-membered ring. Image reproduced from ref.16.

Due to its hollow structure, fullerene can also host small molecules, ions or metal clusters of many types. These materials are known as endohedral fullerenes ($X@C_n$, where X is the trapped atom or molecule and n is the size of the fullerene) and a huge amount of research has been focused on them in the last decades.^[17,18] This is considered in more detail in section 1.1.1.4.

In the next paragraphs some of the reactions of C_{60} are presented.

1.1.1.1 Cycloadditions on C_{60}

C_{60} can undergo different types of cycloadditions. $[1+2]$ cycloadditions, $[2+2]$, $[3+2]$ and $[4+2]$ cycloadditions are all possible on the 6:6 bonds of fullerene's hexagons. This bond can act as diene or as a dienophile depending on the reaction conditions. Most important amongst the various cycloadditions with fullerenes, are cyclopropanation, Diels-Alder and hetero Diels-Alder $[4+2]$ cycloadditions, and the 1,3-dipole $[3+2]$ cycloadditions.

Cyclopropanation

Cyclopropanation of fullerene C_{60} can be achieved by different methods: (i) thermal addition of diazo compounds, followed by thermolysis or photolysis; (ii) addition of free carbenes and (iii) the Bingel reaction.^[19] While the first method leads to both $[6,5]$ -open and $[6,6]$ -closed

methanofullerene structures (**Figure 5**), the addition of free carbenes is selective to the [6,6]-ring junction (**Figure 6**).

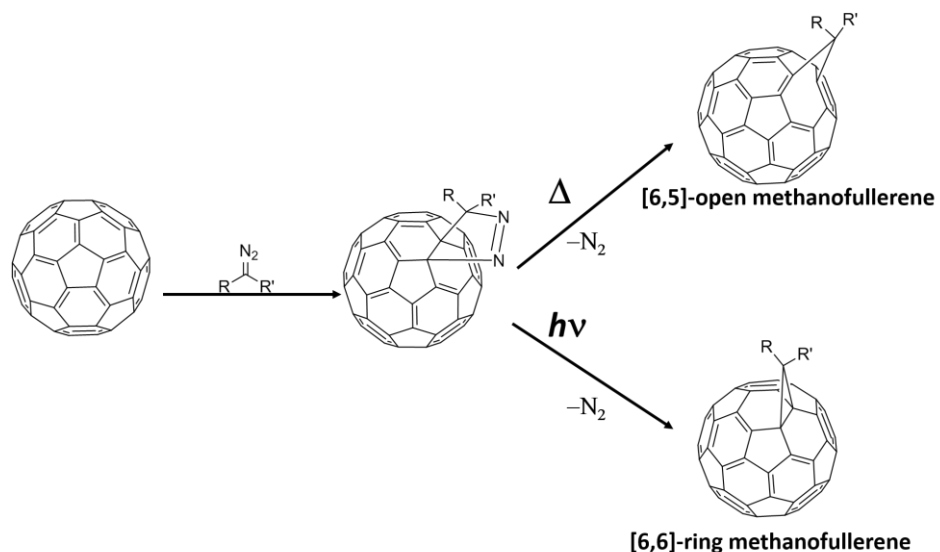


Figure 5: Scheme of the mechanism of the diazo addition on C₆₀ to give methanofullerenes via either thermolysis or photolysis.

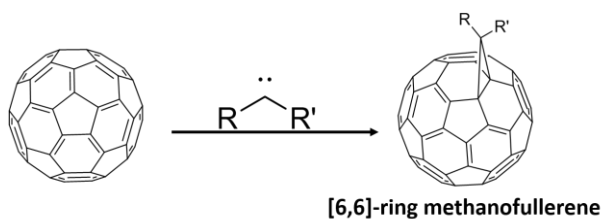


Figure 6: General scheme of the synthesis of methanofullerenes by free carbene addition.

Finally, the Bingel reaction is the procedure which enables the synthesis of C₆₀-methanofullerenes in the highest yields.[20] This reaction provides selectively the [6,6]-closed methanofullerenes products. The reaction conditions are relatively mild. The classic Bingel reaction is carried out on α -halomalonates in the presence of a base.[21] The general scheme of the reaction, which occurs with an addition-elimination mechanism, is reported in **Figure 7**.

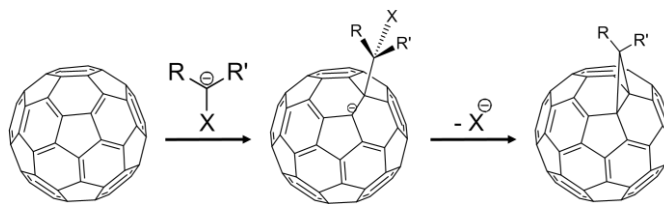


Figure 7: General scheme of the addition-elimination of the Bingel reaction.

The Bingel reaction permits the synthesis of a wide variety of C₆₀ derivatives which present different properties and have been exploited in different fields ranging from photovoltaics,[22] to material sciences[23], to biomedical sciences.[24,25]

In 1998, Diederich, Echegoyen and co-workers reported the discovery of the retro-Bingel reaction.[26] They discovered that via electrolytic reduction at constant potential, it is possible to electrochemically remove the bis(alkoxycarbonyl)methanoaddend formed by the Bingel reaction (**Figure 8**).

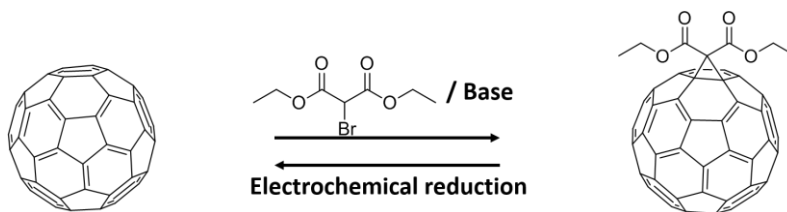


Figure 8: Bingel and retro-Bingel reactions.

The retro-Bingel reaction is an efficient way to remove methano-addends from fullerenes. It is also possible to carry out a retrocyclopropanation by chemical treatments. Both methods allow the selective removal of the Bingel substituent from the fullerene when other addends are present.[27,28]

Diels-Alder cycloaddition

Due to the excellent dienophile character of its (6:6) double bonds, C₆₀ can undergo the classical Diels-Alder cycloaddition reaction with dienes.[29] There are many different examples

of a Diels-Alder reaction on C_{60} and the first was performed using cyclopentadiene as 1,4-diene system (**Figure 9**).[30]

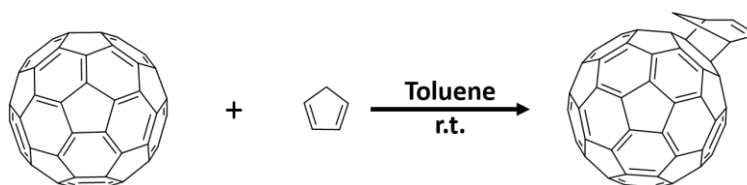


Figure 9: Scheme of Diels-Alder reaction between C_{60} and cyclopentadiene.

Also the retro-Diels-Alder reaction can take place on C_{60} . This particular process has been exploited to improve the morphology of active layers in organic solar cells. Soluble cycloadducts were first introduced into devices in order to obtain the release of C_{60} by means of retro-Diels-Alder reaction above 100 °C. This method permitted the formation of thin-films with improved morphology.[31] Depending on the reactivity of the diene, different reaction conditions (room temperature to reflux in high boiling solvent) are required. An efficient protocol, which leads to higher yields of the cycloaddition product, is to conduct the reaction under microwave (MW) irradiation. The use of MW, in fact, shorten the reaction times and, as a result, retro-Diels-Alder reaction as well as bis-adducts formation are avoided.[32] Although the Diels-Alder reaction is favoured by the presence of electron-rich substituent on the diene, the reaction is also possible with electron-deficient dienophiles. In this case, for example, fulleropyridazines have been prepared by an inverse electron demand Diels-Alder reaction (**Figure 10**), that is a reaction in which the electronic effect on the classic Diels-Alder reactions are inverted. In fact, in an inverse electron demand Diels-Alder, the presence of an electron-withdrawing substituents in the dienophile has the effect to retard the reaction and the presence of an electron-donating groups, to accelerate it. On the contrary, when the electron withdrawing group is on the diene, the reaction will be accelerated whereas an electron-donating group on it will have the effect to retard the reaction. [33]

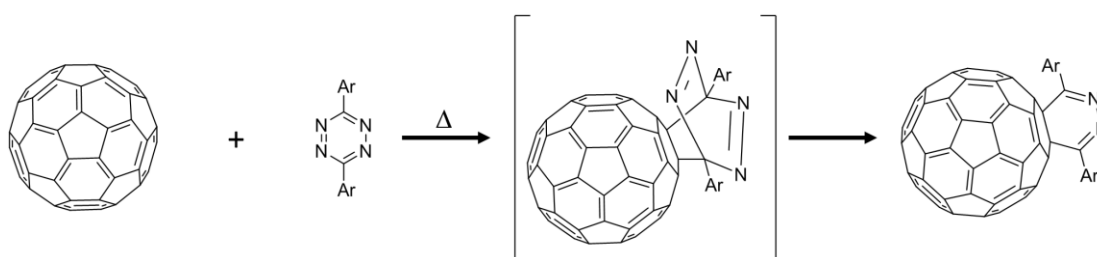


Figure 10: Scheme of Diels-Alder reaction between C_{60} and tetrazine derivative to obtain fulleropyridazine.

Addition of azomethine ylides (Prato chemistry)

Among the various cycloadditions on C_{60} , the 1,3-dipolar cycloaddition of azomethine ylides is of greater interest for this work. This reaction was developed by Prato and Maggini[34] and it is considered one of the most convenient route to functionalized fullerene. An example of this reaction is presented in **Figure 11**. It involves the generation of azomethine ylide via decarboxylation of the immonium salts resulting from the condensation of an α -amino acid with an aldehyde. The azomethine ylide then reacts selectively with a 6:6 bond of the fullerene to give the fulleropyrrolidine.

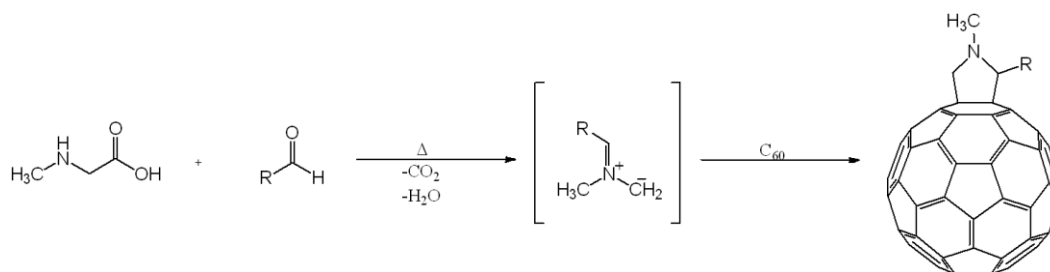


Figure 11: Example of Prato reaction using an aldehyde and *N*-methyl glycine (sarcosine).

The advantages of this method of functionalization are the high selectivity (it specifically attacks 6:6 bonds), the access to a wide range of possible functional groups and the possibility to insert simultaneously up to three substituents into the pyrrolidine ring with a facile reaction.[35] In contrast to the labile derivatives such as Diels-Alder cycloadducts and Bingel methanofullerene, which undergo their corresponding retro-cycloaddition reaction, fulleropyrrolidine had long been considered, to be very stable cycloadducts. However, a highly efficient thermal retro-cycloaddition of fulleropyrrolidine was first reported in 2006.[36] Different substituted fulleropyrrolidines were left in *o*-DCB at reflux for 4 to 24 hours in the presence of an excess of a dipolarophile. The role of the dipolarophile is to trap the ylide that is formed from the thermal retro-cycloaddition reaction in the mixture. With their experiments, Martín, Echegoyen and co-workers demonstrated that the retro-cycloaddition reaction was strongly dependent on the substituents on the pyrrolidine influencing the stability of the corresponding ylide. They have shown, in fact, that passing from unsubstituted *N*-methyl-fulleropyrrolidine to an ester-substituted *N*-methyl fulleropyrrolidine, C_{60} was recovered in 4% yield after 24 h reaction and 96.5% yield after 4 h (100% after 10 h) respectively, as summarized in **Figure 12**. C_{60} itself has been studied as dipolarophile in retro-cycloaddition reaction. When an excess of C_{60} is added to

pyrrolidinofullerene bisadducts in retro-cycloaddition reaction conditions, the mono-functionalized fulleropyrrolidine is obtained (100% yield) after 18 h reflux.

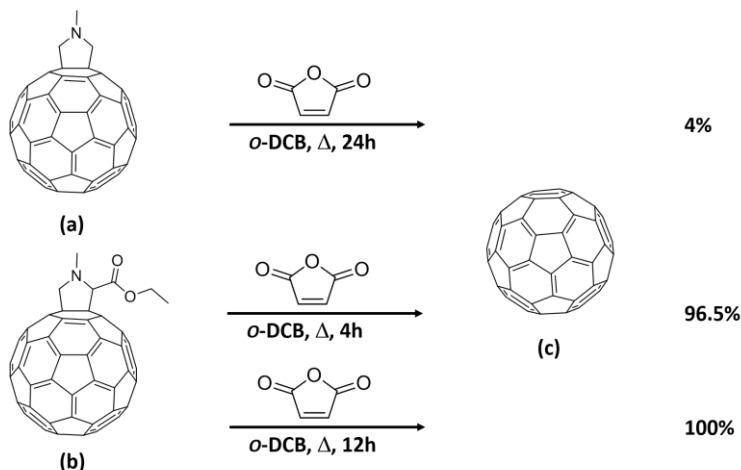


Figure 12: Thermal retro-cycloaddition of unsubstituted N-methyl fulleropyrrolidine **(a)** and ester-substituted N-methyl fulleropyrrolidine **(b)**, to give the parent unsubstituted fullerene C₆₀ **(c)**, and the respective yields showing the influence of the substituents on the efficiency of the reaction; maleic anhydride is used as dipolarophile.

In some cases the presence of dipolarophile, even if it increases the efficiency, is not necessary for the retro-cycloaddition to take place. Compound **a** in **Figure 13**, for instance, can undergo thermal retro-cycloaddition in the absence of dipolarophile (90% yield of C₆₀ after 24 h).[37]

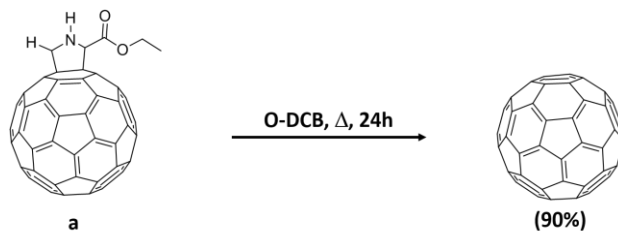


Figure 13: Thermal retro-cycloaddition of fulleropyrrolidine in the absence of dipolarophile.

The retro-cycloaddition efficiency has been shown to be improved by the use of Lewis metal, such as copper(II) triflate, or Wilkinson's catalyst. The retro-cycloaddition of pyrrolidinofullerenes can also be obtained via electrochemical oxidation, as reported in 2006.[38]

1.1.1.2 Nucleophilic additions

Nucleophilic additions are possible with C₆₀. The first examples can be found in the addition of organolithium or Grignard compounds, but also the addition of cyanide groups and of

hetero-groups containing phosphorous or silicon follow the same route. Nucleophilic additions result in monofunctionalized fullerene and usually occur in a 1,2-addition fashion. As reported by Hirsch, the reaction with nucleophiles starts with the formation of an intermediate $\text{Nu}_n\text{C}_{60}^{n-}$ that can be later stabilized by the addition of an electrophile (E^+) or neutral E-X to give $\text{C}_{60}(\text{ENU})_n$, an $\text{S}_{\text{N}}1$ or internal addition reaction to give methanofullerenes and cyclohexenofullerenes, or by oxidation to give C_{60}Nu_2 . [39] It is to be noticed that, technically, the Bingel-reaction described above, belongs to this class of reactions. A general scheme of the nucleophilic addition on fullerene is shown in **Figure 14a** with typical examples of nucleophilic addition reactions **Figure 14b**.

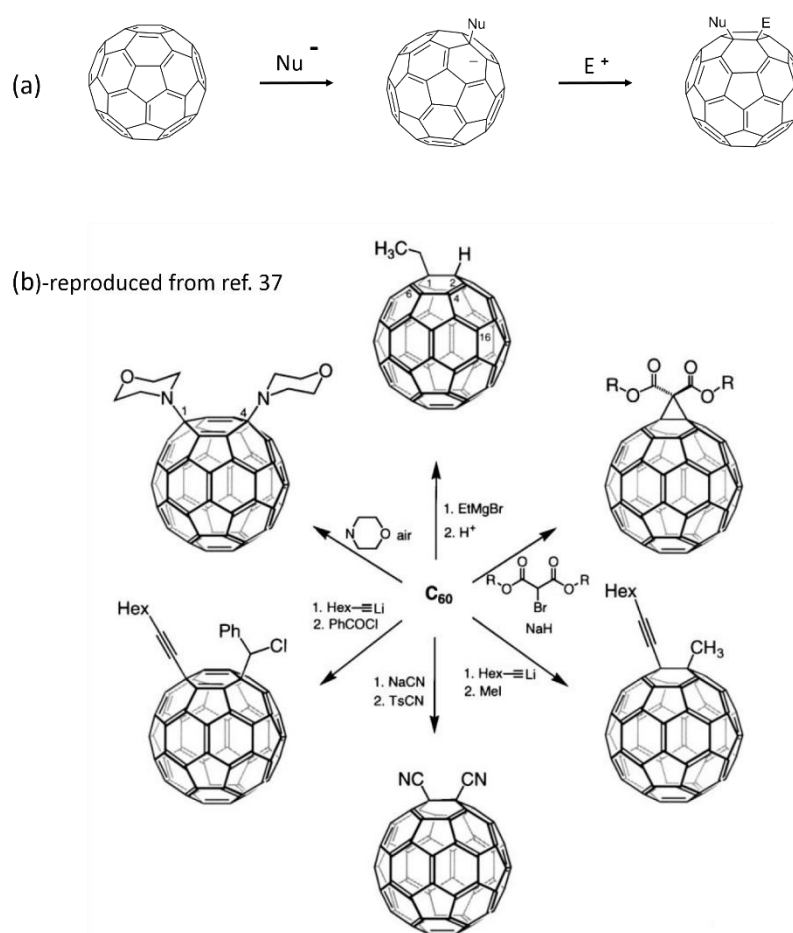


Figure 14: (a) general scheme of the nucleophilic addition on fullerene; (b) typical examples of nucleophilic additions.

1.1.1.3 Radical functionalization

Fullerene C_{60} is usually referred to as “radical sponge”. The electrophilic 6:6 bonds readily react with radicals and often occur as 1,4-additions. The facile addition of up to 11 phenyl groups, 15 benzyl groups, and 34 methyl groups to fullerene are remarkable examples of this aptitude of C_{60} to react with radicals.[40] Over the years, many different radical additions on fullerene have been studied.[41,42] The general scheme of radical addition on C_{60} is represented in **Figure 15**.

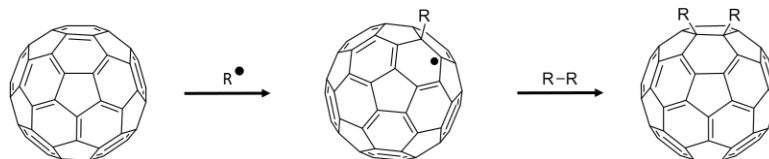


Figure 15: general scheme for the radical addition reaction on C_{60} .

Radical additions on C_{60} have been used to synthesize new materials of technological interest and fullerene-containing polymers. Moreover, the high affinity of C_{60} and its derivatives for radical species makes them potential radical scavengers.[43] In materials science, this high affinity for radical species has been exploited for the thermal and thermo-oxidative stabilization of various polymeric materials against free-radical-mediated degradative processes.[44] For example, C_{60} has been proved to prevent any low-temperature thermal degradation of poly(methyl methacrylate) (PMMA).[45] The efficient scavenging properties of fullerene are investigated also in medical and biological fields where the unique capacity of C_{60} and its derivatives for scavenging reactive oxygen species (ROS) make them of primary interest in many applications.[5,46]

1.1.1.4 Endohedral fullerenes

Endohedral fullerenes ($X@C_n$, where X is the trapped atom or molecule and n is the size of the fullerene) are an important class of fullerene derivatives. They have been first isolated in a pure state in 1994.[47] The empty structure of fullerene cage is apt to host atoms, small molecules and metal clusters of different nature. It is to be taken into account though, that the transition metals and noble metals that exhibit strong catalytic behaviour cannot be host in fullerene cages.

The combination between host molecules and fullerene gives as results the combination of the properties of the components, plus new properties deriving from the interaction between

them. In particular, electron transfer from the encapsulated metallic species to the fullerene cage takes place. These properties are very attractive for material scientists and this explain the huge development that this class of molecules has seen in the last decades. These materials can be classified into three main classes, taking into account the metals contained in the fullerene (mono-, di-, and cluster- endohedral metallo fullerene). Example of mono and di- endohedral metallo fullerenen are shown in **Figure 16**.

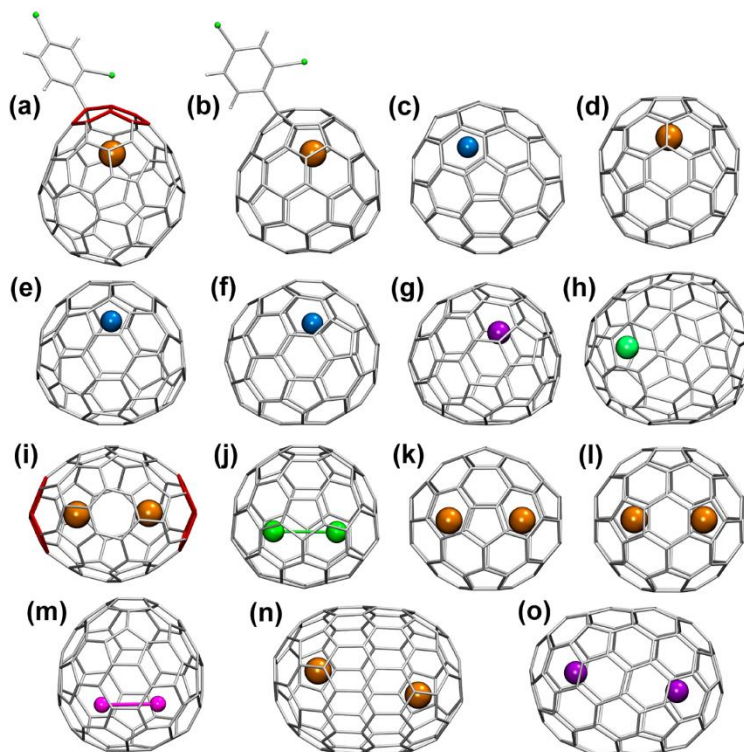


Figure 16: Molecular structures of selected mono- and dimetallofullerenes: (a) $C_6H_3Cl_2$ adduct of $La@C_{72}-C_2(10612)$; (b) $C_6H_3Cl_2$ adduct of $La@C_{74}-D_{3h}(1)$; (c) $Yb@C_{80}-C_{2v}(3)$; (d) $La@C_{82}-C_{2v}(9)$; (e) $Yb@C_{82}-C_2(5)$; (f) $Yb@C_{82}-Cs(6)$; (g) $Sm@C_{82}-C_{3v}(7)$; (h) $Tm@C_{94}-C_{3v}(134)$; (i) $La_2@C_{72}-D_2(10611)$; (j) $Lu_2@C_{76}-T_d(1)$; (k) $La_2@C_{78}-D_{3h}(5)$; (l) $La_2@C_{80}-I_h(7)$; (m) $Sc_2@C_{82}-C_{3v}(8)$; (n) $La_2@C_{100}-D_5(450)$; (o) $Sm_2@C_{104}-D_{3d}(822)$. Carbon atoms are grey except for the atoms in the adjacent pentagon pairs, which are shown in red; metal atoms are dark orange (La), blue (Yb), violet (Sm), lime (Tm), light green (Lu), and magenta (Sc). The lines connecting metal atoms in $Lu_2@C_{76}$ and $Sc_2@C_{82}$ denote covalent bonds between them. Image reproduced from ref.48.

The smallest mono-endohedral metallo fullerene that has been characterized is $La@C_{72}$.^[49] In the case of di-endohedral metallo fullerene, two different metal atoms are incorporated into the fullerene. It has been found that in the case of medium fullerenes (C_{80} and C_{82}), the two metal atoms tend to rotate in the cage.^[50] This is not the case for larger cages (C_{100} , C_{104}) or small fullerenes (C_{72} , C_{78}), where the atoms stay in fixed positions.^[51,52] Various synthetic methods are

possible, depending on the nature of molecule to incorporate. When a metal is to be inserted into fullerene, harsh conditions are needed and arch discharge methods are used.[53] The mechanism of formation of endohedral metallo fullerene is not completely elucidated yet and the synthesis of these materials leads to regioisomeric mixtures. Purification is an important step in order to obtain the desired material. In general, the separation of regioisomers to obtain a pure hybrid compound is done via HPLC chromatography, but other methods have been proposed.[54,55] Once formed, the endohedral fullerene can undergo other reactions. Diels–Alder, Prato and Bingel-Hirsch chemistry as well as radical additions on these material have been published.[48] The endohedral fullerenes find potential application in many technological fields: nanomedicine, pharmaceutical, biology, imaging, catalysis and photovoltaic are some examples. In photovoltaic technology, endohedral fullerenes have been proposed with success as acceptor materials in devices.[56,57]

1.2 Organic photovoltaics

The development of new technologies for renewable energy is of crucial importance nowadays. The increasing global demand for energy, in fact, is in big contrast with the decrease of the availability of fossil fuels, which are currently the main energy source, and with the long-term effect of the CO₂ and other greenhouse emissions caused by their combustion. Different sustainable energies technologies are under studies and are now exploited to alleviate the use of fossil fuels. Among the renewable energies, solar energy is one of the most promising as it is worldwide available. The direct conversion of solar energy into electricity is due to the photovoltaic effect which was first discovered by the French physicist Alexander-Edmond Becquerel in 1839 on inorganic materials.[58] Becquerel, in fact, observed the presence of photocurrent when platinum electrodes, covered with silver bromide or silver chloride, were illuminated in aqueous solution. It is only in the 1900s that photoconductivity was observed also for organic compounds thanks to studies conducted on anthracene.[59] In the early 1960s it was discovered that many common dyes had semi-conducting properties and lately those dyes were proved to exhibit also the photovoltaic effect.[60] The first device which exploited this effect to obtain an electric flux towards an external circuit was developed at Bell laboratories in 1954.[61] This was a Si-based device with a 6% efficiency. Further investigations in Bell's laboratory led to the development of single crystals Si-based devices with efficiencies that could reach 24%. Despite the huge amount of research on organic materials for photovoltaic devices, today Si-

based solar cell still lead the PV-world market. This dominance of inorganic-based devices on the market is due to their stability and efficiency which exceed 44% in the case of multijunction cells, and 25% and 20%, for single crystalline-based devices and multicrystalline silicon-based devices respectively.[62] These efficiencies are very high when compared to those obtained with organic-based devices, as shown in **Figure 17**. Nonetheless, there is great interest in the development of the alternative types of solar cells as the inorganic-based ones have drawbacks mostly due to their high production and installation costs.

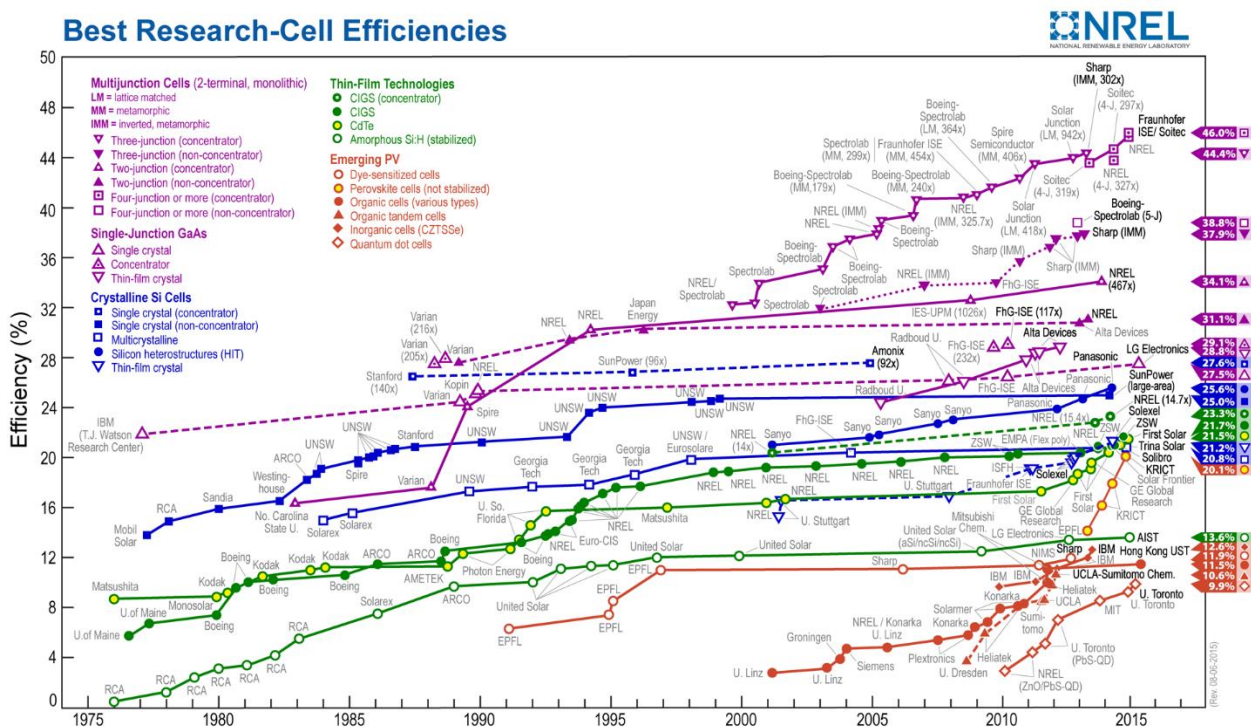


Figure 17: NREL- chart on record cell efficiencies.[62]

The photovoltaic devices are in general divided by generations. To the first generation are devices that exploit silicon to obtain a photovoltaic effect. Second generation NREL devices are those based on thin film technologies which hold the promises of lowering the cost of production by lowering the amount of material needed and by using more convenient manufacturing processes. The use of thin films, in fact, makes it possible to have devices with less Si, which is energy-intensive to prepare, and to obtain devices with lower thickness that can also be flexible. To the third generation solar cells belong the new technologies such as the so called dye sensitized solar cells devices (DSSCs),[63,64] first developed by Grätzel and co-workers, which are

electrochemical cells, the multijunction cells fabricated from group IV and III–V semiconductors,[65] and the organic photovoltaic devices (OPVs), which will be the focus of this section. Examples of a DSSC solar cell and of a multijunction cell are shown in **Figure 18**.

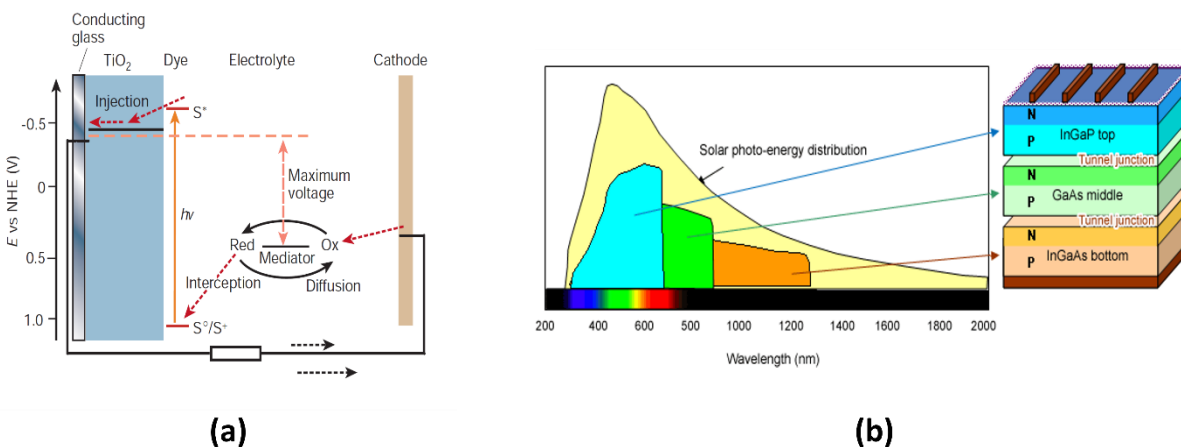


Figure 18: Selected examples of third generation solar cells: (a) Scheme of operation of the dye-sensitized electrochemical photovoltaic cell. The photoanode, made of a mesoporous dye-sensitized semiconductor, receives electrons from the photo-excited dye which is thereby oxidized, and which in turn oxidizes the mediator, a redox species dissolved in the electrolyte. The mediator is regenerated by reduction at the cathode by the electrons circulated through the external circuit. Figure courtesy of P. Bonhôte/EPFL-LPI - Image reproduced from ref.64; (b) wavelength distribution of solar photo-energy and the structure and wavelength sensitivity of a triple-junction compound solar cell –Image reproduced from ref.66.

Organic photovoltaic technology, characterized by the exploitation of organic semiconductors as active layer materials in the devices, has attracted a tremendous amount of interest over the last two decades. This class of solar cells holds promises of low cost and large volume production due to the relatively low energy input in fabrication.[67] Organic semiconductors are solution-processable materials that allow low temperature and high throughput production methods such as roll-to-roll printing. “Market-killing” advantages include the possibilities of fabricating lightweight and flexible devices which can be easily integrated into buildings, vehicles and many different manufacturing processes that can range from textiles to small gadgets. Last but not least, the possibility of colored and semitransparent devices make OPV very promising for the market.

The strengths and limitations of OPV are the use of organic semiconductors itself. The physics is different from that of inorganic materials. This has a great impact on the design of the devices.[68] A first difference between inorganic and organic semiconductors is found in the charge carrier formation upon photo-excitation. In contrast to what happens in inorganic semiconductors,

where optical absorption results in the immediate creation of free charge carriers, in an organic semiconductor this process results in the formation of a spatially localized electron-hole pair, i.e., a Frenkel-type exciton, which is electrically neutral and which needs to undergo dissociation process in order to provide the desired free-charges. Dissociation is possible if the binding energy of the exciton is overcome. This is possible if a strong electric field is present. The device's architecture has then to take into account that, in order to dissociate, excitons need to experience a suitable electric field within their diffusion length, which ranges, depending on the technique used to characterise and materials from around 1 to around 30 nm. To a large extent, this determines the ideal nano morphology of a successful OPV device. If this does not happen, recombination takes place and the exciton decays to its ground state. A second difference is found in the charge carrier mobilities in the materials. While wide valence and conduction bands and large charge carrier mobilities are present in crystalline inorganic semiconductors, due to the three-dimensional character and rigidity of the lattice, in organic semiconductors the weakness of the electronic couplings, the large electron-vibration, and the disorder effects lead only to modest carrier mobilities. In the latter semiconductors charge transport relies on hopping processes through the material rather than proceeding within a band.[69] However, the disadvantages of lower mobility are partially balanced by the relatively strong absorption coefficients (usually $\geq 10^5 \text{ cm}^{-1}$) of these materials, which allows high absorption in even <100 nm thin devices.[70]

1.2.1 Operating principles and device architecture

The photovoltaic process in OPVs requires four steps: (i) light absorption by the photoactive material with the formation of an excited state, a Frenkel-type exciton (bonded electron-hole pair); (ii) exciton diffusion to the interface between n-type and p-type material; (iii) charge separation and generation of free charges carriers at the interface; and (iv) charge transport and collection at the electrodes.

Each step of the photovoltaic process is influenced by the choice of the donor-acceptor pair in the active layer. Light absorption is of course dependent on the nature of the photoactive component. Moreover, the good electronic match between the two materials, as well as a good morphology of the layer are crucial in order to have exciton diffusion and charge separations. The driving force for the charge separation is determined by the difference in energy between the lowest unoccupied molecular orbital (LUMO) of the donor material and the LUMO of the acceptor

material. This energy gap has to overcome the binding energy of the exciton. The scheme of this process is shown in **Figure 19**.

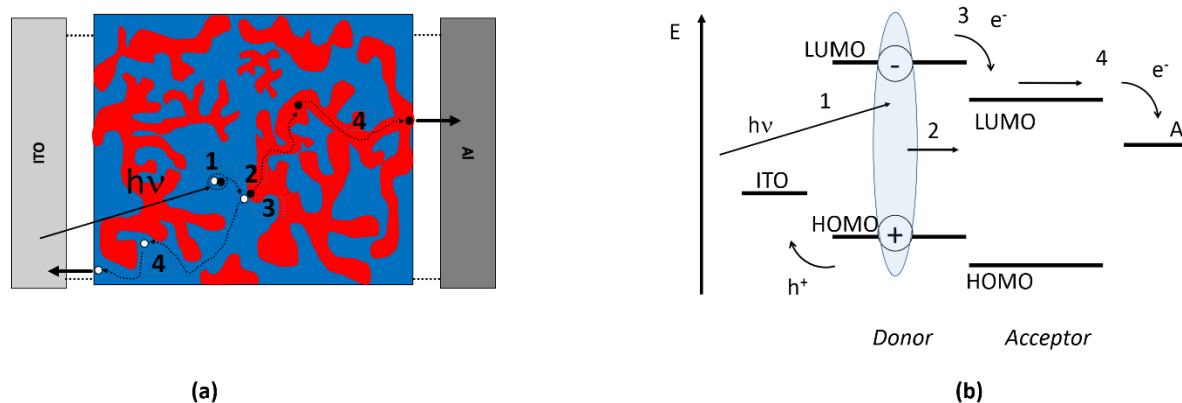


Figure 19: (a) Scheme of the photovoltaic process in an organic-based device and (b) a sketch of the energy level; 1-absorption of light and formation of an exciton; 2- exciton diffusion to the interface; 3- charge separation; 4- charge transport and collection at the electrodes.

The obtained electric current corresponds to the number of the created charges that successfully arrive and are collected at the electrodes. This number depends on three different factors that determine the overall photocurrent efficiency, η (**Equation 1**).

$$\eta_j = \eta_{abs} \times \eta_{diss} \times \eta_{out} .$$

(Equation 1)

The first factor is the fraction of photon absorbed by the photoactive material (η_{abs}). This factor is a function of the absorption spectrum and absorption coefficient and though of the nature of the material and the thickness of the absorbing layer. The second factor takes into account the fraction of hole-electron pairs that are dissociated (η_{diss}). Not all the created excitons diffuse to an interface region where a charge separation can occur, and only a fraction of those which reach the interfaces between the two types of materials actually undergoes charges dissociation. As mentioned above, excitons created in domains larger than their diffusion length cannot reach the interfaces and recombine to decay to the ground state. The last factor, η_{out} , is the fraction of charges that actually reach and are collected at the electrodes (recombination process are possible during the charge transport to the electrodes and, in order to have an efficient collection of the charges, it is necessary to overcome the potential barrier of organic/metal interface).

A crucial role in the efficiency of the solar cells is then played by the device architecture. Although the general structure of a solar cell is constituted by active materials sandwiched between two electrodes, one of which has to be transparent to allow light penetration. Over the years, different OPV device architectures have been used with the aim of improving the performance of the cell. In the first possible structure, a single active layer is sandwiched between two electrodes (**Figure 20**). In this kind of architecture the driving force for the charge separation is the presence of an electric field due to the work function asymmetry of the electrodes. In general the electrode with higher work function consists in a transparent layer of indium tin oxide, ITO. Low work function metal, such as Ag, Al, Mg or Ca can be used as second electrode. The efficiency of these devices is very low because of the low efficiency of their exciton dissociation processes. In order to overcome the exciton binding energy, two processes are possible: the first relies on the thermal energy, and the second on the dissociation at the contacts. Under the operating conditions of solar cells, the temperature is not high enough and the sample thickness is much thicker than the exciton diffusion length.[60]

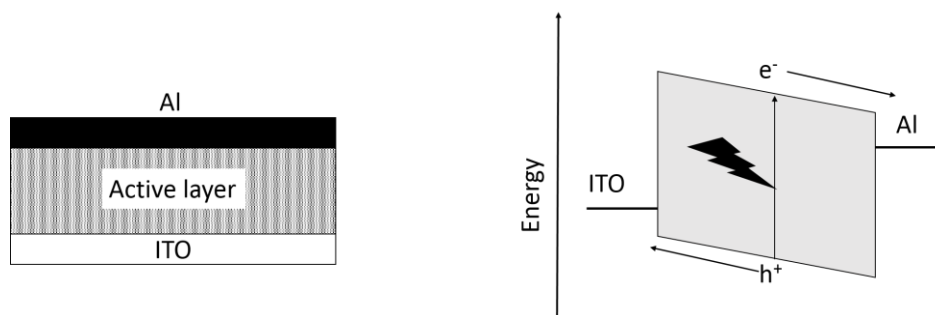


Figure 20: Schematic representation of single-layer OPV device and a sketch of the energetic levels.

A second possible device architecture is obtained using two layers of two different materials, one acting as an electron donor material and the second one as an acceptor. The first example of this device architecture has been published in 1986 by Tang.[71] The device, its schematic representation is reported in **Figure 21**, was prepared with a phtalocyanine derivative (CuPc) as p-type semiconductor and a perylene derivative (PV¹) as n-type semiconductor sandwiched between a transparent conducting oxide and a semitransparent metal electrode. This bilayer-based device is more efficient than the single-layer because charge separation is now driven by

¹ Note that PV, used here to identify the perylene derivative reported by Tang, to be in agreement with reference 71, is used as abbreviation for “photovoltaic” through the rest of this work.

the difference in potential between the two materials. In his work, Tang published a maximum power conversion efficiency of almost 1%.

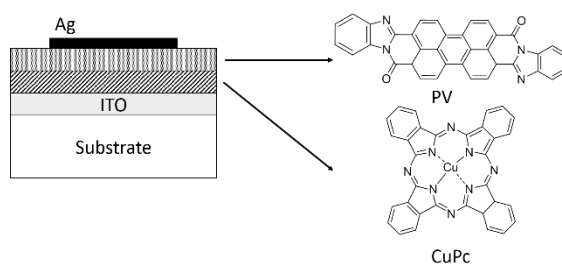


Figure 21: Schematic representation of the bi-layer heterojunction device used by Tang for his work.

The difference in electron affinities results in a driving force at the interface between the two materials which permits the dissociation of the excitons. Once free charges are formed, the electron travels within the acceptor and the hole through the donor material. Thus the opposite charges are physically separated from each other and unlikely to recombine. However, the bilayer type architecture is limited by the exciton diffusion length, and only the excitons formed near the donor/acceptor interface can reach and dissociate at this interface.

To overcome this limitation and improve the efficiency of charge separation by keeping an acceptable active layer thickness in order to absorb most of the light, the bulk heterojunction (BHJ) concept was developed and has been used over the last two decades. The BHJ is obtained by blending donor and acceptor material in a solution process or by co-evaporating the two materials onto the electrode. These techniques allow to obtain dispersed nanostructured domain in the active layer in which more excitons are likely to reach the interface donor-acceptor (**Figure 22**). One disadvantage is that the separation of the charge carriers can result more difficult due to the increased disorder and that the percolation pathways to the respective electrodes are not always given in the disordered material mixtures. Moreover, recombination between trapped charges with mobile ones are more likely to happen. The first dispersed polymer heterojunction was prepared in 1994 via solution process and it was a ITO/MEV-PPV:C₆₀/Ca.[72] Since then, the BHJ morphology is the most widely used in OPV.

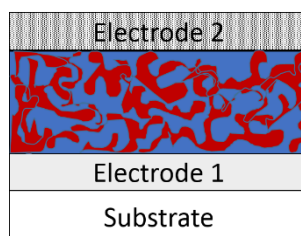


Figure 22: Schematic representation of OPV devices with a bulk heterojunction active layer morphology.

Nowadays there are three most common OPV device architectures which use this concept: (a) normal geometry BHJ, (b) inverted geometry BHJ and (c) tandem devices. The different architectures are represented in **Figure 23**.

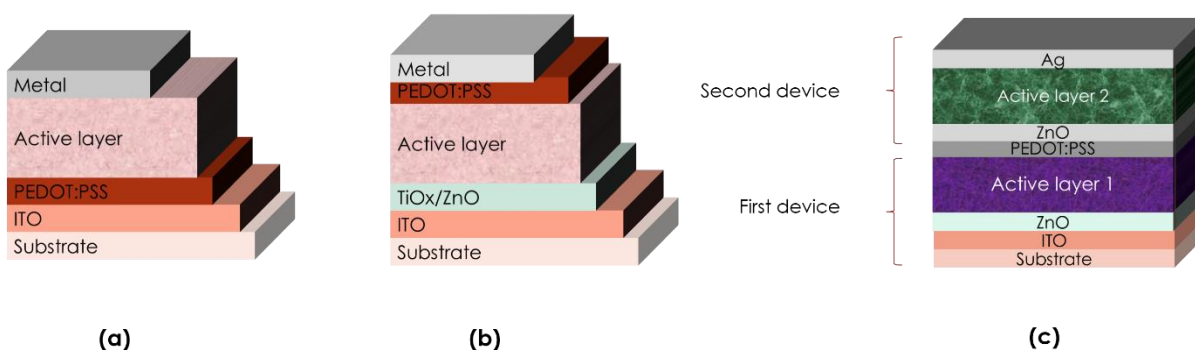


Figure 23: common OPV devices architecture; (a) regular geometry OPV; (b) inverted geometry OPV; (c) tandem OPV solar cell.

The normal and the inverted BHJ geometries differ by way of the direction in which the charges flow.

The normal geometry BHJ is a type of device in which the active layer is sandwiched between two electrodes of different work functions. In this type of solar cells the holes are transported to the anode and the electrons are collected at the cathode. In general the anode consists of indium-tin oxide (ITO) coated glass substrates on the top of which an electron blocking layer, typically PEDOT:PSS, is deposited from solution. The cathode consists in a low work function metal which is separated from the organic active layer by an electron selective interlayer. Most commonly the low work function metal used for this role is aluminium. The main issue encountered with this architecture is the use of the low work function cathodes. These materials have high reductive properties and can easily react with oxygen, water and with polymers. These reactions represent

a degradation pathway for the devices that is added to the already complex degradation pathways of an organic solar cell.

A strategy to diminish this additional degradation pathway has been developed in the last decade and consists in the use of the inverted geometry solar cells.[73] In this configuration, ITO is typically coated with a low work function metal oxide (generally ZnO) and used as cathode. The anode is now constituted by a metal, such as Ag or Au, which has the advantage of a better stability to oxidation.

Finally the third common device architecture for OPV is represented by the tandem geometry. In a tandem device two or more active layers are stacked, one on top of each other, separated by an interconnecting layer which permits the recombination of the opposite charges coming from the two different layers. The tandem architecture has the advantage of an enhanced light harvesting while maintaining each single layer in the range of optimum thickness for charge transport to electrodes (or to the interconnecting layer). The tandem solar cell technology has recently reached the record of 12% efficiency with a device developed by Heliatek.[74]

1.2.2 Influence of the nanoscale morphology

In the BHJ configuration the intimate intermixing of the donor and the acceptor material is of crucial importance. The morphology has a strong impact on the overall solar cell performances as it directly affects the excitons diffusion and dissociation (η_{diss}) as well as the charge transport to the electrodes (η_{out}). A good balance between exciton dissociation and charge transport requirements has to be ensured by an optimum domain size of the phase separation between the two materials. This has also been suggested by Walker *et al.* who used a dynamic Monte Carlo model to study the relationship between the BHJ nanostructure of an organic solar cell and its efficiency.[75] The optimization of the nanomorphology has to be taken into account for the design of advanced organic solar cells, together with the optimization of the molecular structure and the device properties. Considering the requirements for those processes, the ideal nanostructure of the active layer has been found to be an interdigitated structure where donor and acceptor present large interfacial area, small domain in the order of the exciton wavelength, and well ordered to permit an efficient charge transport towards the electrodes. This type of nanostructure, in **Figure 24**, is difficult to obtain with organic materials. The disordered nature of the classic polymer mixtures makes difficult to obtain well-organized nanostructure. However,

this nano-organization can be introduced employing organic materials with self-organization capability or inorganic templates that are then filled with the organic photoactive materials.[76]

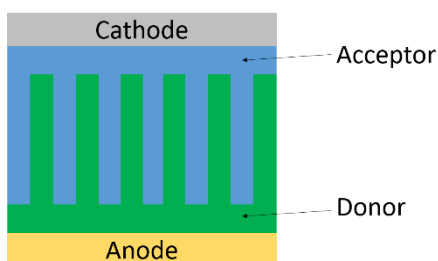


Figure 24: Ideal morphology for BHJ solar cell with inter digitated donor and acceptor material to ensure good exciton separation and charge transport.

To ensure a good morphology of the active layer, different approaches have been proposed.[77] For instance, plasticizer additives and compatibilizers[78] have been applied in the preparation of active layers in order to increase the miscibility of the donor and the acceptor materials and therefore lead to a fine phase segregation. The choice of the good solvent for the active layer deposition is a second way to control the nanostructure morphology. It has been proved that for solvent processed systems, there is a strong dependence of the final morphology on the chosen solvent, solvent evaporation time, and postproduction annealing.[79–81] For example, studies on the solvent-dependent cluster formation in phenyl-C₆₁-butyric acid methyl ester (PCBM):P3HT active layer systems have been conducted.[82] While only a few PCBM clusters are found in films produced using chloroform (CF) and chlorobenzene (CB) as solvents, a higher density of clusters is present in those made using toluene and xylene (**Figure 25**). Thus the cluster-formation process is solubility driven.

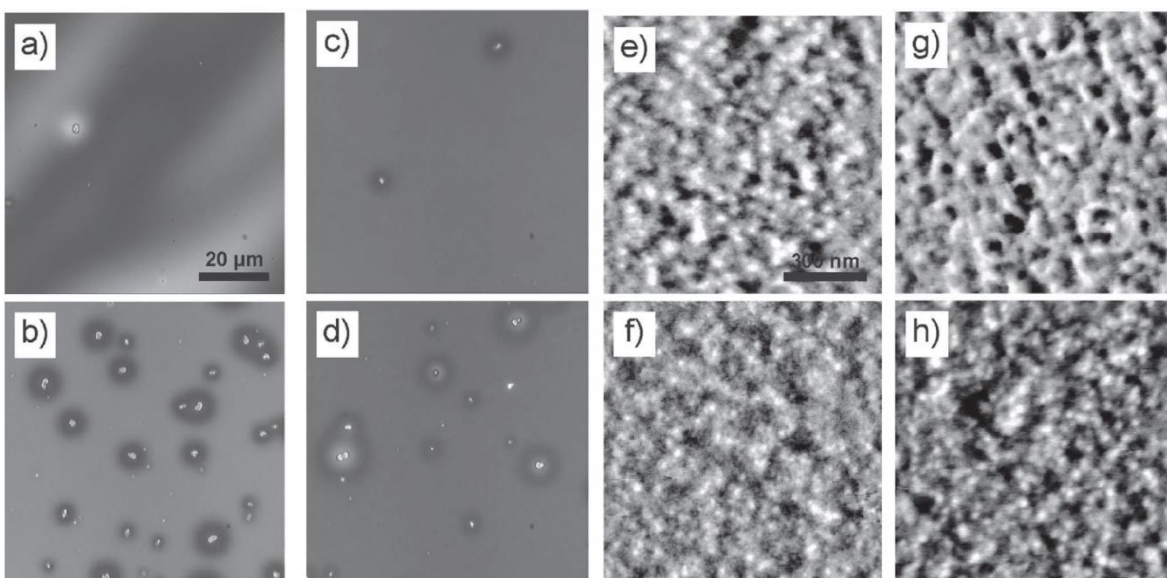


Figure 25: a–d) Optical micrographs and e–h) AFM images ($2 \times 2 \mu\text{m}^2$) showing the topography of annealed P3HT:PCBM films made using a), e) CF, b), f) toluene, c), g) CB, and d), h) xylene solutions. The scale bars demonstrate the scale for all micrographs and AFM images. e)–h) The grayscale code is adapted for each image separately. The grey range covers 3.5, 6.0, 8.0, and 1.0 nm in e), f), g) and h), respectively. Image reproduced from ref.82.

The use of cross-linkers has also been proved successful.[83,84] A very different approach includes the application of inorganic nanostructures. Inorganic nanostructures are first prepared and then used as template for the organic semiconductors to obtain the desired morphology.[85–87]

Together with approaches that take advantages from external factors, strategies based on molecular-design have been proposed to improve the morphology of the devices. One strategy is to covalently link donor and acceptor to have the intermixing profile. The use of self-assembling diblock copolymers to obtain controlled and stable separation between the active materials has been adopted in organic electronic devices.[88–90] Also the use of the so called double-cable polymers, where the acceptor material is covalently grafted onto the backbone of the donor polymer, has been proposed to improve the control on the bicontinuous phase separation between the two materials. The first double-cable polymers used in photovoltaic cells has been reported by Ramos *et al.* in 2001.[91] The layered structure of the self-assembled diblock copolymers and of the double-cable polymers were expected to facilitate the efficiency of charge transport in the active layer.[92] However, double-cable systems result in a too fine nanostructure between the donor and the acceptor material. This morphology results more in facilitating the recombination processes and actually reduce the device performances.

1.2.3 Device characterizations

To characterize the performance of OPV devices, different parameters are used. In this paragraph we briefly discuss some of these parameters.

As for conventional p–n solar cells (inorganic solar cells), an organic photovoltaic device can be approximated by an equivalent circuit, shown in **Figure 26**. To obtain a realistic description of the physics of the devices, different parameters have to be included in the equivalent circuit. A first element to be included is a diode with reverse saturation current density J_0 (current density in the dark at reverse bias) and ideality factor n . A second element is a current source (J_{ph}), which corresponds to the photocurrent upon illumination. In addition to these elements, two resistances have to be added: a series resistance (R_S), and a shunt (R_P) resistance. R_S is a parameter that takes account of the finite conductivity of the semiconducting material, the contact resistance between the semiconductors and the adjacent electrodes, as well as the resistance associated with electrodes and interconnections and has to be minimized. In contrast, the shunt resistance, needs to be maximized as it takes into account the loss of charge carriers via possible leakage paths.[70,93]

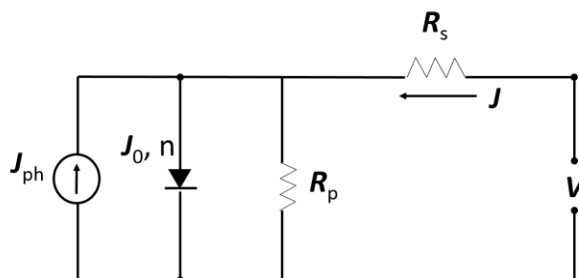


Figure 26: Scheme of the equivalent circuit for an organic solar cell. J_{ph} is current source, J_0 is the diode reverse saturation current, n represent the ideality factor, J is the current through the circuit, V is the voltage, and R_s and R_p are two resistance that takes into account the resistance sources in the device (finite conductivity of the semiconductors, resistance of electrodes and connections) and the possible leakage paths respectively.

Solving for this circuit provides the Shockley equation for the current–voltage (**Equation 2**)

$$J = \frac{1}{1 + R_S/R_P} \left\{ J_0 \left[\exp\left(\frac{V - JR_S A}{nkT/e}\right) - 1 \right] - \left(J_{ph} - \frac{V}{R_P A} \right) \right\}$$

(Equation 2)

The current density–voltage (J - V) curve of an OPV solar cell in dark conditions is shown in **Figure 27a**. For a device in the dark, the J - V curves pass through the origin of the axes. Almost no current

flows until large forward bias. When the cell is under illumination, the J - V curve shifts down as shown in **Figure 27b**.

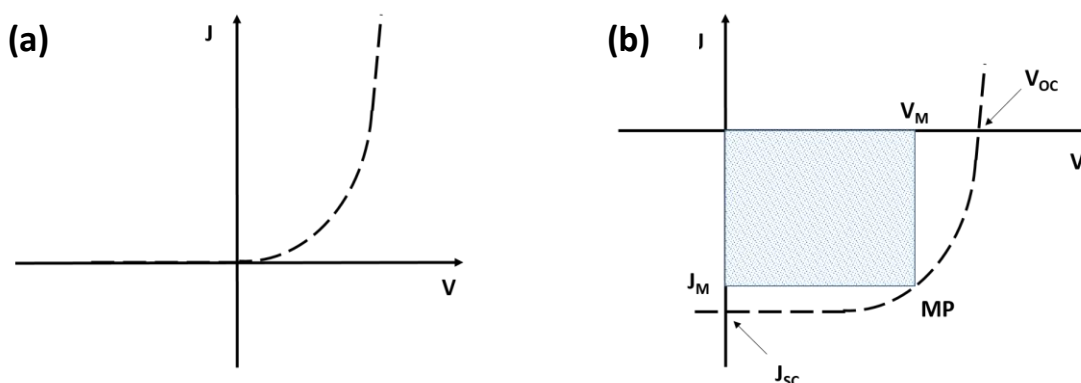


Figure 27: J - V curves of an OPV solar cell under (a) dark and (b) illuminated conditions.

The different metrics to describe the device performances can be obtained from **(Equation 2)**, or experimentally from the J - V curve. The short-circuit current, J_{sc} , is the maximum current that can flow in the device under illumination when no bias is applied. It depends on the illumination strength and on the efficiency of each single steps of the photovoltaic process. This parameter gives information on the efficiency of processes such as charge separation and charge transport in the cell. When a bias is applied and no current runs through the cell, the device is in open circuit condition and the applied voltage is the open circuit voltage (V_{oc}). The V_{oc} is the maximum voltage obtainable from the device. This parameter depends drastically on the nature of the active layer materials. In first approximation, the V_{oc} is proportional to the difference between the HOMO of the donor material and the LUMO of the acceptor material. In the case of a conjugated polymer-PCBM system, the V_{oc} can be estimated using **(Equation 3)**. [94]

$$V_{oc} = (1/e)(|E_{HOMO}^{Donor}| - |E_{LUMO}^{PCBM}|) - 0.3V$$

(Equation 3)

The value 0.3V is an empirical corrective factor related to the coulombic attraction of an electron-hole pair.

At any point on the electrical characteristic in the fourth quadrant of the J - V curve, J_{sc} negative and V_{oc} positive, the device produces an electrical power density which is given by the product

of voltage and current density. The square $J_M V_M$ gives the maximum power (MP) that can be obtained from the cell. Using the parameters described above, it is possible to calculate the Filling Factor (FF) of the cell (**Equation 4**). This metric is used to determine the power conversion efficiency (PCE) of the device. This factor, indeed, gives an indication on how easy is the charge extraction process in the cell and allows to take into account only the part of the product of V_{OC} and J_{SC} that can be used. The PCE of a solar cell is the ratio between the maximum electrical power, P_{OUT} obtained from the device and the total incident optical power, P_{IN} . The complete formula for PCE is presented in

$$PCE = \frac{P_{OUT}}{P_{IN}} = \frac{J_M \times V_M}{P_{IN}} = FF \times J_{SC} \times V_{OC} \div P_{IN}$$

(Equation 5).

$$FF = \frac{J_M \times V_M}{V_{OC} \times J_{SC}}$$

(Equation 4)

$$PCE = \frac{P_{OUT}}{P_{IN}} = \frac{J_M \times V_M}{P_{IN}} = \frac{FF \times J_{SC} \times V_{OC}}{P_{IN}}$$

(Equation 5)

Another important factor to evaluate is the external quantum efficiency (EQE) of the solar cell which is the device efficiency as a function of the energy of the incident radiation. EQE is obtained from the ratio between the collected photogenerated charges and the number of incident photons and describes the overall efficiency of the four steps of photovoltaic process in the solar cell.

To characterize quantitatively the performance of solar cells for terrestrial applications, and in order to have comparable values between the research laboratories, standardized illumination conditions are used. Generally in these conditions, the spectrum of the light source simulates the solar spectrum and has an intensity on the order of 1000 mW m^{-2} (**Figure 28**), which corresponds to the average intensity of sun light with an angle of incidence $\theta=48^\circ$ relative to the normal to the earth's surface. This standard condition is denoted AM 1.5 G where AM is for air mass, equal to $1/\cos\theta$, and G stands for global and refers to small contribution of diffusive light to the direct incident light.[95,96]

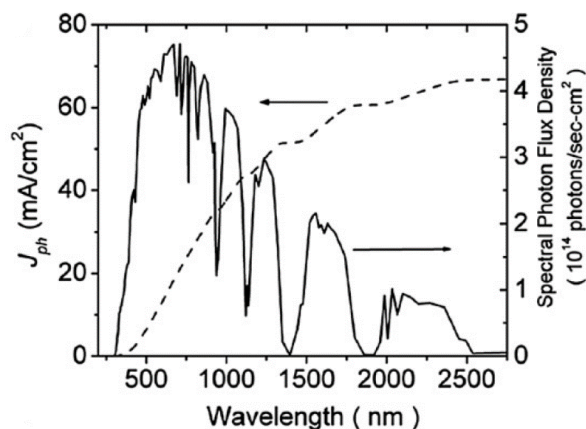


Figure 28: Spectral photon flux density in the standardized AM 1.5 G illumination conditions and corresponding integrated current that would be produced if each photon contributes to current with unity efficiency. Image reproduced from ref.93.

1.2.4 Device stability

Organic solar cells degrade during illumination. Photo-induced degradations are not the only degradation processes that interest OPVs. Chemical and physical degradation phenomena, take place in an organic solar cell under illumination and in the dark. Understanding the stability/degradation in organic solar cell is one of the greatest challenges in the field. Moreover, alleviating the degradation phenomena is necessary to successful application of this technology. Long operational lifetime, in fact, together with low cost production and good efficiency is a basic requirement for real-life application of organic solar cell devices.

Depending on the significance of air exposure, intrinsic degradation (caused by the thermal interdiffusion of species inside the device) and extrinsic degradation (caused by the intrusion of air) can be found.[97] The former includes phase separation at the organic cathode interface, phase segregation of the organic materials and inter-diffusion at buffer interlayers. Also macroscopic changes such as delamination, formation of particles, bubbles, and cracks influence the device's lifetime. A schematic illustration of some degradation processes in OPV devices is reported in **Figure 29**.

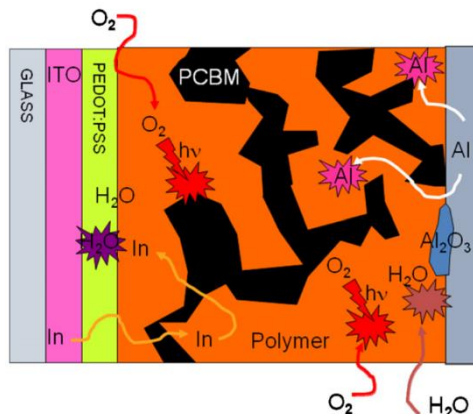


Figure 29: Schematic illustration of some degradation processes in OPV devices. Image reproduced from ref.98.

Chemical degradation are mainly due to oxygen, water and electrode materials reactions with the polymer active layer. When a device is exposed to air, the oxygen and the water can diffuse into it and react with the active layer materials. Oxygen is considered the main cause of chemical degradation because the electron-transport properties of fullerene suffer from the exposure to oxygen in air[99] and, moreover, oxygen increases the work functions of metals by forming surface dipoles.[100] This generally deteriorates the performance of conventional devices, but may temporarily enhance the performance of inverted OPV.[101] The diffusion of this molecule through the outer electrode was shown to proceed via microscopic pinholes in the electrode. Although the oxidation of the organic materials occurs also in the dark, illumination accelerates this process. The mechanism of the photo-oxidation of a polymer is well-known. Singlet oxygen is formed by energy transfer from the photo-excited polymer to adsorbed ground state oxygen molecules. The singlet oxygen reacts then with the polymer itself to give the oxidation products. Chambon *et al.* have reported that the presence of a large amount of PCBM, in a MDMO-PPV polymer, efficiently quenched the excited state whereby sensitization of singlet oxygen is suppressed.[102] They concluded that the radical scavenger properties of PCBM protects the polymer MDMO-PPV from oxidation. Chemical degradation can occur also at the device's electrodes. Electrodes can react with water and oxygen, but interaction between fullerene derivatives in the active layer and Al electrode is also possible. The use of solar cell geometries with a low work function metallic cathode is likely to have significant degradation mechanisms and instability linked to the interface with the active layer. On the other side of the solar cell, also the ITO/PEDOT:PSS interface is interested by degradation. This interface is sensitive to air and,

in addition, the hygroscopic nature of PSS allows water absorption that facilitate the etching of ITO. Not only PEDOT:PSS is in part responsible for the presence of water in the device, but Norrman *et al.* observed that particles due do PSS oxidation are formed from this layer in Al/C₆₀/C₁₂-PPV/PEDOT:PSS/ITO.[103] It is clear that from the chemical point of view, obtain an air stable solar cell is more than challenging. The loss in the device efficiency with time is to be attributed also to physical degradation, in the first place, the physical instability of the active layer morphology. Once formed, the bulk heterojunction nanostructure is not static. It has been shown that small molecules such as PCBM and even polymers e.g. P3HT can have some freedom to diffuse within the layer or recrystallize over time. These phenomena are facilitated at elevated temperature. An example of this phenomenon has already been shown in this work (**Figure 25**).

The role of light in degradation can be described in three points: it can accelerate the intrinsic degradation processes by increasing the temperature in the device; it causes the photo-degradation of the organic semiconductors and accelerates the diffusion of oxygen and water in the BHJ.[104–107]

Light-induced degradation in organic solar cell can usually be recovered in dark[108] and this recovery is temperature independent.[109] In a recent study has been showed that there is no clear correlation between the intensity of the incident light and the degradation itself.[110]

Different approaches have been proposed to improve the stability of the devices. A general approach is to use metal oxides as buffer layers, and silver as the top anode. To reduce the amounts of oxygen and water in the devices, generally, encapsulation glasses or membranes are used.

1.2.5 Materials for the active layer

As described above, the photoactive layer in an organic solar cell is composed by an electron donating material (donor material, D) and an electron accepting material (acceptor material, A). The presence of these two materials ensure the exciton formation upon light absorption, the charge dissociation (at the D/A interface), and the electron/hole transport to the respective electrodes. Tremendous efforts have gone into the design, synthesis and characterization of the active layer materials in order to improve device performances. Different studies have been conducted and general guidelines on the choice and on the design of donor and acceptor

materials have been published in the past years. Scharber and co-workers, for example, have described the design rules for donor materials in BHJ solar cells.[94] The Scharber diagram (Figure 30), which permits to estimate the PCE of a devices by using the electronic properties of the donor, is nowadays a valid instrument to base donor material design development.

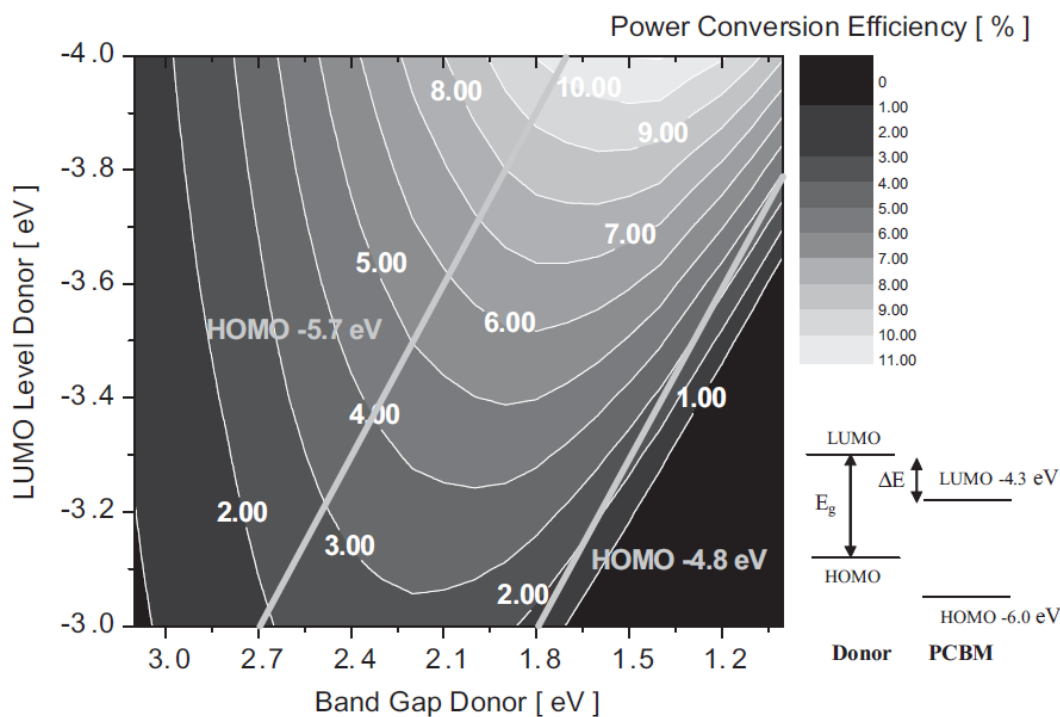


Figure 30: Contour plot showing the calculated energy-conversion efficiency (contour lines and colors) versus the bandgap and the LUMO level of the donor polymer. Straight lines starting at 2.7 eV and 1.8 eV indicate HOMO levels of -5.7 eV and -4.8 eV, respectively. A schematic energy diagram of a donor PCBM system with the bandgap energy (E_g) and the energy difference (ΔE) are also shown.

In particular, this model suggests that the energy-conversion efficiency of a bulk-heterojunction solar cell should be much more sensitive to changes of the donor LUMO level compared to variations of the donor bandgap. According to Scharber's model, for energy conversion efficiencies exceeding 10 %, the donor polymer must have a bandgap < 1.74 eV and a LUMO level < -3.92 eV. In the case of acceptor materials, they have a variety of design requirements that are application specific. For application in OPV, it is necessary that the acceptor material is compatible with the donor and with the manufacturing process. With this in mind, general guidelines for n-type materials have been found in: (i) good solubility and film-forming properties; (ii) strong and broad bandwidth absorption; (iii) high electron mobility; (iv) suitable

HOMO/LUMO energy levels relative to the p-type electron donor to guarantee photo-induced electron transfer.[111]

In the next paragraphs a short overview on the main classes of the developed materials is given.

1.2.5.1 Donor material

As mentioned above, the active layer materials have to fulfil strict requirements in order to obtain a good charge separation and extraction. Regarding the donor polymers for instance, when blended with PCBM, they need to fulfil the requirements of a HOMO energy level lower than -5.20 eV and a bandgap between 1.30 and 1.90 eV.[112] Over the last decades, a great number of donor materials has been designed, synthesized and studied. Both small molecules and polymers have been proposed and used as donor materials in OPV.

The main advantages held by small molecules are their well-defined molecular structures, which permit high reproducibility, and the possibility of a vapour-deposition process. This type of process gives highly controlled and well-defined layers of high purity. Among the different classes of conjugated small molecules proposed for OPV applications, there are (**Figure 31**) oligothiophenes(a),[113] triphenylamines(b),[114] EDOT-based systems (c),[115] diketopyrrolopyrroles (d),[116] dicyanopyrane derivatives (e),[117] merocyanines (f),[118] oligoacenes (g),[119] squaraines (h), as well as indigos (i).[120]

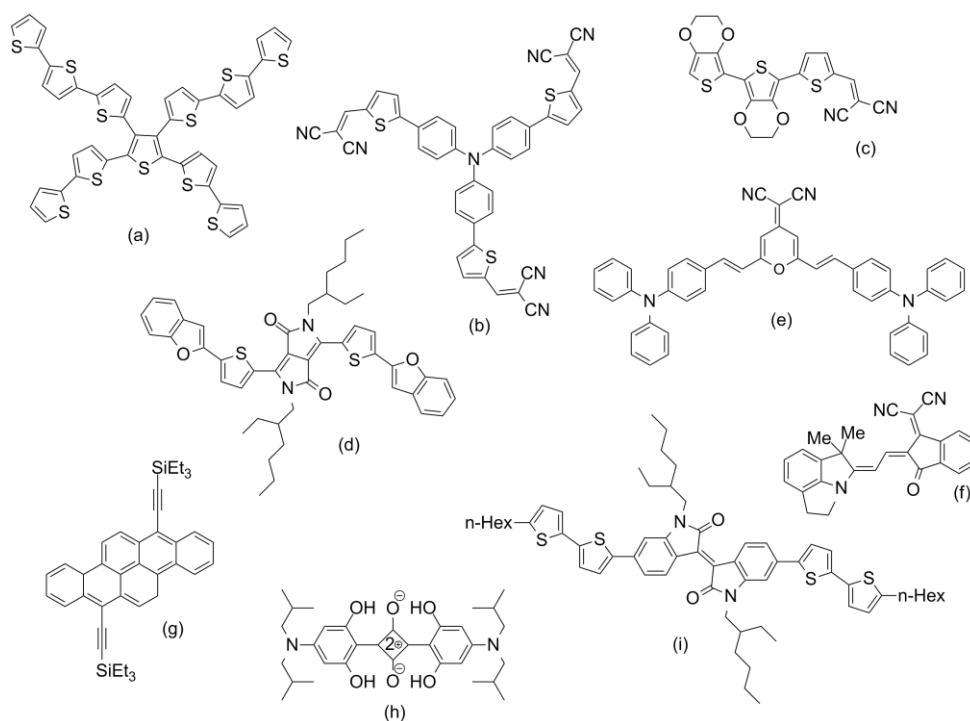


Figure 31: Examples of small molecules used as donors in OPVs - (a) oligothiophenes, (b) triphenylamines, (c) EDOT-based systems, (d) diketopyrrolopyrroles, (e) dicyanopyrane derivatives, (f) merocyanines, (g) oligoacenes, (h) squaraines, and (i) indigos.

Conjugated polymers have gained great importance in many organic-based electronic devices such as OLEDs, solar cells, sensors, transistors, or electrochromic devices. The reason of the increasing interest for these type of material is found in their mechanical characteristics, in their low cost of production, in the possibility of tuning the electronic levels via structural modifications to obtain desired properties and in the processibility of the material.

When designing a polymer for OPV applications, it has to be taken into account that the choice of the monomers determines the HOMO and the LUMO levels of the polymer, and thus its bandgap and optical properties. It also has to be taken into account that appropriate structural changes on a defined monomer can lead to the control of the opto-electronic characteristics of the polymer. It is not surprising, though, the wide variety of polymers proposed for organic electronic devices applications. A first breakthrough in the field of conjugated polymer has been the synthesis of high conductive polyacetylene, first reported by Alan J. Heeger, Alan MacDiarmid and Hideki Shirakawa in 1977.[121] This research, for which the authors have been awarded the Nobel Prize in Chemistry encouraged the rapid growth of the field. Other important families of conducting polymers are (**Figure 32**) the poly(*p*-phenylenvinylene)s (PPV)s and polythiophenes (PT)s and

their alkyl- and alkoxy-derivatives. Poly (*p*-phenylenevinylene) (PPV) has been the first polymer used in polymer based LEDs[122] and the PPV derivatives are still amongst the most studied conjugated polymers for OLED and OPV applications. PPVs have good conductive character and good photoluminescence properties. Moreover, small modifications of the structure have proved to tune electronic properties of the polymers. The HOMO and LUMO levels of the unsubstituted PPV, for instance, were reported at -5.1 and -2.7 eV, respectively, with a band gap of 2.4 eV. When two alkoxy groups on the phenylene ring are introduced, the bandgap is reduced by 0.2 eV.[123] Also, the incorporation of substituents on the vinylene-bridge allows to tune the energy levels of PPV derivatives. For instance, PPV derivatives containing a cyano group attached to the double bond have been designed and synthesized (CN-PPV) following this strategy. For years, PPV-based derivatives (MEH-PPV or MDMO-PPV) have been used in polymer solar cells blends with C₆₀ or PCBM.[124,125] Unfortunately the low conductivities of these derivatives limits their application in devices.[126,127]

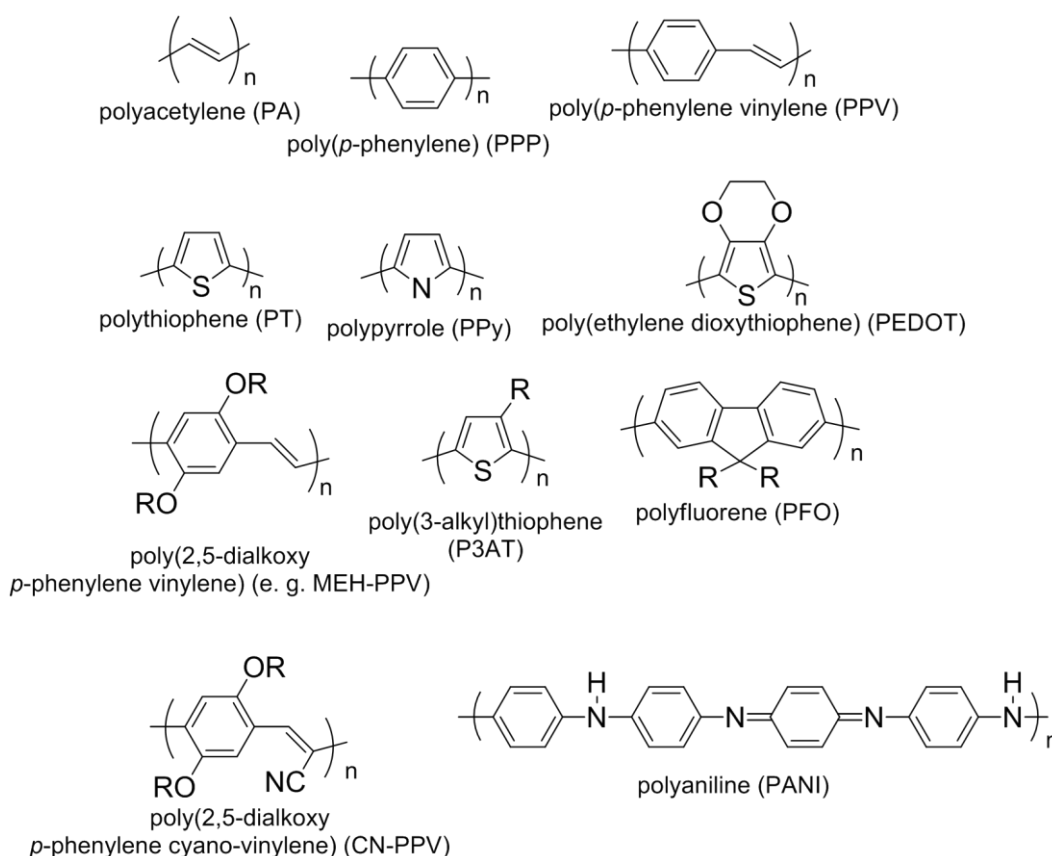


Figure 32: First and Second Generation semiconducting polymers.

Polythiophenes (PT) are one of the major families of conjugated polymers for applications in chemical sensors, light emitting diodes, field effect transistors and organic solar cells. Compared to PPVs, it presents improved electronic and electrical properties, as well as thermal and chemical stabilities. Among the different polythiophene, poly(3-hexylthiophene) (P3HT) is the most used in OPV cells. While for systems such as MDMO-PPV:PCBM, the efficiency is limited to around 3%, the efficiency of a P3HT:PCBM solar cell is typically 4-5%.

The efficiency of the P3HT-based devices are limited by the relatively large bandgap (1.9 eV) of this polymer. The absorption spectrum of P3HT allows a good light harvesting only in a small range of the solar emission spectrum as shown in **Figure 33** where the absorption spectrum of P3HT (purple) is compared with the emission spectrum of the sun (black). The green line in the **Figure 33** is representative of the absorption spectra of a different class of donor material which will be now discussed.

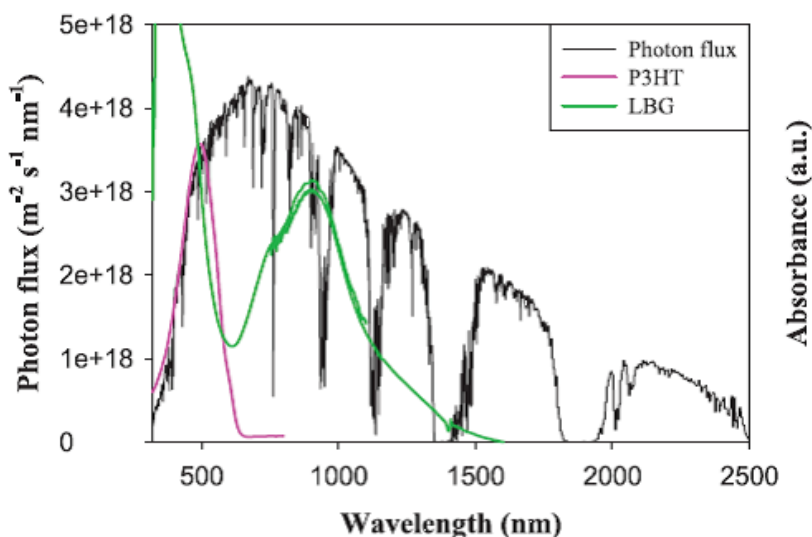


Figure 33: Absorption Spectra of P3HT (purple), a (green) LBG and (black) the Solar Emission Spectra at AM 1.5 G.

With the aim to better match the absorption spectra of the polymers with the solar emission spectrum, and thus increase the light harvesting by the active layer; *low band-gap* (LBG) polymers have been developed in the past few years.[127–131] Among the low band-gap polymers investigated in OPV devices, there are polythiophenes, polybenzodithiazoles (BT), poly-(pyrrolo[3,4-c]pyrrole-1,4-dione)s, which is also named poly(diketopyrrolopyrrole)s (DPP), and poly(benzo[1,2-b:4,5-b']dithiophene)s (BDT). To obtain LBG materials from the

already known conducting polymers, different strategies have been employed. P3HT has been modified by Li *et al.* by introducing a conjugated lateral chain at the 3-position of the thiophene. This modification induced a broader absorption spectrum for the polymer. Other polythiophene derivatives have been tested. A different strategy is the use of push-pull copolymers. In these type of polymers an electron-rich comonomer (fluorene, carbazole, dibenzosilole, benzodithiophene, etc.) is coupled with a second electron-deficient comonomer (benzodithiazole, diketopyrrolopyrrole, etc.). The application of this new class of conjugated polymers into devices has led to remarkable increase in the devices efficiency. Efficiency of 10.3% and 11.5% have been reported for single junction and tandem devices respectively.[132] Some example of LBG polymers are reported in **Figure 34**.

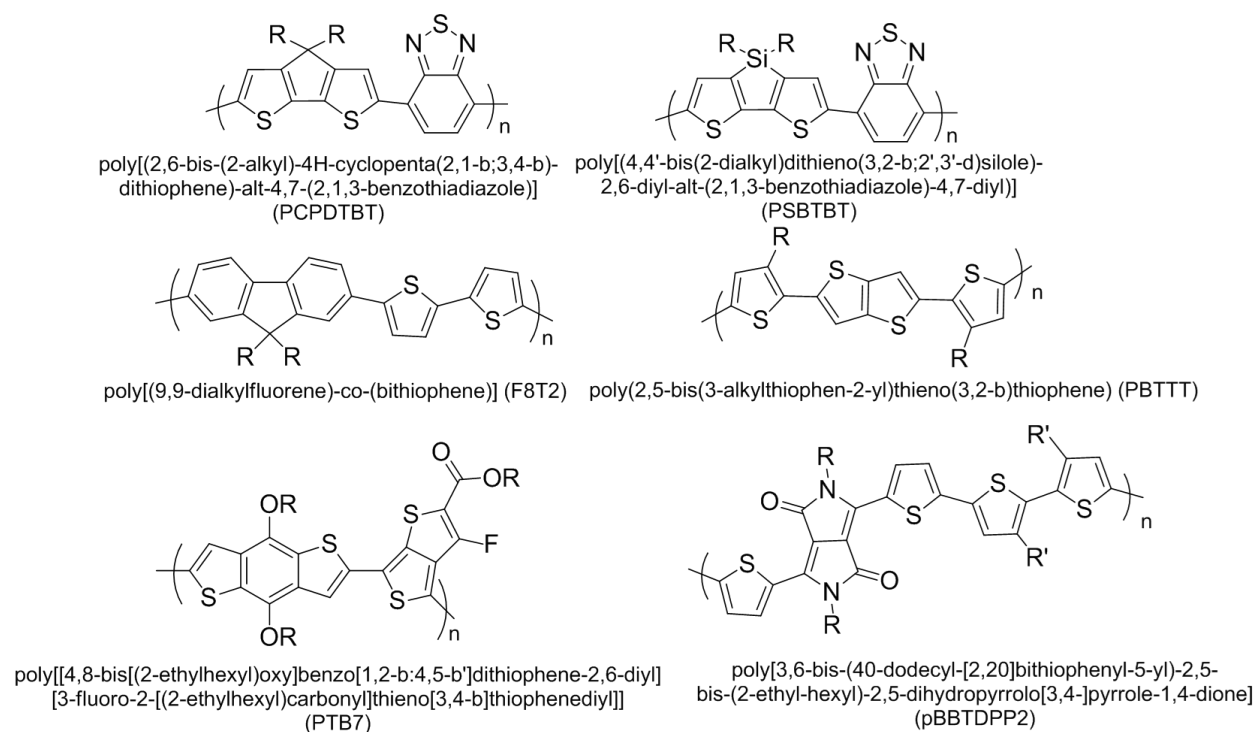


Figure 34: Low band-gap semiconducting polymers. R=alkyl chain.[133,134]

1.2.5.2 Acceptor materials

Compared to the enormous research focused on the donor-type material for OPV, the studies on the design of acceptor materials are few. n-Type materials have design requirements that are application specific (OLEDs, OPVs or OFET devices do not necessary lead to the same requirements on the electron-transport material). Nonetheless, some of the desirable characteristics such as high mobility, material stability, ease of synthesis and processibility, can

apply across the spectrum of electron-transport materials. A brief discussion on some concepts that helps to design electron-transport materials for organic electronic devices is found in the work by Anthony *et al.* In their work, the authors present three concepts that are crucial for n-type material design: i) electron-transport material should be electron deficient; ii) π -Stacking leads to higher mobility; iii) tailoring the molecules in the right way can make them electron deficient to facilitate injection, stability, and in some cases hole blocking.[135]

Fullerene derivatives have a particular relevance among the different n-type materials. The most used acceptor materials for organic solar cells, indeed, are the fullerene derivatives and in particular phenyl-C₆₁-butyric acid methyl ester (PCBM), which is soluble in most organic solvents. Fullerene derivatives as acceptor in OPV devices will be discussed in more detail in section 1.3.1. While most of the applications are historically covered by fullerene derivatives, other small molecules have been developed to fulfill the role of acceptor in organic electronic devices. Some examples are shown in **Figure 35** and include siloles derivatives, acenes, perylene diimide, naphthalene derivatives, and diketopyrrolopyrrole derivatives.[136–142] Also metallophthalocyanines, which are known as p-type materials, have been studied as acceptor material in OPV.[142]

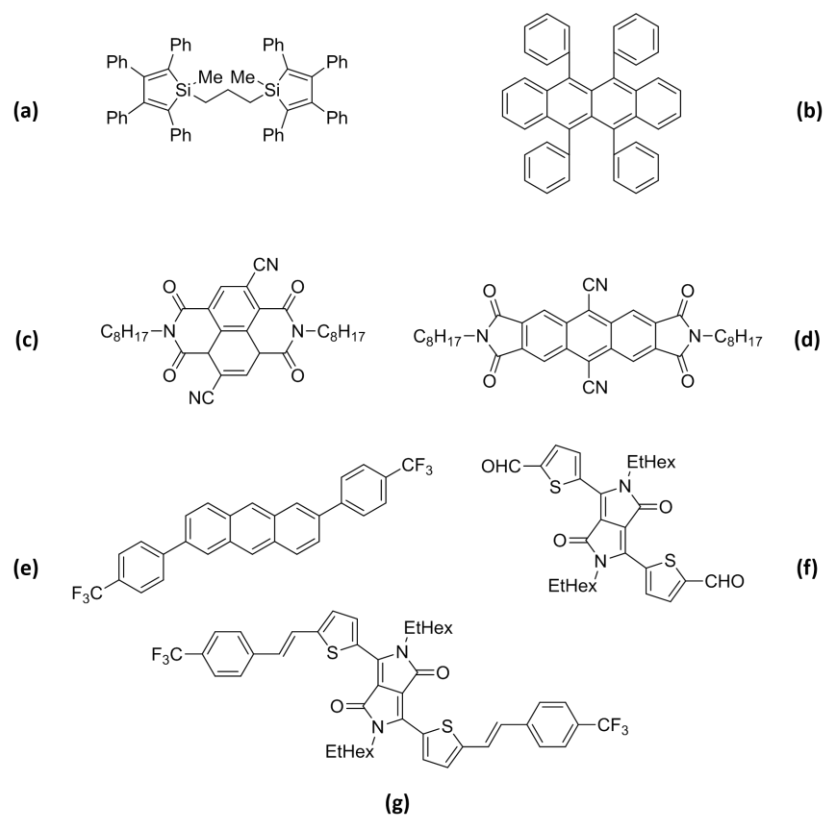


Figure 35: Examples of n-type molecules used as acceptors in OPV and OFET applications; (a) acenes, (b-e) rylene diimides, and (f, g) diketopyrrolopyrroles.

Polymers have also been studied as acceptors. The interest in polymers is in the possibility of having low cost materials which are potentially more stable than fullerene derivatives and in general can have a broader absorption spectra in the visible-near infrared region. Moreover, as for the case of the donor materials, one of the main advantages of the polymers is their easy tunability. Polymer donor – polymer acceptor solar cells holds the promises of great modularity of the components as well as an improved morphological stability with respect to the polymer/fullerene systems.[143] In the past decade, however, they had demonstrated a lower efficiency with only few reports on systems with PCE over 2%.[144–147] In the last years, a renewed attention has been given to the all-polymer solar cells technology[148–150] following the announcement by Polyera of a polymer-polymer solar cell achieving a PCE of 6.47%.[151] More recently Hwang, Courtright, Ferreira, Tolbert and Jenekhe have reported a high-performance all-polymer solar cells with record 7.7% PCE.[152] The device uses a polymer-polymer active layer composed of a high-mobility crystalline naphthalene diimide (NDI)-

selenophene copolymer acceptor and a small band gap benzodithiophene-thieno[3,4-b]thiophene copolymer donor (PNDIS-HD:PBDTT-FTTE). The molecular structures of acceptor polymer and donor polymer as well as their energy level diagrams and their optical absorption spectra are shown in **Figure 36**.

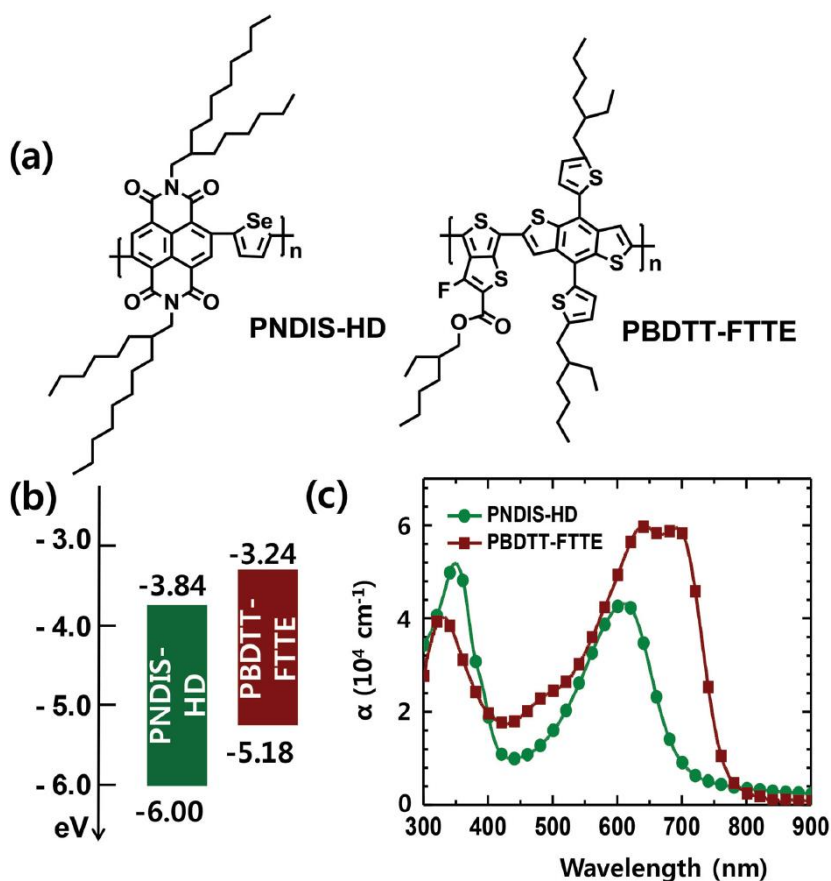


Figure 36: a) Molecular structures of acceptor polymer (PNDIS-HD) and donor polymer (PBDTT-FTTE). b) HOMO/LUMO energy levels of the acceptor and donor polymers. c) Optical absorption spectra of the acceptor and donor polymers

The chemical structures of selected acceptor polymers used in all-polymer blends for BHJ solar cells are reported in **Figure 37**.

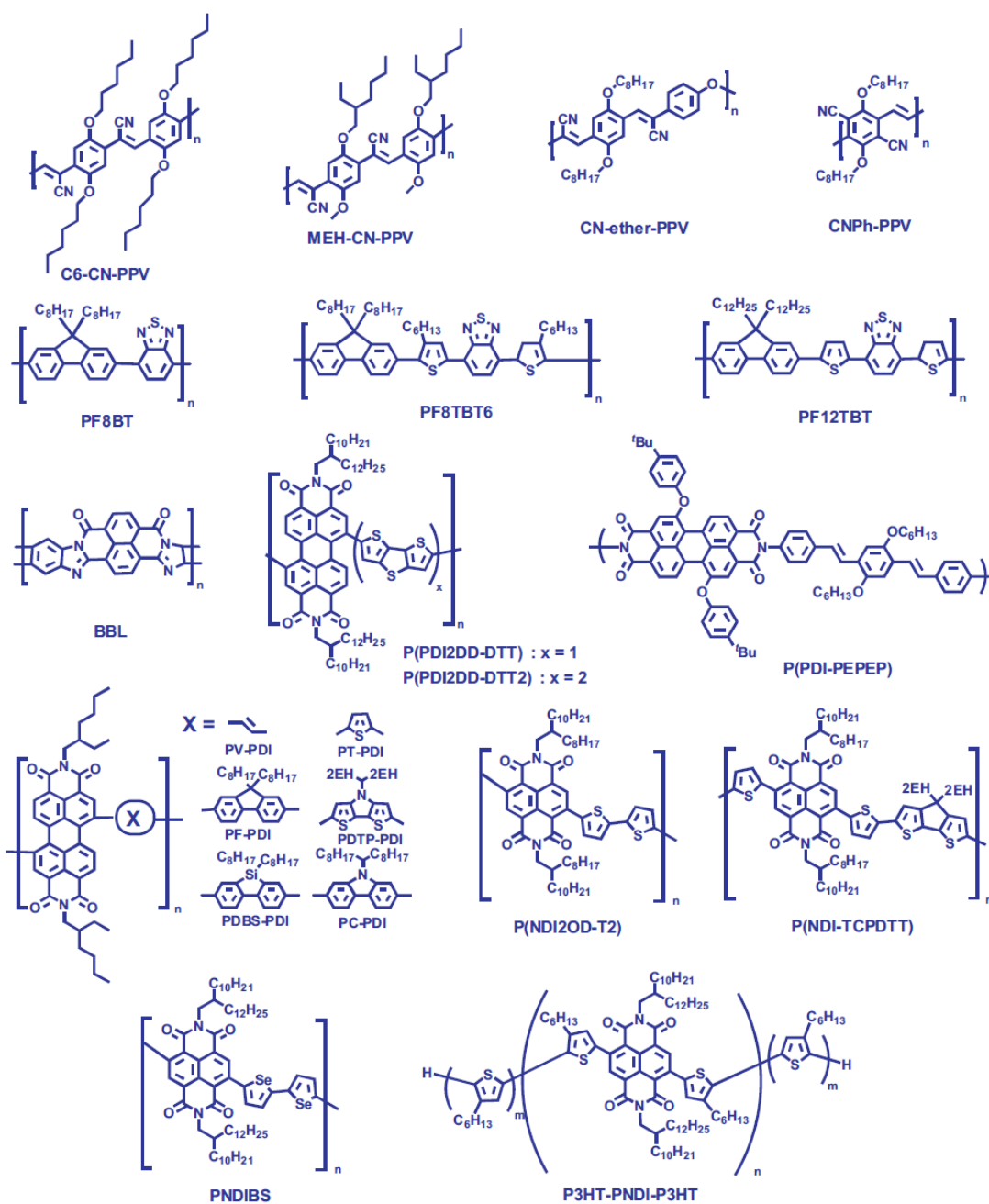


Figure 37: Chemical structure of selected acceptor polymers used in all-polymer blends for BHJ solar cells. Image reproduced from ref.153.

1.2.6 Material Characterizations

Together with their chemical characterization, obtained for instance by NMR spectroscopy, IR spectroscopy, SEC, UV-vis spectroscopy, it is important to investigate and understand the electronic properties of the materials used in organic photovoltaics as the good match between the energy levels of the single components are crucial to the efficiency of the whole device. In this section, the photoemission spectroscopy techniques UPS and XPS are introduced. The two techniques are used to evaluate the energy levels structure of the materials. The section ended with the description of the Integer Charge Transfer (ICT) model, which has been used to discuss the spectroscopic data in this work.

1.2.6.1 Photoemission spectroscopy, XPS and UPS

Understanding the energy level-alignment at the interfaces involving semiconducting and/or conducting molecules and polymers is crucial for all organic electronic technologies. The performance of the devices depends, not only on the properties of the organic material, but also on the properties of their interfaces.

A valuable tool to investigate these properties is photoemission (PES). Both X-ray photoelectron spectroscopy (XPS) and ultraviolet photoelectron spectroscopy (UPS) are extremely surface sensitive techniques which are widely used for studying the bulk and the surface chemical and electronic structure of condensed matter. XPS is used to study in a qualitative and semi-quantitative way the chemical composition of the near surface region of a solid sample. Moreover, the chemical state of the considered element can be investigated. UPS is typically used to study the electronic structure of the valence band and the energy level alignment at interfaces.

1.2.6.2 Working principle

When a sample is irradiated with high energy photons, it is possible to remove an electron from a bound state of the material. In a first approximation, this photoemission process can be regarded as an elastic scattering process where the energy of the exciting photon is transferred completely to the excited electron. If the energy of the incident photon, $h\nu$, is sufficient to overcome the binding energy of the electron E_B and the work function (ϕ) of the sample, the

electron can leave the sample with a certain kinetic energy E_k . The schematic representation of the photoemission process is shown in **Figure 38**.

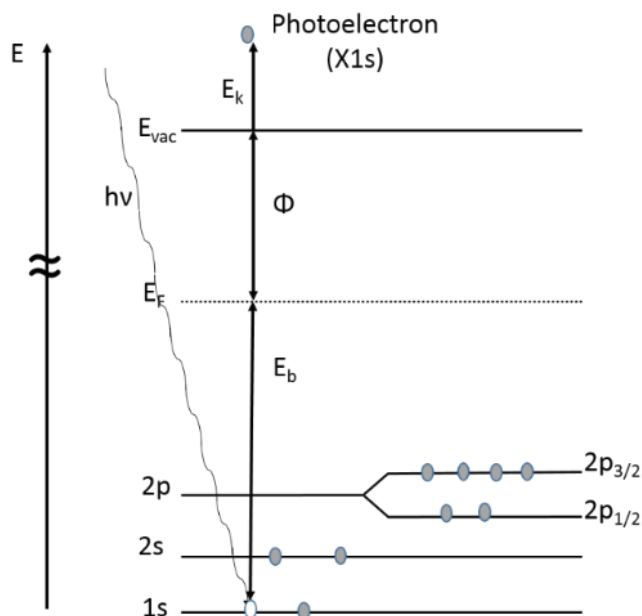


Figure 38: Schematic representation of photoemission process. The incident photon excites an electron from the 1s core shell to an unbound state above the vacuum level (E_{vac}).

The photoelectron spectrum is obtained by detecting the emitted electrons according to their kinetic energy and counting their intensity. The basic components of a photoelectron spectrometer are the photon source, the sample holder, the electron energy analyzer and the detector. The entire system works in ultrahigh vacuum (UHV) conditions. These conditions are required first because the emitted photoelectrons could easily interact with molecules of the atmosphere. Thus, if the ambient pressure increases the mean free path of the electron is drastically reduced. UHV regime ensures that a sufficient number of electrons reaches the analyser and can be detected. Moreover, as the PES techniques are high surface sensitive, possible contamination needs to be avoided in order to analyse the properties of the clean surface.

The binding energy of the electrons in photoemission can be calculated according (**Equation 6**).

$$E_B = h\nu - E_K - \phi$$

(Equation 6)

1.2.6.3 Information from data

XPS data are usually shown on a binding energy scale. Due to the higher $h\nu$ (> 100 eV) compared to UPS, electrons from core levels determine the spectrum. The information obtained from the core level peaks can help to elucidate electronic and chemical properties of the sample. For instance, the binding energies are in general characteristic for the different atoms. From the binding energy and the relative intensities it is possible to identify the atomic composition at the surface of the sample and the relative concentration of the respective element. Due to the spin-orbit coupling, the line shape of core level spectra is characteristic for the type of orbital involved in the photoemission process. As example, a photoemission process involving p and d orbitals results in doublet with characteristic intensity ratio of 2:1 for $p_{3/2}$ and $p_{1/2}$ and 3:2 for $d_{5/2}$ and $d_{3/2}$, respectively. For s -orbitals no splitting is observed. XPS is also an important tool to determine the chemical state and oxidation state of the species, in particular at the surface or interface. Although so-called final state have to be considered in photoemission,[154,155] initial state effects such as the Madelung potential and the ground state valence atomic charge determine the detailed binding energy. As a consequence, distinct shifts of the peak position (chemical shifts) can be observed as a function of the electron density at the considered site. This enables the analysis of the chemical state; typical binding energies of elements in chemical groups are even tabulated.

The interpretation of the XPS spectra is not always an easy task. In some spectra also signals of so-called shake-up and shake-off satellites can be observed on the high binding energy site. These features can sometimes coincide with components with high chemical shifts, but their origin is completely different. The shake-up contribution originates from the excitation of valence electrons into excited bound states in the time scale of the photoemission process. In the shake-off process a valence electron is excited into an unbound state above the vacuum level.

UPS analysis can provide more information about the valence electronic structure of a material. In a first approximation, in UPS the density of states (more exactly the "Joint Density of States") is mapped. In general the electrons with highest kinetics energy are those originated from the highest occupied states of the analyzed material (Fermi level for the metals, valence band maximum, VBM, for semiconductor materials and highest occupied molecular orbital, HOMO, for organic semiconductors). At a kinetic energy of 0 eV the intensity of the spectra drops down as the (secondary) electrons have no energy left to overcome the work function (φ) of the sample (the work function of a material is the minimum amount of energy necessary to remove an

electron from the material and excite it above the vacuum level). This point corresponds to the maximum binding energy measured and depends on the incident photon energy. From the UPS spectra, the change in the work function, Δ , that can e.g. occur upon partial coverage of the substrate surface can be measured. To obtain these values from the photoemission spectra, the energy of the incident photon ($h\nu$) must be known. The work function of the material is then obtained by measuring the energy of the secondary-electron cutoff of the photoemission spectrum and subtracting this value from the exciting photon energy (*Equation 7*).

$$\phi = h\nu - E_{cutoff}$$

(Equation 7)

In general, for UPS experiments the photon sources used in this work are HeI ($h\nu = 21.2 \text{ eV}$) or HeII radiation ($h\nu = 40.8 \text{ eV}$). The physical interpretation of an UPS spectrum is showed in *Figure 39*.

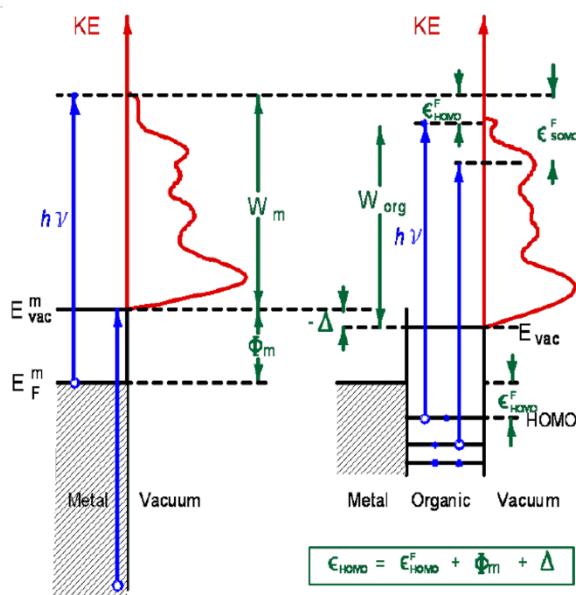


Figure 39: Energy relationship scheme for UPS spectra (left) for Au and (right) for an organic layer deposited on the metal substrate.[100]

1.2.6.4 Integer charge-transfer model

When two materials are brought into contact, the interface is formed depending on the nature of the materials. In order to describe the different interface phenomena, various models have been developed. One approach is the classification of interfaces by the strength of the interactions. It has to be noticed that the strength of the interactions depends both on the materials and on the preparation of the interface. A classification of the different type of interfaces have been given by Fahlman and co-workers.[156]

Although several models may describe the situation at interfaces,[157–161] we will briefly discuss here the integer charge-transfer model (ICT), first introduced by the group of W. R. Salaneck. The ICT model is in particular well suited for interfaces with weak interaction and applied in this work. It was shown that interfaces prepared in ambient conditions, semiconducting organic/organic interfaces, as well as interfaces formed with substrates that are passivated by oxides or residual hydrocarbons can be well described with this model. These interfaces are characterized by a negligible hybridization of π -electronic molecular orbitals and substrate wave functions. The electron transfer across the interface can occur via tunneling. This process implies a transfer of an integer amount of charge into a well-defined charged state of the organic material which becomes energetically allowed. An integer charge transfer can be expected, if the work function of a substrate is higher than the HOMO (electron from HOMO to substrate) or lower than LUMO (electron from substrate to LUMO). The new allowed states can be defined as follow:

- E_{ICT+} (energy of a positive integer charge-transfer state): is the energy required to take away one electron from the organic material to obtain a fully relaxed state.
- E_{ICT-} (energy of a negative integer charge-transfer state): is the energy gained when one electron is added to the organic material producing a fully relaxed state.[156]

Note that both electronic and geometrical relaxation are included in the E_{ICT+} and E_{ICT-} , as well as effects from inter- and intra-molecular order at the interface.[162] Thus, the $ICT+$ and $ICT-$ states are separated from the HOMO and LUMO of the neutral molecule/polymer, typical values are between 0.5 and 0.8 eV.[163]

These two energy levels can be determined by the measurement of the work function of a material on substrates with different work function. When the range of the substrate's work

functions is wide enough for a specific material to be found in its ICT- status from one side and in its ICT+ status on the other, a “Mark of Zorro”-type plot is observed (**Figure 40**)

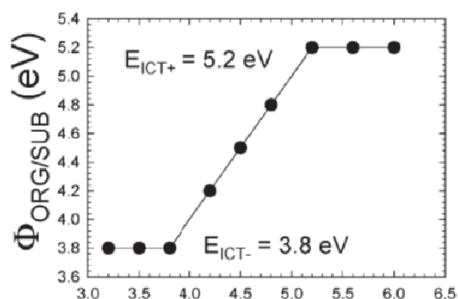


Figure 40: General $\phi_{\text{ORG/SUB}}$ versus ϕ_{SUB} dependence predicted by the ICT model. Reproduced from ref. [156]

A scheme of the energetic level alignments which explains this shape is reported in **Figure 41**. The processes shown in the figure are explained here below.

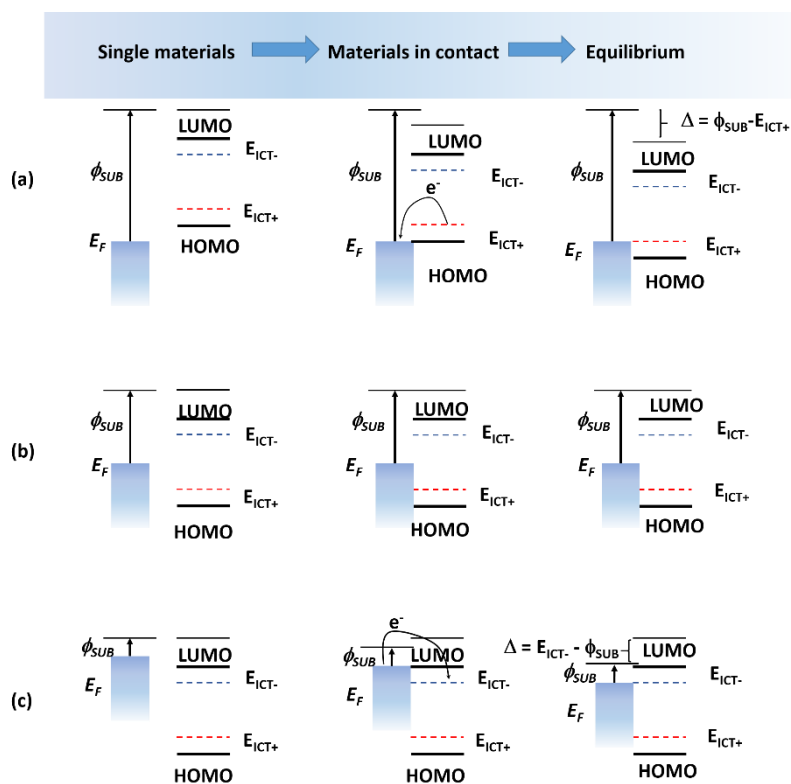


Figure 41: Schematic illustration of the evolution of the energy-level alignment when a π -conjugated organic molecule or polymer is physisorbed on a substrate surface when a) $\phi_{\text{SUB}} > E_{\text{ICT}^+}$: Fermi-level pinning to a positive integer charge-transfer state, b) $E_{\text{ICT}^-} < \phi_{\text{SUB}} < E_{\text{ICT}^+}$: vacuum level alignment, and c) $\phi_{\text{SUB}} < E_{\text{ICT}^-}$: Fermi-level pinning to a negative integer charge-transfer state. The charge-transfer-induced shift in vacuum level, Δ , is shown where applicable.

According to this model, when a substrate is put in contact with the organic material, three different regimes for the energy level alignment are observed for: (i) $\Phi_{\text{SUB}} > E_{\text{ICT}^+}$; (ii) $E_{\text{ICT}^-} < \Phi_{\text{SUB}} < E_{\text{ICT}^+}$; (iii) $\Phi_{\text{SUB}} < E_{\text{ICT}^-}$.

In the first case (i), and in the third (iii) case, a pinning of the Fermi level to the ICT levels (ICT^+ for (i) and, ICT^- for (iii)) is established while the vacuum level alignment regime is found for (ii). In fact, when organic material and substrate are put in contact, depending on the relative values of Φ_{SUB} and ICT levels, charge transfer from one material to the other can take place at the interface. If $\Phi_{\text{SUB}} > E_{\text{ICT}^+}$, the contact between the two materials induces a flow of electrons from the organic one to the substrate. On the contrary, when $\Phi_{\text{SUB}} < E_{\text{ICT}^-}$, the opposite situation is established and a spontaneous flow of electrons from the substrate to the organic material takes place until equilibrium is reached. The continuous charge transfer from one site to the other at the interface induces the formation of a dipole that results in a down-shift (in the first case) or an up-shift (in the second case) of the vacuum level. In both cases, when the equilibrium is reached, no charges flow is present anymore. If the initial condition was $\Phi_{\text{SUB}} > E_{\text{ICT}^+}$ ($\Phi_{\text{SUB}} < E_{\text{ICT}^-}$), then at equilibrium it is $\Delta = \Phi_{\text{SUB}} - E_{\text{ICT}^+}$ ($\Delta = E_{\text{ICT}^-} - \Phi_{\text{SUB}}$). It is then clear that the resulting work function for the organic material on the substrate ($\Phi_{\text{ORG/SUB}}$) is equal to E_{ICT^+} and E_{ICT^-} respectively. Moreover, if the initial conditions $\Phi_{\text{SUB}} > E_{\text{ICT}^+}$ or $\Phi_{\text{SUB}} < E_{\text{ICT}^-}$ are fulfilled, a variation of Φ_{SUB} will not affect the measured value for $\Phi_{\text{ORG/SUB}}$. In other words, a measure of this work function in these two cases allows the mapping of the corresponding ICT level of the organic compound. In the case (ii), when $E_{\text{ICT}^-} < \Phi_{\text{SUB}} < E_{\text{ICT}^+}$, no electron flow occurs neither from the substrate to the organic material, nor in the opposite direction and thus, no vacuum level offset is observed. Therefore, the resulting $\Phi_{\text{ORG/SUB}}$ is not indicative of the position of the ICT levels of the organic compound. This model has been applied to organic-metal interfaces and organic donor-acceptor systems. It is proposed that the position of ICT levels determines the energy level alignment at organic-organic and organic-electrode interfaces. In particular, between the two organic materials (blend) an additional dipole can be formed. The size of the dipole depends on the difference between ICT^+ (donor) and ICT^- (acceptor).[164,165] With this in mind, it is important to determine the energy of these level for the single component.

Together with their chemical characterization, obtained for instance by NMR spectroscopy, IR spectroscopy, SEC, UV-visible spectroscopy and other common techniques, it is important to investigate and understand the electronic properties of the materials used in organic photovoltaics as the good match between the energy level of the single components are crucial

to the efficiency of the whole device. In this section, the photoemission spectroscopy techniques UPS and XPS are introduced. The two techniques are used to evaluate the energy levels structure of the materials. The section ended with the description of the Integer Charge Transfer (ICT) model, which has been used to discuss the spectroscopic data in this work.

1.3 The role of fullerenes in organic photovoltaics

Fullerene and fullerene derivatives play a very important roles in the field of organic photovoltaic. In the following sections, the different uses of fullerene derivatives in devices are briefly presented.

1.3.1 Fullerene acceptors

Fullerene derivatives are good acceptor materials for OPV due to their high electron affinity and good electron mobility. They also can provide favourable nanoscale morphology necessary for charge separation and charge diffusion in the bulk. A great part of OPV technology is based on devices which use fullerene derivatives as acceptor. This is somehow surprising as most of the non-fullerene small molecules used as acceptor have stronger light absorption in the visible region respect to fullerene derivatives and also, one would expect that the use of planar or semi planar molecules is preferable to achieve good electron transport. In the bulk heterojunction solar cells, the most commonly used C_{60} soluble derivative is the Phenyl- C_{61} -butyric acid methyl ester PCBM followed by the C_{70} analogous PC₇₀BM. The structure and the synthetic route for PCBM is showed in **Figure 42**.

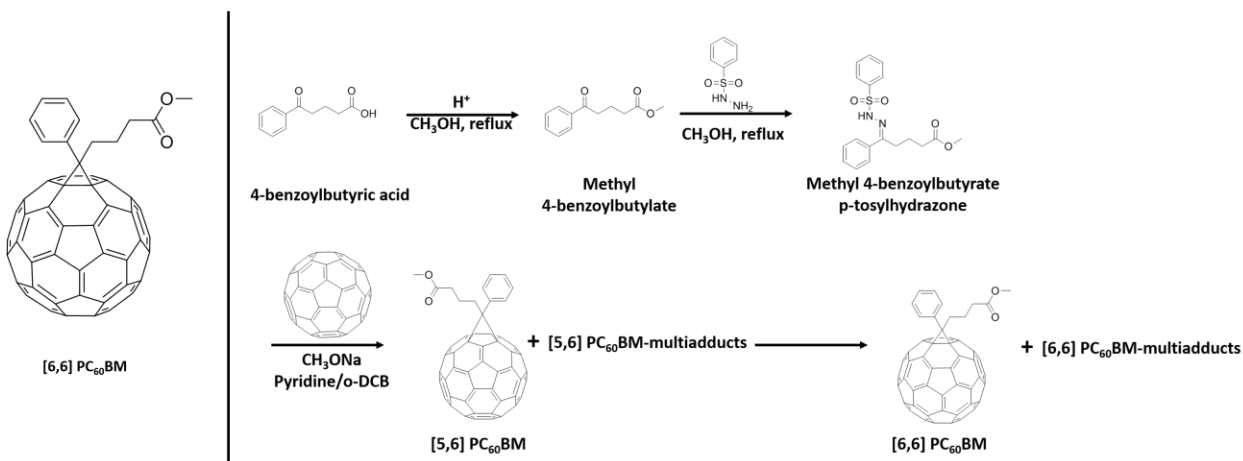


Figure 42: (a) Structure and (b) synthesis of 6,6-phenyl- C_{60} -butyric acid methyl ester (PCBM).

PCBM was first introduced by Wudl *et al.* in 1995 for photo-diode and photo-detector applications[166] and shortly after used as acceptor material in blends with conjugated polymers.[167,168] PCBM has good acceptor properties and good miscibility with conductive polymers. Although it preserves the high electron affinity and good electron mobility (2×10^{-3} and $4,5 \times 10^{-3} \text{ cm}^2 \text{V}^{-1} \text{s}^{-1}$)[169] of its parent C_{60} , it has also a very low light-harvesting ability in the visible region of the light spectrum and therefore it limits the PCE of the devices. The most representative polymer donor/fullerene acceptor system used in PSCs reached a PCE of about 4%. One strategy to avoid this problem consisted in replacing it with PC₇₀BM. This molecule is less symmetric than PCBM and therefore shows a stronger absorption in the visible region as it has more allowed optical transitions. Different fullerene derivatives have been synthesized in order to obtain an up-shifted LUMO energy level respect to PCBM. As a consequence of the direct proportional relationship between the difference $\text{LUMO}_{(\text{acceptor})}$ and $\text{HOMO}_{(\text{donor})}$ and the V_{oc} of the cell, to up-shift the LUMO level of the fullerene derivative results in a higher V_{oc} of the devices when the material is used to replace PCBM in the blend with a determined polymer.[170] For instance, Kooistra *et al.* reported ten new fullerene derivatives for photovoltaic applications[171] showing how the V_{oc} of cells in which the derivatives were blended with MDMO-PPV was modified with a variation in the LUMO level of the acceptor. The structures of the derivatives as well as the obtained results are shown in **Figure 43**.

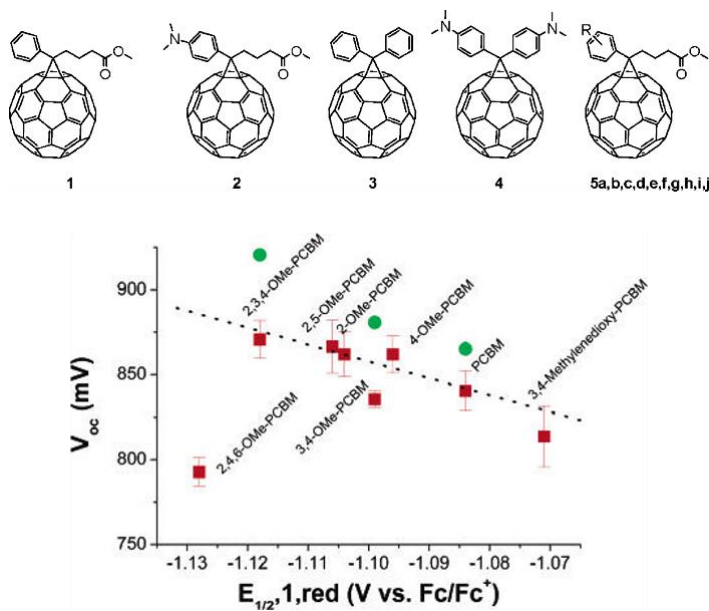


Figure 43: top - Structures of [60]PCBM (1), 4-N,N-dialkylamino[60]-PCBM (2), diphenylmethano[60]fullerene (3), bis-4-N,N-dialkyl-amino-diphenylmethano[60]fullerene (4) and substituted PCBM compounds (5): R) 4-OMe (a), 3,4-OMe (b), 2,3,4-OMe (c), 2-OMe (d), 2,5-OMe (e), 2,4,6-OMe (f), 3,4-methylenedioxy (g), 2-SMe (h), 4-SMe (i), and pentafluoro (j). Bottom - V_{oc} of devices from MDMO-PPV blends vs the first reduction potential, $E_{1/2,1,red}$ (V vs ferrocene/ferrocene⁺) of the PCBM derivatives: squares, from ODCB; circles, from chlorobenzene. The dotted line is to guide the eye for a 1:1 relationship between V_{oc} and $E_{1/2,1,red}$. [19]

The use of functionalized substituents on the C_{60} is not the only direct way to increase the LUMO energy level of the fullerene derivatives respect to PCBM. A second strategy is to have bis- or multi- adducts on the C_{60} cage. The LUMO energy is raised as a consequence of the saturation of the double bonds on the C_{60} hexagons.[172] A remarkable C_{60} derivative designed with this strategy is the indene- C_{60} -bisadducts (IC₆₀BA), first reported by He *et al.*, which has a LUMO level up-shifted by 0.17 eV respect to the LUMO of PCBM and is more soluble.[173] There are also some examples of endohedral fullerenes used as acceptor in photovoltaic devices. More exhaustive list of fullerene derivatives used as acceptor material in organic solar cells can be found in recent reviews[174–176] and in particular, Mi *et al.* divide the derivatives according to the principle used for their design. The authors divided the synthesized molecules in two groups: the derivatives which have been designed in order to tune the LUMO energy of the acceptor and then to increase the V_{oc} of the cells, and those designed to enhance the devices performances by obtaining a higher J_{sc} or FF. Many efforts have been done to further improve the solubility and to optimize the phase segregation of fullerene derivatives in the bulk. Some examples are given by **PCBB**[177] where the alkyl-chain length of the ester-group is modified, **ThCBM**[178] in which

the phenyl group of PCBM is substituted by a thiophene ring, and the dihydronaphthyl bridge ester C_{60} in which is the methylene bridge to be substituted. Another fullerene used in organic photovoltaic is the C_{70} and its derivative phenyl- C_{71} -butyric acid methyl ester (**PC₇₁BM**)[179]. The C_{70} has an asymmetric structure, with a stronger absorption in the visible region than C_{60} , and it has been used in combination with many conjugated polymers and in particular with low band gap polymers.[180,181]

1.3.2 Fullerene interlayers

To improve the efficiency of a solar cell, an additional n-type interlayer can be used in the device architecture. Many different fullerene-based derivatives have been developed in order to fulfil this role of interlayer between the active layer and the inorganic component of the cell.[182] Those derivatives help improve the efficiency by either enhancing the interfacial charge-transport efficiency or by modifying the work function of cathodes. For instance, C_{60} -SAMs (self assembled monolayers) can be deposited over ZnO or TiO_x layer to act as electron selective and hole blocking layers and this improves the charge transfer from the organic active layer to the oxide. Other C_{60} -derivatives have been used to tune ITO work function or Ag work function and have better energy levels alignment and enhance device performances. Though the C_{60} -based interlayers can be used both for the regular and for the inverted geometry solar cell devices, it has to be taken into account that orthogonal solvent-processed strategies have to be used when incorporating them in normal devices. The use of organic solvents that dissolve also the active layer would lead to a mixing of the two layers with a loss of the desired morphology. Hydrophilic fullerene derivatives which can be dissolved in polar solvent systems can then be used for conventional devices and deposited from solution without destroying the morphology of the active layer.

1.3.3 Fullerene additives

The morphology of the active layer strongly influences the performance of the BHJ type solar cell device and the maintenance in time of the optimal morphology is crucial for the device's lifetime. One of the major problems with fullerene derivatives, and in particular with PCBM, is their tendency to diffuse to the polymer matrix and self-aggregate into larger crystals or clusters under

continuous heating. This behaviour causes, together with other factors, the loss in performance of the cell. In general the desired morphology of the active layer can be achieved by using different methods during the different stages of device fabrication. For instance, employing solvent mixtures to deposit the active layer, adding high boiling solvent additives or post-deposition treatments like solvent vapour or thermal annealing can help to have the right morphology that enables a good balance between charge separation and charge diffusion in the bulk. To stabilize the morphology and improve thermal stability, various strategies have been applied in the years. Many studies are focused on the direct modification of the donor or the acceptor material in order to obtain photocrosslinkable structures[183] or bulky substituents on PCBM. The use of diblock copolymers incorporating both the donor and the acceptor material has also been attempted to freeze the optimum morphology in the bulk. In the last few years, the use of fullerene-based additive in the BHJ has been introduced. Tai *et al.* reported the synthesis of a fullerene end-capped poly(ethylene glycol) which has been used as an additive in a P3HT/PCBM device resulting in the increase of the long-term stability of the cell.[184] Following the same concept, polystyrene-tethered fullerene has been successfully developed to reduce the initial domain size of PCBM as well as their growth over time.[185] A new successful approach to morphology stabilization was introduced by Schroeder *et al.* In their work covalently linked PCBM dimers were added in solution prior the deposition of the active layer.[186] The structure of the dumbbell-shaped dimeric fullerenes developed by the authors is shown in **Figure 44**.

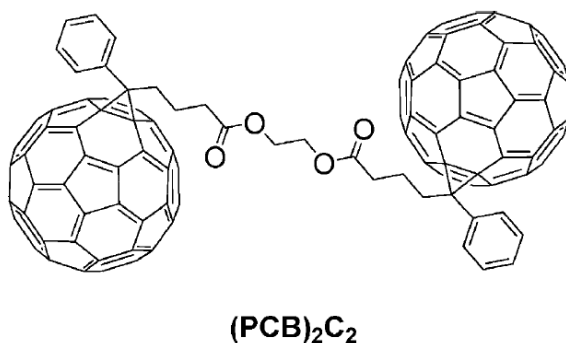


Figure 44: Structure of PCBM dumbbell (PCB)₂C₂. [186]

The loading of 20% of this fullerene dimer in a carbazole-based PCDTBT polymer blended with PCBM system, not only does not influence negatively the PCE of the device, but also can lead to

an enhanced morphological stability that is explained by an effect of frustration of molecular packing of PCBM by the additive.

1.3.4 Fullerene as donor materials

The bipolar nature of fullerene permits them to transport both electrons and holes. Studying a MDMO-PPV:PCBM blend, Melzer et al. discovered a hole mobility of only one order of magnitude lower than the electron mobility in PCBM.[187,188] Due to this characteristic, fullerene derivatives could also be used as donor materials in devices when combined with an acceptor with a LUMO energy in a proper offset. Some work have been published in which fullerene derivatives are used with this new uncommon role. PCBM and ICBA have been recently employed for the first time as donors materials in planar heterojunction all fullerene solar cells[189] showing the possibility of new applications for fullerene derivatives. In the cells C_{70} has been used as n-type component and the resulting PCE for the optimized ICBA/ C_{70} system reaches 0.8% under AM1.5 G (100 mW cm^{-2}) conditions. A FF of 0.27 and a PCE of 0.21% for PCBM/BCN-HH-BCN with conventional BHJ and a FF of 0.29 with a PCE of 0.34% for a PCBM/BCN-HH-BCN BHJ solar cell have been published.[190] The acceptor material (**Figure 45**) has been developed by Ie *et al.* and is a hexyl-substituted bithiophene difunctionalized with dicyanomethylene-substituted cyclopenta[*b*]thiophene units.[191] Also C_{70} has been investigated as p-type donor in PHJ OPV devices in combination with 1,4,5,8,9,11-hexaazatriphenylene hexacarbonitrile (HAT-CN). High FFs of more than 0.70 as well as PCE of up to 2.83% have been achieved with this system.[192] Further examples of C_{60} or metal doped C_{60} with an electron donor role can be found in literature.[193–195]

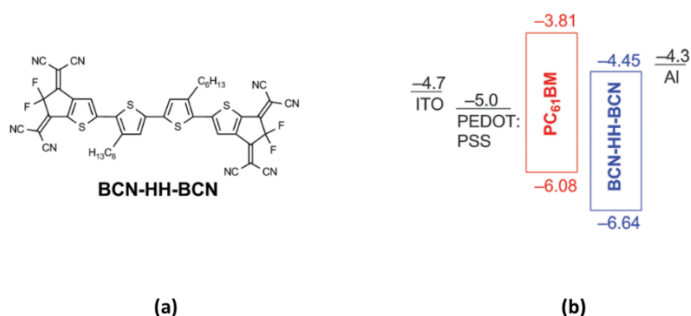


Figure 45: (a) Structure of BCN-HH—BCN molecule; (b) Energy level diagram for BCN-HH-BCN/PCBM.[191]

1.4 Polyfullerenes

Since fullerene and fullerene derivatives are interesting materials for photovoltaic applications due to their good electronic properties, the possibility to merge them with the mechanical properties and facile processibility of polymers has attracted many researchers. In the last years, polymers containing fullerene have been studied for different applications in organic photovoltaic. In this section, general characteristics of polyfullerenes are presented before their application in OPV are reviewed.

1.4.1 Polyfullerenes: introduction

The first example of a polyfullerene was published in 1991 by Olah *et al.* [196] The authors prepared polyarenefullerenes, $C_{60}(H-Ar)_n$, via acid-catalyzed Friedel-Crafts reaction with polystyrene. Since then many polyfullerenes have been prepared and several of them have been used as active materials in electroluminescent,[197–200] non-volatile flash,[201] and photovoltaic devices.

According to their chemical structure, polyfullerenes can be classified into 9 families. To these types of materials, C_{60} -supramolecular polymers can be added.

1.4.1.1 All-carbon polyfullerenes

The all- C_{60} polymers, also named “intrinsic polymers”, are constituted of just C_{60} molecules. In these materials, the C_{60} cages are covalently linked and do not present any substituents. These all-carbon polyfullerenes can be prepared via different strategies. The first example of this class of material was prepared via photopolymerization,[202] but pressure-induced polymerization, electron beam-induced polymerization and plasma-induced polymerization have also been exploited. The polymerization proceeds via $[2+2]$ cycloadditions which involves two 6-6 double bonds of neighbouring C_{60} molecules.[203] The formation of the all carbon C_{60} -polymers is shown in **Figure 46**.

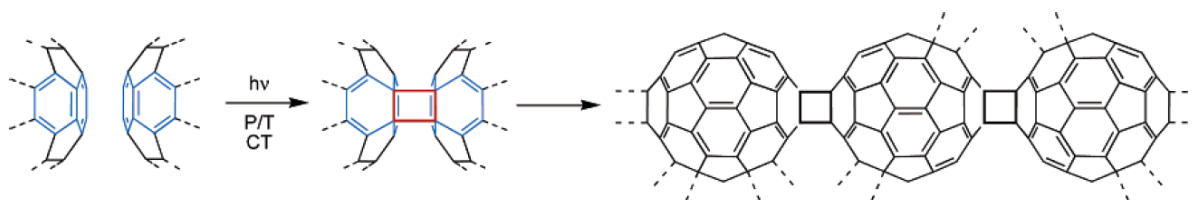


Figure 46: Scheme of the synthesis of all- C_{60} -polymers.[204]

1.4.1.2 Organometallic polyfullerenes

These are compounds contain metals or heteroatoms in their structure. They are considered as a subclass of all-carbon polyfullerenes. The first evidence of the possibility of such a class of polymers was published by Forrò in 1994. He discovered that the fulleride phase AC_{60} , where A is K, Rb or Cs, could undergo $[2+2]$ cycloadditions and give polymers with the alkali metal in the crystal voids. The very first example of an organometallic polymer of C_{60} , however, was published in 1992 by Nagashima and co-workers and it was a Pd-containing polymer.[205] Other polymers were prepared using Pt(II), Rh(II) and Ir(I).

1.4.1.3 Crosslinked polyfullerenes

A large class of polyfullerenes is represented by cross-linked polymers. These polymers have attracted great interest in the last two decades. Polymers such as polystyrene, polyurethane, poly(vinyl ketone) and others have been used to produce cross-linked polymers with C_{60} . The

main interest is the possibility of having a network in which the fullerene is morphologically stable.[206,207] The drawback is the low solubility and poor processibility that these materials generally present. Different strategies to synthesize cross-linked C_{60} -containing polymers include: i) C_{60} and C_{60} derivatives are mixed together with a monomer and left to react randomly; ii) fullerene is first modified to obtain multisubstituted derivative that is then homopolymerized in three-dimensions; iii) C_{60} or its derivatives are allowed to react with a preformed polymer which has been functionalized at the chain ends; iv) the fullerene is left to react with polymers which present pendant reactive moieties. Strategies (i), (iii) and (iv) are summarized in **Figure 47**.

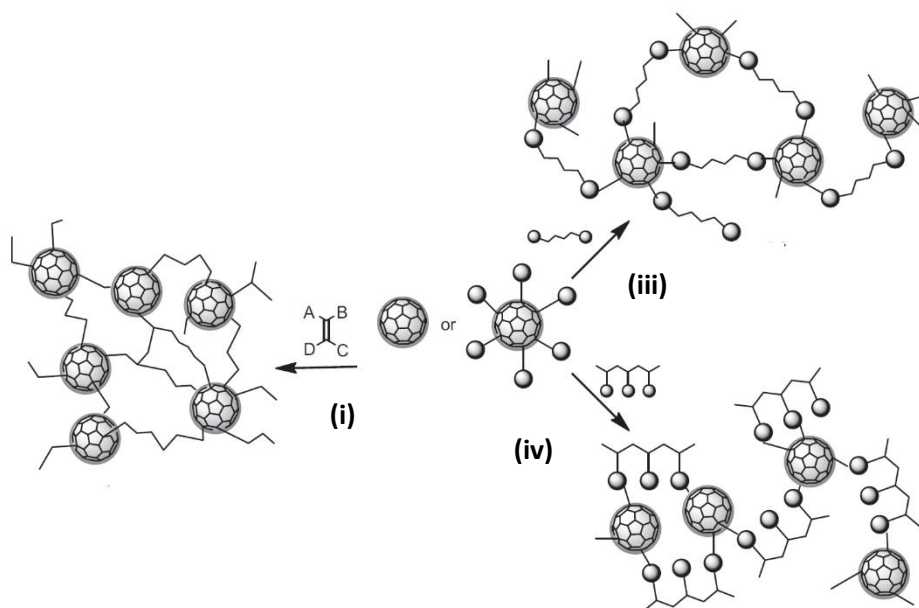


Figure 47: Synthetic pathway leading to cross-linked polyfullerene: (i) C_{60} and C_{60} derivatives are mixed together with a monomer and left to react randomly; iii) C_{60} or its derivatives are allowed to react with a preformed polymer which has been functionalized at the end termini; iv) fullerene is left to react with polymers which present pendant reactive moieties. Image reproduced from ref.208.

1.4.1.4 End-capped polymers

Chain end-capped polyfullerenes are polymers which present one or two C_{60} units at their terminal positions. Two different synthetic strategies are possible. The first is to synthesize the polymer and then incorporate the fullerene. The second, less widely employed, is to grow the polymer on a C_{60} derivative.

Mono and di- C_{60} -end-capped poly(ethylene glycol)s (PEG) were synthesized by Goh and coworkers and showed an extremely interesting capacity to form interpolymer complexes via hydrogen-bonding interactions, when mixed with H-donating polymers.[209] Moreover, films of double C_{60} -end-capped PEG showed good mechanical properties and a very large resistance to elongation.[210] Also four-arm C_{60} -end-capped poly(ethylene oxide)s (PEO) has been prepared,[211] as well as C_{60} -end-capped polystyrene (PS).[212] Fullerene end-capped polystyrenes have been largely investigated. The first example of this class of C_{60} -containing polymers has been synthesized amino-terminated PS; other examples have been prepared by using TEMPO-terminated PS²¹³ or TEMPOL-terminated PS.[214] Although “living” anionic polymerization is the most traditionally used route used to prepare these macromolecules due to the possibility of good control over the molecular weights and their distributions, atom transfer radical polymerization (ATRP) has found large use due to its ease. Along with well-defined C_{60} -end-capped PS, this polymerization has been successfully exploited with other polymers to obtain the correspondent C_{60} -end-capped derivatives.

1.4.1.5 Star-shaped polymers

Star-shaped polymers take their name from their structure, recalling sea stars as shown in **Figure 48**. In this class of polymers, from two to twelve polymer chains are covalently linked to the fullerene cage. PS- C_{60} star polymers have been largely investigated. It has been found that both the number of PS chains linked to C_{60} , and the dimensions of the final macromolecule can be controlled in the $C_{60}(\text{PS})_x$ species when “living” anionic polymerization is performed under high-purity conditions.[215,216] Different strategies were employed to obtain star-shaped C_{60} -containing polymers, for example that by Mignard et al. in 2002.[217] In their work, the authors have reported the synthesis of 6-star- C_{60} [styrene-poly(1,4-phenylene)-*block*-polystyrene] and 6-star- C_{60} [polystyrene-*block*-poly(1,4-phenylene)] by grafting “living” polystyrene-*block*-poly(1,3-cyclohexadiene)-*block*-styryllithium and poly(1,3-cyclohexadiene)-*block*-polystyryllithium onto C_{60} . In this case the fullerene was observed to limit the number of linked polymeric chains to six. The star-shaped polyfullerenes have been obtained also using C_{70} and multisubstituted fullerene as the central core. Examples are given by the work of Chen et al., where C_{70} has been used with living polystyrene anions to obtain polystyrene-substituted [70]fullerene,[218] and the work of Goswami and co-workers who prepared ether-connected star-shaped C_{60} -polymer (**Figure 48**) starting from fullerenol, $C_{60}(\text{OH})_n$.[219]

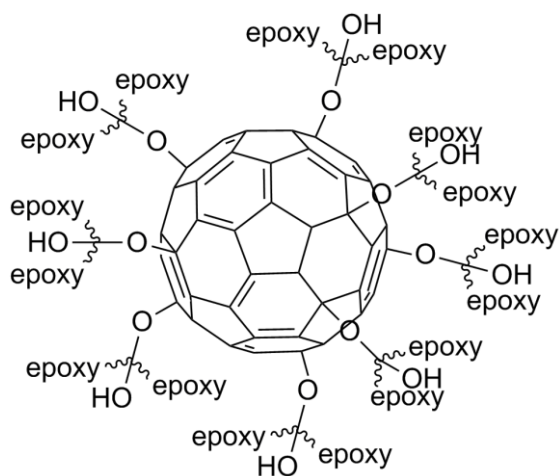


Figure 48: Example of a star-shaped fullerene-containing polymers. Image adapted from ref. 204

1.4.1.6 C₆₀-dendrimers

Dendrimers can reach high molecular weights. For this reason, and considering that fullerenes are good candidate as core for hosting dendrons, C₆₀-dendrimers are classified as polyfullerenes. The first example of this family is given by Fréchet and Wudl in 1993.[220] In this first work, the authors coupled compact dendritic macromolecules with pre-functionalized fullerenes to obtain well-defined polymer-fullerene hybrids. As shown in **Figure 49**, they used phenol-functionalized fullerene as a core and attached polyether dendrimers to it.

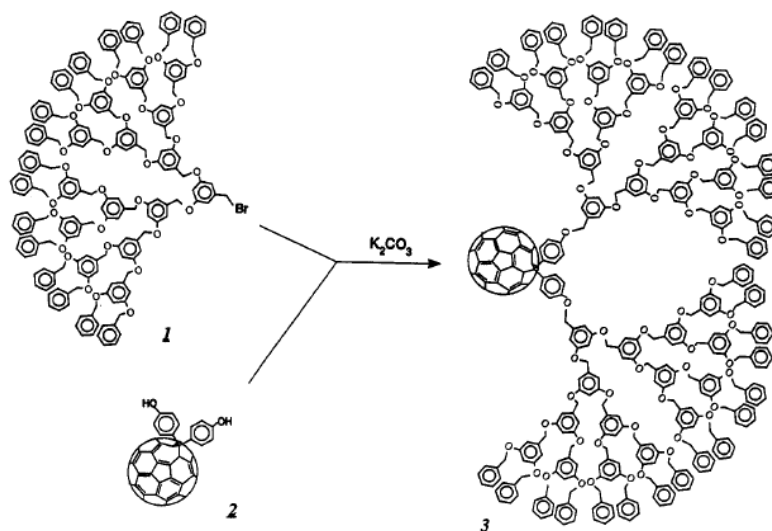


Figure 49: Scheme of the formation of fullerene-dendrimer; **1**: fourth-generation dendrimer [G-4]-Br; **2**: diphenolic fullerene; **3**: obtained polymer-fullerene hybrid structure. Reproduced from ref. 220

This class of polyfullerene has attracted growing interest in the last decades for their nanostructure and organization and the good solubility in many solvents. In the field of nanotechnology, for instance, and in particular in the field of liquid-crystals, fullerodendrimers represent a promising family of materials. Functionalize dendrimers with mesogenic elements leads to the formation of liquid-crystalline materials. The incorporation of fullerene into these liquid-crystals structures opens to the possibility of new molecular devices that can link the extraordinary electrochemical and photophysical characteristics of fullerene with the self-assembly capacity of liquid-crystals. The materials obtained by the association of C_{60} with redox-active units and second-generation liquid crystal dendrons have been studied in supramolecular switches and in solar cell technologies.[221–225] Also dendritic structures that have fullerene units on their surface or in the dendritic branches are found in literature.[226–228] In order to prepare these macromolecules, two different synthetic strategies are possible: divergent synthesis and convergent synthesis.[229] The divergent synthesis is the easiest one. In this strategy fullerodendrimers are obtained by grafting C_{60} units on the peripheral reactive groups on commercially available dendrimers. The C_{60} -containing polypropylene dendrimers shown in **Figure 50(a)** have been prepared with this strategy.[230] The convergent strategy has been introduced by Hawker and Fréchet and it results more efficient in order to obtain monodisperse dendrimers.[231] In this second strategy the peripheral dendrimers are synthesized first and then there are attached to the central unit. An example of molecule prepared with this approach is shown in **Figure 50 (b)**. [232]

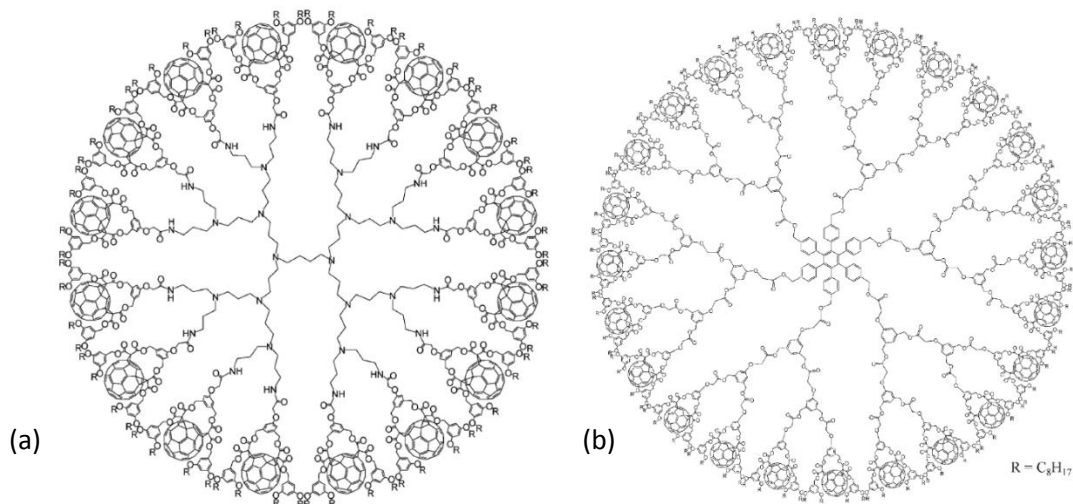


Figure 50: Structure of a (a) C_{60} -containing polypropylene dendrimers prepared by grafting C_{60} units onto commercially available dendrimers, and (b) C_{60} -containing dendrimers prepared by attaching synthesized peripheral dendrimers to the central unit.

1.4.1.7 Main-chain polymers

Main-chain polyfullerenes, also called in-chain or pearl necklace polymers, have interesting structures, but are probably the least represented among the C_{60} -containing polymers. The fullerene resides in the polymer backbone. If these materials are less common than the other types it is because the double addition on the fullerene cage, necessary to obtain the in-chain structure, is difficult to control and often yields complex regioisomeric mixtures. Also the formation of cross-linked products by multiple additions on C_{60} makes the synthesis of these materials more difficult. Two strategies are possible for the synthesis of main-chain polyfullerenes: i) reaction between C_{60} and a symmetrically difunctionalized monomer and ii) polycondensation between a fullerene bisadduct and a difunctionalized fullerene. One of the first examples of this family of materials was published by Rotello and Nie, in 1997, who reported a thermoreversible material based on a C_{60} main-chain polymer. The material was obtained by Diels-Alder cycloaddition at room temperature and underwent a cycloreversion process when heated between 60 and 75 °C.[233] This result was a promising hint towards the development of recyclable and thermally processable polymers based on thermoreversible polymerisation-depolymerization. A new route of main-chain polyfullerenes was proposed by Hiorns et al. in 2009.[234] The obtained poly{(1,4-fullerene)-*alt*-[1,4-dimethylene-2,5-bis(cyclohexylmethyl ether)phenylene]}s (PFDP)s, whose the preparation scheme is reported in **Figure 51**, were tested in OPV, blended with P3HT. The non-optimized device reached a promising efficiency of 1.6%.

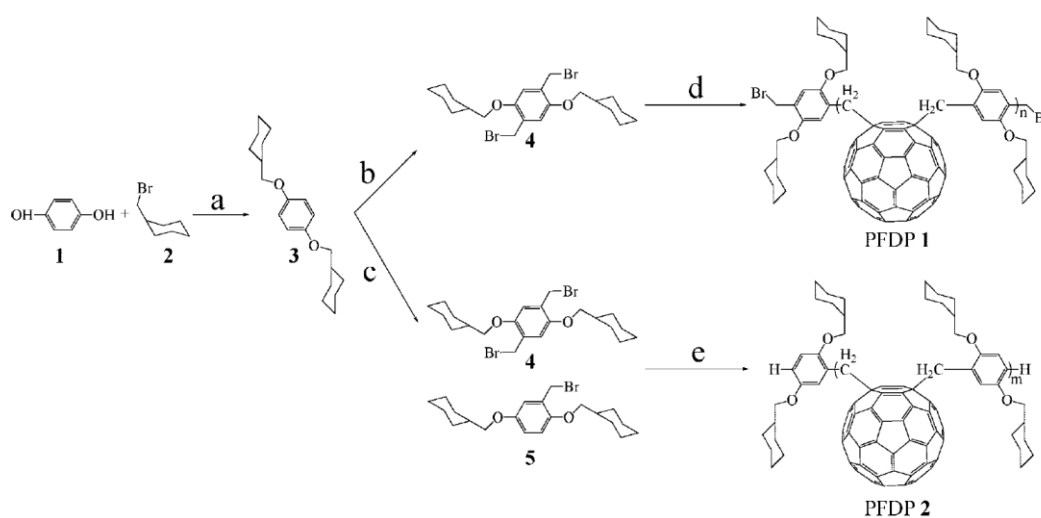


Figure 51: a) K_2CO_3 , acetonitrile, 90 °C, 40 h; (b) paraformaldehyde, HBr, 65 °C, 80 min; (c) paraformaldehyde, HBr, 45 °C, 24 h; and (d and e) fullerene, CuBr, bipyridine, 22 h, 115 °C. Reproduced from ref. 234

The obtained materials were of facile synthesis and presented a modular structure, electronic activity, and novel solid-state behaviour that make them promising materials for photovoltaic applications. This work is the starting point of part of the work presented in this manuscript. The synthetic route reported by Hiorns *et al.*, the atom transfer radical addition polymerization (ATRAP) has been extended to produce PCBM-based polymers (*vide infra*). The chemistry is facile and breaks only the 6-6 double bonds on the fullerene. It is based on the atom transfer radical addition (ATRA) mechanism shown in **Figure 52**.

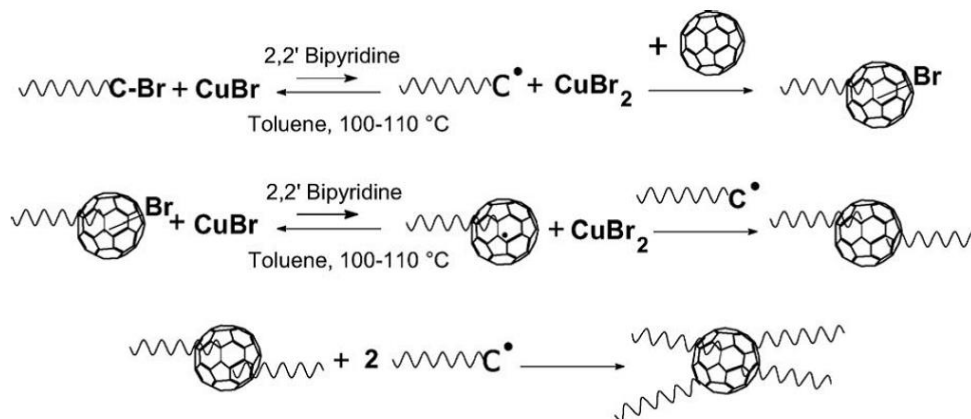


Figure 52: Addition mechanism of PSBr chains onto C₆₀ through an ATRA.

Once one substituent is attached onto the C₆₀ cage via an ATRA reaction, a second addition is highly favoured. Mathis and co-workers showed in their work on the addition on PSBr onto C₆₀, that no mono-adducts were formed. Moreover, they showed that only products with an even number of grafted chains were obtained. This property of the products is directly connected with the reaction mechanism. Any C₆₀-A bond between the fullerene cage and an atom A, is weaker than a 'normal' C-A bond. That means that the C₆₀-Br bond which is formed after the first addition of PSBr on the fullerene, is easier to break than the PS-Br bond. The concentration of the radical PS-C₆₀• is always large and the possibility to have recombination between it and the radical PS• is very likely. The UV-vis characterisation conducted by the authors demonstrate that the attack position of two substituent is more probable on the 1,4 position of the same hexagon. Together with demonstrate that mono-adducts were not obtained even when C₆₀ was used in 10-fold excess, they showed that the number of branches on fullerene was controlled by the ratio PSBr/C₆₀. Pure bis-adducts were obtained only when this ratio was kept lower than 2. They also demonstrate that pure tetra-adducts were obtained only if the reaction were performed with a large excess of PSBr (PSBr/C₆₀ > 4).[235-236]

Another very interesting main-chain polyfullerene was first introduced by Geckeler and co-workers.[237] They reacted C_{60} directly with β -cyclodextrine-bis-amino complexes as shown in **Figure 53**; the reaction proceeds via a nucleophilic polyaddition reaction. The product of this reaction was the first water-soluble polyfullerene reported in literature. In addition to water solubility, the cyclodextrine avoids the multi-addition on the C_{60} sphere thanks to its steric hindrance. This polymer has been successfully employed as DNA-cleaving agent.

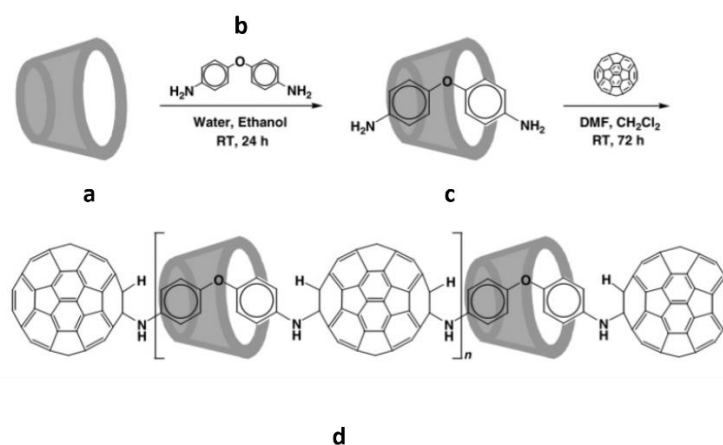


Figure 53: Reaction scheme for the synthesis of the polyfullerene reported by Geckeler and co-workers. (a) β -cyclodextrine, (b) p -phenylenediamine, (c) cyclodextrine-amine complex and (d) resulting polymer. Image adapted from ref.237

Despite the difficulty to obtain bis-substituted C_{60} , the second strategy has been the most employed. For example, Taki *et al.* after reporting an elegant route to obtain well-defined fullerene bis-adducts,[238] used the obtained compounds as monomers to synthesize pearl-neckless polyesters containing C_{60} moieties in the main-chain.[239] Their method consists in the reaction of C_{60} with two α,α' -dibromo-*o*-xylene moieties connected by an oligomethylene chain. Depending on the length (n) of the oligomethylene ($-(CH_2)_n-$) chain, only *cis*-2- and *cis*-3-bisadducts ($n = 2$ and 3) or *e*-bisadduct ($n = 5$) were selectively obtained. Finally the cleavage of the oligomethylene chain produced the corresponding C_{60} derivatives possessing two phenol moieties that can be then employed in further functionalization of the system. The scheme for the synthesis of the C_{60} bisadducts is reported in **Figure 54**.

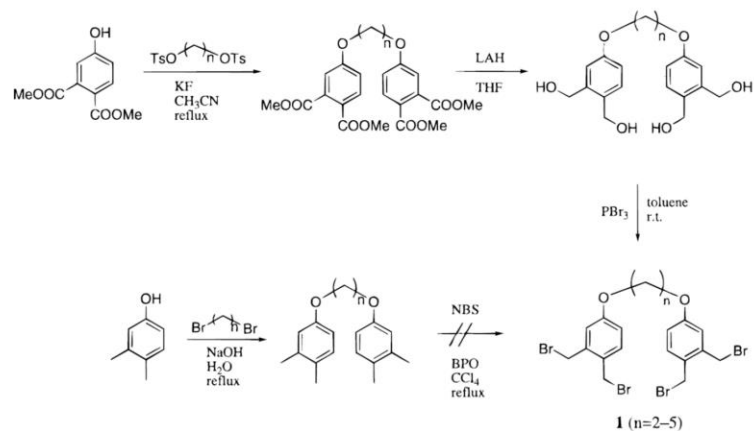
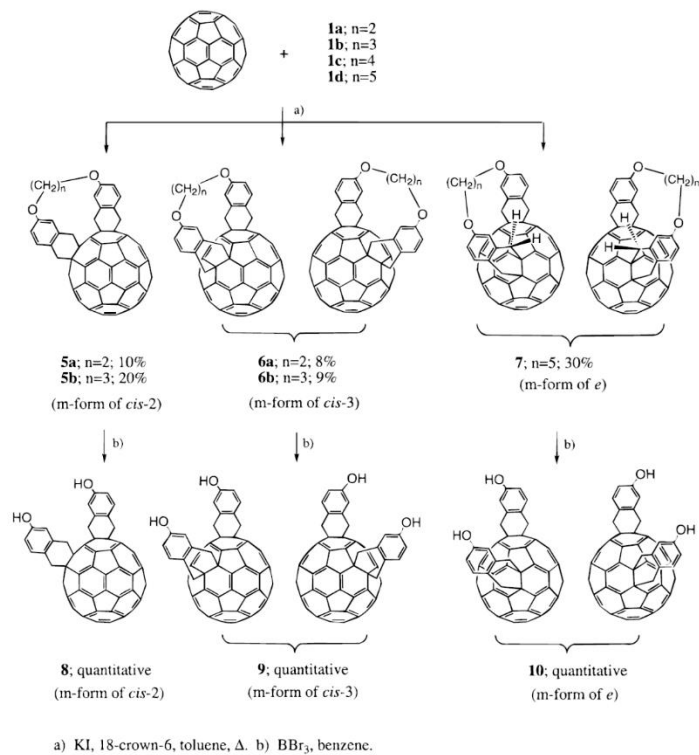


Figure 54: Scheme of the synthesis of α, α' -dibromo-o-xylene moieties connected by an oligomethylene chain. Image reproduced from ref. 238

After conversion of the phenol groups in correspondent salts to improve their water solubility, the authors let them react with C₆₀ in a condensation polymerization to yield the main-chain polyfullerenes. The scheme of the just presented strategy is reported in **Figure 55**.

Scheme a:



Scheme b:

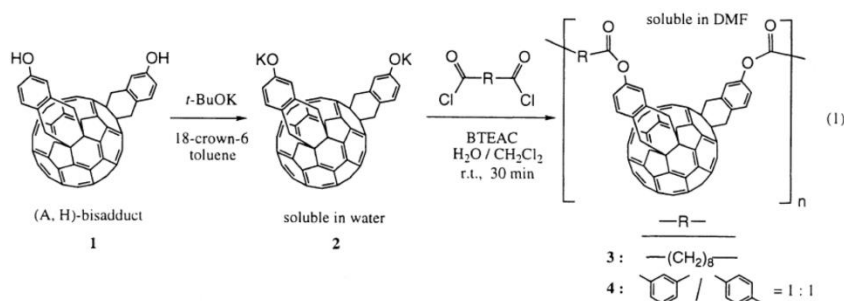


Figure 55: (Scheme a) Synthesis of well-defined C_{60} bis-adducts, with reference to **Figure 54** for compounds 1a-d (image reproduced from ref. 238); (Scheme b) Synthesis of C_{60} -main-chain polyesters (image reproduced from ref. 239).

Using the ideas that the construction of main-chain polymers is possible by repetitive cycloaddition of C_{60} , Gügel *et al.*[240] obtained polyfullerenes by repetitive Diels-Alder cycloaddition of bis-hexyloxy-substituted bis-sulfone on the fullerene as reported in **Figure 56**. With this method, using appropriate solubilizing functional groups and avoiding cross-linking by means of addition of mono-*o*-quinodimethane in the reaction mixture, they obtained high molecular weight polymers with good solubility.

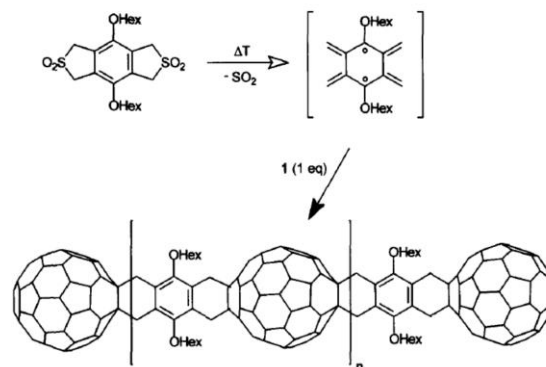


Figure 56: Scheme of the synthesis of main-chain polyfullerene by repetitive Diels-Alder cycloaddition. Image reproduced from ref. 240

Alternative main-chain polyfullerenes were prepared reacting a mixture of C₆₀-bis adducts with amino-propyl-end-capped-PDMS in 1999 (**Figure 57**)[241], but other examples are present in literature.[242–244] Also pure fullerene regioisomers have been used to prepare main-chain polyfullerenes.[245] In general, the polymers obtained have the advantage of a very good processibility.

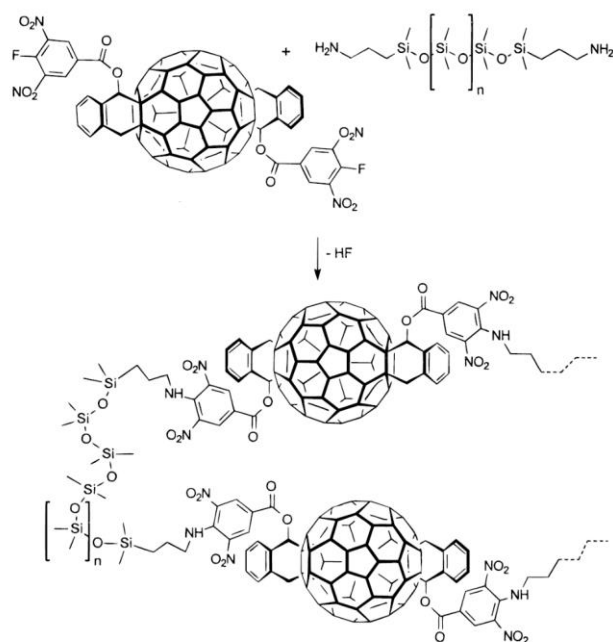


Figure 57: main-chain polyfullerenes have been prepared reacting a mixture of C₆₀-bis adducts with amino-propyl-end-capped-PDMS. Image reproduced from ref.241.

1.4.1.8 Side-chain polymers

Side-chain polyfullerenes are the most studied fullerene-containing polymers and count a large number of macromolecules. Also for this family of polymers there are two different synthetic strategies (**Figure 58**): the first strategy (i) is the direct introduction of fullerene or fullerene derivatives into a preformed polymer; in the second strategy (ii) fullerene derivatives are first synthesized and then homopolymerized or copolymerized to obtain the desired polyfullerene.

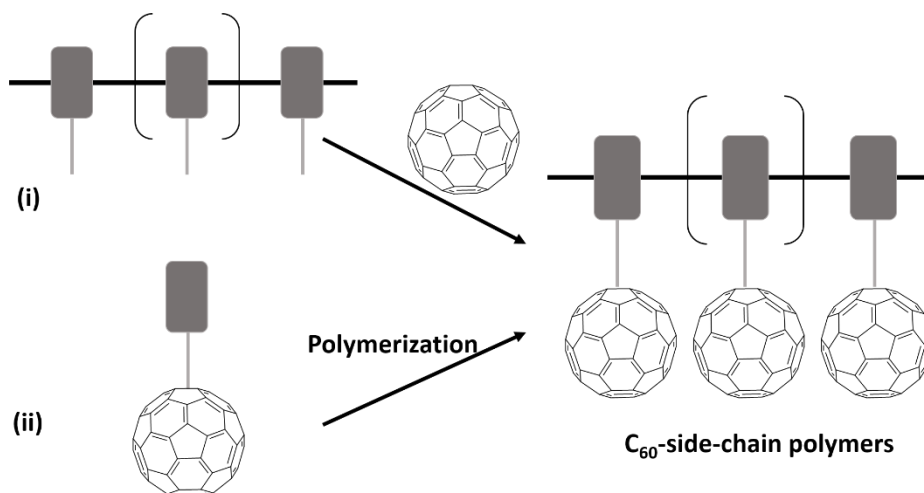


Figure 58: Synthetic strategies for the synthesis of side-chain C_{60} -polymers.

Many common polymers, such as PS,[246–248] polyacrylate,[209,249–251] polycarbonate,[252,253] polyvinylcarbazole,[254] polyphosphazenes,[255] polysiloxane,[256] polysaccharides,[257] as well as polyethers and polythiophenes have been exploited to produce side-chain polyfullerenes. In order to link the C_{60} to the polymer chain, different routes have been used. Due to the well-known addition of amines to fullerene double bonds, amino- or imino-linked fullerene-polymers have been one of the first studied ways to prepare this class of macromolecules.[258] Other approaches involve the grafting of C_{60} via Friedel-Crafts reaction, the “azido” route, [4+2] cycloaddition reaction and “living” radical reaction, but also MW irradiations have been exploited.

1.4.1.9 Double-cable polymers

Double-cable (D-C) polymers have found applications in electro-optical devices due to their electronic properties. These polymer are constituted, of a π -conjugated polymer, as main chain polymer, to which a number of n-type materials, C_{60} for instance, are covalently linked. The concept of double-cable polymers for organic optoelectronic devices was first introduced by Cravino and Sariciftci in 2002.[259] They bring the advantages of the possibility of large donor-acceptor interfacial area, good tunability of the components as well as good stability upon phase separation and clustering. Together with the strategies used to synthesised side-chain polymers, along with electropolymerization of aromatic monomers has been one of the most employed strategies to obtain C_{60} -containing D-C. As example, electropolymerization giving a double cable polymer in which C_{60} was used as n-type material with terthiophene as the main-chain monomer is shown in **Figure 59**. [260]

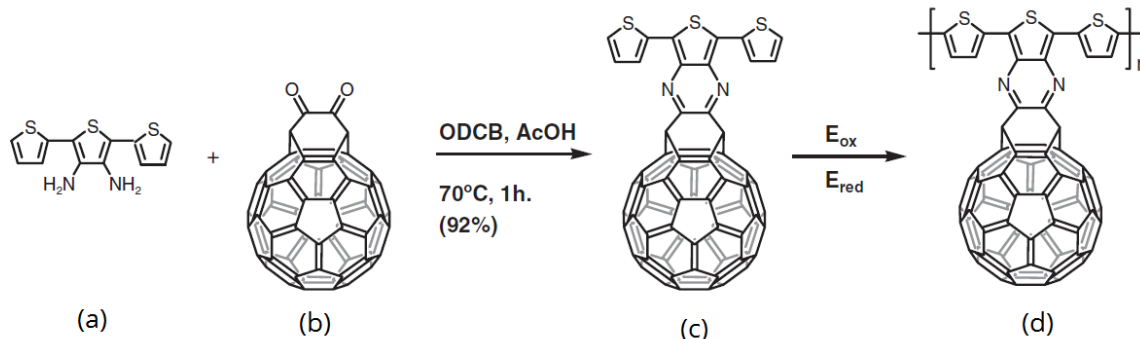


Figure 59: Synthesis and polymerization of the monomer c containing (b) bisfulleroid, as electron-acceptor and (a) terthiophene as donor material; the two components are linked by a [3,4-*b*]-pyrazine bridge. Electropolymerization gives D-C polymer (d).

1.4.1.10 C_{60} -supramolecular polymers

This class of macromolecules has been its developed only very recently. This push has come by the possibility of avoiding the formation of large C_{60} clusters dispersed in a polymeric matrix that are commonly found with polyfullerenes.[261] A supramolecular polymer, is kept together by non-covalent bonds and results from any type of self-assembly process that creates polymer-like aggregates. The reversible nature of the interaction can avoid phase segregation of the components, but a more important advantage of this type of macromolecules is the possibility to

obtain additional order in the solid state.[262] Based on the synthetic strategy used for their preparation, supramolecular polyfullerenes can be divided into four classes: (i) supramolecular polyfullerenes based on interaction between suitably functionalized polymers and C_{60} derivatives; (ii) supramolecular polyfullerenes based on self-assembly of fullerene derivatives; (iii) supramolecular polyfullerenes based on functionalized C_{60} and complementary backbones; (iv) complementary interactions between C_{60} and concave guests.

The interactions that keep the structures together are weak interactions of varying natures and are displayed in **Figure 60**.

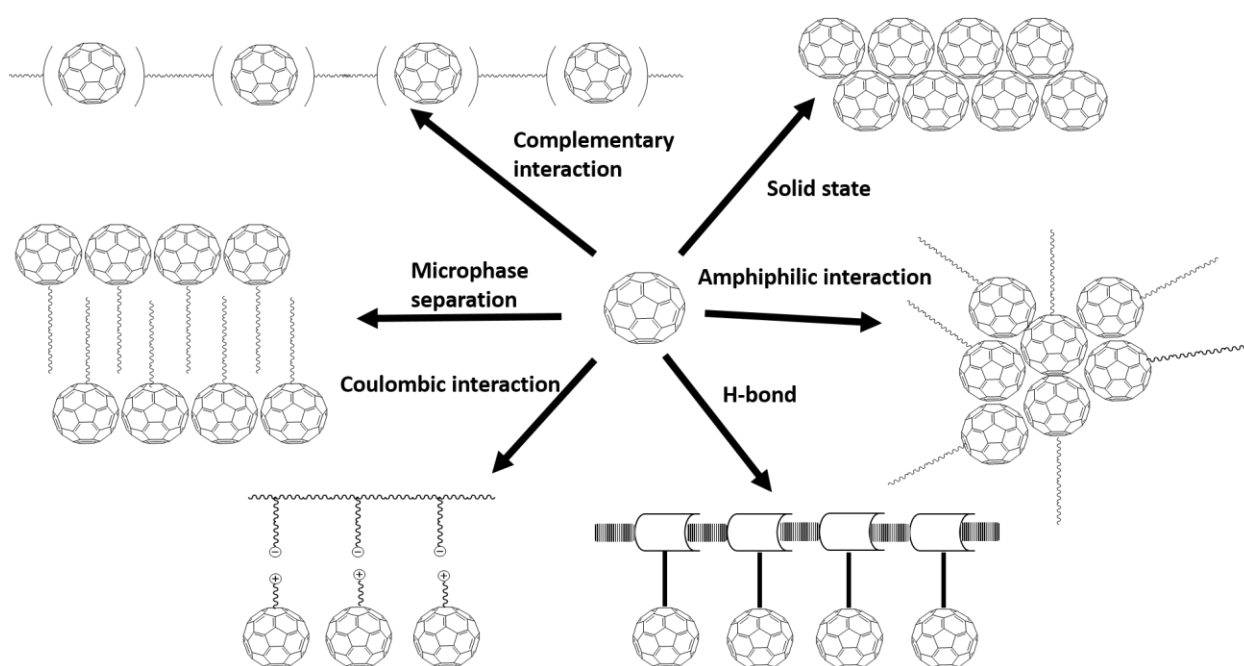


Figure 60: Type of interaction that forms fullerene-based supramolecular ensembles.

1.4.2 Polyfullerenes in organic photovoltaics

The association between the electronic properties of fullerene and the mechanical properties, the stability, as well as the processibility of polymers gives a promising mixture that is interesting in photovoltaic applications. Over the years, polyfullerenes have been proposed in the role of n-type material in all-polymer blends and as electron-selective-layer (ESL) in devices. The most exploited type of polyfullerenes in OPVs are the D-Cs, presented in section 1.4.1.9.[263] The first

observation of a photo-induced charge transfer in these type of materials was reported for the first time by Cravino et al. and this opened the possibility of using them as active layers in organic solar cells.[264,265] The author studied a D-C polymer composed of a polythiophene backbone with tethered fullerene units (**Figure 61**). Spectroscopic studies showed that the two components did not interact in the ground state while electron transfer occurred in the polymer in its excited state. The photo-induced absorption spectrum, shows the two typical bands (1.4 and 0.6 eV) of positive polarons on a thiophene-based backbone. The two bands showed an excitation intensity dependence which is an indication of the charge carrier behaviour of the material. The photo-induced charge transfer between the donor and the acceptor components were confirmed by ESR.

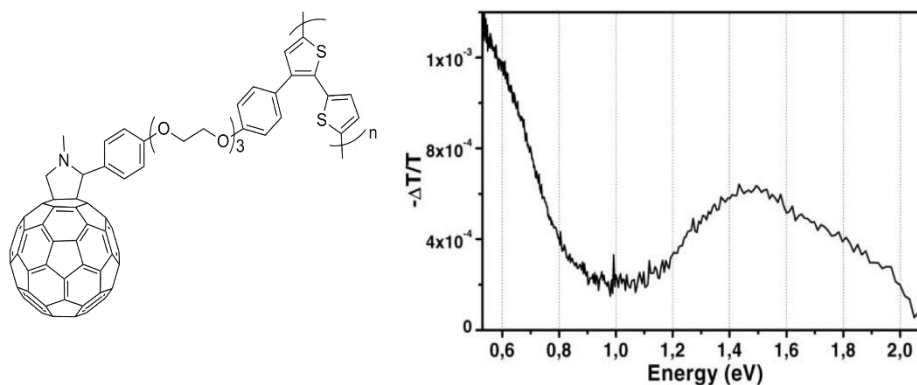


Figure 61: Structure of double-cable C₆₀-containing polymer investigated for charge-transfer processes (left) and its published absorption spectrum (right) showing the bands typical for positive polarons on a thiophene-based backbone. Image adapted from ref.265

Some years later, Tan *et al.* investigated the photovoltaic properties of a D-C polyfullerene based solar cell obtaining a PCE of 0.52% under AM 1.5 illumination conditions.[266] They used the solar cell structure ITO/PEDOT:PSS/PT-F/Ca/Al where PT-F was a D-C polythiophene with a high-content of pendent C₆₀ units (**Figure 62**).

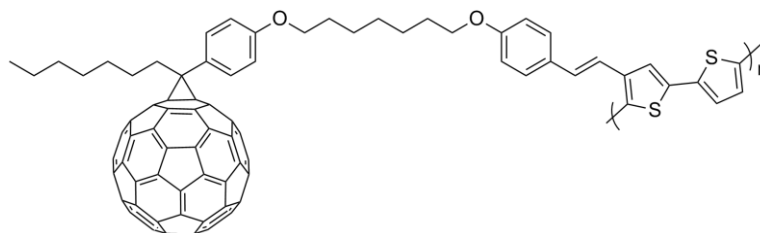


Figure 62: structure of double-cable polythiophene with high-content of C₆₀ pendent units.

Even if the double-cable approach seems to be the most rational one to obtain well controlled and defined morphology of the solar cell active layer, the efficiency of the devices fabricated with these materials is very low. This is the result of poor charge separation and a high recombination rate caused by the too intimate mixing of D and A units. The main limitations for the application of D-C systems are their challenging synthesis and processibility. [92,259,267]

Also main-chain polyfullerenes have been proposed for the active layer. They were thought to be a good alternative because they allow an easier access to the correct geometry and can lead to optimum domain sizes. The main-chain polyfullerenes proposed by Hiorns and co-workers and already discussed in paragraph 1.4.1.7 give one example.

The use of a cross-linked network is a common method in organic electronic to obtain robust materials. Cross-linkable fullerene derivatives, in particular modified PCBM molecules bearing either styryl groups (PCBS and PCBSD) or oxetane groups (PCBO and PCBOD) have been successfully proposed as ESLs. The structure of these molecules are shown in **Figure 63** and their cross-linking obtained by thermal treatment.[268] The authors reported enhancement up to 26% with respect to the reference devices when the cross-linked fullerene are used.[269] This enhancement was attributed to the capability of the materials to self-assemble onto the TiO_x surface and simultaneously cross-link and generate a dense, robust, and pinhole-free multimolecular interlayer that improve the interface characteristics.

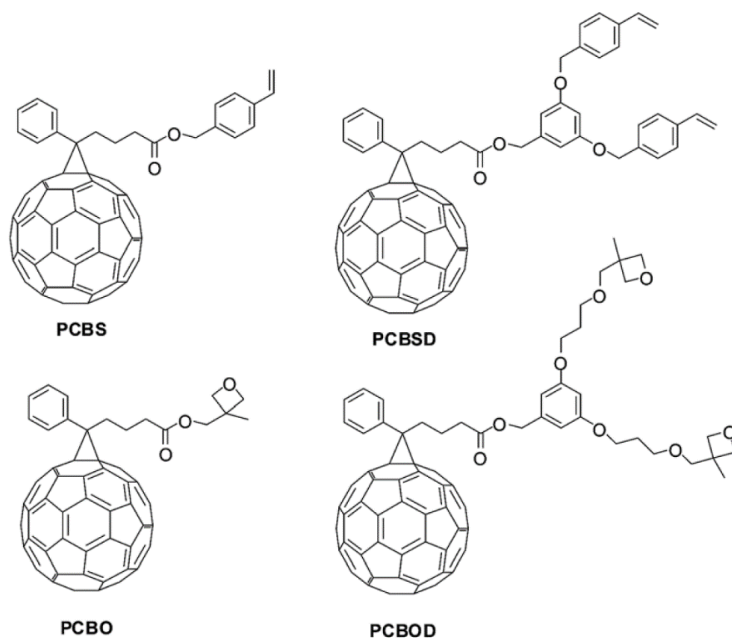


Figure 63: Structure of crosslinkable PCBM derivatives.[268]

An alternate use of polyfullerenes in OPV is as a compatibilizer between n- and p-type materials in the active layer. For example, BHJ based on P3HT:PCBM blends have been stabilized by the C₆₀-containing polythiophenes showed in **Figure 64**. The hybrid material is, suitable to go at the interfacial surface between the donor and the acceptor material, reducing the interfacial energy and leading to a better compatibility between the components.

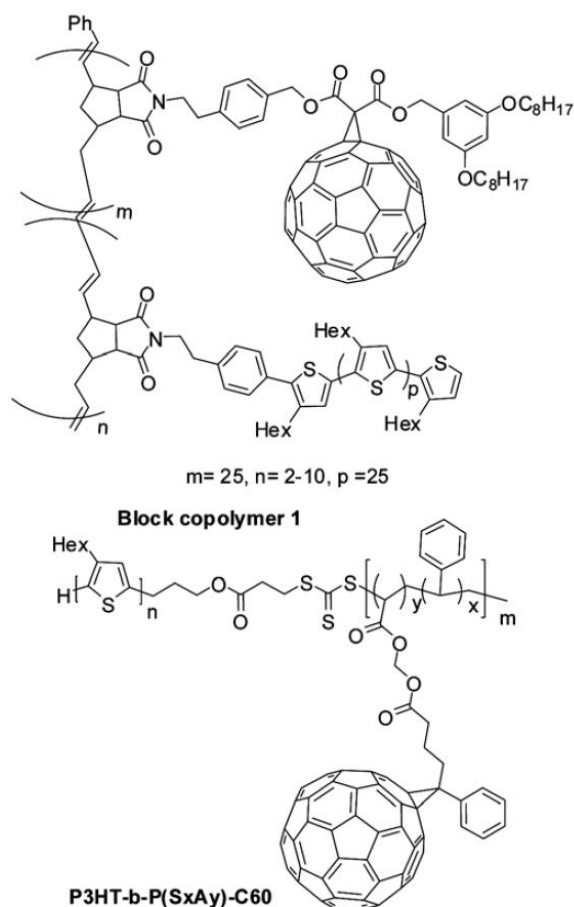


Figure 64: used as Structure of C₆₀-containing polymers compatibilizer in OPV devices.[270,271]

In this last section we have introduced and given a non-exhaustive review of the various classes of polyfullerenes. Moreover, their applications in organic photovoltaics have been briefly discussed. Polyfullerenes are very versatile materials that remain relatively unexplored. As discussed in the last part of this section, polyfullerenes can be potentially used in the OPV active layer as well as an interlayer to optimize the device interfaces and enhance the performances. Thanks to their polymeric natures, polyfullerenes are also good candidates for organic photovoltaics when the issue of stability is addressed. It is expected that all-polymers active layer can reach a better miscibility of the materials avoiding the formation of macroscopic fullerene clusters with time. This effect is also expected in a ternary blend where, for example, a polyfullerene is mixed with donor:acceptor materials. However, in order to be used in industrial application, polyfullerenes must fulfil different requirements such as facile production, good solubility and easy processibility.

2 Synthesis and characterization of novel polyfullerenes

Abstract

Here we present the synthesis of new classes of soluble main-chain polyfullerenes. The first type of materials presented in this section are PCBM-based oligo- and polyfullerenes synthesized using the ATRAP route. In the second part of this Chapter, a novel polymerization route, based on fulleropyrrolidine-chemistry and developed during this PhD is presented. This new route employs C_{60} as monomer to yield highly soluble main-chain polyfullerenes.

Part of the results on the first type of materials have been presented in national and international conferences:

1. Fullerene-based polymers for photovoltaic applications

Hasina H. Ramanitra, Simon A. Dowland, Graham E. Morse, Hugo Santos Silva, Didier Bégué, Thomas Chassé, Andreas Distler and Roger C. Hiorns

ESOS European training school and conference on organic photovoltaic stability, June 2015, Cargèse, Corsica, France

2. Fullerene-based polymers for photovoltaic applications (Polymères à base de fullerene pour applications photovoltaïques)

Hasina H. Ramanitra, Simon A. Dowland, Graham E. Morse, Hugo Santos Silva, Didier Bégué, Thomas Chassé, Andreas Distler and Roger C. Hiorns

Congrès 2015 de la Société Chimique de France, July 2015, Lille, France

3. Fullerene-based polymers for photovoltaic applications

Hasina H. Ramanitra, Simon A. Dowland, Graham E. Morse, Hugo Santos Silva, Didier Bégué, Thomas Chassé, Andreas Distler and Roger C. Hiorns

12th International Symposium on Functional π -Electron Systems (F π -12), July 2015, Seattle, Washington, USA.

Part of the results will be published in:

Patent pendent 'Semiconducting mixtures'

R. C. Hiorns (CNRS), H. H. Ramanitra (UPPA), D. Bégué (UPPA), H. Santos Silva (UPPA) A. Distler (Belectric OPV GmbH), S. Dowland (Belectric OPV GmbH), G. Morse (MERCK). Merck/CNRS/UPPA/Belectric OPV GmbH.

“It’s ATRAP! PolyPCBM and its oligomers for the stabilization of polymer:PCBM bulk heterojunctions”

Hasina H. Ramanitra, Simon Dowland, Hugo Santos Silva, Didier Bégué, Sambatra Rajoelson, Michael Salvador, Andres Osvet, Christoph J. Brabec, Hans-Joachim Egelhaaf, Graham Morse, Andreas Distler, Roger C. Hiorns

A Facile Metal-free Route to Main-chain Fullerene Polymers

Hasina H. Ramanitra, Hugo Santos Silva, Abdel Khoukh, Craig. M. S. Combe, S. A. Dowland, Didier Bégué, Christine Dagron-Lartigau, Andreas Distler, Graham Morse, Roger C. Hiorns

This work has also permitted the preparation of the article:

PCBM polymerized! SACAP gives soluble main-chain polyfullerenes

Meera Stephen, Hasina H. Ramanitra, Simon Dowland, Didier Bégué, Kristijonas Genevičius, Kestutis Arlauskas, Gytis Juška, Andreas Distler, Roger C. Hiorns

"The research leading to these results has received funding from the French Region Aquitaine under the grant agreement FULLINC 2011 and from European Union Seventh Framework Program (FP7/2011) under grant agreement ESTABLIS no. 2900

To merge the excellent electronic properties of fullerenes and the mechanical properties of polymers is a very attractive proposition to find novel materials for photovoltaic applications. Many different fullerene-containing polymers have already been synthesized and some of them have been proposed in different roles in solar cells showing promising, even if not yet market competitive, results. The production of polyfullerenes still has to face many difficulties due, in the most part, to the nature and reactivity of fullerene itself. In particular, when main-chain polyfullerenes are desired, the synthesis is made challenging by the difficulty of arresting the functionalization of fullerene to bis-adducts, which are necessary to obtain this type of macromolecules. Moreover, the synthesis of bis-adducts generally results in a mixture of regioisomers. In fact, 8 regioisomers are possible for the bis-functionalisation of a C₆₀ fullerene cage.

Different methods have been developed to obtain controlled bis-functionalised C₆₀ and it has been shown that great importance in controlling the synthesis is the steric hindrance of substituents. As stated in paragraph 1.4.1.7, two strategies are possible for the synthesis of main-chain poly[60]fullerenes: i) reaction between C₆₀ and symmetrically difunctionalized monomer; ii) polycondensation between a fullerene bisadduct and a difunctionalized fullerene. There are few examples in literature of main-chain polyfullerene, but they generally require multi-steps synthesis.

In this work, we therefore explore two different routes to obtain main-chain polyfullerenes which have the advantage of being facile one-pot synthesis and which results in two novel type of C₆₀-containing polymers with promising performances in organic solar cells. In the first type of synthesis, PCBM is exploited as monomer. The synthesis is based on ATRAP polymerisation route following a previous work by Hiorns and co-workers. As suggested by the authors, with the aim of avoiding multiple additions to the fullerene, and hence cross-linking reactions, a co-monomer with quite large steric groups, namely 1,4-bis(bromomethyl)-2,5-bis(octyloxy)benzene (**2**) was chosen.

The second polymerization route is based on Prato chemistry which is, to our knowledge, exploited for the first time for the synthesis of main-chain polyfullerenes. To explore this novel polymerisation route, three different comonomers have been employed. For this work we have chosen 3 symmetrical benzene-core based comonomers with symmetrical substituents with increasing chain-lengths (terephthaldehyde, 2,5-bis(octyloxy)terephthaldehyde, 2,5-

bis(hexadecyloxy)terephthalaldehyde). This choice of comonomers has permitted to study the effect of the substituent chain length in the polymerisation.

In the following sections, the syntheses of the comonomers are reported and the syntheses of the novel PolyPCBM and PPC₆₀ are discussed in detail.

2.1 Syntheses of the comonomers

Four different monomers were used during this study. Terephthalaldehyde (**6**), is commercially available and was used as received. 1,4-Bis(bromomethyl)-2,5-bis(octyloxy)benzene (**3a**), bis-2,5-(octyloxy)terephthalaldehyde (**5a**) and bis-2,5-(dodecyl)terephthalaldehyde (**5b**) were synthesized following modified protocols from literature.

The scheme for the synthesis of the different monomers is reported in **Figure 65**.

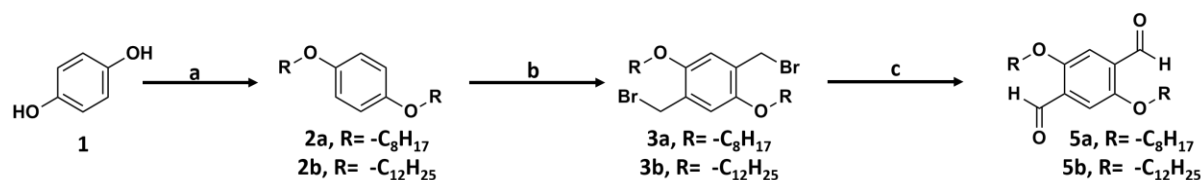


Figure 65: Scheme for the synthesis of the monomers used in this work: **a-2a**) 1-bromooctane, K₂CO₃, **1**, acetonitrile; **a-2b**) 1-bromododecane, K₂CO₃, **1**, acetonitrile; **b-3a**) (CH₂O), acetic acid, **2a**, HBr; **b-3b**) (CH₂O), acetic acid, **2b**, HBr; **c-5a**) NaHCO₃, **3a**, dimethyl sulfoxide; **c-5b**) NaHCO₃, **3b**, dimethyl sulfoxide.

The choice to use aromatic-oxy-alkyl side-groups was made from their expected photostability,[272] high solubility, and ease of preparation via a Williamson condensation with hydroquinone (**1**). The etherification of hydroquinone to obtain **2a** and **2b** was realized in reasonable yields (60-70%) using the respective alkyl bromides.[273] It was expected that the subsequent bisbromomethylation might be sensitive to the presence of large alkyl chains; indeed, prior work by Made *et al.* showed with small substituents yields of around 95% could be obtained,[274] but in our case we had to be content with yields around 75%. Attempting to make 2,5-bis(bromomethyl)-1,4-bis(hexadecyl)benzene we found yields were variable.

From the bromomethylated molecules, to the bis-aldehyde ones, different synthetic routes are possible. In a first attempt, the route proposed by Wang *et al.* was chosen.[273] This route, shown in **Figure 66**, requires five steps in all from the hydroquinone to the desired formylated aromatic ether **5a** or **5b**.

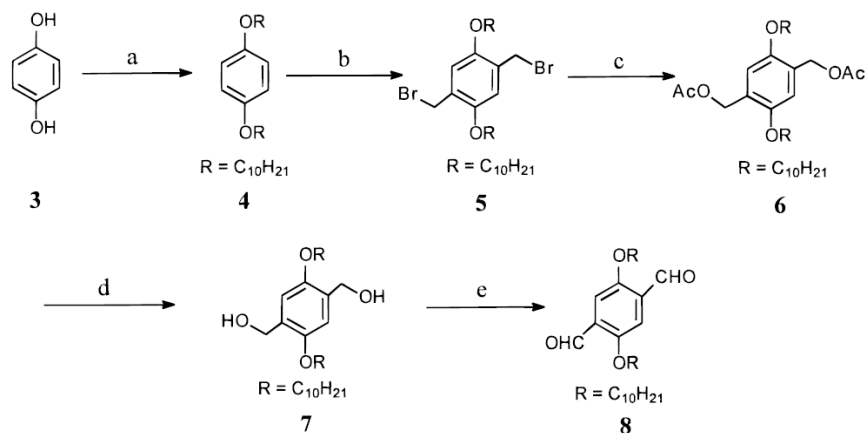


Figure 66: (a) Bromodecane, K_2CO_3 , acetonitrile, reflux, 36 h, 85%; (b) paraformaldehyde, HBr, 60 °C, 2 h, 86%; (c) KOAc, Bu_4NBr , acetonitrile, reflux, overnight, 100%; (d) $LiAlH_4$, THF, room temperature, 2 h, 99%; (e) PCC, CH_2Cl_2 , room temperature, 2 h, 87%;

Therefore, a “short cut” was found by going from the bromomethylated products to the aldehydes by oxidation with dimethyl sulfoxide (DMSO) with excessive sodium bicarbonate ($NaHCO_3$) as auxiliary agent.[275,276] This reaction is known as Kornblum oxidation and its mechanism is shown in **Figure 67**.

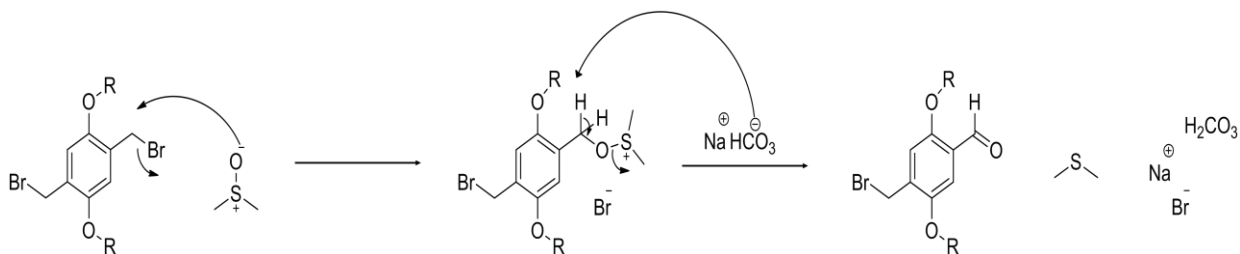


Figure 67: Mechanism of Kornblum oxidation using $NaHCO_3$ as base.

The reaction was conducted at 115 °C for 30 minutes to limit the formation of by-products. The changes in the colour of the reaction mixture was used to monitor the process itself. The initial transparent mixture turns into pale yellow when the desired product is formed and, as the reaction continues and more by-products are present in the mixture, this turns into orange. This method can be applied under N_2 atmosphere or air. The choice to carry out the synthesis in ambient atmosphere is for convenience. Moreover with this choice only low to reasonable yields (21-47%) were found. Although the obtained yields are lower than the ones expected with the Wang route (60-75%) for 1,4-alkoxy-2,5-bis(bromomethyl)benzenes with alkoxy-chains with 1

to 12 carbon units, this method was retained as three synthetic steps were replaced by just one. At each step of the synthesis, the structures were confirmed via NMR spectroscopy. The spectra are reported in this manuscript in the experimental section (section 5). Once the co-monomer was obtained, the synthesis of two different types of C_{60} -containing polymers is proposed.

2.2 Synthesis and Characterisation of PolyPCBMs

PCBM is the most widely used fullerene C_{60} derivative in organic photovoltaics. The success of PCBM lies in its good solubility and electronic properties. As mentioned in section 1.3.1, PCBM has also some limits such as the relative low absorbance. Moreover, PCBM has a tendency to self-aggregate under device operational conditions. The segregation of PCBM, and though the formation of larger PCBM-rich domains, is one of the reason for the loss in efficiency of the device. Different strategies have been proposed to overcome these limits by keeping the desired properties of PCBM. For instance, substitution of the alkyl-chain, the substitution of the aromatic group, or the substitution of the ester group have been investigated. Also PCBM bis-adducts have been proposed and actually results in an increase of 18% of PCE over that of PCBM.[277,278] In this section we propose a different approach: the insertion of PCBM into a main-chain polymer.

The reaction scheme for the synthesis of the oligo- and polyPCBM is shown in **Figure 68**.

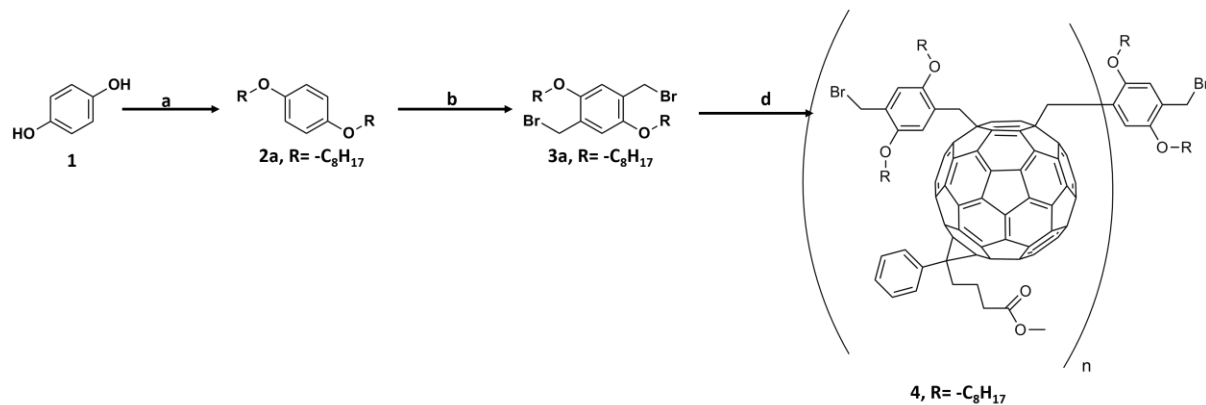


Figure 68: Scheme for the synthesis of oligo- and polyPCBM.

The synthesis of the comonomer **3a** has already been discussed (see section 2.1). The polyPCBM (**4**) are prepared following the general protocol for the atomic transfer radical addition polymerization (ATRAP), introduced in section 1.4.1.7. PCBM was used as monomer, dissolved at

room temperature in distilled toluene and mixed with an equimolar amount of 1,4-bis(bromomethyl)-2,5-bis(octyloxy)benzene (**2a**). 2 equivalents of CuBr and 4 equivalents of bipyridine were added and the temperature of the vigorously stirred mixture slowly raised to 100 °C to start the reaction. After 16 h, the mixture was precipitated in methanol to stop the reaction. The resulting brown precipitates were filtered under N₂ and dried under reduced pressure for 3 d at 30 °C. To purify the product, the recovered solid is washed in a Soxhlet apparatus with acetone overnight to eliminate the unreacted monomers. The scheme of the proposed mechanism for the polymerization is shown in **Figure 69**.

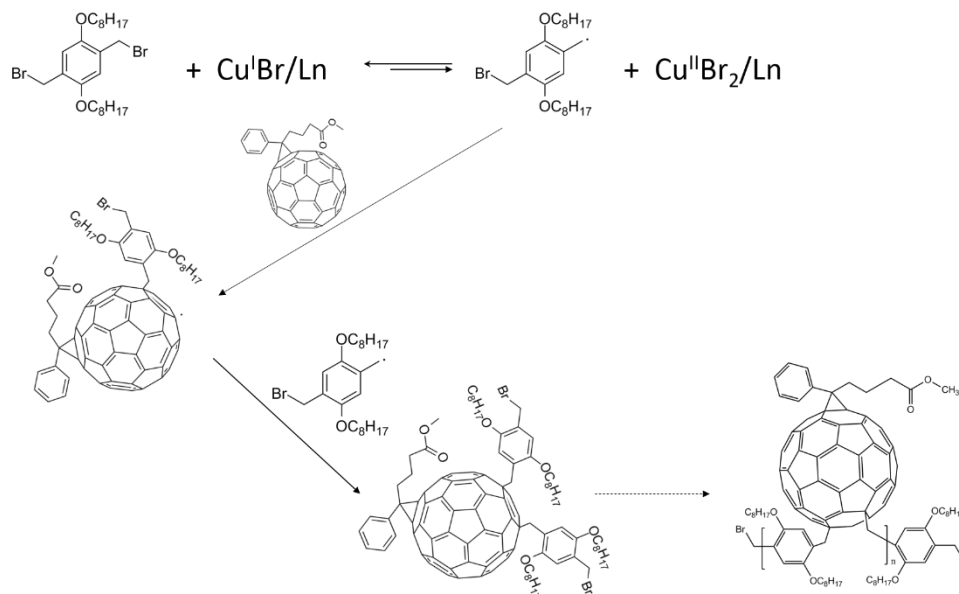


Figure 69: Proposed mechanism of reaction for the preparation of polyPCBMs.

In order to characterize the obtained materials, we have performed size-exclusion chromatography in tetrahydrofuran (SEC-THF), ¹H and ¹³C nuclear magnetic resonance (NMR) measurements, thermogravimetric analysis (TGA), differential scanning calorimetry (DSC) and, UV-VIS optical absorption in solution (UV-VIS). The results are presented and discussed below.

2.2.1 Size-exclusion chromatography (SEC)

The synthesized products are very soluble in common organic solvents such as chloroform, benzene, toluene, and have remarkable solubility in THF. Size-exclusion chromatography (SEC), of the materials have been performed using this last solvent as mobile phase and toluene as flow

marker. This technique is one of the most widely used for polymer characterization as it gives information on the molecular weights and molecular weight distributions of the macromolecules in a sample.

SEC is based on the separation of a mixture based on the size of the components. The dissolved materials are pushed through the instrument's columns which are filled with materials

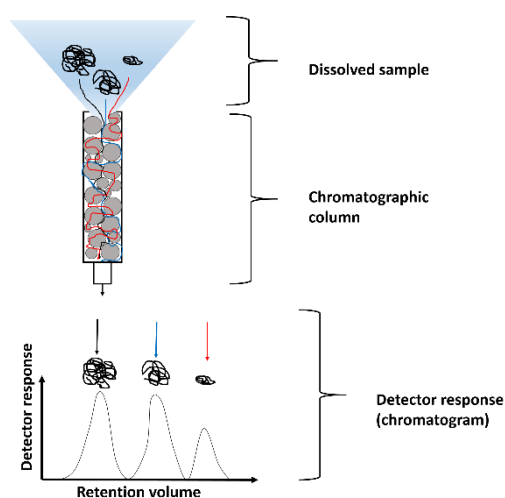


Figure 70: Schematic illustration of the separation mechanism in size-exclusion chromatography.

containing many pores (stationary phase). While passing through the column, smaller dissolved molecules flow more slowly because they can penetrate deep into many pores, whereas large dissolved molecules flow quickly because they interact in a minor extent with the pores. Consequently, larger molecules elute from the column sooner and smaller molecules later, which effectively sorts the molecules by size. As the components exit the column they are detected in various ways, and the elution behaviour of the sample is displayed in a chromatogram. For more clarity, the separating mechanism in a SEC is shown in **Figure 70**. Information on the

molecular weight of the samples are not obtained in a direct way. The conversion from the elution time, obtained considering a constant flow rate of the mobile phase, to the molecular weight of the sample is done by a calibration with standard polymers of known weight. In general polystyrene standards are used. Although SEC chromatography is a valid instrument to understand the nature of the synthesized materials, one has to take into account that it does not give reliable molecular weight values in the case of fullerene derivatives.[279,280]

It is known that the weight extracted from SEC experiments should be considerably lower than they really are. In their work, Gügel, Müllen and co-workers proposed that a correction factor of 2 – 4 has to be applied in order to obtain reliable molecular weight values from SEC data.[240] An empirical method to evaluate the number of repeating units in the macromolecule by using the SEC traces consists in counting the number of peaks identifiable in the chromatogram and considering that each additional peak at lower elution volume, correspond to the presence of an additional unit, as illustrated in **Figure 71**.

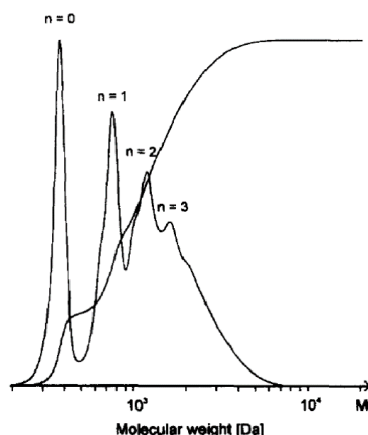


Figure 71: SEC chromatogram of oligo-fullerenes showing the empirical method to evaluate the number of repeating units in the macromolecules. Image reproduced from ref.240

The obtained chromatograms of the synthesized compounds showed that the syntheses led to products with variable molecular weights (

Figure 72), and range from oligomers to polymers. With exception for polyPCBM_F, which was obtained from a reaction in which the starting amount of PCBM was 3 g, all the compounds were obtained using 0.4 g of initial PCBM. The ratio between the reagents was the same for all the reactions (PCBM: bis-bromo-comonomer: CuBr: bipyridine, 1:1:2:4). It is also interesting to note that some batches of the materials show the presence of products that are eluted after 35.05 mL (PCBM retention volume).

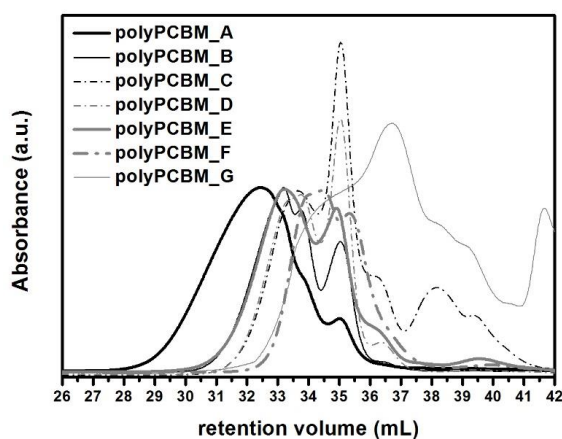


Figure 72: SEC chromatogram of polyPCBM_A-G in THF (30 °C, $\lambda=300\text{nm}$, with toluene as flow marker).

One can notice that in the elution diagrams of the materials, specific peaks are present and can be attributed to an integral increasing of the chain. Surprisingly, not all the samples present the same peaks even in the lower molecular weight region. The big differences that can be seen in the chromatogram denounce the high sensibility of the polymerization reaction towards CuBr purity and external agents such as impurities, water, oxygen that, despite the great attention used during the experiments, were probably present in some of the reaction mixtures. The obtained values for the molecular weight, as obtained from the instrument, and the dispersity are reported in **Table 3**. From this can be stated that particular care with handling of C₆₀ and PCBM with respect to oxygen and light, and great care with respect to the pre-cleaning of the CuBr are necessary to obtain a controlled reaction.

Product label	M _n (g/mol)	M _w (g/mol)	M _p (g/mol)	M _z (g/mol)	Đ
polyPCBM_A	2 410	4 130	3 040	6 720	1.71
polyPCBM_B	1 510	2 130	2 200	2 870	2.41
polyPCBM_C	80	1 070	720	2 260	14.18
polyPCBM_D	1 010	1 720	770	2 600	1.70
polyPCBM_E	810	1690	1860	2850	2.09
polyPCBM_F	710	980	980	1270	1.37
polyPCBM_G	330	880	500	1 670	2.71

Table 3: SEC-THF parameters against polystyrene standards. All the reaction have been conducted in the same condition with exception for polyPCBM which has been conducted using a larger amount of material (x 7.5).

As expected for the type of polymerization used to produce these materials, the recorded dispersities ($\text{Đ} = M_w/M_n$) are quite low. An exception is the case of polyPCBM_C for which the dispersity, 14.18, is impressively high. This result, together with the very low molecular weight of the sample, indicates a probable failure of the reaction.

Performing the aforementioned exercise of counting off oligomers and considering that the peak at around 35 mL represents PCBM and though, the peak that elutes straight before represents one bis-adduct, the one before a three-adduct and so on,[240] one could be able to determine the PCBM units incorporated in the chain. When we do this exercise, we find that the obtained macromolecules presents 4 - >8 PCBM units in the chain.

In order to better understand the reaction, the polycondensation was followed over time. Naphthalene was added as internal standard. Following the polymerization process by SEC for the first 6 h 30 min of reaction, allowed us to corroborate the assumption taken for the determination of PCBM units in the chain. As a matter of fact, in the elution graphs, reported in **Figure 73**, it can be seen how new species with higher molecular weights, are formed with time. The number of repeating units displayed in the image is indicative, but the shift of the curves towards lower retention volume values, shows the increasing in the molecular weight of the samples. In addition, the consumption of PCBM is indicated by the diminishment with time of the peak at around 35 mL of retention volume. However, from the obtained results, this reduction does not seem to be constant with time.

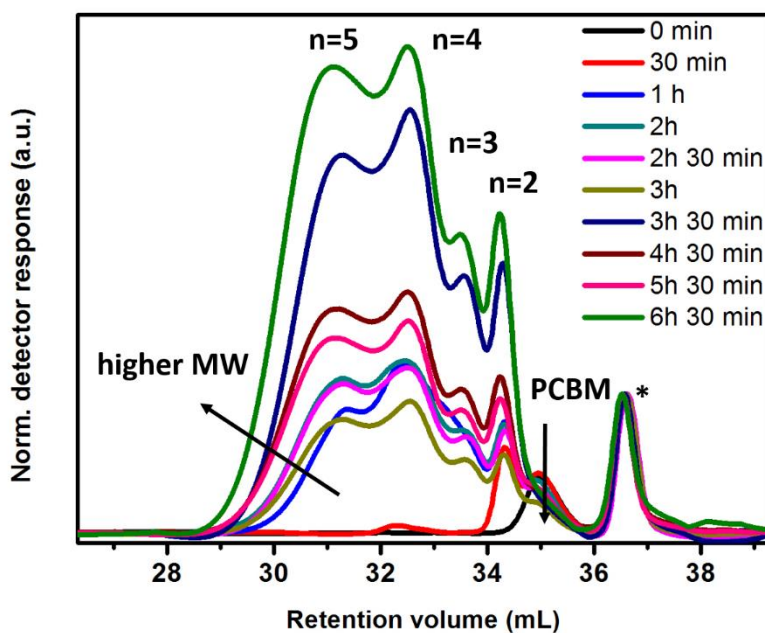


Figure 73: SEC chromatograms showing the evolution of molecular weight and composition of the reaction mixture with time for the synthesis of polyPCBMs via ATRAP polymerization.

In this work, only the analyses of two selected macromolecules are presented and discussed. This allows to investigate the property of oligo- and polyPCBM. Indeed, the two selected products differs in their molecular weight. The first one, polyPCBM_A, presents the highest molecular weight obtained while the second, polyPCBM_F, has a modest molecular weight.

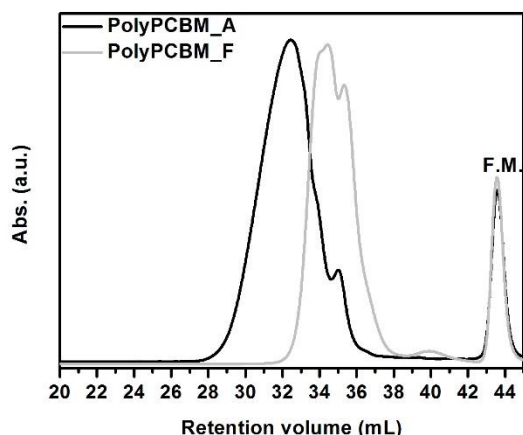


Figure 74: SEC chromatogram (THF, 30 °C, $\lambda=300\text{nm}$, toluene flow marker) of polyPCBM_A and polyPCBM_B

The SEC chromatograms of the two selected materials are shown in **Figure 74**. In the chromatograms, the signal for toluene (retention volume ~ 43 mL), used as a flow marker, is shown. The two curves are broad and have quite different shapes. PolyPCBM_A presents a shape which is typical for polymers, while polyPCBM_F curve is more multimodal. The deconvolution of the two curves in different contributions is shown in **Figure 75**. The curves have been fitted with Gaussian distributions only with the purpose to show the complexity of the systems. However, if one calculates the contribution of the PCBM peak by comparing the area under the curves, and if one accepts the hypothesis that the absorbance are proportional to the PCBM content in the samples, some indicative values can be obtained. Importantly, it can be concluded that PCBM contributes to polyPCBM_A to the extent of 3% while the percentage drastically increases to 35% in polyPCBM_F.

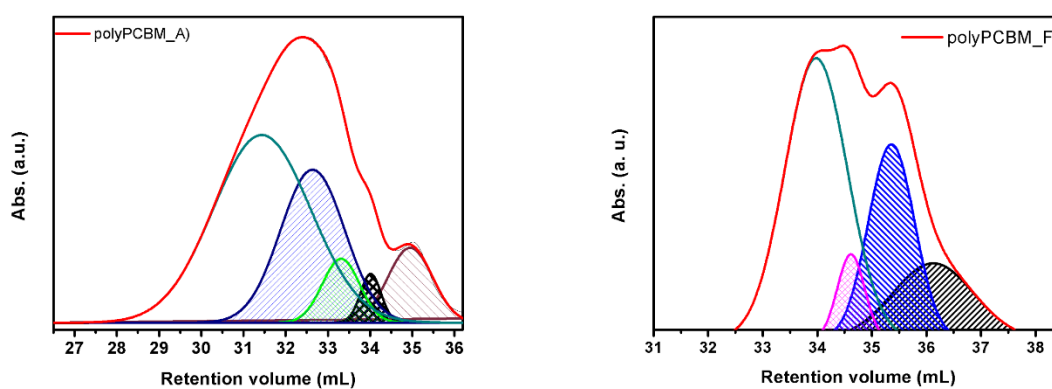


Figure 75: Deconvolution of SEC chromatograms of polyPCBM_A and polyPCBM_F with Gaussian functions.

2.2.2 Nuclear magnetic resonance (NMR)

Thanks to good solubility of the compounds, both chloroform-*d* (CD_3Cl) and benzene-*d*₆ (C_6D_6) were used as solvents to prepare the NMR samples. Nonetheless, the materials were dissolved in the solvent with the help of a low-power sonication bath to ensure a better dissolution and to reach the higher possible concentration (in general around 30 mg/mL). In order to obtain good spectra from the analyses, long acquisition times that could extend over 24 h in the case of 2D experiments, and extended number of cycles were required for both proton and carbon signals. The ^1H -NMR of polyPCBM_A and polyPCBM_F were recorded in benzene-*d*₆ and are displayed in **Figure 76a** together with the proton NMR of PCBM, recorded in the same conditions, for comparison. A magnification of the spectra in the range between 3.4 and 4.9 ppm is also reported (**Figure 76b**) to underline the differences in the structure of the two synthesized products with respect to commercial PCBM. In particular, three peaks, although they are very broad and low in intensity, are found at around 3.75, 4.07 and 4.45 ppm in the spectra of the first two products and are not found in the PCBM spectrum. The signals in this range of chemical shift also show that the structure of polyPCBM_A and polyPCBM_F are similar. The main difference is in the width of the signals. While the signals in polyPCBM_F are quite sharp, passing to polyPCBM_A the peak in the ^1H -NMR are broader.

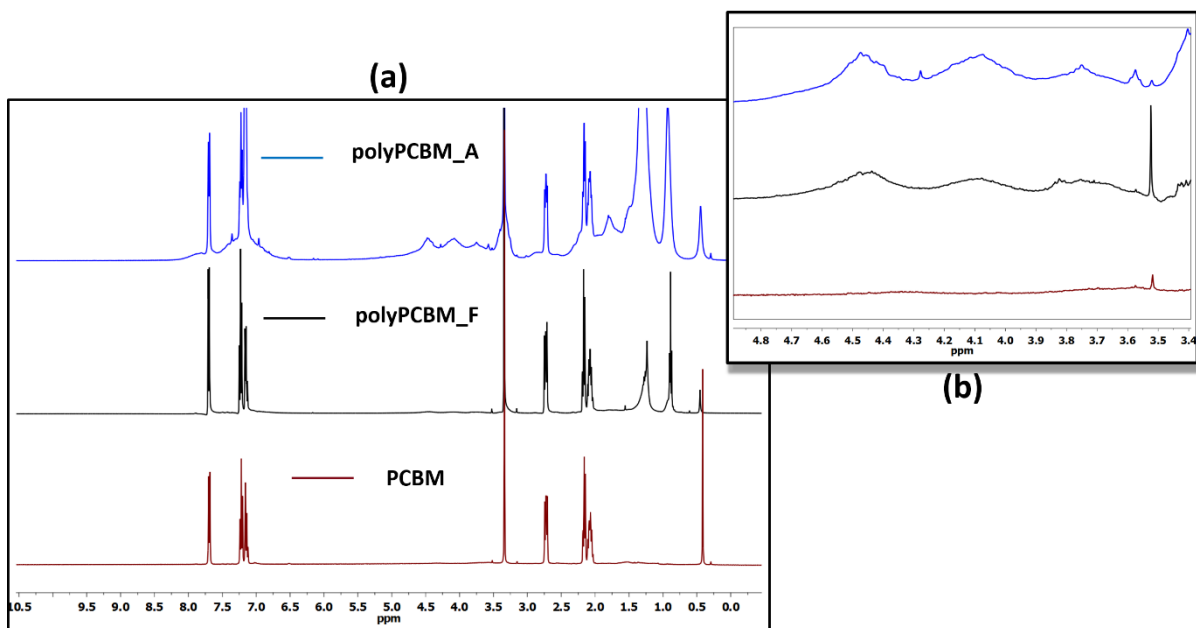


Figure 76: (a) ^1H -NMR of (red) PCBM, (noir) polyPCBM_F and, (blue) polyPCBM_A; (b) magnification of ^1H -NMR spectra in the range 3.4-4.9 ppm.

This similarity in the structures of the compounds is also confirmed by the ^{13}C -NMR spectra in **Figure 77**. It is to be noticed that in the case of carbon NMR, the main differences are found in the region between 4 and 42 ppm. Considering the expected molecular structures, one would expect to find differences also in the region between 40 and 120 ppm where the carbon-NMR signals for the $-\text{O}-\text{CH}_2-$ groups, the $-\text{CH}$ aromatics and the $-\text{CH}_2\text{Br}-$ of the co-monomers should appear.

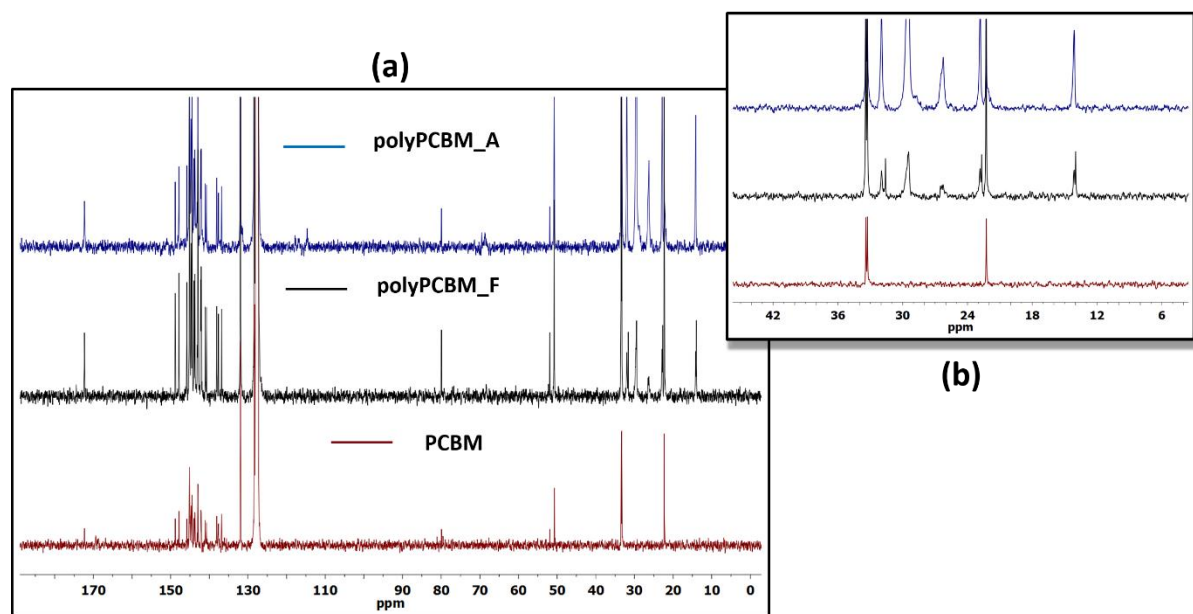


Figure 77: ^{13}C -NMR of (red) PCBM, (noir) polyPCBM_F and, (blue) polyPCBM_A; **(b)** magnification of ^{13}C -NMR spectra in the range 4-45 ppm.

As said, the peaks are not well resolved in the ^1H -NMR spectra, and are more in the form of broad signals typical for polymers, and fullerene oligomers at much high concentration where aggregation can occur. Nonetheless, one can recognize the characteristic peaks reported in literature for similar systems. In particular, according to published works, the $-\text{CH}_2-$ groups linked to the fullerene should result in double doublets, one located at 4.0 and the other at 4.4 ppm. These two signals are found, in our cases, at 4.07 and 4.45 ppm. Moreover, the broad signal at 3.75 in the spectra of polyPCBM_A and polyPCBM_F, can be assigned to the α -protons in the alkoxy groups of the comonomers. 2D-NMR of correlation have been obtained with HSQC experiments in the same condition used to measure the ^1H and ^{13}C NMR spectra. In the HSQC spectra of the two materials, one can find confirmation of the prior attributions for the different signals. In particular, two distinct correlation pairs (4.17;42.83) and (4.78;42.96), labelled **a** in **Figure 78**, are due to the $-\text{CH}_2-$ groups linked to the fullerene cage, as said in the discussion for

the proton NMR spectra; these correlations are more evident for polyPCBM_A. Furthermore, the extended correlation pairs that is found from 3.5 up to 4.0 ppm for proton NMR, with a carbon signal at around 69 ppm (**c**), is attributed to the signals due to $-CH_2-$ in α -position to the alkoxy groups. Other correlations that are found in the spectra are due to the aromatic protons and the carbons on the hexagon rings of the comonomer (**b**, 6.82;114.88 and 7.30;117.45). The reader will notice a correlation signal at 4.41;28.63. This correlation pair corresponds to the $-CH_2Br$ groups on the comonomer at the chain-end.

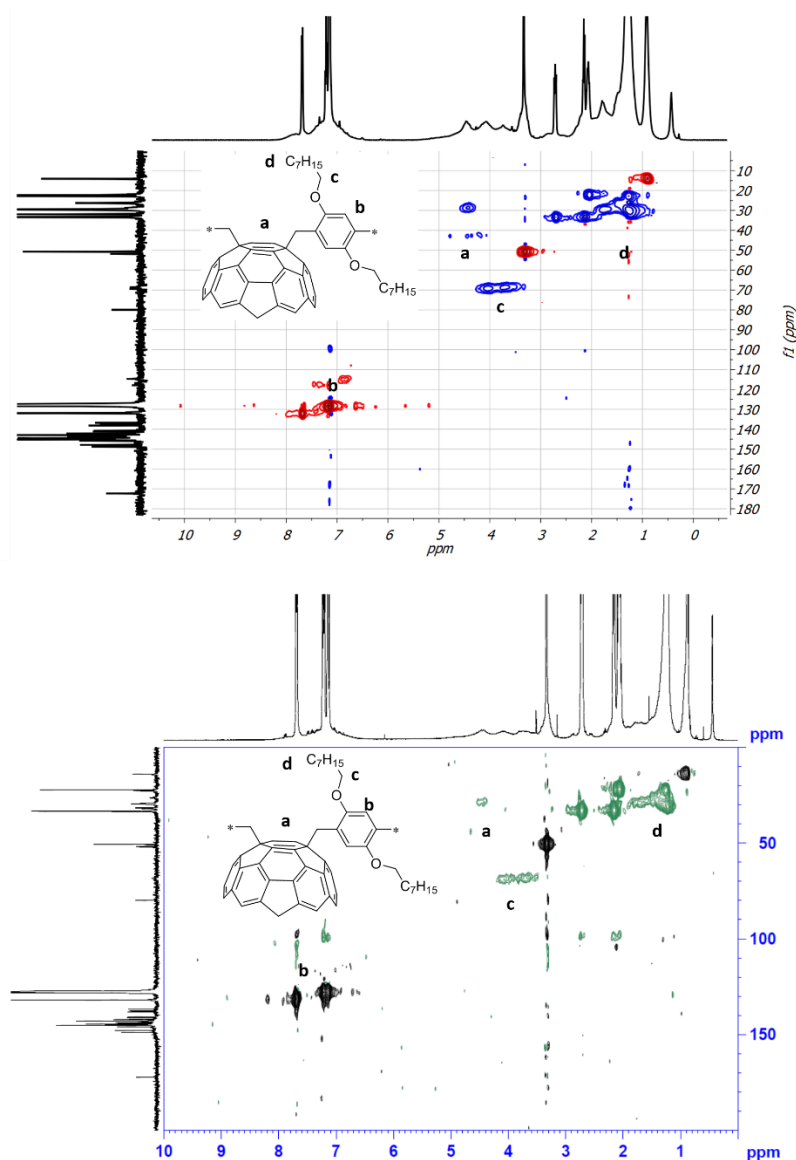


Figure 78: 2D-NMR HSQC spectra of (top) polyPCBM_A and, (b) polyPCBM_F.

In common between polyPCBM_A's and polyPCBM_F's spectra is the presence of sharp peaks due to PCBM structure. Diffusion-ordered spectroscopy (DOSY) is a valid instrument to distinguished between the contribution of the different molecules in the sample. DOSY spectroscopy, which seeks to separate the NMR signals of different species according to their diffusion coefficient, has been used to better understand the composition of the synthesized products. The spectra are reported in **Figure 79**. The ^1H -NMR spectra are reported on the top of each image, while the intensity of the signals correlated to each diffusion coefficient are displayed on the right.

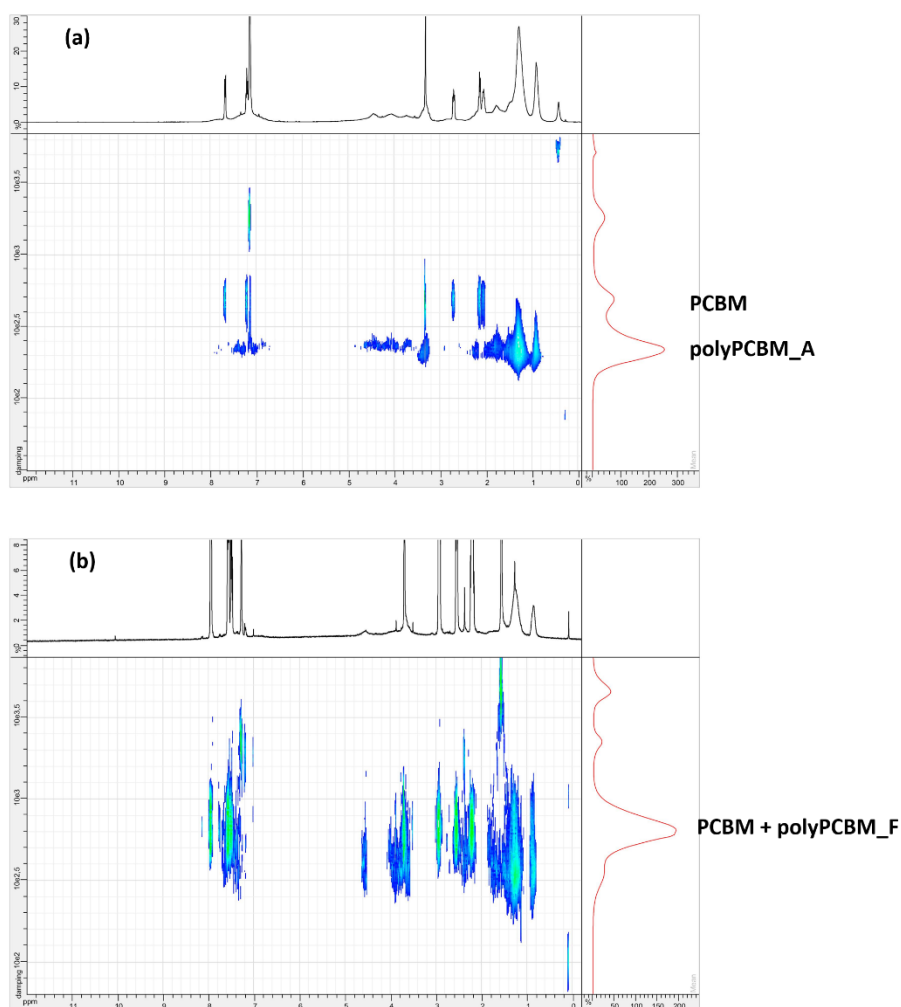


Figure 79: DOSY-NMR spectra of (a) polyPCBM_A and, (b) polyPCBM_F.²

² Nonessential, in the spectrum of polyPCBM_A, one can find clear signals for silicon grease (around 0 ppm) and benzene (7.16 ppm), while in the spectrum of polyPCBM_F, both acetone (1.55 ppm), and benzene (7.16 ppm) are found.

In **Figure 79a**, two different traces are evident for PCBM and for polyPCBM_A, indicating that the two compounds actually coexist in the synthesized product. This is not the case in **Figure 79b** where the traces are broader and it is difficult to discern between the two different components. This is indicative also of the fact that, while the diffusion coefficients of PCBM and polyPCBM_A, and though the molecular weight of the two compounds, are considerably different, PCBM and polyPCBM_F have diffusion coefficient values close to each other corroborate the results obtained from SEC analysis and the $^1\text{H-NMR}$ spectra.

2.2.3 Thermogravimetric analysis (TGA)

The thermal degradation profile of the two compounds have been obtained via thermogravimetric analysis (TGA). The recorded thermograms are shown in **Figure 80** together with their first derivative (DTG) in dot lines. In **Figure 80c** also the thermogram of PCBM, recorded in the same conditions, is displayed for comparison.

We first compare the thermogram for PCBM and polyPCBM_F that, according to NMR and SEC results, presents a high content of its parent PCBM.

The thermal degradation profiles of polyPCBM_F, is very similar to that of PCBM. However, the first two weight loss steps are at slightly higher temperatures for the polymeric material. In both cases the two steps account for a weight loss of about 1%. These weight losses can be associated with the loss of residual solvent contained in the crystalline structure of PCBM.[281] This type of residual solvent in the crystalline structure is not exclusive of fullerene derivatives and has been reported by Tung *et al* [282] for polyaniline (PANi) crystallite.

The third step of the thermograms represents the degradation step for the investigated compounds. The onset of the third weight loss step is 380 °C for PCBM, and 379 °C for polyPCBM_F. This is consistent with the release of C_{60} -links reported by Pozdnyakov *et al.*[283] and can be related to the cleavage of the link $\text{C}_{60}\text{-C}_{\text{comonomer/substituent}}$.

The thermal stability of methylene bonds on C_{60} , at least those of polystyrene, can be low but vary greatly depending on the size of the addend and the number of additions around the sphere. Pozdnyakov *et al.* studied the degradation of polystyrene stars with a C_{60} core and observed the release of styrene at around 350 °C. This temperature which is about 100 °C lower than the normal depolymerization temperature for polystyrene. To explain the differences in temperature

a decomposition mechanism that follows a partial depolymerization of each PS arm induced by the radical produced by the breaking of its terminal ‘weak’ PS-C₆₀ bond has been proposed. This interpretation is also in agreement with the work of Mathis and co-workers, [235,284] as well as with the work of Audouin *et al.* [285] where they found that the link between C₆₀ and a polystyrene chain is weaker than the carbon-carbon bond in the PS chain, for their case.

For polyPCBM_F, we can conclude that the weight loss that started 379 °C is actually due to the decomposition of the chemical structure of phenyl-butyric acid methyl ester in PCBM. This process is concomitant with a second decomposition, probably involving the comonomer (bis(octyloxy)benzene), as it is suggested in **Figure 81** where the first derivatives of the thermal degradation profiles of PCBM and polyPCBM_F are compared. The reader can observe how more local maxima are present in the range of interest (320-440 °C) in the case of the degradation of polyPCBM_F suggesting the loss of a higher number of segments.

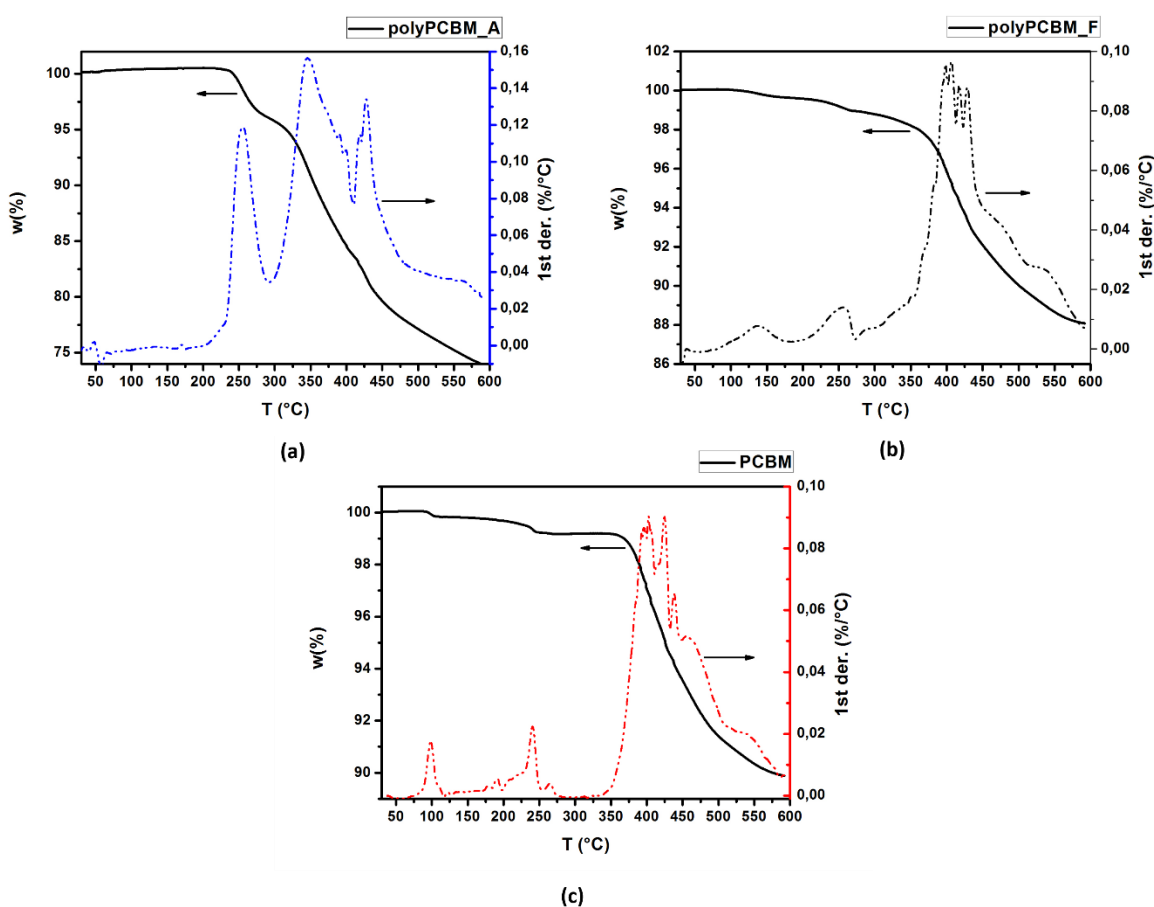


Figure 80: TGA/DTG studies (a) polyPCBM_A, (b) polyPCBM_F and (c) PCBM. For this analysis, a temperature rate of 10 K min⁻¹, from 30 °C to 600 °C, has been applied to the samples in N₂ atmosphere.

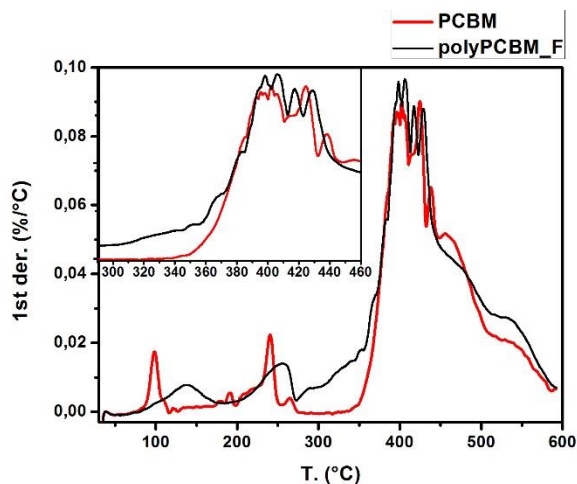


Figure 81: comparison between the TDG of (red) PCBM and (black) polyPCBM_F.

We discuss now of the thermal degradation profile of polyPCBM_A. Despite it presents comparable decomposition temperatures, the thermodegradation profile of polyPCBM_A (**Figure 80a**) differs remarkably from the above discussed thermograms. The weight loss at 250 °C, attributed to enclosed solvents, is more important in this case. Besides, the decomposition step that starts at around 350°C counts for the 20% of the total weight loss. This value is far from the 10 % (polyPCBM_A) and 9% (PCBM) weight loss of the other compounds in the same range of temperature. The reasons for these differences have probably to be searched in the higher content of polymeric material in polyPCBM_A with respect to polyPCBM_F and obviously, the PCBM sample.

2.2.4 Differential scanning calorimetry (DSC)

Differential scanning calorimetry (DSC) is a technique that permits to analyse the thermal behaviour of the materials during heating and cooling cycles or under isothermal treatment in controlled atmosphere. DSC measurements were performed for polyPCBM_A, polyPCBM_F and PCBM.

Taking into consideration the very close thermodegradation profile of polyPCBM_F and PCBM, the two compounds have been analysed using the same experimental conditions. From room temperature, they first were heated up to 320 °C before being cooled down to -40 °C. The heating entire cycle has then been repeated once more. An isothermal program of 5 minutes has been

applied at the end of every segment of each cycle. The DSC curves for PCBM and polyPCBM_F are shown in **Figure 82**. The PCBM curves are consistent with the data in literature.[286] The only difference is that the endothermic peak at 247.6 °C (10.7 J/g) is found also in the second heating cycle at 240.4 °C (1.15 J/g). The temperature of this transition is close to the one of the second weight loss step in the TGA diagram and is attributed to the evaporation of residual solvent in the PCBM crystalline structure as already mentioned. During the first heating (**Figure 82a**), polyPCBM_F presents an exothermic transition at 192.8 °C (3.6 J/g) and a large melting peak transition at 272.1 °C (13.9 J/g). While the first transition seems to be irreversible, the second one is partially reversible and a smaller melting peak is found again at 278 °C (1.276 J/g), as one can observe in **Figure 82c**. The interpretation of the irreversible melting is still under discussion: it could be due (i) to a concomitant degradation of the material, even if the TGA diagram shows a degradation onset only from about 379 °C and not before, or (ii) to the fact that the cooling rate is too fast to allow a proper recrystallization of the compound. In the second heating cycle of polyPCBM_F, also a glass transition is found at 136°C.

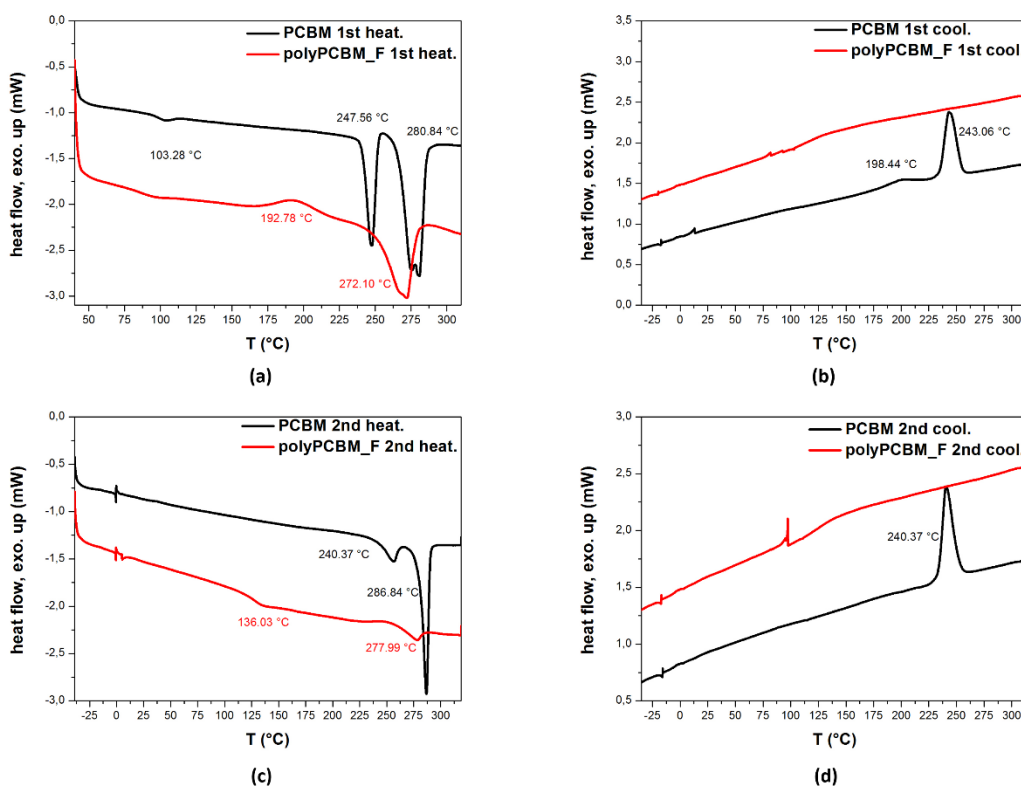


Figure 82 : DSC thermograms, solid samples in aluminium crucibles at a heating/cooling rate of 10 °C min⁻¹ under a flux of N₂ maintained at 20 mL min⁻¹, for (black) PCBM and (red) polyPCBM_F in the -40 to 320 °C temperature range; (a) first heating ramp, (b) first cooling ramp, (c) second heating ramp and, (d) second cooling ramp.

In the case of polyPCBM_A, a different temperature program was chosen. Taking into account the TGA graph of polyPCBM_A, we have chosen to limit the upper temperature to only 200°C. Although the weight loss at 250 °C (**Figure 80a**) is attributed to the evaporation of incorporated solvents and not to the degradation of the macromolecule itself, its magnitude is large enough to possibly disturb the DSC analysis. As shown in **Figure 83**, even if an order-disorder reorganization seems to take place during the first heating, no thermal activated transition is detected between -40 ° and 200 °C in the second heating/cooling cycle for polyPCBM_A. This material is in a stable phase at the considered temperature range.

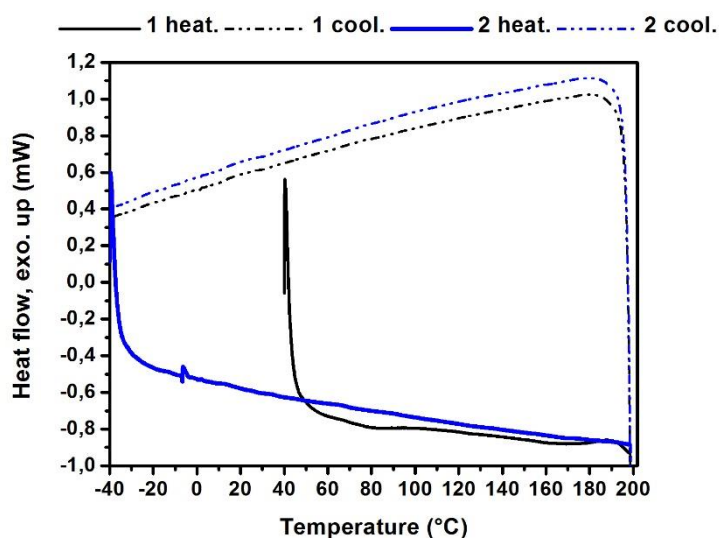


Figure 83: DSC thermograms for polyPCBM_A in the -40 to 200 °C temperature range.

2.2.5 UV-visible optical spectroscopy

The absorption properties of a material are very important to complete their characterization, and it is even more important when the material is designed for photovoltaic applications. The capacity of absorption of the materials, especially in the visible region, will actually have an impact on the device efficiency as discussed in paragraph 1.2.1.

The application of UV-visible spectroscopy is then an easy and direct way to obtain those information. Moreover, in fullerene chemistry, UV-VIS spectroscopy has proven itself as an efficient tool to characterize fullerene multi-adducts.[279,287] For instance, fullerene 1,4-bisadducts and fullerene 1,2-bisadducts exhibit two different absorption properties. While the first show a broad absorption around 440 nm, the second results in the presence of a sharp

absorption at lower wavelengths (400 nm). Interestingly, the comparison between the absorption spectra of PCBM and polyPCBM_F, in **Figure 84**, is inconclusive. As one can remark, the two spectra are identical. This disappointing result can in part be justified by the great amount of PCBM still presents in polyPCBM_F mixture. A different hypothesis can be that the symmetry of PCBM is not much perturbed by the functionalization in polyPCBM_A. For instance, Liu *et al.*[288] reported the synthesis of dumb-belled PCBM derivatives in which the fullerene core of PCBM, and though its symmetry, was not perturbed. The UV-visible spectra of the resulting derivatives have similar shape with the sharp peak at 430 nm characteristic for C_{2v} symmetry of PCBM.

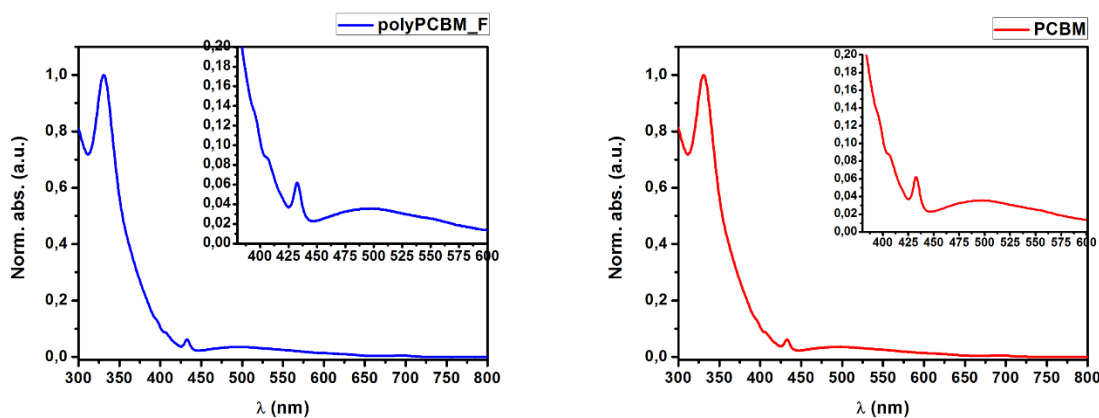


Figure 84: Measured UV-VIS optical absorption spectra for (red) PCBM and (red) PCBM with the respective expansion in the 350-600 nm range.

2.2.6 X-ray photoemission spectroscopy

As discussed in paragraph 1.2.6.1 of this manuscript, X-ray photoemission spectroscopy (XPS) is sensitive to the composition and the chemical nature of the samples, giving insight in the chemical structures of the materials. With this in mind, we prepared thin films of PCBM and polyPCBM_F via doctor blade deposition from solution in o-xylene on ITO-coated glasses for XPS analysis. In **Figure 85** the overview spectra for the two materials are shown. The intensity of carbon and the oxygen core level signals could be used to analyse the stoichiometry of the materials, but the quantitative analysis reveal some deviations from expected results. In **Table 4** the obtained results are summarized.

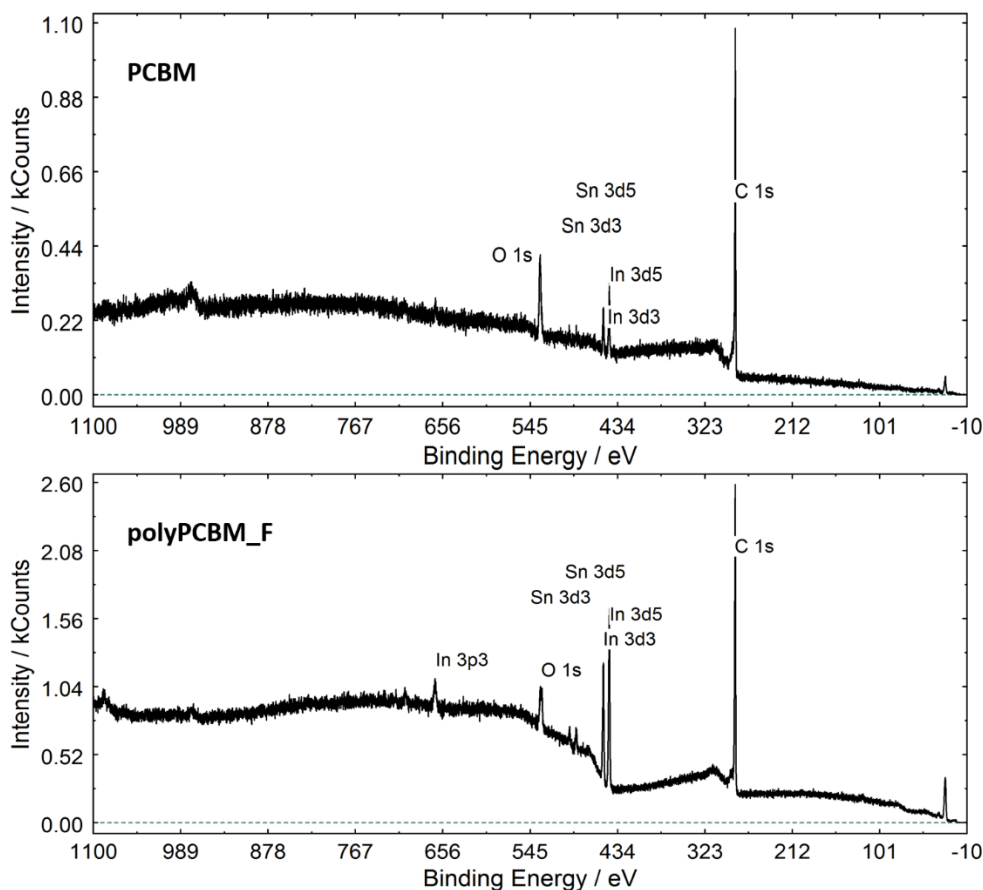


Figure 85: XPS overview spectra of (top) PCBM ad, (bottom) polyPCBM_F films on ITO-coated glass substrates.

Peak	PCBM		polyPCBM_F	
	<i>expected³ conc. (%)</i>	<i>Experimental conc. (%)</i>	<i>expected conc. (%)</i>	<i>Experimental conc. (%)</i>
C1s	96.43	87.47	94.69	84.55
O1s	3.57	12.53	5.31	15.45
O1s*	3.57	11.17	5.31	9.12

Table 4: Relative concentration of carbon and oxygen in PCBM and polyPCBM_F obtained via XPS analysis. * value obtained subtracting the contribution of ITO determined by O1s peak fitting.

A possible reason for the observed deviation is the low thickness or surface inhomogeneity of the samples, In 3d and Sn 3d signals of the substrate are still visible in the spectra. In particular, this imply that the oxygen present in the ITO, contribute to the overall oxygen core level signal of the

³ Value calculated from the chemical structure of the compound.

samples. Therefore, a peak fit analysis of the oxygen core signals seems to be necessary to analyze the atomic composition of the two compounds. As shown in **Figure 85**, at least four different components are necessary to describe the oxygen signals for both compounds.

The O1s spectrum of PCBM sample (**Figure 86a**) shows two distinct oxygen species which correspond to the two different oxygen binding sites in PCBM. The two components have almost equal intensity (an equal intensity is expected from the molecular structure). The component (**c**) at 531.8 eV is attributed to the oxygen in the carbonyl group while the signal at 532.9 eV (**d**) is generated by the oxygen in the methoxy group. The two remaining signals are attributed to the substrate.

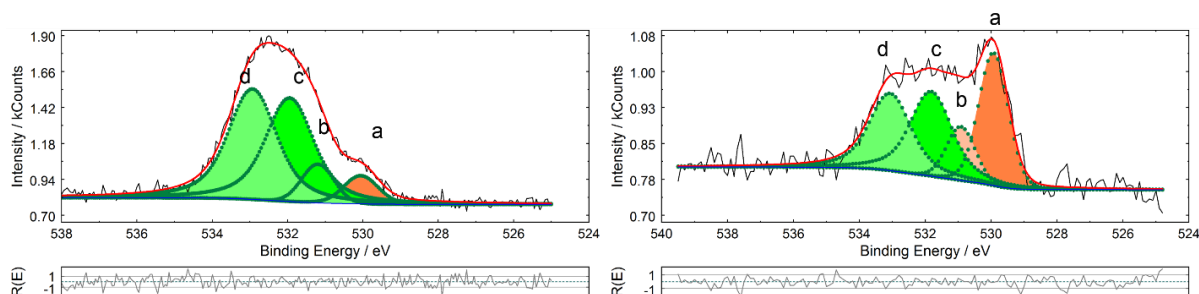


Figure 86: Oxygen O1s peak of (left) PCBM and (right) polyPCBM_F.

In the O1s spectrum of polyPCBM_F (**Figure 86b**), the same components are found, but their relative intensity is different to PCBM. The two signals attributed to the two oxygen binding sites of the PCBM structure are again very close in intensity; however, now the signal at 531.8 eV is more intense than the one at around 533.0 eV. Moreover, there is an increase in the signal at 529.9 eV that results more than 2 times greater than the signals b and that is due to the higher intensity of the substrate's signals. Considering the structure of the two compound, here reported in **Figure 87**, it is expected that also the contribution of the oxygen in the linked comonomer structure plays a role in these differences. The obtained values for the O1s core spectra are reported in **Table 5**. Looking at the obtained results, the relative intensity of the oxygen components are not the expected ones and contamination can't be excluded.

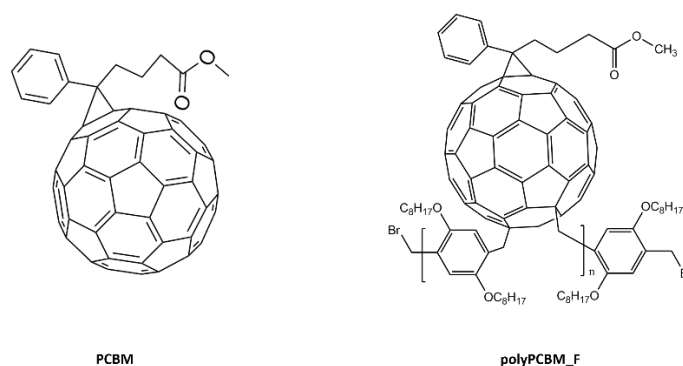


Figure 87: Chemical structure of PCBM and polyPCBM_F.

Peak label	PCBM		polyPCBM_F	
	Position (eV)	Relative intensity (%)	Position (eV)	Relative intensity (%)
a	529.9	5.45	529.9	29.6
b	530.9	5.4	530.9	11.39
c	531.8	43.46	531.8	30.83
d	532.9	45.69	533	28.19

Table 5: Relative intensity of the oxygen O1s peak components for PCBM and polyPCBM_F.

2.2.7 Matrix Assisted Laser Desorption/Ionization - time-of-flight mass spectrometry (MALDI-TOF)

Considering the observed properties for polyPCBM_A, this polymeric material represents an encouraging results towards a further studies and developments of this class of compounds. A better understanding of the structure of this compound is then crucial. An attempt to obtain this desired knowledge has been performed using MALDI-TOF spectrometry. The fragmentation spectrum is reported in **Figure 88** with a magnification in the region between 1014 and 3900 m/z. Although this spectroscopy has been successfully used to characterize fullerene derivatives, in recent times it has been shown that this technique can also result in further reactions between the radical species formed by the incident beam and in the formation of new species in the analysis samples. For instance, Bottari *et al.* carried out MALDI experiments with monofunctionalized fulleropyrrolidines, which revealed the formation of bisadducts that were not present in the samples.[289] The authors concluded that consequently to this discovery, the establishment of the number of ligands attained on a fullerene, and though of the structure of the

derivative, based exclusively on the MALDI experiments, has to be taken with caution. Nonetheless, an interpretation of the mass spectrum data have been proposed. A first element to notice, is that a peak at 720.6 m/z, corresponding to C₆₀, is present in the mass spectrum meaning that the analysis conditions are capable of fragmenting the PCBM structure which signal is also present (910.1 m/z).

The interpretation of the mass spectrum is not straightforward and is not definitive. Signals corresponding to one comonomer linked to one PCBM (1270.3 m/z), twice substituted PCBM (1630.5 m/z) and twice substituted C₆₀ (1441.3) can be found. More interestingly, some of the fragmentation peaks are compatible with structures in which the linker between two fullerene cores is not composed by one comonomer but two (**Figure 89**). For instance the higher molecular weight fragment found in the analysis, is compatible with the structure reported in **Figure 89b**. Due to the mechanism involved in ATRAP polymerization, the possibility that radical methylene are co-terminating is very low as the number of active sites at any moment during the reaction is tiny. So, if the detected fragments actually present the discussed methylene-methylene link, these products are more likely produced during MALDI-TOF analysis.

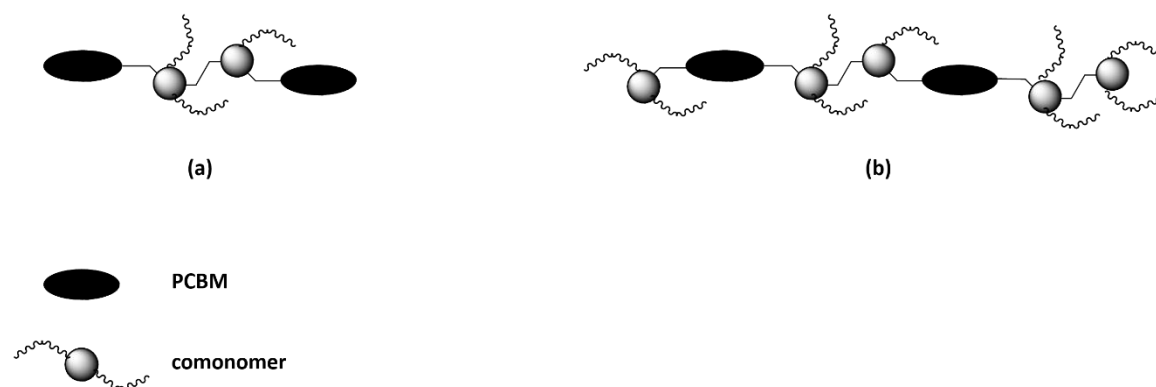


Figure 89: Schematic representation of (a) fragmentation product with two comonomers as linker between the two PCBM and, (b) structure compatible with the higher molecular weight fragment in the mass spectrum of polyPCBM_A.

2.3 Synthesis and characterization of poly-C₆₀-pyrrolidine

In this section, we present the synthesis of novel main-chain polyfullerenes based on the azomethine ylide cycloadditions to fullerene (C₆₀) that have been discussed in section 1.1.1.1. Due to their facile nature and adaptability to numerous groups, these types of cycloadditions have provided pyrrolidinofullerenes of interest for photovoltaics, organic-electronics, medicine and molecular machines.

The scheme for the synthesis of the polymers is shown in **Figure 90**. As one can see, three different co-monomers, namely terephthalaldehyde (**6**), 2,5-bis(octyloxy)terephthalaldehyde (**5a**) and, 2,5-bis(dodecyloxy)terephthalaldehyde (**5b**), have been employed in the reactions. The synthesis of the monomers have been discussed in section 2.1.

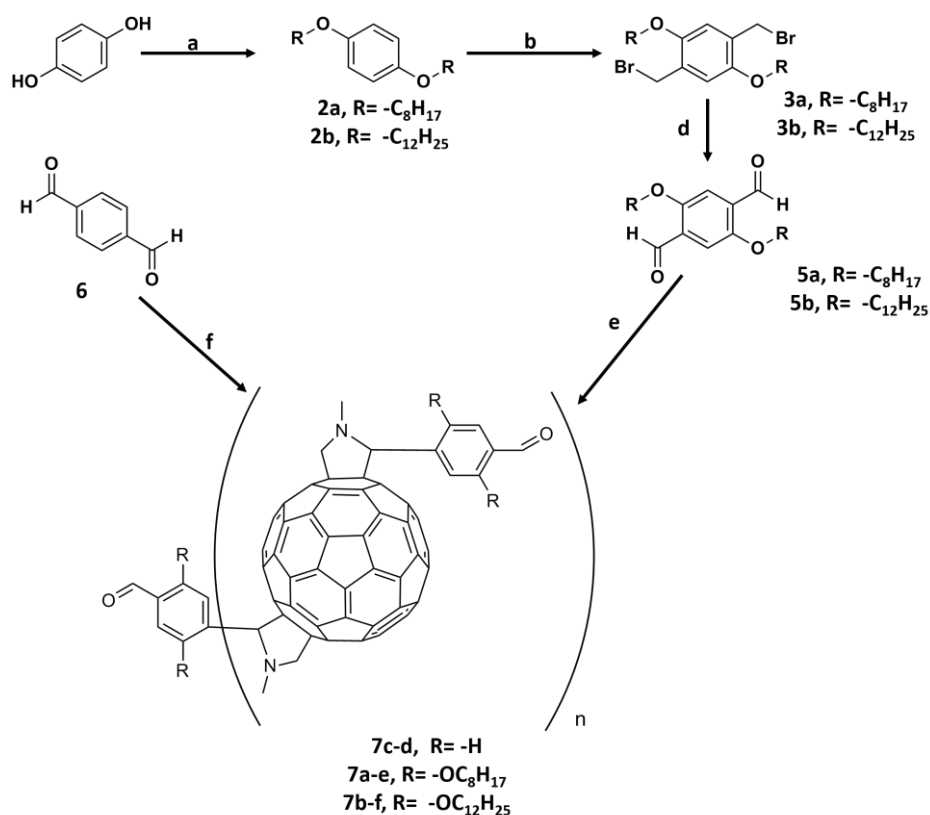


Figure 90: Syntheses of the oligo- and poly- main-chain poly(fulleropyrrolidines). **a-2a**) 1-bromooctane, K₂CO₃, **1**, acetonitrile; **a-2b**) 1-bromododecane, K₂CO₃, **1**, acetonitrile; **b-3a**) {CH₂O}, acetic acid, **2a**, HBr; **b-3b**) {CH₂O}, acetic acid, **2b**, HBr; **d-5a**) NaHCO₃, **3a**, dimethyl sulfoxide; **d-5b**) NaHCO₃, **3b**, dimethyl sulfoxide. **e**) C₆₀, N-methylglycine, **5a**, toluene or DCB, respectively, for **7a**, and **7e**; C₆₀, N-methylglycine, **5b**, toluene or DCB, respectively, for **7b** and **7f**. **f**) C₆₀, N-methylglycine, **6**, toluene or DCB, respectively, for **7c**, and **7d**.

In order to maximise bis-additions so that high molar mass polymers could be formed, the reagents were mixed at absolute ratios, i.e., **6** or **5a** or **5b** : C₆₀ : *N*-methylglycine, respectively, at 1:1:2. Moreover, to attain high molar masses, it was expected that long reaction times (i.e., *ca* 18 h) would be required. Two extreme sets of conditions were employed to better understand the reaction, namely: (i) toluene, 110 °C, and *ca* C₆₀ 0.91 mg toluene mL⁻¹; or (ii) 1,2-dichlorobenzene (DCB), 150 °C, C₆₀ 20 mg DCB mL⁻¹. The concentrations were chosen as the highest possible without risking fullerene precipitation. The reaction conditions for the synthesized materials are reported in **Table 6**.

Label	Co-monomer	Solvent	Temp. (°C)	Yield (%)
PPC1-7c*	6	toluene	110	37.5
PPC2-7d*	5a	o-DCB	150	30
PPC3-7a*	5b	toluene	110	40.6
PPC4-7e*	6	o-DCB	150	57.5
PPC5-7b*	5a	toluene	110	42.3
PPC6-7f*	5b	o-DCB	150	35

Table 6: reaction conditions for poly(fulleropyrrolidines). * with reference to **Figure 90**.

It is known that the removal of C₆₀ from macromolecules can be troublesome. An alternative to the Soxhlet treatment could have been the use of repeated reprecipitations from chlorobenzene into hexane. Unfortunately, this intensive manipulation risked invoking chain-crosslinking through oxygen-bridge formation with air[37] and 2+2 cycloadditions with light.[38] So for the purification of the synthesized materials Soxhlet was performed with hexane. Light and oxygen were excluded. While with this technique all C₆₀ was removed from **PPC5 (7b, in Figure 90)**, traces are observable in **PPC1 (7c)**, **PPC3 (7a)**, **PPC4 (7e)** and **PPC6 (7f)** in the order of 3%, as estimated from integration over SECs performed at 300 nm. Moreover, residue of the order of 47 mol% of C₆₀ could not be removed from **PPC2 (7d)**. This would suggest a trapping of C₆₀ in a crosslinked matrix.

2.3.1 Size-exclusion chromatography (SEC)

The synthesized materials have been analysed by SEC chromatography. As one can see in **Figure 91**, the elution graphs of **PPC1-6** show an increase in molecular weights with the increasing size of the comonomer chains, whether the reaction is in toluene (**Figure 91a**) or in DCB (**Figure 91b**).

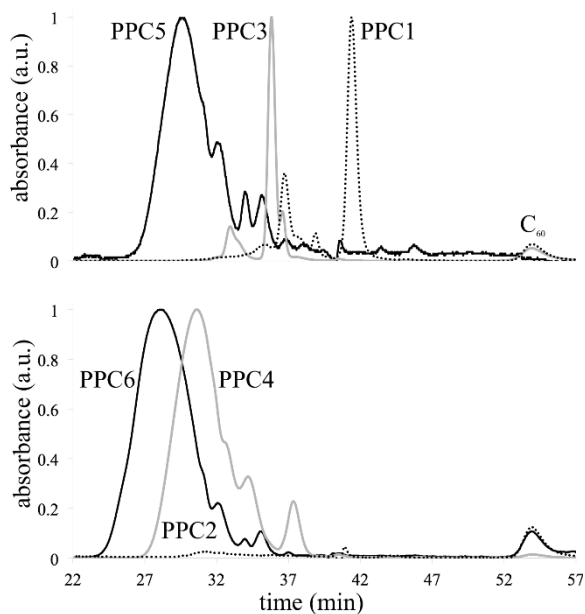


Figure 91: SECs of OPCs and PPCs (THF, $\lambda = 300$ nm): a) from toluene 110 °C; and b) from DCB at 150 °C.

From these results, we can conclude that the choice of the comonomer has a great role in determining the molecular weights of the final products: the greater the bulk of the comonomers, the more effective the blocking of multiple attacks on the fullerene and the reduced number of cross-links. **PPC1** and **PPC2**, made with small comonomers, show weak signals in the column – due to their low solubility. This is a strong indicator of their cross-linked nature. Furthermore, their low molar masses, high dispersities and multi-modal curves indicate reactions limited by cross-linking and precipitation. Turning to poly[fullerene-alt-(1,4-bisformyl-2,5-bisocetyloxybenzene)] (**PPC3** and **PPC4**), made with sterically larger comonomers, there is a clear increase in mass. In this case, while cross-linking cannot yet be ruled out, it is no longer present enough to dominate the solution properties of the material. This effect is further strengthened when considering **PPC5** and **PPC6**, made with the most cumbersome comonomers. **Table 7** brings together values from SECs shown in **Figure 91**.

Polymer	Condition set ^a	$M_w^{[b]}$ (g mol ⁻¹)	$\bar{D}^{[b]}$	M_p (g mol ⁻¹) [repeating units] ^[c]
PPC1	i	820	4.4	900 [1]
PPC2	ii	1850	9.8	8000 [12]
PPC3	i	3360	1.1	5850 [5]
PPC4	ii	4640	2.2	15200 [13]
PPC5	i	4630	1.7	19100 [15]
PPC6	ii	10840	1.9	24300 [19]

Table 7: Molecular characteristic of the materials studied. Notes: [a] i = refluxing toluene; ii = o-dichlorobenzene, 150 °C; [b] SEC (polystyrene standards, THF, 30 °C, UV 300 nm); and [c] most probable M_p by deconvolution of SEC curves.

As already discussed for the SEC results for polyPCBMs (paragraph 2.2.1), the normal polystyrene-based calibration is SEC analysis, is inadequate for these polymers: C₆₀ elutes extremely late from the column, as shown by peaks at ca 54 min, 13 min after the toluene marker. Thus, the values in **Table 7** severely underestimate the actual value for the molar masses of the polymers. Also in this case, the approach used by Müllen and co-workers,[240] leads to a better, if approximate, estimation. According to this method, the estimation is made by inspecting the number of peaks from right to left in the SEC curves and assuming that each is due to an integral number of repeating units. Once discrete peaks are no longer discerned then, by definition, a polymer has been attained.[290] In addition to the influence of the co-monomer hindrance, discussed above, we have noticed that also using high concentrations and high temperatures can increase the molecular weights. For instance, according to the SEC measurements, **PPC3** and **PPC4** present M_p of around 5850 and 15200 g mol⁻¹ respectively. The former, made in toluene, has a growth inhibited by the low temperature of the reaction. **PPC4**, prepared at 150 °C in DCB, demonstrates polymer like qualities, with the formation of a smooth SEC peak uninterrupted at high molar masses, and only few lower molar mass oligomers. This effect is further strengthened when considering **PPC5** and **PPC6**. The molecular weights obtained from counting off peaks are, respectively, around 19100 and 24300 g mol⁻¹, and the materials show high solubilities. However, it has to be said that the use of high concentrations of reagents and temperature in method *ii*

permits high yields of soluble long chains with sterically cumbersome **PPC4**, but also leads to low yields and crosslinking with **PPC2**. In effect, we can conclude that the use of large comonomers is more critical to high polymer formation under high temperature and concentration conditions.

2.3.2 Kinetics

Considering the novelty of this approach to obtain main-chain polyfullerene, preliminary kinetics studies have been performed on the reaction. To investigate, the formation of **PPC4** in DCB was followed by SEC, as shown in **Figure 92**. The reaction was performed in 1,2-dichlorobenzene at 150 °C at a starting concentration of C_{60} of 20 mg mL⁻¹. In **Figure 92**, the curves are normalised to the standard naphthalene, employed at 10 mg mL⁻¹ and eluting at *ca* 20.6 – 20.8 mL. A toluene marker elutes at *ca* 22.3-22.6 mL. C_{60} elutes at *ca* 26.8 mL (later than toluene) due to retention in the column. The values of M_w , M_n and \mathcal{D} are given in **Table 8**. It has to be noticed that the data were obtained by OMNISEC software which estimates limits around the main peaks (elution volume < *ca* 22.5 min) to obtain M_n , M_w , and dispersity. The oligomers and polymers suffer similar column retentions to those of C_{60} , and therefore the values given underestimate actual masses by several orders of magnitude. Even though the values for M_n are clearly erroneous due to the just discussed retention of polymers, oligomers and C_{60} in the column, the data can be explored when assuming it to be a self-consistent set. Given the mechanism of the cycloaddition to C_{60} , it was expected that the formation of macromolecules would be essentially in accordance with step polymerization kinetics³² modified by aggregation effects, steric constraints, or precipitation.

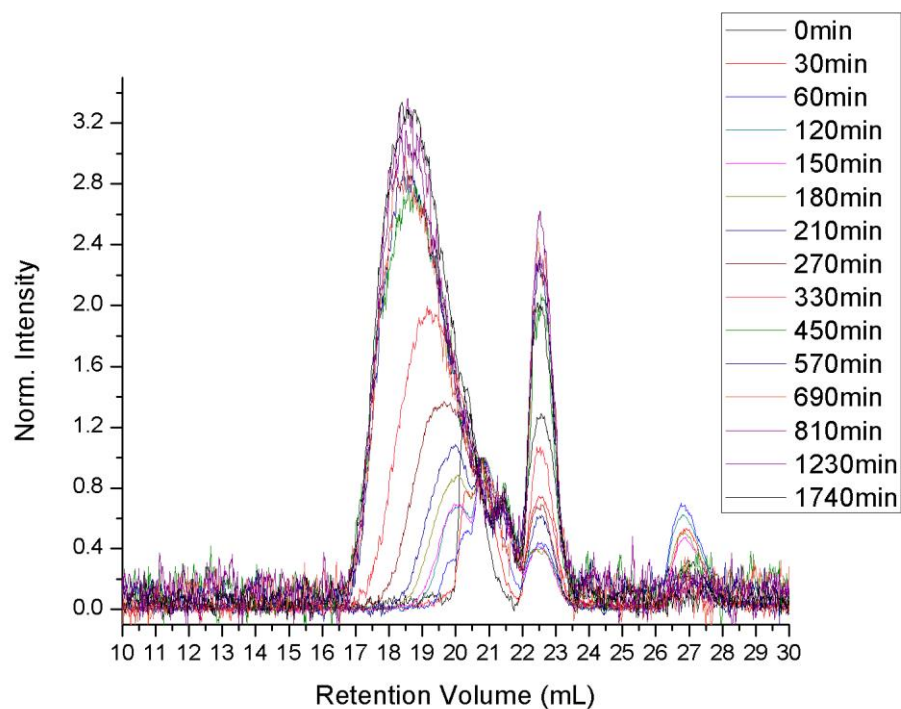


Figure 92: SEC curves following the formation of oligo and polymeric **PPC4** with time (THF, 30 °C, 280 nm).

Time (min)	M_n (g mol ⁻¹)	M_w (g mol ⁻¹)	M_p	\mathcal{D}
0	320	410	490	1.3
30	220	350	240	1.6
60	180	370	240	2.1
120	170	490	220	2.9
150	180	630	220	3.5
180	190	700	225	3.8
210	240	900	780	3.7
270	310	1420	1190	4.6
330	480	2340	2150	4.9
450	680	4060	4010	6.0
570	740	3860	3530	5.2
810	620	3990	4119	6.4
1230	790	4080	4260	5.2
1740	790	4330	4830	5.5

Table 8: Average molar masses obtained with time for **PPC4** and plotted in Figure 3 in the main text.

Plotting the variation of the obtained M_n with time (**Figure 93a**), one can see that M_n does not increase linearly with time; it initially decreases. This is most likely due to the dissolution of reagents with time, aggregates of C_{60} disappearing over a period of an hour or so. Indeed, this is further confirmed when considering the reaction in terms of the consumption of C_{60} , as in **Figure**

93b. There is an initial increase in C_{60} concentration due to the delay in its dissolution; it is still in aggregates that are filtered out prior to injection in the machine. There then follows a phase of about three hours where there is a negligible increase in M_n due to a formation of either or both ylides and low molar mass oligomers.

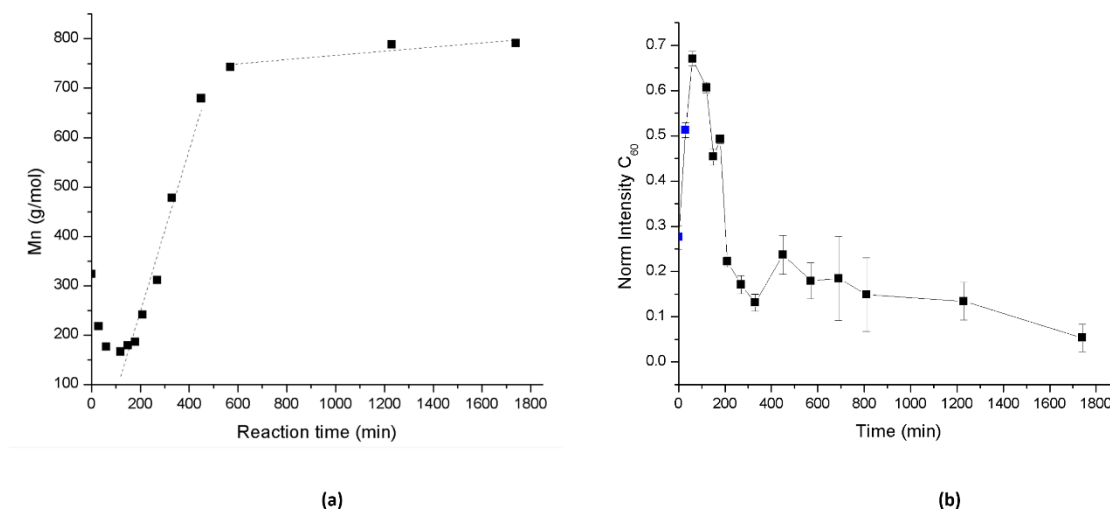


Figure 93: (a) Variation in indicated M_n (against PS standards) with time and, (b) consumption of C_{60} with time in the preparation of **PPC4**.

Assuming that the second part of the reaction, between ca 180 min and 600 min, is a second-order polyaddition (other order plots did not give better results) between that of the ylide and C_{60} , and given that the average degree of polymerization (x_n) is related to the extent of the reaction (p) through the Carothers equation i.e., [291–293] the polymerization can be better understood as a function of its progress, as detailed in **Table 9** and shown in **Figure 94a**. The typical curve for a polyaddition is obtained, however, it falls well-short of $p=1$, i.e., a complete reaction. This limit to the reaction indicates that the polymers aggregate once high molar masses are achieved. This is confirmed by the considerable differences between the measured and calculated ideal dispersities (obtained from the Flory equation, $\bar{D} = 1+p$) listed in **Table 10**. Towards the end of the reaction, for a pure polyaddition one would expect $\bar{D} = 2$, however, actual values upwards of 5 are obtained, not unusual for reactions hampered by precipitation.

<i>time</i>	x_n	<i>p</i>
60	1	0
120	0.94318	-0.06024
150	1.01705	0.01676
180	1.05682	0.05376
210	1.36932	0.26971
270	1.76705	0.43408
330	2.71591	0.6318
450	3.85795	0.7408
570	4.22159	0.76312
1230	4.47727	0.77665
1740	4.49432	0.7775

Table 9: Average degree of polymerization (x_n) and extent of the reaction for **PPC4** with time.

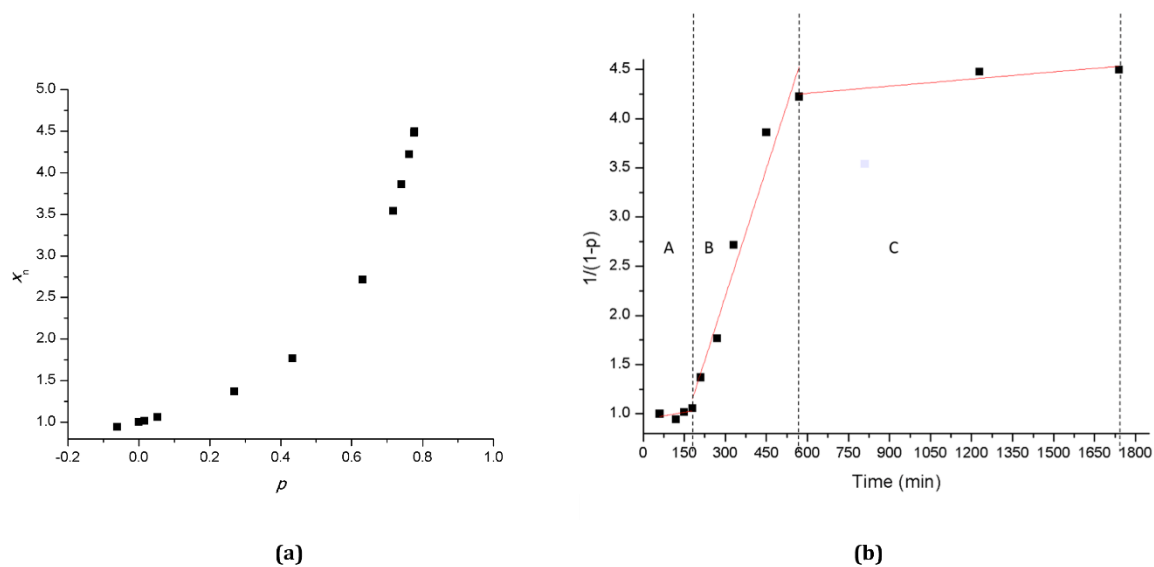


Figure 94: Plots for **PPC4** of: a) the variation in x_n with p for the formation of **PPC4**; and b) of $1/(1-p)$ against time showing three different regimes (A, B, C). Straight lines are linear fits within each domain.

Time (min)	\bar{D} (calculated)	\bar{D} (measured SEC, THF 30 °C)
60	1	2.1
120	0.93976	2.9
150	1.01676	3.5
180	1.05376	3.8
210	1.26971	3.7
270	1.43408	4.6
330	1.6318	4.9
450	1.7408	6.0
570	1.76312	5.2
810	1.7175	6.4
1230	1.77665	5.2
1740	1.7775	5.5

Table 10: Change in dispersities with time for **PPC4**, both measured (SEC, THF 30 °C, UV) and calculated using the Flory distribution equation ($\bar{D} = 1 + p$).

Again, making the not unreasonable assumption that the main part of the polymerisation is a second order step polymerisation by plotting $1/(1-p)$ against time (**Figure 93b**), an indication of the rate constant (k) during the reaction can be found in accordance with (**Equation 8**).

$$[M]_0 kt = \frac{1}{(1-p)} - 1$$

(Equation 8)

where $[M]_0$ is the initial concentration of C_{60} .

Confirming the prior results, **Figure 94b** shows three distinct regimes:

- A. a period of induction, where C_{60} dissolution or ylide formation or both are rate determining up to the 180th minute;

- B. a period where the polymerisation proceeds in accordance with a typical step growth reaction to around 10 h;
- C. where the polymerisation is limited by product precipitation.

For each region, the value of the rate constants have been calculated and shown in Table S4. $[M]_0$ is assumed to be the initial C_{60} concentration. For regime B, k is of the order of $7.1 \times 10^{-4} \text{ L mol}^{-1} \text{ s}^{-1}$, nearly three times the rate constant ($2.9 \times 10^{-4} \text{ L mol}^{-1} \text{ s}^{-1}$) for the induction period in regime A. The final domain C gives a rate constant of around $4.5 \times 10^{-4} \text{ L mol}^{-1} \text{ s}^{-1}$, and is most likely slowed by precipitation. The possibility of retro-cycloadditions cannot be completely excluded,³⁵ however, for them to occur in a relevant yield, the presence of either a strong dipolarophile or substituents, such as ester and aryl groups, which stabilize the in-situ-generated azomethine ylide is needed.

Regime	t_i (min)	t_e (min)	Fitting slope	$[M]_{0,x}$ (mol L)	k ($\text{L mol}^{-1} \text{ min}^{-1}$)	k ($\text{L mol}^{-1} \text{ s}^{-1}$)
A	60	180	4.82×10^{-4}	0.02775	1.74×10^{-02}	2.89×10^{-4}
B	180	570	8.65×10^{-3}	0.0202501	4.27×10^{-01}	7.12×10^{-3}
C	570	1740	2.40×10^{-4}	0.0088367	2.72×10^{-02}	4.54×10^{-4}

Figure 95: Calculated rate constants for the formation of **PPC4** divided into 3 regimes A, B and C. The initial concentration of C_{60} $[M]_0$ is $0.02775 \text{ mol L}^{-1}$. Elsewhere it is assumed that C_{60} consumption is directly proportional to the UV absorbance at 280 nm.

2.3.3 Nuclear magnetic resonance (NMR)

All the polymers have been characterized by NMR spectroscopy. The complete set of spectra is reported in section 5. **PPC1** was difficult to treat and due to its low solubility, it was not possible to obtain complete spectra even when employing 1,4-dichlorobenzene- d_4 at 85°C . This was due to crosslinking, as confirmed by the presence of trapped fullerene and hexane in well-washed and dried samples and confirmed by the spectra (**Figure 96**). However, in the soluble parts of **PPC1** samples, a partial characterisation was possible. Pyrrolidine adducts were found by way of double-doublets centred at 4.50 ppm (4.14 and 4.85 ppm) due to pyrrolidine methylenes, a singlet at 4.5 ppm from pyrrolidine methines, and a singlet at 2.3 ppm of amino methyl groups.

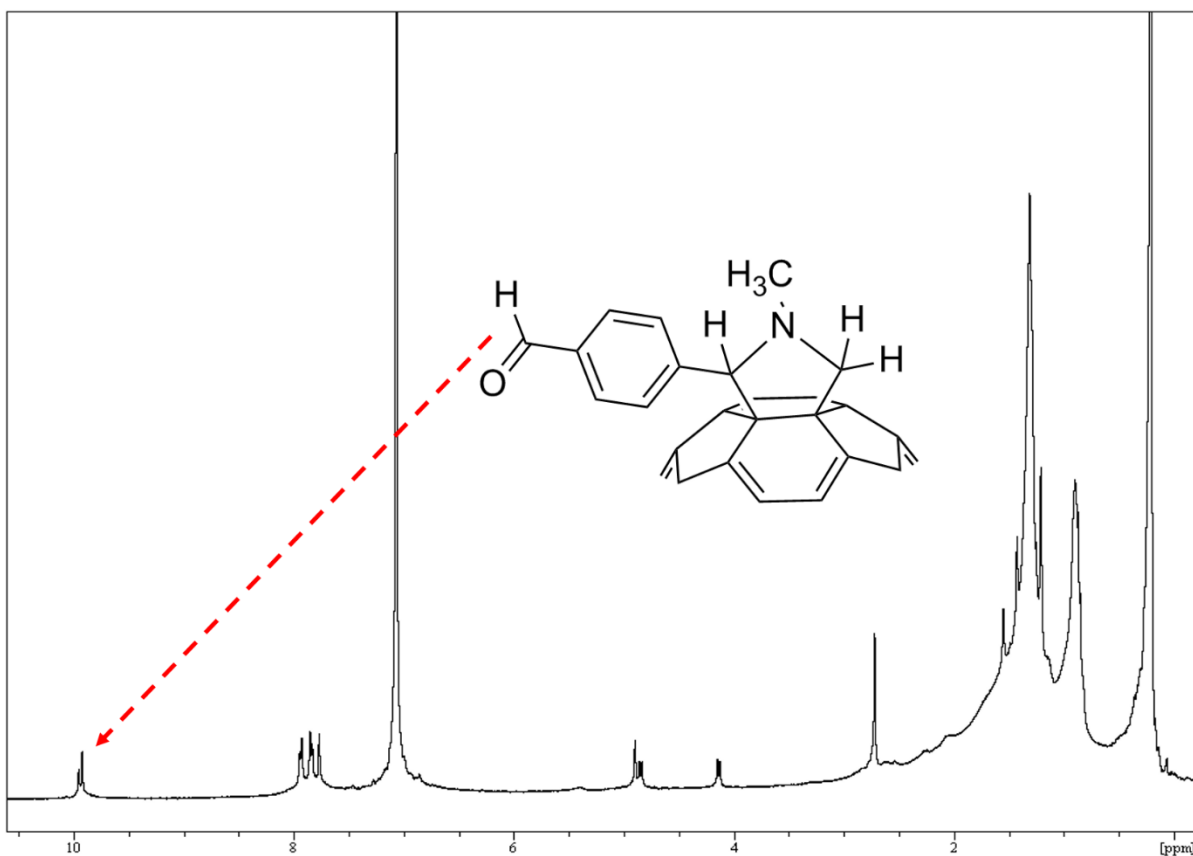


Figure 96: ^1H - NMR spectrum (85 °C, 1,4-DCB- d_4) of **PPC1** showing two signals for the HC=O group.

While the ^1H NMR of **PPC1** showed two aldehyde peaks around 10 ppm, the HSQC NMR (**Figure 97a**) uncovered three at 9.57, 9.52 and 9.45 ppm. The ^{13}C NMR showed three peaks (one a shoulder to the other at 189.9 and 190.0 ppm, respectively) and one very weak peak (189.7 ppm) discerned by adding comonomer as an impurity (**Figure 97 b-c**). This suggested that the mixture contained symmetrical bis-adducts, tris-adducts, and comonomer. **PPC2** could not be characterised as it was insoluble; the higher reaction temperature permitted an even greater level of crosslinking than that found for **PPC1**.

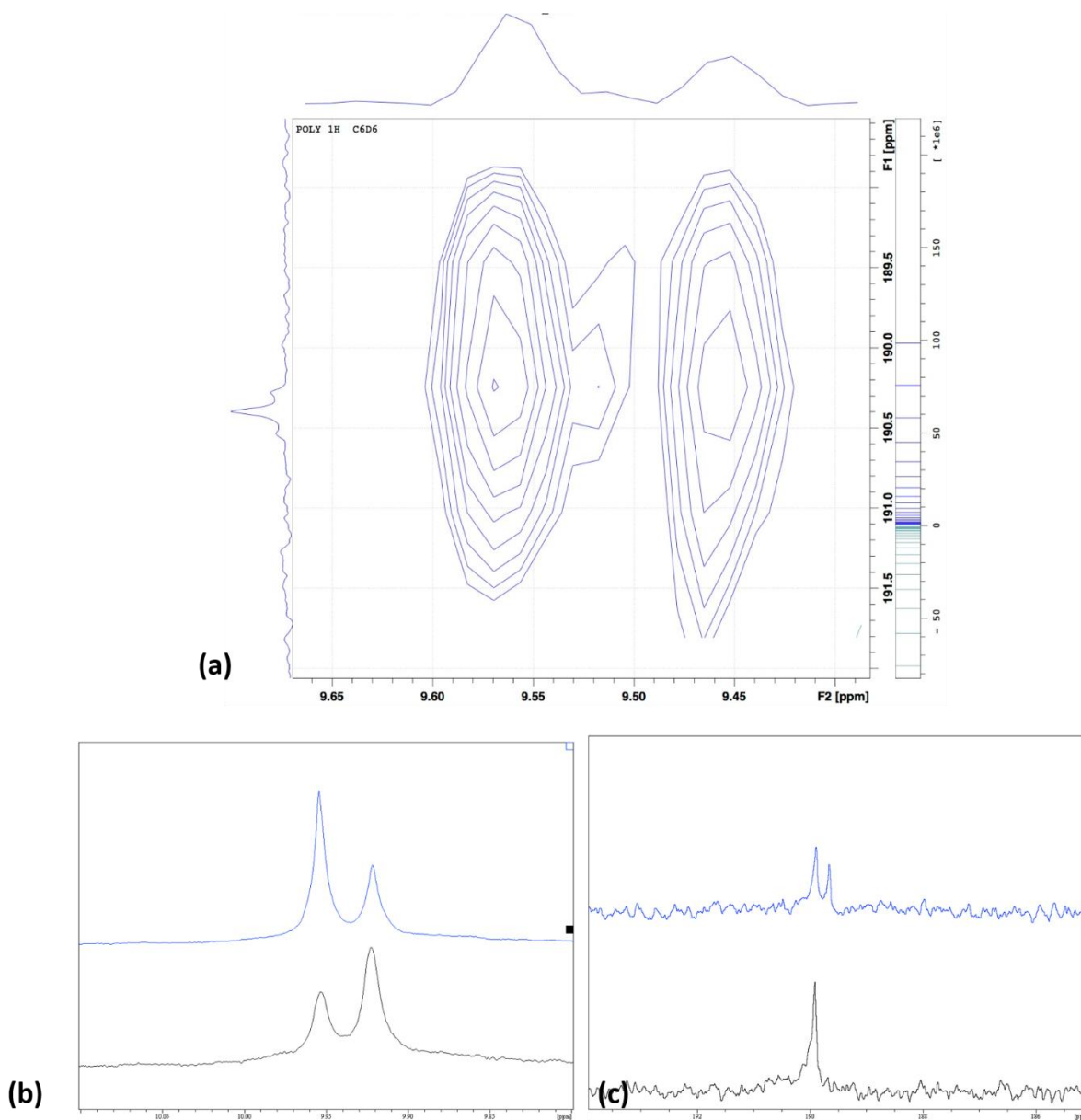


Figure 97: (a) . HSQC spectra of **PPC1** (85 °C, 1,4-DCB- d_4) showing zoom on aldehyde peaks; (b) ^1H NMRs and (c) ^{13}C NMRs of **PPC1** (black, bottom) and the **PPC1** + comonomer (blue, top); all 85 °C, 1,4-DCB- d_4 .

Turning to **PPC3**, the ^1H NMR in **Figure 177** of section 5, shows more soluble well defined samples indicating reduced cross-linking and less tris-adduct formation. The aldehydes form a large singlet at 10.67. A ^{13}C NMR of the brut sample (**Figure 178**) and the starting material indicated that one peak was due to a comonomer impurity, while the other, carrying no shoulder, was due to single type of CHO group on the **PPC3**, confirming that the product was mostly made of symmetrical bis-adducts. **Figure 98** shows a zoom in the range 6 to 2.5 ppm wherein the -N-CH₃

peaks (2.8 – 3.0 ppm) show one major peak due to the trans-3 adduct and several minor peaks, probably due to the aforementioned trans-2, and other isomers. Peaks associated with pyrrolidinone groups are labelled in **Figure 98**. In this figure one can also notice that, going up through the series from **PPC3** to **PPC6**, the increase in the polymeric character of the materials is clearly shown through the peak broadening of the ^1H NMRs. This change is present in all the ^1H , ^{13}C and HSQC spectra.

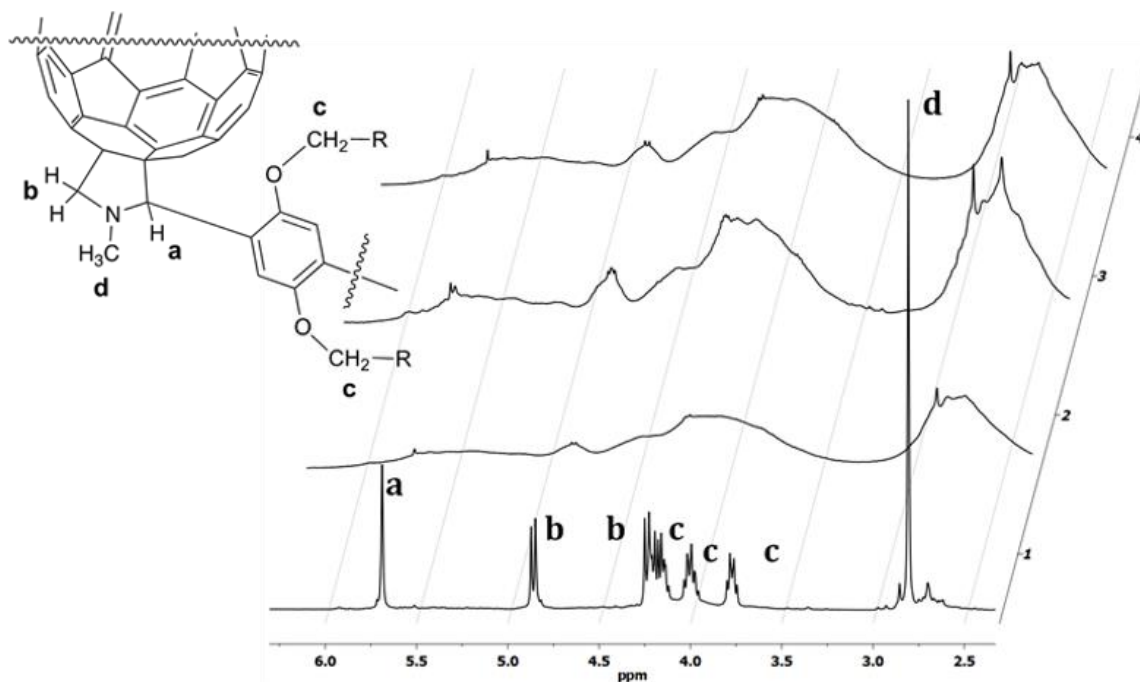


Figure 98: ^1H - NMR spectrum for **PPC3-6** in the range 2.5 – 6 ppm.

The **PPC3** HSQC NMR spectrum (**Figure 99**) has been recorded in the same conditions. The spectrum shows the correlations confirmed pyrrolidine with methylene double doublets at 4.3 and 4.9 ppm, a methine singlet at 5.8 ppm, and an amino methyl singlet at 1.6 ppm. Remarkably, there are multiplet correlations at 4.2, 4.1, and 3.8 ppm (^1H) arising from the asymmetry in the $\text{O-CH}_2\text{-C}_6\text{H}_{13}$ side-chains of these short oligomeric species showing that this group is surrounded by different groups in the macromolecule.

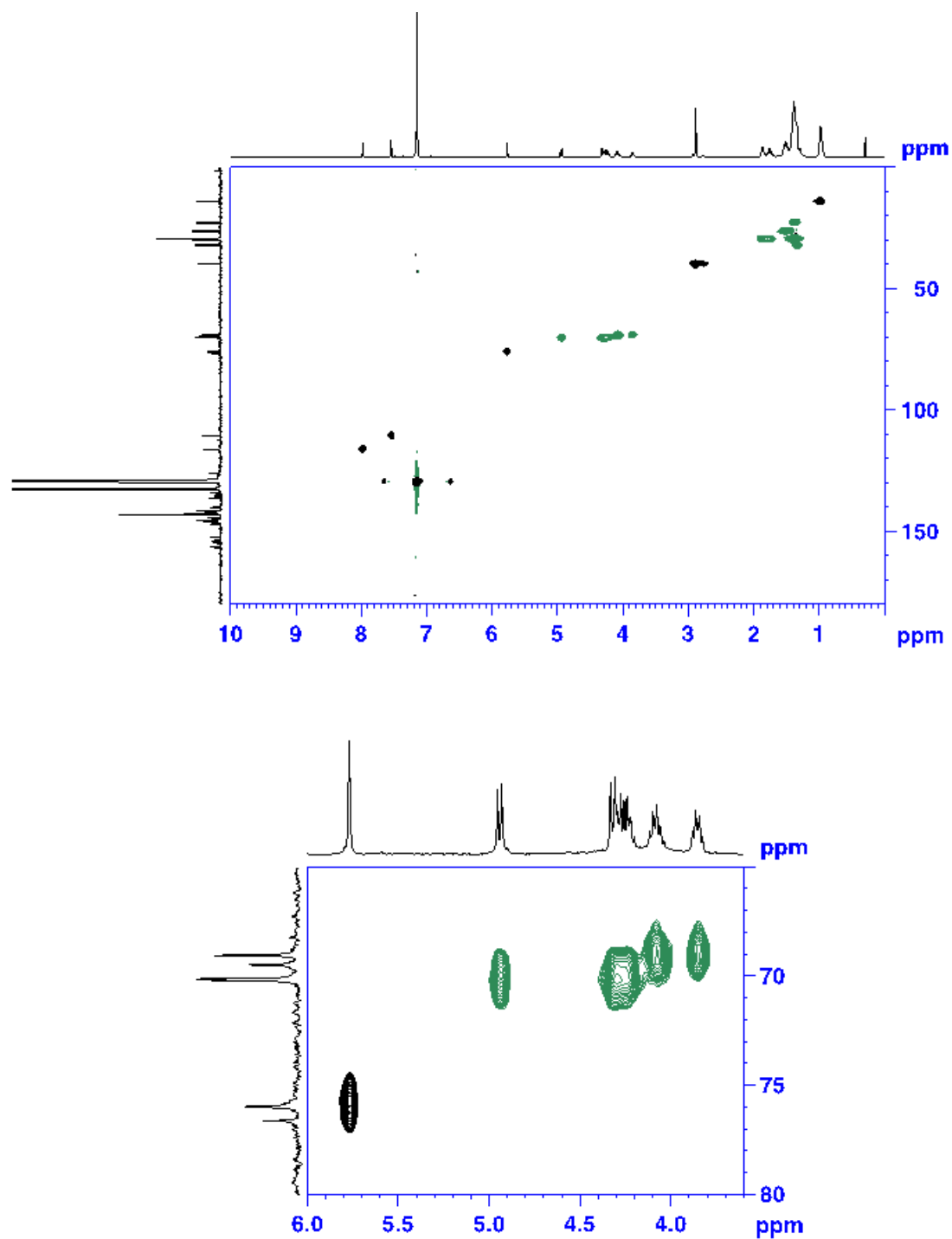


Figure 99: HMQC 2D NMR spectrum (1,4-DCB-d₄, 85 °C) of **PPC3** with zoom below.

In the ¹³C NMR of **PPC3** (**Figure 100**) more than 30 resonances are present in the region between 133 and 158 ppm. This is due to a mixture of fullerene derivatives with various

symmetries. The four resonances around 70 and 76 ppm are characteristic for pyrrolidine sp^3 carbons and confirm the presence of at least two different adducts.

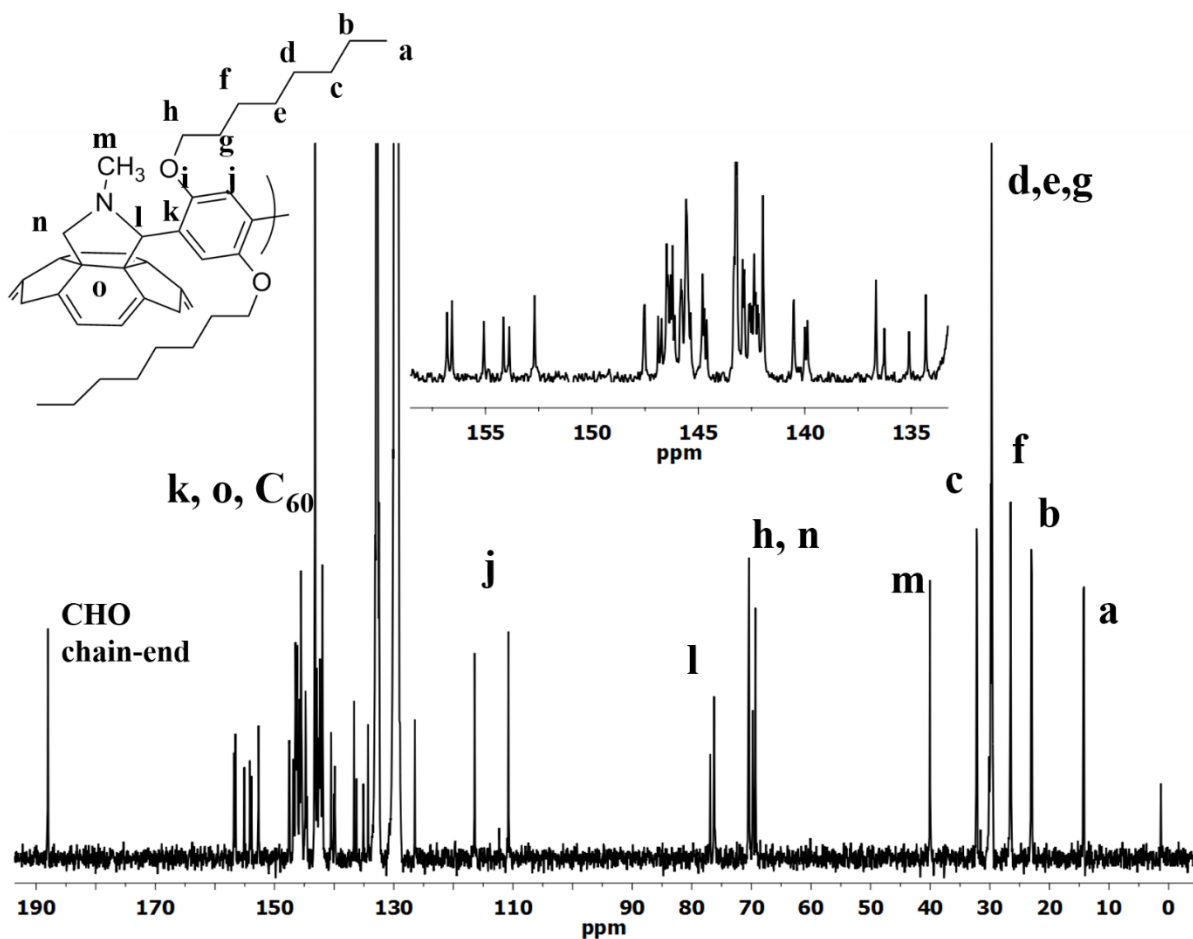


Figure 100: ^{13}C -NMR spectrum (1,4-DCB- d_4 , 85 °C) of PPC3.

Variations in ^{13}C asymmetries (**Figure 101**) appear to decrease going up through the sample series (reduction in the peak at ca 76.7 ppm) and tentatively confirm increased selectivity with increasing adduct size.

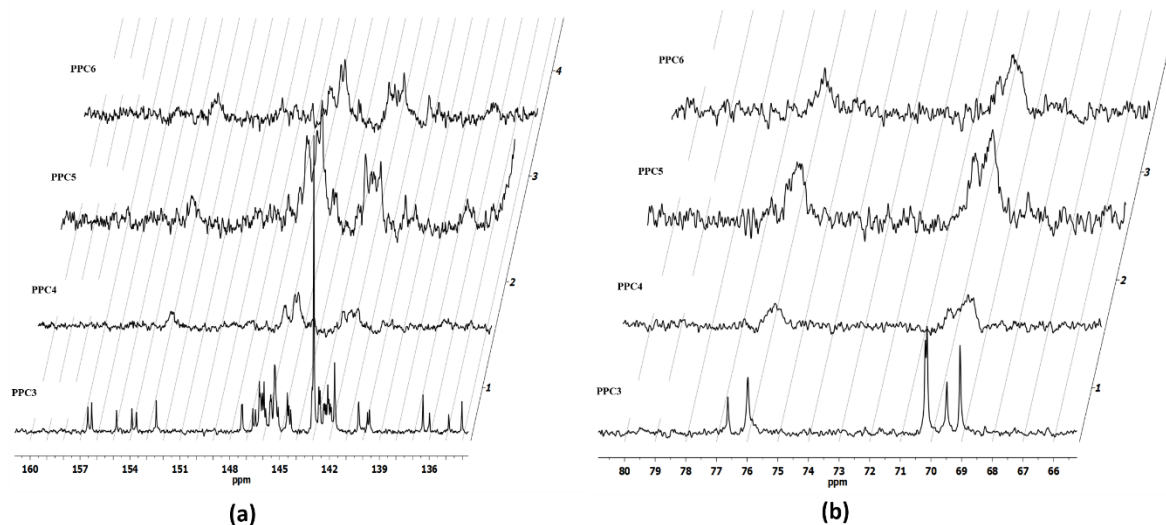


Figure 101: Comparisons of: a) ¹³C NMR spectra (1,4-DCB-*d*₄, 85 °C) of the sp² carbon region in the ¹³C-NMR (135 – 160 ppm) for the poly(fulleropyrrolidines) **PPC3**, **PPC4**, **PPC5** and **PPC6**; and b) ¹³C NMR spectra (1,4-DCB-*d*₄, 85 °C) of the sp³ carbon region (66 – 80 ppm) for **PPC3**, **PPC4**, **PPC5** and **PPC6**.

Given that the SEC values for molar masses were either inaccurate or estimated from peaks, NMR was used to give a more exact estimate of the degree of polymerization (DP_n) and the M_n. Assuming that all chains carried on average one aldehyde group and one C₆₀ at the chain-ends, as would be expected for a polyaddition, and that each repeating unit contained two phenylic and six alkyl methylic protons, the DP_n was calculated as a ratio of proton integrals in accordance with **Equation 9**:

$$DP_n = \frac{[\int(\text{phenyl}/2) + \int(\text{methyl}/6)]}{2 \int \text{CHO}}$$

Equation 9

PPC3 and **PPC5** gave masses of 3600 g mol⁻¹ (DP_n = 2.4) and 26 900 g mol⁻¹ (DP_n = 21), respectively. The former value confirms that the material is essential low molar mass oligomers, with the aforementioned asymmetries probably arising through mid-chain and chain-end groups, whereas **PPC5** shows a strong polymeric character. These values indicate that molar masses are best calculated using NMRs and peak estimations, even the former may overestimate due to some tris-additions being present, and the latter underestimating as peaks are easily missed. The “real” values are most likely somewhere between these two. Either way, the data

confirms how PS standards can lead to extremely underestimated values for high polymers made from C_{60} . **PPC4** and **PPC6** did not carry identifiable -CHO groups, either due to minor crosslinking at chain-ends, or the presence of excess C_{60} .

2.3.4 FTIR characterization

Fourier transform infrared spectroscopy, FT-IR, have been performed to investigate the structures of the synthesized compounds. The IR spectra of **PPC3**, **PPC4**, **PPC5** and **PPC6**, have been obtained in vacuum conditions using KCl pellets samples. The obtained spectra are reported in **Figure 102** together with the spectrum of C_{60} for comparison.

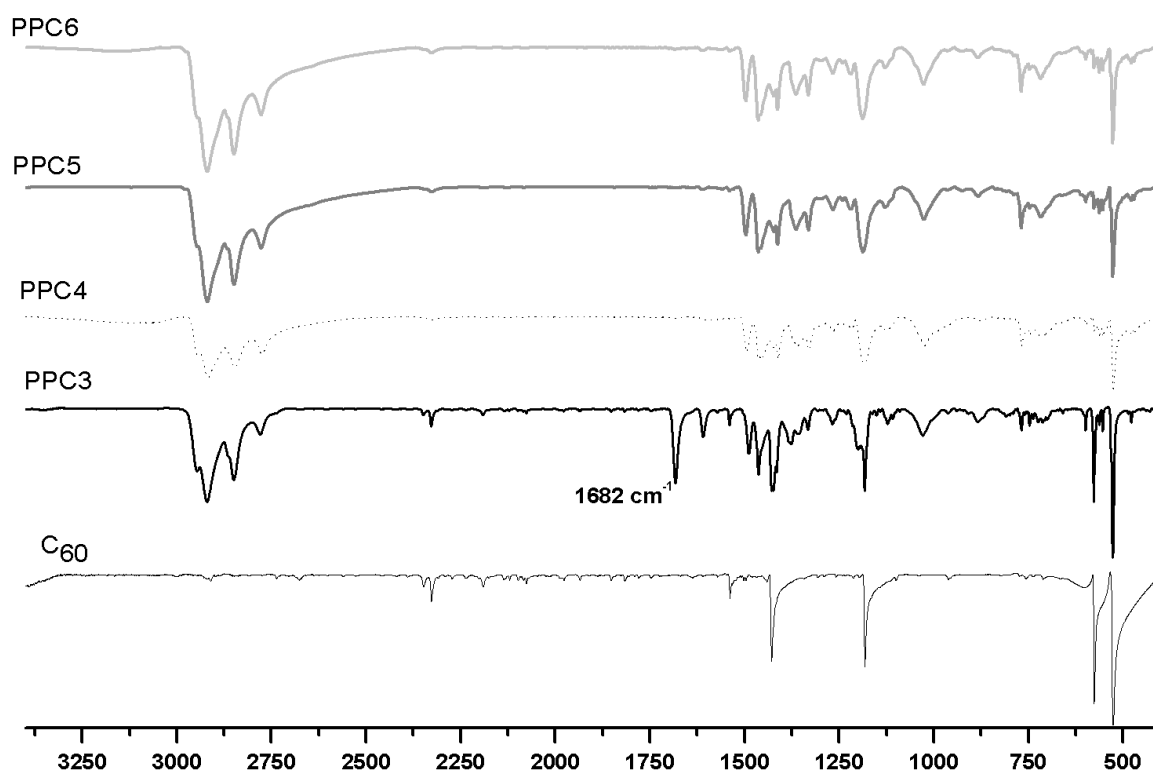


Figure 102: FTIR spectra of C_{60} and **PPC3-6**, KCl

The IR spectra confirm the polymeric structures and are consistent with literature values for comparable, small molecule systems.[294] Absorption bands at 1428, 1182, 576 and 526 cm^{-1} are present in all materials and are attributed to C_{60} vibrations.[295] In **PPC3** spectrum the

contribution of C_{60} is strong, confirming its presence as an impurity; the C=O band stretching band at 1682 cm^{-1} , for the aldehyde functions also confirms the relatively low molecular weight of **PPC3**. The vibrational spectra of the compounds confirms their general similar structures. Going from **PPC3** to **PPC6** peaks between 2500 and 3000 cm^{-1} become stronger and broader confirming both the higher percentage of alkyl chains in the macromolecules and the materials' increasingly polymeric nature; these bands are due to symmetric and asymmetric stretching of C-H groups, and out of plane C-H bending at aromatic rings and pyrrolidine groups. The absorption bands for the corresponding bendings participate in the more complex features between 1100 and 1500 cm^{-1} : the presence of alkyl aryl ethers are confirmed by the bands at 1025 cm^{-1} , characteristic of C-O-C group stretching. Absorption bands due to the asymmetric stretching of this group are hidden by absorptions due to fullerene in the region 1200 - 1275 cm^{-1} .

2.3.5 Thermogravimetric analysis (TGA)

Thermogravimetric analyses have been performed for the compounds in N_2 flux with a program temperature of 10 or $20^\circ\text{C}/\text{min}$. The thermogravimetric characterisations of **PPC1-PPC6** could be used to follow the gradual changes in properties while going through the series. For **PPC1**, in **Figure 103a**, there are 4 steps of decomposition, starting at ca 120 , ca 250 , 350 and 500°C ; **PPC2**, in **Figure 103b**, a less pronounced but similar multi-step process is shown starting at ca 135 , 250 , 350°C , and 500°C . The lowest temperature for both samples, respectively 120 and 135°C , are due to the loss of trapped solvents and reagents. This can be taken as a confirmation of the fact that **PPC2** is more crosslinked than **PPC1**; the impurities are more strongly trapped in the matrices.

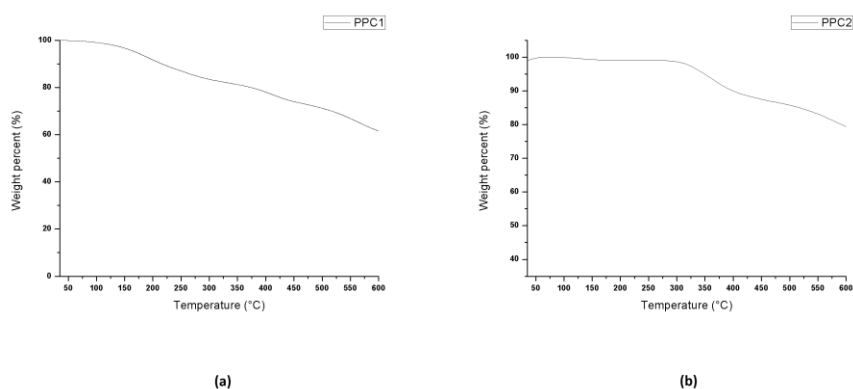


Figure 103: (a) TGA curve of **PPC1** ($dT/dt\ 10^\circ\text{C min}^{-1}$); (b) TGA curve of **PPC2** ($dT/dt = 20^\circ\text{C min}^{-1}$).

The polymers **PPC3-6** show a higher thermal stability with a decomposition temperature around 350 °C to 400 °C and a loss of around 20% weight in all cases (**Figure 188a-d**). These values indicate that it is the alkyl side chains which are lost first in this process, as expected. Interestingly, **PPC4** has a slightly higher degradation temperature than the other samples which may point to a better crystallisation of this material.

2.3.6 Differential scanning calorimetry (DSC)

DSC characterisations of **PPC3**, **PPC4**, **PPC5** and **PPC6** were performed, on powder, up to 180 °C in N₂ atmosphere. **Figure 104** shows complete first and second heating and cooling passages. After solvents were removed from **PPC1** at *ca* 120 °C, there is a featureless curve, indicative of an unstructured material. Indeed, all samples gave featureless curves on their second passages, an expected result for materials containing such cumbersome groups. In all cases, minor transitions were observed around 120-130 °C on the first passage. As for the case of the synthesized polyPCBMs, discussed in section 2.2.4), these transitions are most likely due to solvents being removed, the possibility that these are arising from disorder-order transitions cannot be excluded. It is to be said that, of these transitions, the most remarkable is the endothermic transition of **PPC4** in **Figure 104c** at 128 °C ($\Delta_H = 0.26 \text{ J g}^{-1}$) which may result from a reorganisation of the polymer.

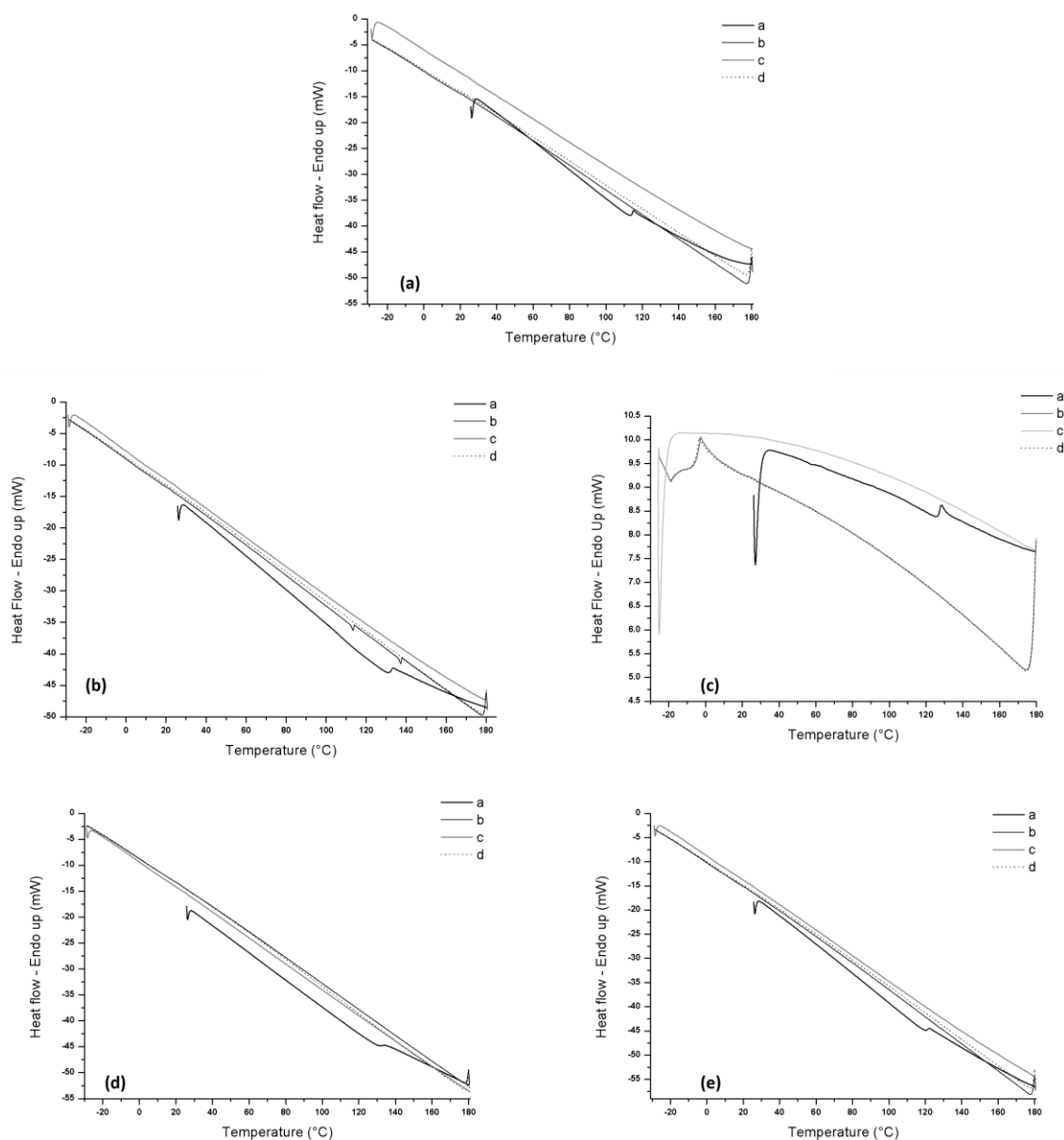


Figure 104: DSC curves of (a) PPC1, (b) PPC3, (c) PPC4, (d) PPC5 and, (e) PPC6 ($dT/dt = 20\text{ }^{\circ}\text{C}/\text{min}$). For each thermogram (a) first heating; (b) first cooling; (c) second heating; and (d) second cooling cycles.

2.3.7 UV-visible optical spectroscopy

As discussed above in this work, the polymeric nature of the products results in a difficult NMR characterisation which was expected to be complicated by the variety of possible in-chain isomers and the multiplicity of environments for each repeating unit. This is valid also for UV-visible characterisation. Furthermore, UV-visible spectra were not expected to give diagnostic

information due to the admixing of multiple absorptions. As mentioned in section 2.2.2, a mixture of multiadducts is found in the products. In particular, a mixture of predominantly *trans*-3, equatorial, *trans*-2, *trans*-4, and *cis*-2 isomers would be expected in the polymer chains.[287, 296] *Cis* isomers are generally excluded by steric effects. Dr. Hugo Santos-Silva has then explored modelling to determine: first, what UV-spectra might be expected for the possible isomers; and second, identify the most preferred isomer formed by the reaction. While details on the method are found in appendix A, we present here the main results obtained from this study. Comparing the calculated electronic transitions for a representative compound with the UV-vis spectrum of **PPC3**, we observed that the closest correlation was found for the *trans*-3 isomer, as shown in **Figure 105**.

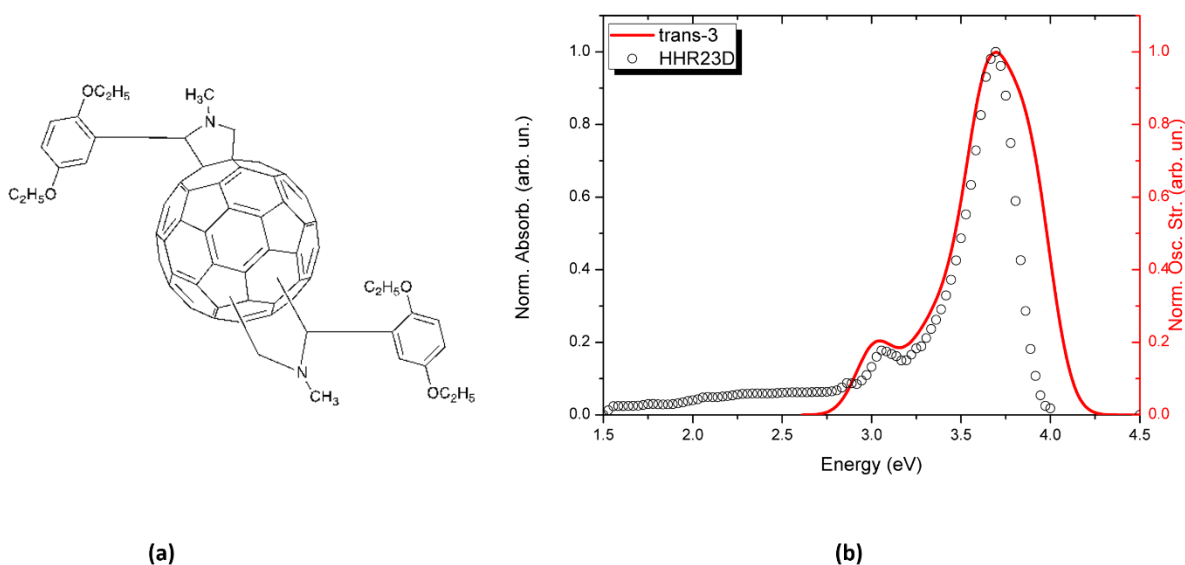


Figure 105: (a) Representative structure employed for treatment by time dependent density functional theory (TDDFT); (b) comparisons between the obtained spectra for the generic compound in a and **PPC3**.

However, one can see also a minor ‘bump’, at ca 2.7 eV, in the spectrum, which can be associated with the *trans*-2 adduct, indicating a mixture of both in the chains, and in agreement with prior work.[287] An unexpected result is that *trans*-4 and equatorial products appear limited.[296] Interestingly when looking at **PPC6**, in **Figure 106**, the bump at ca 2.7 eV is very much reduced, indicating a further, greater reduction in *trans*-2 additions, and suggesting that the larger -OC₁₂H₂₅ chains are enforcing steric control over the product. However, the correlation between calculated and actual values is poor in the zone below 2.8 eV as shown in **Figure 189** and in **Figure 190** in appendix A.

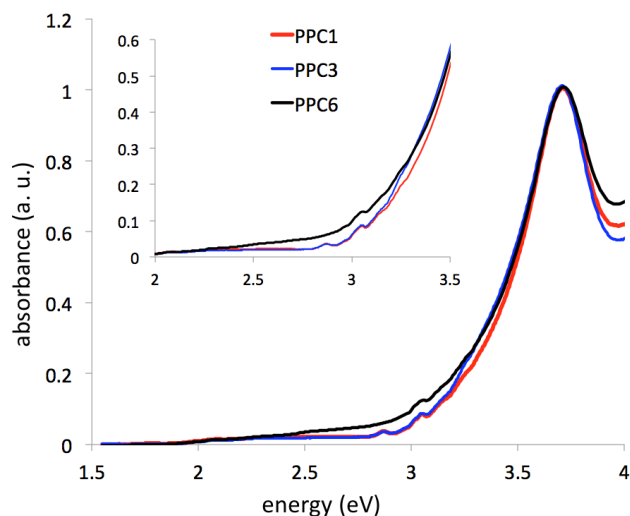


Figure 106: comparison of UV spectra for **PPC1**, **PPC3** and **PPC6**.

2.3.8 X-ray photoemission spectroscopy

In this section, results of the XPS and UPS characterizations of three different fullerene derivatives are presented. The derivatives used for the studies are PCBM, **PPC4** and **PPC6**. Thin films of the compounds have been prepared by solution casting procedures (doctor blade or spin coating, depending on the substrate). An attempt of characterization has been also done with **PPC1**, but the bad homogeneity of the obtained film, did not permit a consistent study. The **Figure 107** shows how upon doctor blade deposition on ITO-coated glass, **PPC1** forms aggregates which auto assemble in a well organize pattern. Similar result is obtained by spin coating deposition on ITO-coated glass.



Figure 107: Film of **PPC1** on ITO-coated glass substrate. The film was obtained by doctor blade deposition from a solution of 2.5 mg mL^{-1} **PPC1** in *p*-xylene.

branched polyethylenimine (PEI) has been deposited on ITO-coated glass substrate from a solution in *i*-butanol to obtain a substrate with a work function of 3.45 eV. During the deposition of the polymer layer, the choice of the parameters are crucial as PEI is a large band-gap insulator and only ultrathin layers (< 10 nm) are desired to modify the substrate's work functions without obtaining an insulator surface. The structure of PEI is displayed in **Figure 109** together with the XPS spectrum of PEI on ITO-coated glass. Signals due to In and Sn core levels are still evident in the spectrum. The presence of these elements indicates the low thickness of the PEI layer but also the not homogeneity of it.

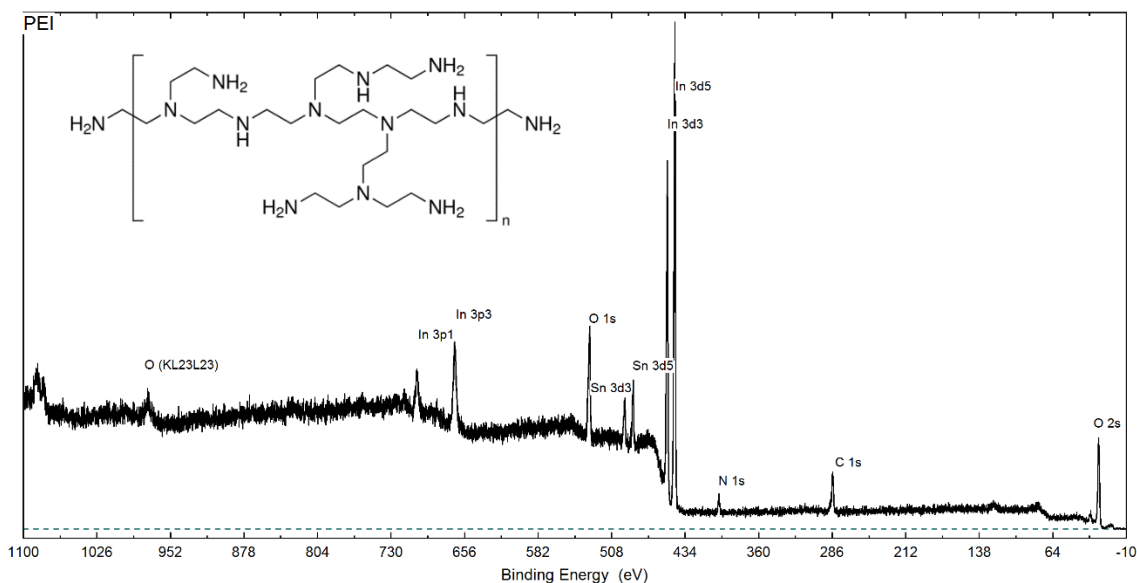


Figure 109: XPS spectrum for PEI on ITO-coated glass and PEI structure (top left).

When a thickness estimation is attempted using parameters the ratio between the In 3d5 and the C 1s peaks, a value of ~ 2 nm is obtained. It has to be said that this estimation is not very correct and a lower value of the thickness has to be considered as also contaminants contributed to the carbon's peak.

ITO-coated glasses with different surface cleaning methods

A second strategy used to modulate ITO-coated glass work function is the use of different surface cleaning method. The dependence of the ITO work function on the surface cleaning method has been investigated, for example, by Sugiyama *et al.*[298] In their studies, ITO substrates were cleaned with three different methods and analysed by XPS and UPS spectroscopies. The first

method used was the treatment in organic solvent. For this method the ITO substrate was subjected to ultrasonic agitation in acetone and then exposed to *i*-propanol vapour. In the second method, after the solvent treatment, the substrate was cleaned by UV-ozone treatment. In the third method, an Ar⁺ ion sputtering was performed under vacuum after solvent cleaning. From the obtained results, they could conclude that after the organic solvents cleaning, carbon contaminants remained on the surface and thus work function was lowered. They also observed that the UV-ozone treatment removed the carbon contaminants without much change in the chemical composition of the surface. This removal of contaminants increased the work function. Finally, Ar⁺ sputtering was found to reduce not only the carbon contamination but also the oxygen content on the ITO surface resulting in a decrease of the work function.

A similar study was repeated in this work in order to choose suitable cleaning methods to obtain desired broader range of work functions of ITO substrate. Four different cleaning protocols were considered:

- Method 1: soft mechanical polishing (the substrate was gently cleaned with a soft paper tissue)
- Method 2: solvent cleaning using *i*-propanol (ultrasonic bath for 15 min)
- Method 3: solvent cleaning using first acetone (ultrasonic bath for 15 min), then *i*-propanol (ultrasonic bath for 15 min)
- Method 4: UV-ozone treatment, after solvent cleaning as in method 3.

The XPS spectrum of the ITO substrate, treated with method 4, is shown as example in **Figure 109**. It shows signals for In, Sn and O core levels for ITO.

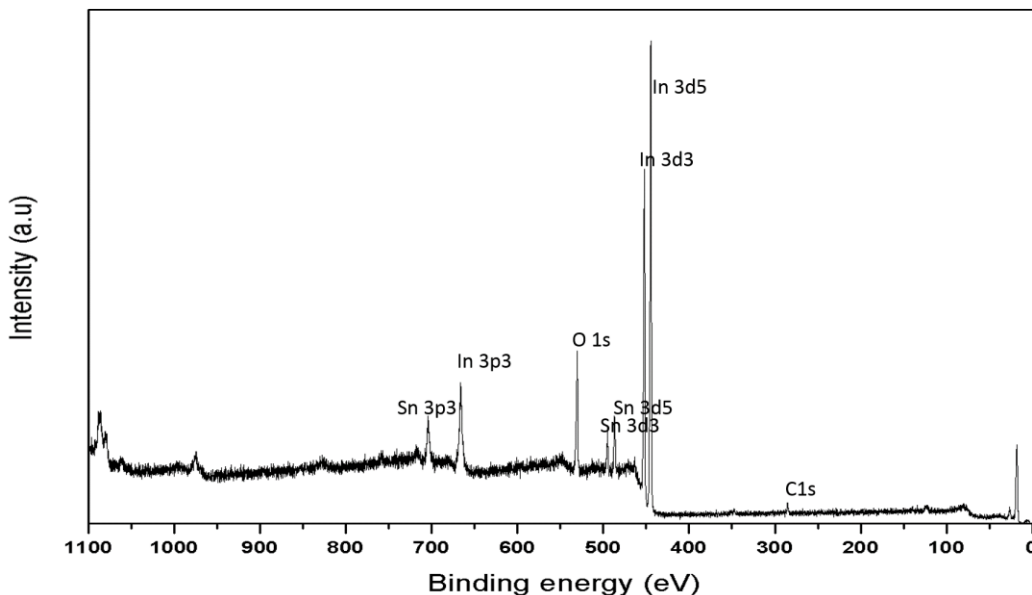


Figure 110: XPS spectrum of ITO showing the In, Sn and O core levels due to ITO and the C species due to contaminants on the surface.

The XPS spectra of the substrates after different cleaning protocols are similar. From these spectra, shown in **Figure 111**, it can be noticed that the most effective protocol to reduce the carbon contamination content on the substrate surface is method 4 which contemplates the use of UV-ozone treatment. Compared to ITO treated with method 1, in fact, the content of carbon contaminants is reduced by the 82 % in the ITO treated with method 4. The cleaning effect of the UV-ozone treatments is a result of photo-oxidation processes of the contaminants. The UV light, in fact, excites or dissociates the contaminant molecules while producing atomic oxygen and ozone, which can undergoes dissociation itself, from O_2 . The excited molecules as well as the free radicals formed in this process react readily with the molecular oxygen to form small volatile molecules that are then removed from the surface.[299]

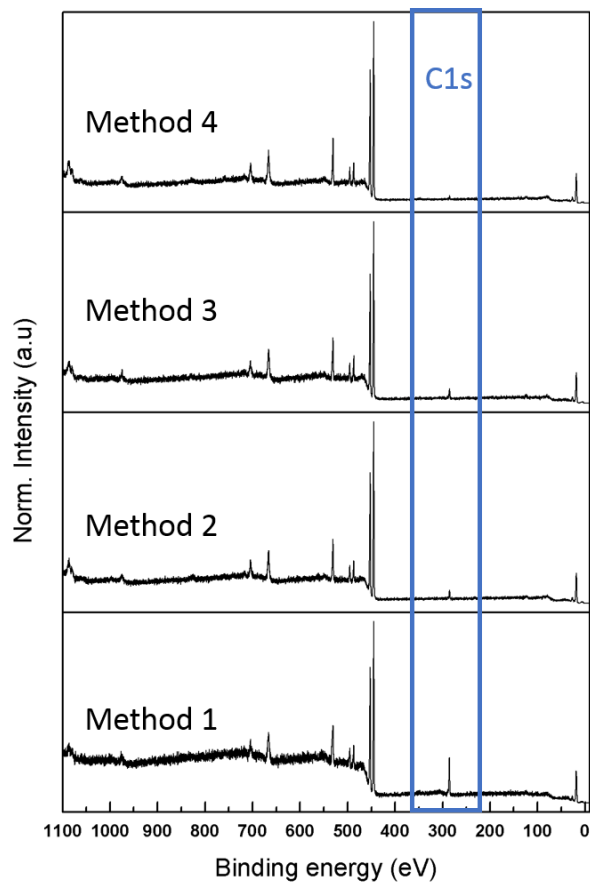


Figure 111: XPS spectra of ITO substrates after different cleaning method (method 1: Method 1: soft mechanical polishing; method 2: solvent cleaning using i-propanol; method 3: solvent cleaning using first acetone, then i-propanol and method 4: UV-ozone treatment, after solvent cleaning as in method 3).

The work functions of the substrates have been measured by UPS spectroscopy with negative bias on the samples to overcome the work function of the analyser. The UV-ozone treatment is also known as one of the most effective technique to increase the work function of ITO.[300] This has been confirmed by the experiment. The increase of the binding energy of the secondary electron cut off shows clearly how the cleaning method 1 produces a substrate with the lower work function. The secondary electron cut off for the substrate treated with method 2 exhibit a small shoulder, pointing to region with different work function, e.g. due to remaining islands of contamination. The calculated work functions for the substrates are reported in **Table 11**.

Cleaning method	Work function (ϕ) /eV
Method 1	$2.6 \pm 0.1^*$
Method 2	$4.14 \pm 0.05^*$
Method 3	$3.75 \pm 0.05^*$
Method 4	$4.21 \pm 0.05^*$

Table 11: work function of ITO substrates cleaned with different methods. * additional experimental errors occur.

The value are taken as indicative for the trend in the work function modification with the cleaning protocol. Method 2 and method 3 have been discarded as from XPS spectra. It is to notice that the obtained substrate using method 2 shows the same composition, in particular the same amount of carbon contaminant, as the substrate treated with method 3, but the UPS spectrum does not result in a defined secondary electrons cut off, pointing to an inhomogeneous surface (**Figure 112**). The method 1 and method 4 have been used for the studies on fullerene derivatives.

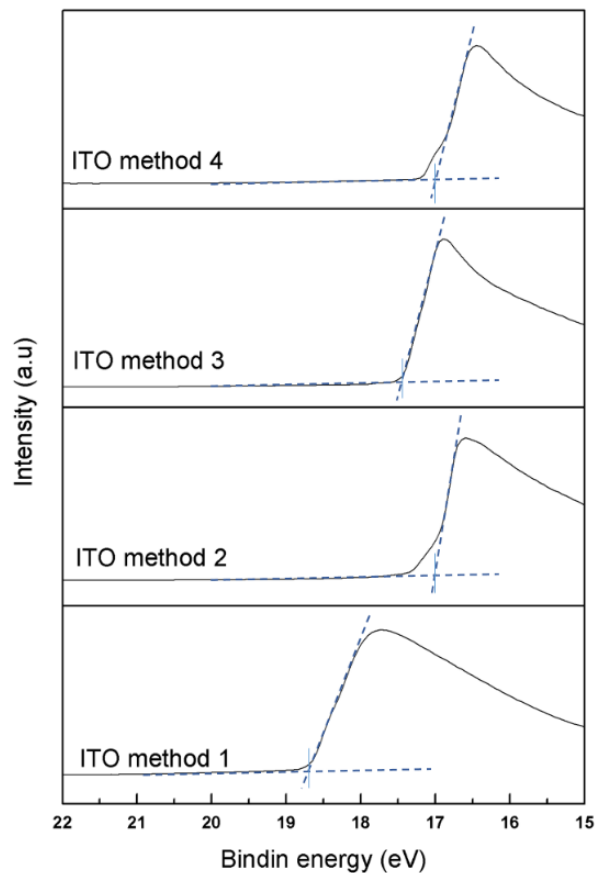


Figure 112: UPS secondary electrons cut-off spectra of ITO substrates treated with different cleaning protocols.

Au layer co-evaporated on Si wafer

Gold (Au) has a quite high work function. For this study thin layer of gold have been co-evaporated on Si wafer in order to obtain substrates (Au@Si) with higher work function than ITO. The substrates were then be used in two different conditions:

- The Au@Si substrates left to air exposure before polymer deposition have a work function of 4.65 eV.
- The Au@Si UV-ozone treated (10 min) substrates have a work function of 4.78 eV.

From XPS analysis carbon as well as oxygen species are detectable on the surface of the substrates (Table 12). The ratio between the species does not change in a radical way upon 10 min treatment with UV-ozone (Figure 113). This explains why the work function of the substrates are close to each other.

Species	EB (eV)	Quant. (%) Au@Si air exposed	Quant. (%) Au@Si UV-ozone treated 10 min
Au 4f7	83.4	52.1	53.07
C 1s	284.1	27.59	25.29
O 1s	531.0	20.31	21.64

Table 12: Analysis of Au@Si samples XPS spectra.

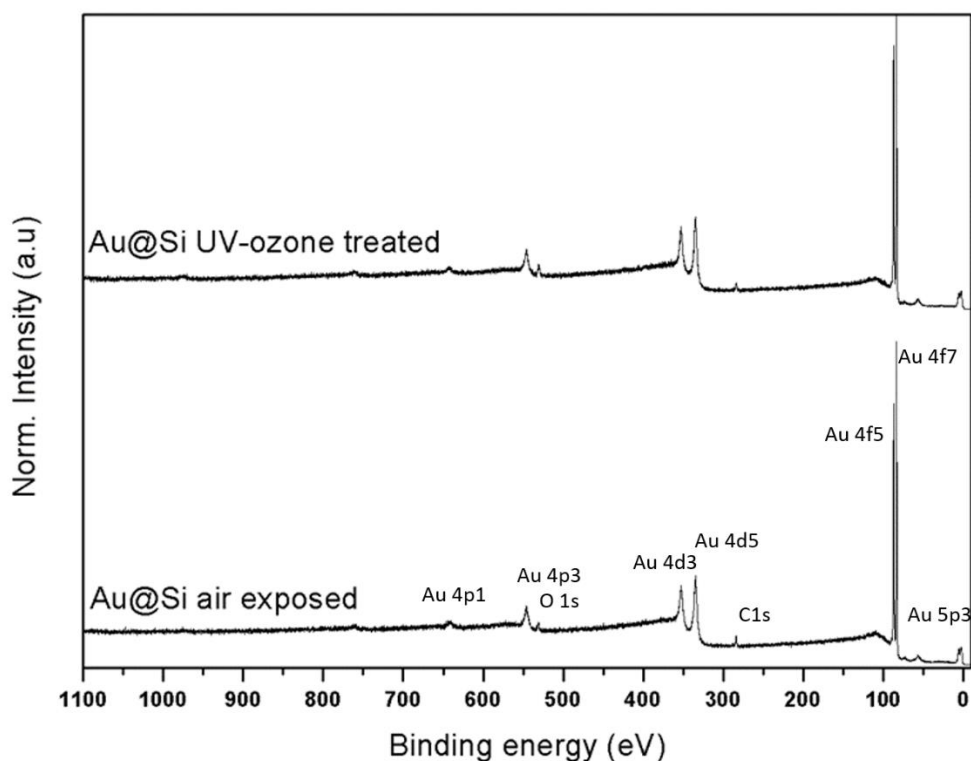


Figure 113: XPS spectra of Au@Si air exposed (bottom) and Au@Si UV-ozone treated (top) showing the presence of oxygen and carbon contaminants on the surface.

The different substrates used are: PEI-coated ITO, not treated ITO-coated glass, ozone treated ITO-coated glass, air exposed Au layers co-evaporated on Si wafer and ozone treated Au layers co-evaporated on Au wafer.

2.3.8.2 Energy level alignment on different substrates

The values of measured work functions and the energy of the valence band maximum (HOMO) of the different compounds on the selected substrates are reported in **Table 13**.

		HOMO (eV)	ϕ (eV)	$\Delta\phi$ (eV)
PEI	<i>Substrate</i>	3.1	3.53	-
	<i>PCBM</i>	1.72	4.31	0.8
	<i>PPC4</i>	1.93	4.0	0.5
	<i>PPC6</i>	1.92	3.9	0.4
ITO not treated	<i>Substrate</i>	1.2	3.76	-
	<i>PCBM</i>	1.6	4.4	0.64
	<i>PPC4</i>	1.77	4.2	0.44
	<i>PPC6</i>	1.9	4.36	0.6
ITO O₃ treated	<i>Substrate</i>	3.83	3.88	-
	<i>PCBM</i>	1.68	4.4	0.5
	<i>PPC4</i>	1.73	4.3	0.4
	<i>PPC6</i>	1.73	4.3	0.4
Au air exposed	<i>Substrate</i>	-1.3	4.52	-
	<i>PCBM</i>	1.35	4.76	0.24
	<i>PPC4</i>	1.66	4.4	-0.1
	<i>PPC6</i>	1.65	4.1	-0.4
Au O₃ treated	<i>Substrate</i>	-7	4.85	-
	<i>PCBM</i>	1.03	4.87	0.02
	<i>PPC4</i>	n.v*	4.98	0.1
	<i>PPC6</i>	1.53	4.34	-0.5

Table 13: Values of HOMO level and work function obtained from UPS spectra of different samples. *not visible.

According to the ICT model, a charge transfer from the substrate to the different fullerenes resulting in a pinning at the ICT- level can be expected if the work function of the substrate is lower as ICT- of the fullerene. For PCBM these levels are known from the literature (5.32 eV for E_{ICT+} and 4.31 eV for E_{ICT-}).[301] Considering the value of the work function of the different substrates, a pinning at the ICT- level can be expected for PCBM when it is deposited on PEI, ITO n.t. and ITO O₃ treated. An opposite charge transfer, from the organic to the metal is not expected, since the work function of all substrates is significantly smaller than E_{ICT+} of PCBM. Indeed, the absence of interface dipoles for PCBM on the gold substrates in **Table 13** confirms the expected vacuum level alignment regime for $E_{ICT-} < \Phi_{SUB} < E_{ICT+}$.

For PEI and the ITO substrates, the UPS spectra before and after deposition of PCBM are shown in **Figure 114**. The shift of the high binding energy cutoff after deposition indicates the formation of an interface dipole, clearly visible for all systems (cf. **Table 13**). The value of the work function of PCBM, extracted from the position of the high binding energy cutoff, corresponds to E_{ICT-} . The found values between 4.31 eV and 4.4 eV are in good agreement to the literature (4.31 eV).[301]

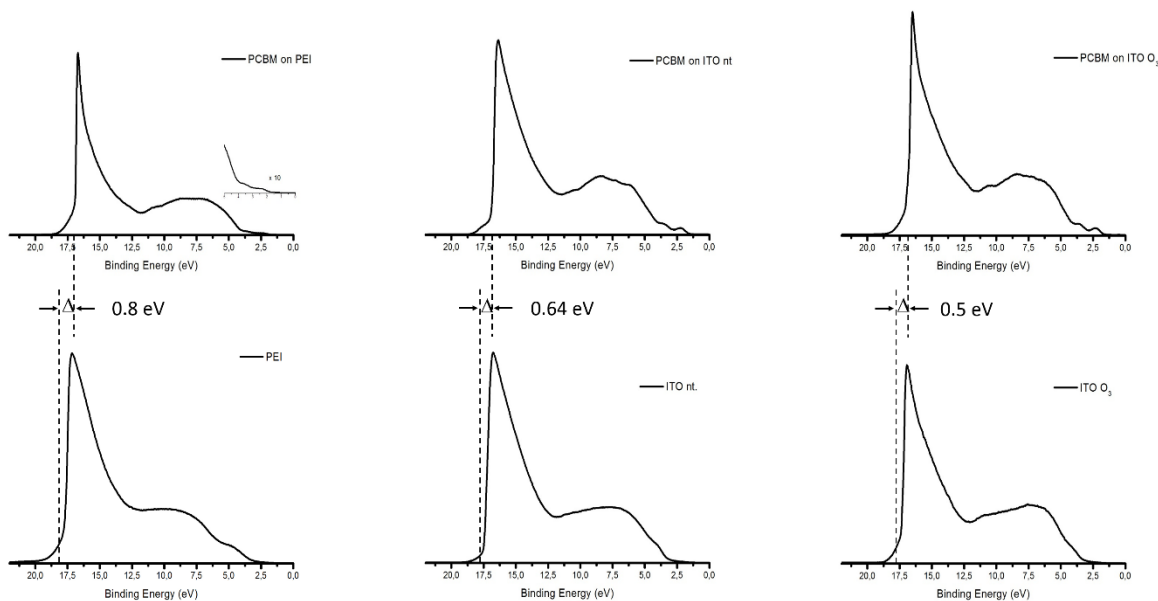


Figure 114: UPS spectra before and after deposition of PCBM on (left) PEI, (center) ITO not treated, (right) ITO ozone treated.

More difficulties were revealed with respect to the deposition of **PPC6**. In the case of **PPC6** on ITO n.t., for instance, the secondary electron cut off appears broader than 0.5 eV. Moreover, on

Au substrates often steps were found in the secondary electron cut off, indicating regions with different work function and thus an inhomogeneous polymer film. Moreover, in particular for **PPC6** a wide spread of the ionization potential (sum HOMO and ϕ in **Table 13**) is observed, ranging from 5.8 to 6.25 eV. Although the ionization potential cannot be generally regarded as a materials' constant, it depends e.g. from the molecular orientation or interfacial doing,[302,303] we would not expect larger variations for the studied (disordered) polyfullerenes. We ascribe these difficulties rather to the film formation on the different substrates. Most likely the polymer was poorly solved, or properties of the substrate surface supported an agglomeration of the polymers resulting in the formation of islands and regions with low material coverage. As a consequence, the ionizing photoemission process generates an inhomogeneously charged polymer film, which may explain the observed spectral features. This difficulty might be overcome by the preparation of thinner polymer films and the analysis of thickness-dependent data. We focus therefore in the following on the PEI substrate only. For this system well-defined UPS spectra with sharp HOMO and cut-off features were obtained (**Figure 115**). In the case of **PPC6** further experiments were performed to confirm the data.

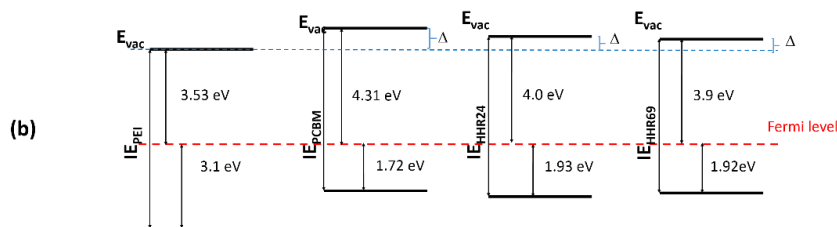
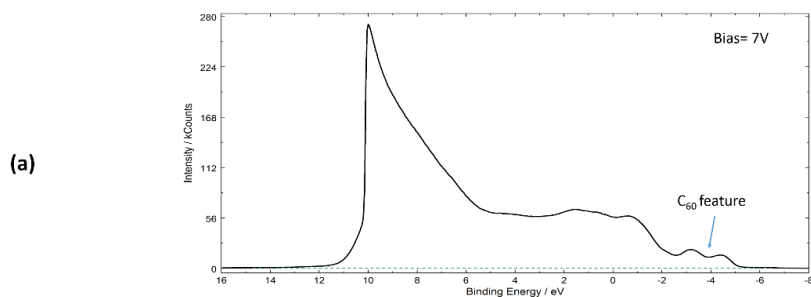
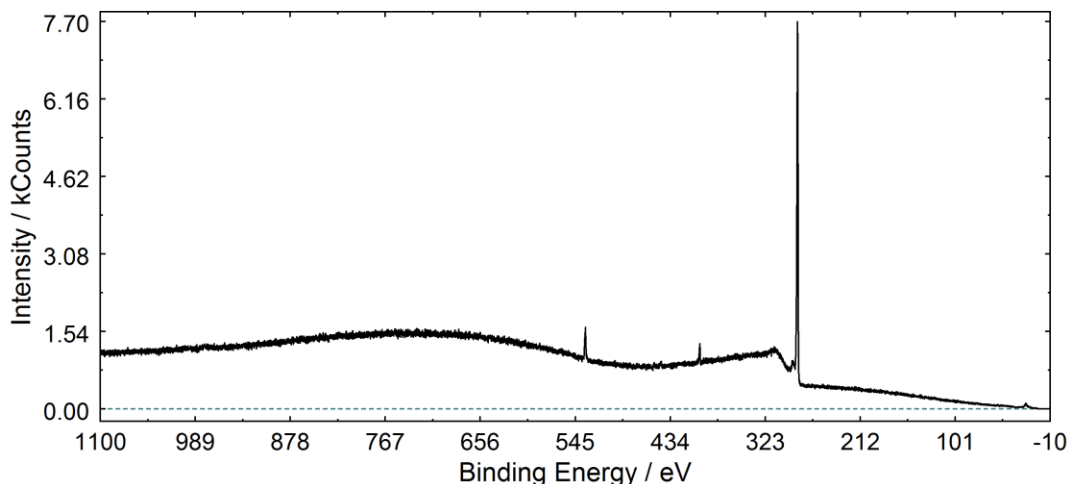


Figure 115: (a) example of well-defined UPS spectrum for **PPC** on PEI and, (b) energy level diagrams for PPCs on PEI systems.

The polymerization of fullerenes changes their electronic properties. As example, in the row PCBM – BisPCBM – TrisPCBM a lowering of the ionization potential was observed (6.1/5.95/5.85 eV). Such effects can be understood by variation of the length of the π -conjugated system or by the introduction of additional electron-withdrawing or electron donating groups, as for example the electro donating alkoxy groups on the benzene ring of the comonomer. Indeed, also in our case, a lowering of the ionization potential (sum HOMO and ϕ in **Table 13**) as a consequence of the polymerization is observed (6.03 for PCBM, 5.93 eV for **PPC4** and 5.8 eV for **PPC6**). At the interface to PEI, interface dipoles of 0.5 eV and 0.4 eV were observed for **PPC4** and **PPC6**, respectively. The formation of such interface dipoles points again to a pinning of the energy levels

at the interface. In our case, the pinning level can be related to the ICT- level of the polymer. The value for E_{ICT} is 4.0 eV (**PPC4**) and 3.9 eV (**PPC6**) and thus significantly lower compared to PCBM.

In the context of organic solar cells, such pinning levels are important for the device performance. Possible barriers toward hole-and/or electron-extraction will decrease the open circuit voltage (V_{oc}) and the overall power efficiency.[162] Our studies confirm the pinning at the ICT- level and thus absence of larger barriers at the interface. However, for electrode materials with slightly higher work function (of about 0.3-0.5 eV), a vacuum level alignment accompanied with a barrier formation might be expected for the studied polyfullerenes, although for related PCBM based devices still a pinning regime is observed. Therefore the use of very low work function electrodes seems to be essential for devices containing polyfullerenes as active layer (electron acceptor). In addition, a change of the potential step at the bulk heterojunction donor-acceptor interface has to be taken into consideration.

In this chapter, two polymerization routes to achieve fullerene-containing polymers in their back-bone have been presented. The first polymerization route is based on atomic transfer addition polymerisation (ATRAP). In the study here reported, PCBM has been employed as monomer to take advantage from its good solubility. This route, chosen because easy to implement, results in oligo- and polyPCBM materials with good solubility. The synthesis is facile but highly sensitive to impurities. SEC chromatography analysis on different batches of materials suggests that particular care with handling of C_{60} and PCBM with respect to oxygen and light, and great care with respect to the pre-cleaning of the CuBr are necessary to obtain a controlled reaction.

In the chapter, more details on the studies of two materials are reported. PolyPCBM_A, presents a polymeric nature, while polyPCBM_F, the second compounds, has an oligomeric nature. The difference in the two materials could be attributed to the different scale of the reactions while temperature, concentration, as well as time of reaction were the same for the two reactions.

Different characterisation techniques show the close similarity between polyPCBM_F and PCBM. This was confirmed by the SEC analysis. Indeed, it has been noticed that PCBM contributes to polyPCBM_A to the extent of 3% while the percentage drastically increases to 35% in polyPCBM_F after purification in Soxhlet apparatus with acetone.

The second route of polymerisation presented in the chapter is based on fulleropyrrolidine chemistry (Prato chemistry), which is, to our knowledge, exploited for the first time for the synthesis of main-chain polyfullerenes.

Three different co-monomers, namely terephthaldehyde, 2,5-bis(octyloxy)terephthaldehyde and, 2,5-bis(dodecyloxy)terephthaldehyde, have been employed in the reactions to study the role of the substituents on the polymerisation process.

The polymerisation results highly dependent on the steric hindrance of the comonomer. In particular, while the small terephthaldehyde results in a multi-substituted fullerene derivatives, the hindrance of the comonomers with longer side alkoxy-chain led to oligo- and polyfullerene.

Also concentration and temperature of reaction play a role in the polymerisation. In particular, despite the use of the same comonomer, higher temperature (150 °C instead of 110 °C), and higher concentration, led to higher molecular weight macromolecules.

Kinetic studies suggest that the polymerization process occurs through three distinct regimes with time:

- A. a period of induction, where C_{60} dissolution or ylide formation or both are rate determining up to the 180th minute;
- B. a period where the polymerisation proceeds in accordance with a typical step growth reaction to around 10 h;
- C. a period where the polymerisation is limited by product precipitation.

Comparing the calculated electronic transitions for a representative compound with the UV-vis spectrum of one of the polymers, revealed that the closest correlation was found for the trans-3 isomer. Trans-2 adduct was detected in smaller amounts in the mixture and resulted very much reduced when larger $-OC_{12}H_{25}$ chains are used in the comonomer. This corroborates the idea that the larger comonomer are enforcing steric control over the product.

XPS and UPS analysis have been conducted on the synthesized materials which have been deposited on various substrates. A lowering of the ionization potential as a consequence of the polymerization is observed (6.03 for PCBM, 5.93 eV for **PPC4** and 5.8 eV for **PPC6**). At the interface to PEI substrate, interface dipoles of 0.5 eV and 0.4 eV were observed for **PPC4** and **PPC6**, respectively, which suggest a pinning of the energy levels at the interface. The pinning level can be related to the ICT- level of

*the polymer. The value for E_{ICT} is 4.0 eV (**PPC4**) and 3.9 eV (**PPC6**) and thus significantly lower compared to PCBM.*

3 Application of polyfullerenes in organic solar cells

Abstract

The study on the photovoltaic performance of representative synthesized oligo- and polyfullerene materials applied to devices is presented here. The material based on PCBM has been tested as an alternative acceptor in the active layer. The novel poly(fulleropyrrolidine) materials have been tested for three applications: (i) as electron acceptor material within the blend; (ii) as an interlayer between the active layer and the electron extraction layer and; (iii) as an additive to stabilize the morphology of the blend under thermal stress.

Part of the results will be published in:

Patent pendent 'Semiconducting mixtures'

R. C. Hiorns (CNRS), H. H. Ramanitra (UPPA), D. Bégué (UPPA), H. Santos Silva (UPPA) A. Distler (Belectric OPV GmbH), S. Dowland (Belectric OPV GmbH), G. Morse (MERCK). Merck/CNRS/UPPA/Belectric OPV GmbH.

"It's ATRAP! PolyPCBM and its oligomers for the stabilization of polymer:PCBM bulk heterojunctions"

Hasina H. Ramanitra, Simon Dowland, Hugo Santos Silva, Didier Bégué, Sambatra Rajoelson, Michael Salvador, Andres Osvet, Christoph J. Brabec, Hans-Joachim Egelhaaf, Graham Morse, Andreas Distler, Roger C. Hiorns

A Facile Metal-free Route to Main-chain Fullerene Polymers

Hasina H. Ramanitra, Hugo Santos Silva, Abdel Khoukh, Craig. M. S. Combe, S. A. Dowland, Didier Bégué, Christine Dagrón-Lartigau, Andreas Distler, Graham Morse, Roger C. Hiorns

Part of the results have been presented in national and international conferences:

1. Fullerene-based polymers for photovoltaic applications (oral presentation)

Hasina H. Ramanitra, Simon A. Dowland, Graham E. Morse, Hugo Santos Silva, Didier Bégué, Thomas Chassé, Andreas Distler and Roger C. Hiorns

12th International Symposium on Functional π -Electron Systems (F π -12), July 2015, Seattle, Washington, USA.

2. Fullerene-based polymers for photovoltaic applications (Polymères à base de fullerene pour applications photovoltaïques) (oral presentation)

Hasina H. Ramanitra, Simon A. Dowland, Graham E. Morse, Hugo Santos Silva, Didier Bégué, Thomas Chassé, Andreas Distler and Roger C. Hiorns
Congrès 2015 de la Société Chimique de France, July 2015, Lille, France

3. Fullerene-based polymers for photovoltaic applications (oral presentation)

Hasina H. Ramanitra, Simon A. Dowland, Graham E. Morse, Hugo Santos Silva, Didier Bégué, Thomas Chassé, Andreas Distler and Roger C. Hiorns
ESOS European training school and conference on organic photovoltaic stability, June 2015, Cargèse, Corsica, France

4. Incorporation of Fullerene into Polymers for photovoltaic Applications (oral presentation)

Hasina Harimino Ramanitra, Hugo Santos Silva, Simon Dowland, Didier Bégué, Christine Dagron-Lartigau, Andreas Distler, Roger C. Hiorns
The 2014 IUPAC World Polymer Congress or MACRO 201, July 2014, Chiang Mai province, Thailand.

5. Fullerene-based polymers for photovoltaic applications (poster presentation)

Hasina H. Ramanitra, Simon A. Dowland, Graham E. Morse, Hugo Santos Silva, Didier Bégué, Thomas Chassé, Andreas Distler and Roger C. Hiorns
EMRS 2015 Spring Meeting, May 2015, Lille, France

6. Incorporation of Fullerene into Polymers for Photovoltaic Applications (poster presentation)

Hasina H. Ramanitra, Hugo Santos Silva, Didier Bégué, Christine Dagron-Lartigau, and Roger C. Hiorns
Jjcnanorga13 : Journées Jeunes Chercheurs NANORGASOL, Nov 2013, Mèze, France

More presentation have been given by Dr. Hiorns Roger and Dr. Simon A. Dowland:

Invited Oral Lectures:

7. PolyPCBM: Polyfullerenes for Organic Photovoltaic Cells

H. H. Ramanitra, H. Santos Silva, S. Dowland, D. Bégué, H. Peisert, T. Chassé, J.-L. Gardette, S. Thérias, A. Rivaton, C. Dagron-Lartigau, G. Morse, A. Distler, R. C. Hiorns
XIV Brazil MRS Meeting, 8th International Summit on Organic and Hybrid Solar Cells Stability (ISOS-8), Rio de Janeiro, September/October 2015.

8. ATRAP as a Route to PolyPCBM... and Stabilising Organic Photovoltaic Devices

H. H. Ramanitra, S. A. Dowland, H. Santos Silva, C. M. Combe, D. Bégué, C. Dagron-Lartigau, Graham Morse, A. Distler, R. C. Hiorns
7th International Symposium on Engineering Plastics, Xining, China, August 2015.

9. Using fullerene as a monomer and stabilizing organic solar cells

H. H. Ramanitra, H. Santos Silva, A. Tournebize, C. M. Combe, D. Bégué, H. Peisert, T. Chassé, J.-L. Gardette, S. Thérias, A. Rivaton, C. Dagron-Lartigau, R. C. Hiorns
The 3rd KIT International Symposium on Advanced Polymer Materials and Fiber Science, Kyoto, Japan, February 2015.

10. Polyfullerenes for photovoltaics

H. H. Ramanitra, B. Bregadiolli, R. Marques Ferreira, H. Santos Silva, C. M. Combe, D. Bégué, F. C. Lavarda, C. Dagron-Lartigau, C. F. O. Graeff, R. C. Hiorns
EMN Meeting on Polymers, Energy Materials and Nanotechnology, Orlando, Florida, USA, January 2015.

11. Polyfullerenes and stabilizing polymer-based organic photovoltaic cells

*H. H. Ramanitra, H. Santos Silva, A. Tournebize, D. Bégué, H. Peisert, T. Chassé, J.-L. Gardette, S. Thérias, A. Rivaton, C. Dagron-Lartigau, R. C. Hiorns**
3rd Kathmandu Symposia on Advanced Materials 2014 (KaSAM), Kathmandu, Nepal, September 2014.

12. Using Fullerene as a Comonomer for Organic Photovoltaic Applications

*H. Santos Silva, H. H. Ramanitra, D. Bégué, C. Dagron-Lartigau, R. C. Hiorns**
6th International Symposium on Engineering Plastics, Xiamen, China, August 2013.

Oral Presentations

13. Teaching an old dog new tricks: Polyfullerenes as a route to the enhanced stability morphological stability of bulk heterojunctions

Dr. Simon Dowland
HOPV15, May 2015, Rome, Italy

14. Polyfullerenes for photovoltaics

H. H. Ramanitra, B. Bregadiolli, R. Marques Ferreira, C. M. Combe, H. Santos Silva, D. Bégué, F. C. Lavarda, C. Dagron-Lartigau, C. F. O. Graeff, R. C. Hiorns
Advanced Materials and Nanotechnology AMN7, Nelson, New Zealand, February 2015.

The devices and experiments presented here were performed by Dr S. A. Dowland, from Belectric OPV GmbH. "

The research leading to these results has received funding from the French Region Aquitaine under the grant agreement FULLINC 2011 and from European Union Seventh Framework Program (FP7/2011) under grant agreement ESTABLIS no. 290022.

3.1 PolyPCBM acceptors in OPV devices

We here present the application of the synthesized materials in solar cell and their characterization. The aim of this study was to test the performance of the novel polymers as alternative acceptor material to PCBM. This application is the straightforward application for which the novel fullerene derivatives are proposed. In our case, the excellent electron properties of fullerene are expected to be only slightly modified and the oligomeric /polymeric character of the material are expected to affect the morphology of the active layer. The synthesized polyPCBM_F has thus been inserted in solar cells blended with the donor archetypal P3HT. A successive work has been the study of the thermal stability of the system. Finally, the oligo-fullerene has been tested as an acceptor in two other systems, namely with the low band gap polymers PCDTBT and Si-PCPDTBT.

3.1.1 Organic solar cells based on polyPCBM:P3HT blends

Each and every single component of an OPV device is nowadays an object for optimization studies. Although the P3HT:PCBM-based solar cells are historically the most studied system, as underlined in 2011 by Dang, Hirsch and Wantz in their paper “P3HT:PCBM, best seller in polymer photovoltaic research”, [304] the quest of novel materials for photovoltaic applications is a hot topic in organic solar cells research. This system is now in fact well known in many of its aspects and generally used as model device for OPV development, but it presents relatively low PCE (~3-6 %), [304,305] and low V_{oc} . In the active layer, much of the effort has been historically focused on the donor material and higher PCE have been actually obtained with low band gap polymers. [306–308] Regarding the n-type materials, PCBM is still the most largely fullerene-based acceptor used in devices. However, different fullerene derivatives have been proposed as alternative to PCBM. [173,309–311] In this paragraph we present the results obtained substituting PCBM with polyPCBM_F in inverted solar cell. We decided to use P3HT:PCBM system as control for the performance of the novel materials. The general architecture of the fabricated devices is shown in **Figure 116**.

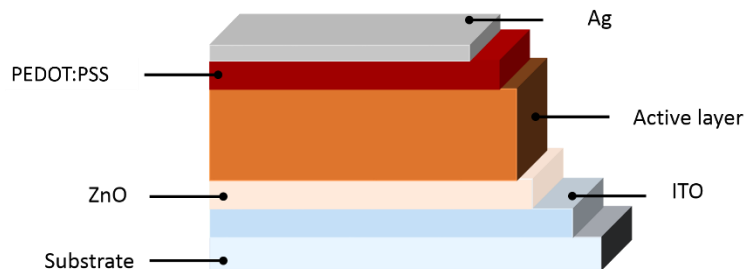


Figure 116: General architecture of the inverted solar cells employed in this work.

Photoluminescence (PL) spectroscopy is used to investigate the interaction between the exciton formed on the P3HT and the acceptor. The extent of eventual photoluminescence quenching gives indication on the mixing between the components in the mixture and on the charge transfer occurring which stops the emission. A preliminary photoluminescence study on P3HT:PCBM and P3HT:polyPCBM_F, in function of the fullerene derivative load, shows that the opto-electronic properties of the two systems are very close. In fact, from the results obtained for 445nm excitation are displayed in **Figure 117** one can observe the same trend with, in particular, a high PL quenching at low loading of the fullerene derivative in both systems.

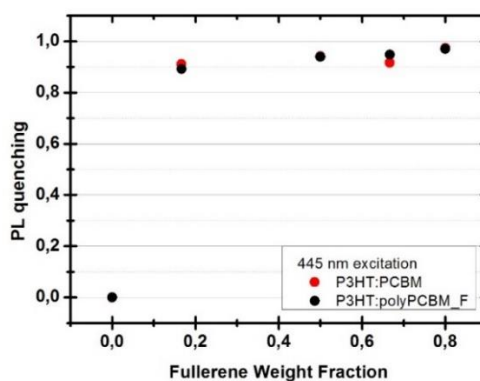


Figure 117: PL quenching of (red) P3HT:PCBM and (black) P3HT:polyPCBM_F as function of the fullerene weight fraction.

The PL data suggest that polyPCBM is mixing as well as the PCBM in the blend. This is in line with the oligomeric nature of polyPCBM_F.

From this and previous results, e.g.. the UV-visible absorption characteristics of polyPCBM_F with respect to PCBM, it was expected that the two materials would result in comparable

performances in solar cells. This is actually the case we have observed. However it has to be said that the film formation properties of the two compounds are quite different when film are blade-casted from *o*-xylene showing the different nature (small molecule in the case of PCBM, and oligomer in the case of polyPCBM_F) of the two compounds. This can be seen in **Figure 118**, where the AFM images of the films are shown. The images indicate a considerable smoothing of the surface, with the RMS decreasing from 2.5 to 0.4 nm; from them it is apparent that PCBM_F is of use to obtain more homogenous films.

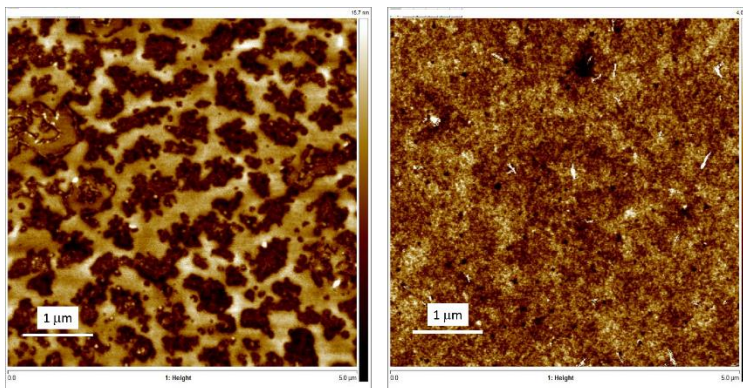


Figure 118: AFM images of (left) PCBM; and (right) oligoPCBM. Films prepared by blade casting from solutions in neat xylene.

When the PCE of different devices are measured as function on the composition ratio of the active layer (**Figure 119**), similar trends are found. The PCE is higher for the devices where the fullerene weight fraction is equal or less than 0.5 and the lowest value is found when this fraction is 0.8. The results here showed are not for optimised devices, but are for blends processed in neat

xylene on flexible substrates. This explains to some extent the low values of PCE obtained in this study. However, this system was used due to its industrial relevance.

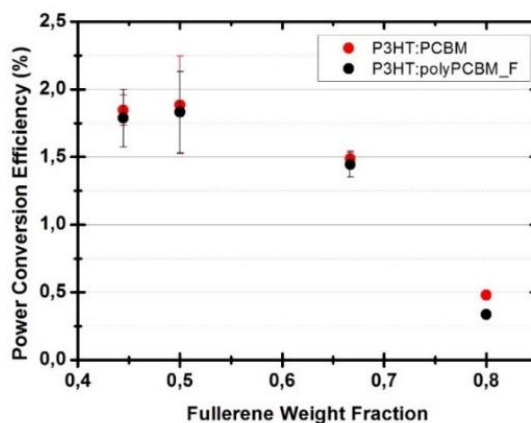


Figure 119: PCE of (red) P3HT:PCBM and (black) P3HT:polyPCBM_F devices as function of the fullerene weight fraction.

The obtained results indicate that both the opto-electronic and the charge-transfer properties of PCBM are not diminished by the presence of polymer in polyPCBM_F, even in extremely high amounts of around 70% (Section 80). It could sound naïve, but we actually consider the obtained results from the devices, as encouraging for the continuation of our research. Indeed, low concentrations of additives can improve device efficiencies and stabilities, but in quantities above a few percent generally result in a rapid decrease in productivity.[312]

3.1.2 Device thermal stability

As not only the performances, but also the lifetime of a device is crucial for its real-life application, when testing a new material in solar cells, it is also interesting to test its performance in different degradation conditions. For this work we focused on an accelerated thermal degradation study at 120 °C. Inverted solar cells containing polyPCBM_F as alternative of PCBM in the active layer with P3HT have been prepared and annealed at 120 °C in a glovebox, where all the performance measurements have been performed. ITO/ZnO/P3HT:PCBM/PEDOT:PSS/Ag devices have been used as control. **Figure 120a** demonstrates that in the experimental conditions, polyPCBM_F

stabilizes device efficiency with T_{80} being 10 times longer than for the control, it also closely follows J_{sc} (**Figure 120b**).

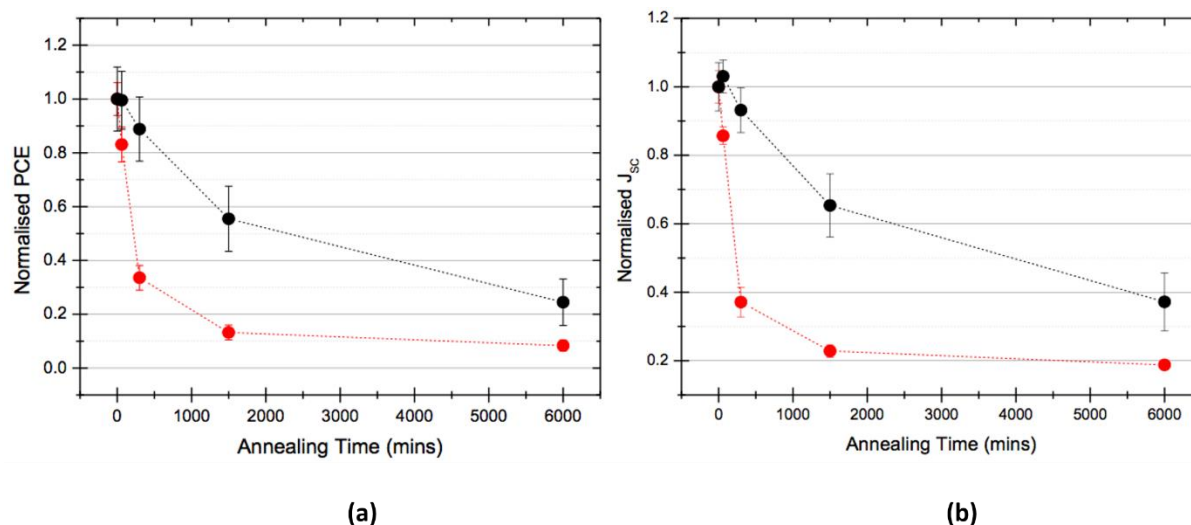


Figure 120: (a) PCE and (b) normalized J_{sc} for (red) ITO/ZnO/P3HT:PCBM/PEDOT:PSS/Ag and (black) ITO/ZnO/P3HT:polyPCBM_F/PEDOT:PSS/Ag devices with annealing time.

One can hypothesize that this is a result of a stabilization of charge transfer that could be due to the fact that the PCBM is migrating to a lesser extent, both vertically towards the interfaces, and in the bulk. To investigate the effect of polyPCBM on the evolution of the morphology of the active layer, we performed optical microscopy of the samples after 100 h. The images (**Figure 121**) suggested a leaching of the fullerene derivative into aggregates. Interestingly, the device with polyPCBM_F forms the larger aggregate structures. This is in contrast with what is normally expected.[313] Studies to elucidate this point are still on going. Nonetheless, different hypotheses can be proposed, that is either there is enough polyPCBM_F being restrained into close contact with P3HT to generate charges.

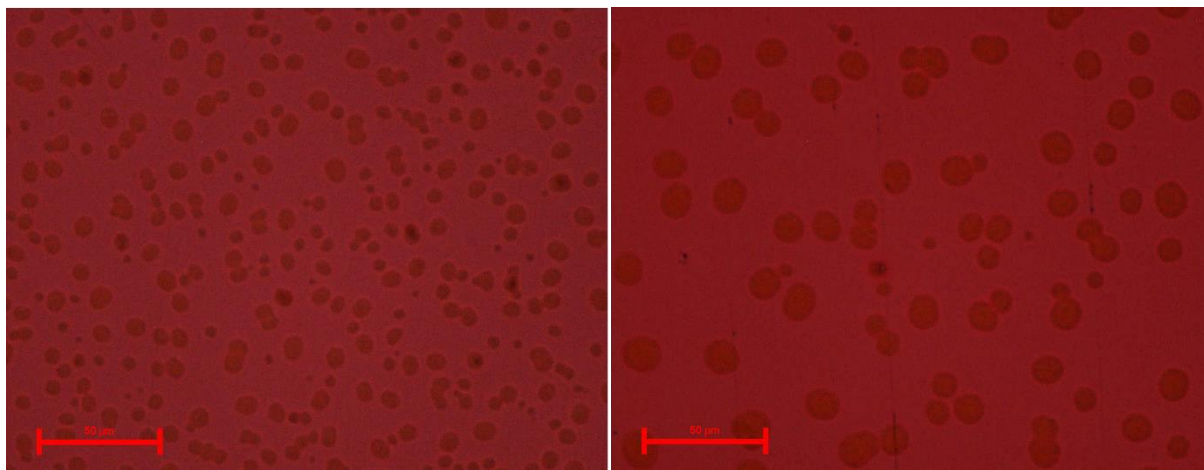


Figure 121: Optical microscopy images of (left) P3HT:PCBM and (right) P3HT:polyPCBM_F blends after 100 h at 120 °C in glovebox.

3.1.3 Low band gap: polyPCBM solar cells

The very promising results obtained on the accelerated thermal ageing of P3HT:polyPCBM_F devices, encouraged us to investigate the eventual thermal stabilizing properties of this polymer within LBG-based systems. We have prepared devices with PCDTBT and Si-PCPDTBT as donor materials. The chemical structures of the polymers are reported in **Figure 122**. The effects of accelerated thermal ageing on PCEs, which are again found to heavily correlate with J_{sc} , on the devices are shown in **Figure 123**.

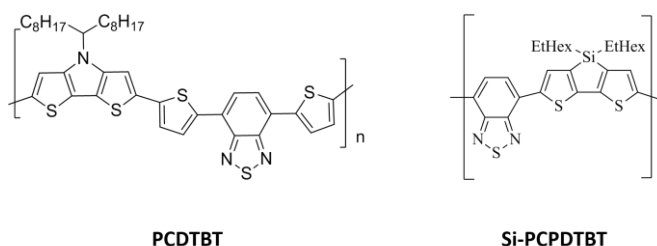


Figure 122: Structure of PCDTBT and Si-PCPDTBT used as donor polymers in the devices.

As one can observe, in all cases, polyPCBM_F is found to stabilize the devices in the experimental conditions. The T_{80} is delayed by polyPCBM_F with respect to PCBM. The morphology of the different systems have been analysed by mean of optical microscopy. The images obtained of the aged samples are shown in **Figure 124**. While PCDTBT:PCBM gives rise to large aggregates of PCBM, the mixture Si-PCPDTBT:polyPCBM_F appears more homogeneous with only few small

aggregates appearing. This would lead to the conclusion that in this polymer the morphology is stabilized with polyPCBM_F. It is important to underline that the experiments presented above are very much initial studies aimed to verify the possible applicability of the novel polyPCBM materials in OPV active layers. From these studies we demonstrate, that while polyPCBM_F is actually applicable to numerous systems, it most likely requires an optimization specific to each partner low band gap polymer.

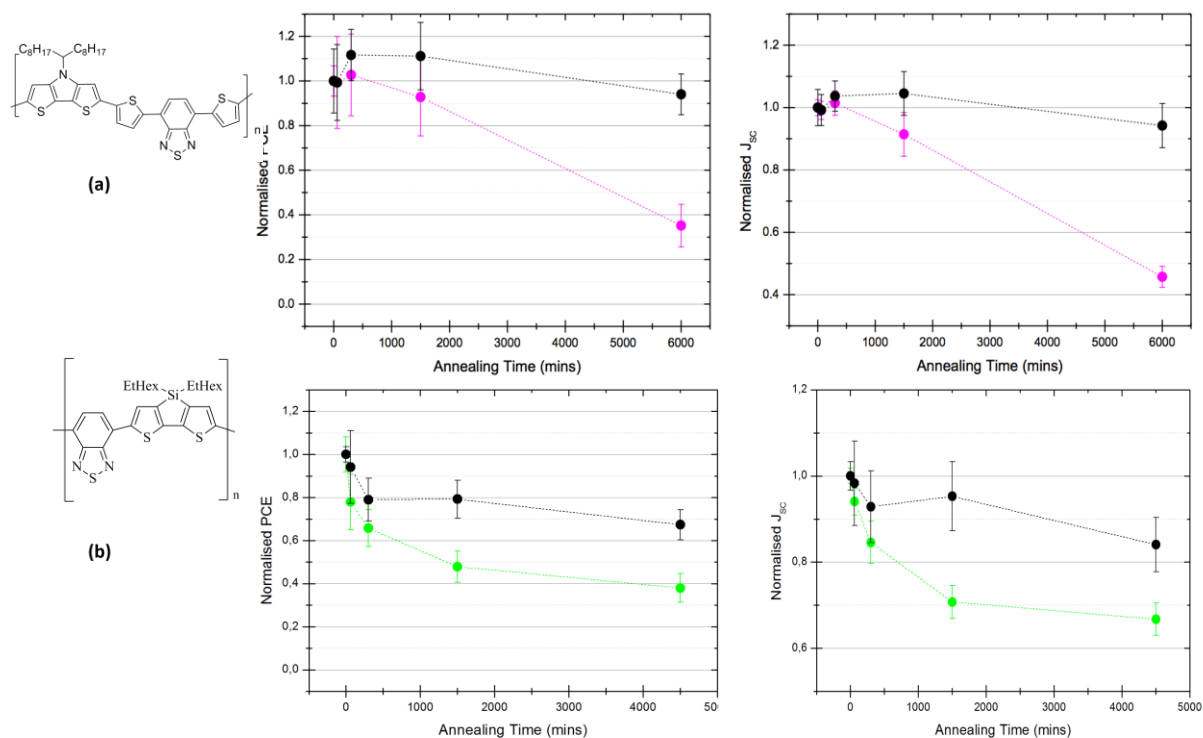


Figure 123: Extracted performances for devices fabricated and thermally annealed at 120 °C with alternative donor polymers and PCBM (colours) or polyPCBM_F (black).

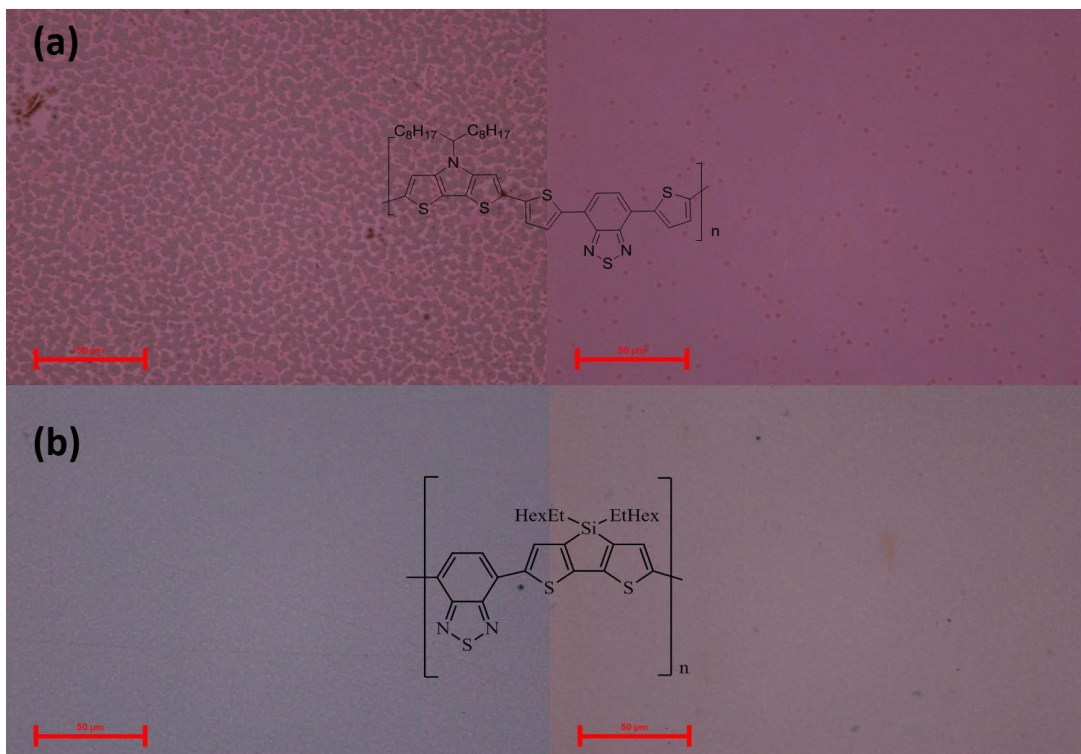


Figure 124: Photomicrographs of thermally treated thin films (120 °C) of (top) PCDTBT and of (bottom) Si-PCPDTBT, mixed with (left) PCBM or (right) oligoPCBM.

3.2 Polyfulleropyrrolidines-based organic solar cells

Fulleropyrrolidines are a very interesting class of materials that find applications in various technological fields due to their ease of production, modification of the substituents and relative stability (Section 2.3). Up to now, although the low performances of these materials in organic photovoltaics have limited the interest for their application in this field, many examples of fulleropyrrolidines as alternative acceptors to PCBM, [310,314–320] as electron transport interlayers, [321] or additives in the active layer [322] can be found in literature. In this study, the success in the incorporation of fulleropyrrolidine into main-chain polyfullerenes has encouraged us to investigate either or not the novel polymers could aspire for a role in OPV devices. We have employed **PPC4** in the three roles prior reported in inverted geometry devices as described in section 3.1.1:

- As a replacement for PCBM in the active layer;
- As an interlayer between the active layer and the electron selective layer;
- As an additive in the active layer.

In all the cases, ITO / ZnO / P3HT:PCBM / PEDOT:PSS / Ag device has been use as control.

In the next paragraphs the results of the different experiments are reported. Since the experiments have been carried out with non-optimized devices, these studies have only comparative value.

3.2.1 Polyfulleropyrrolidine as an acceptor

The first role investigated for the novel polymer has been the role of alternative acceptor to the PCBM. Several devices with active layers obtained from solutions with varying amounts of **PPC4** and PCBM have been prepared. To study the actual effect **PPC4**, the total fullerene content was kept constant across all solutions by adapting the ratio of the two fullerene sources. The performance of the devices with 100%, 80%, 60%, 40%, 20% and 0% control fullerenes from **PPC4** are reported in **Figure 125**. The results from this experiments are not encouraging. As observed in the graphs, as the fullerene content becomes increasingly provided by the **PPC4** the performance of the cells drops (PCE in **Figure 125d**). This drop is primarily due to a loss in the current extracted from the devices, as it is indicated by the changes in J_{sc} which follow the same trend.

While there is no critical changes observed for the fill factor (**Figure 125c**), the V_{oc} of the devices (**Figure 125d**) seems to increase slightly with the increasing of the percentage of **PPC4** in the blend. Further studies have been carried out with equivalent systems that used P3HT as donor material and a polyfullerene equivalent to **PPC4** as acceptor material. Part of the results of this study, are reported in Appendix B.

The PL quenching as a function of blend composition of P3HT:fullerene derivative, processed from xylene with 5%vol 1-methylnaphthaline at different excitation wavelengths, would suggests poor miscibility and poor intermixing between P3HT and **PPC4**.

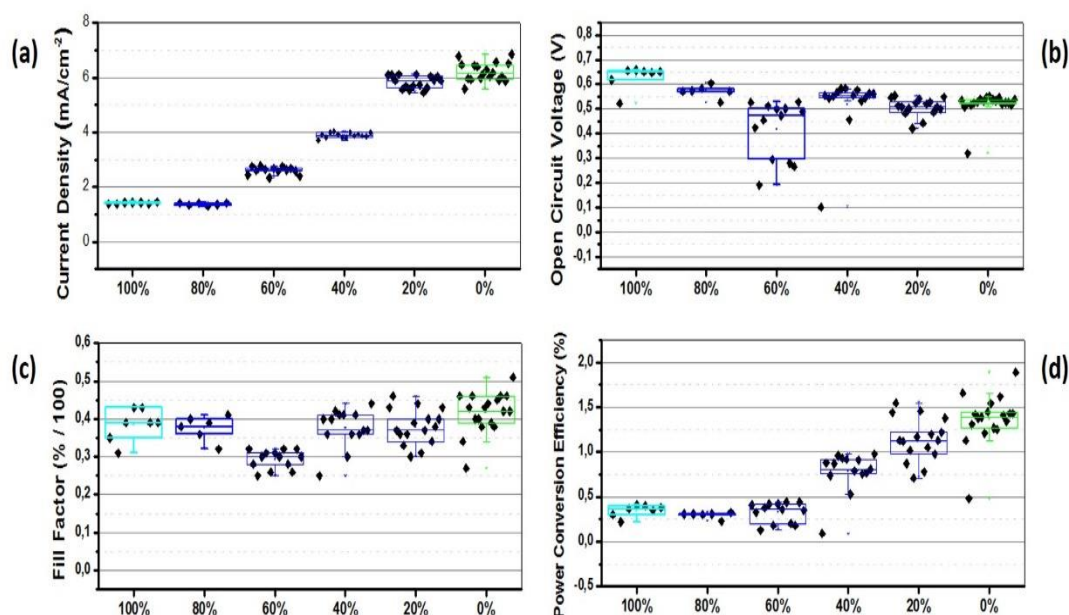


Figure 125: Performance parameters for P3HT:PPC4-based devices with different loading of the fullerene derivative.

3.2.2 Polyfulleropyrrolidine as an interlayer

An important role in the development of organic photovoltaic is currently held by the interfacial hole- and electron-transport layers (HTL and ETL).[323,324] The development of these layers, together with the improvements in the active layer materials and in the device architecture, have recently permitted the achievement of relatively high PCE.[325] We have already treated the topic of fullerene as interlayer in OPV devices in section 1.3.2.

In this section we present the results of the study carried out using **PPC4** as ETL in devices. In the samples, the **PPC4** interlayer has been positioned at the electron selective side of the active layer: ZnO / *Interlayer **PPC4*** / P3HT:PCBM of inverted structure devices.

The interlayer has been deposited from xylene solution at different coating speeds in order to produce different thicknesses. The samples have then been exposed to different annealing temperatures for 20 min. The results reported in **Figure 126** show how the introduction of the interlayer appears to have a detrimental effect on performance (PCE, **Figure 126d**) except for the thinnest layer when unannealed.

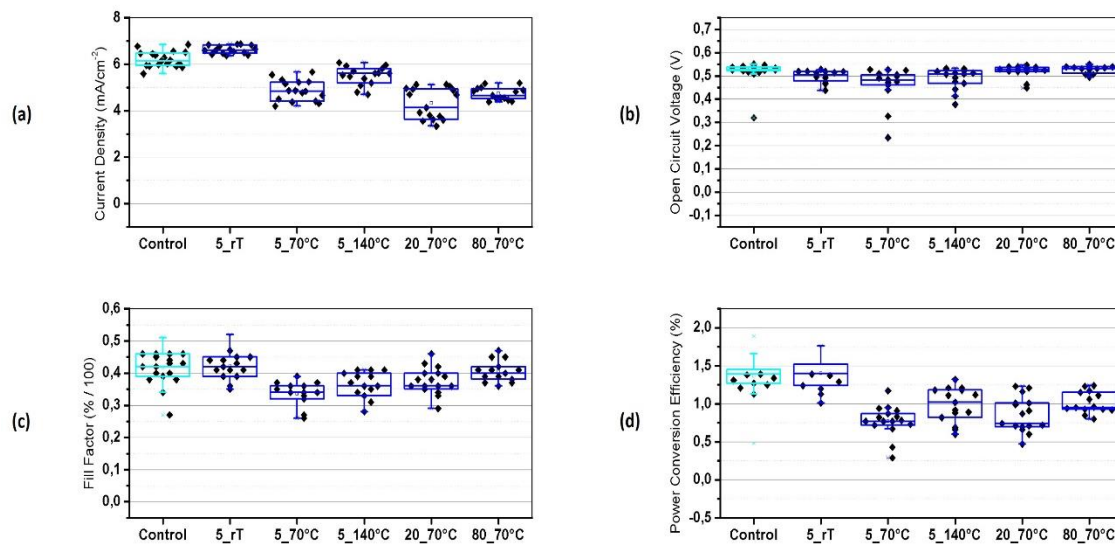


Figure 126: Performance parameters for P3HT:PCBM-based devices with **PPC4** as interlayer between the active layer and ZnO at different annealing time and temperature.

When the devices are annealed, the performances are worse. This can be seen also in the J-V curves of representative devices in **Figure 127** where while the curve for the unannealed sample follows closely the control curve, this is not the case for the annealed samples regardless annealing time and temperature.

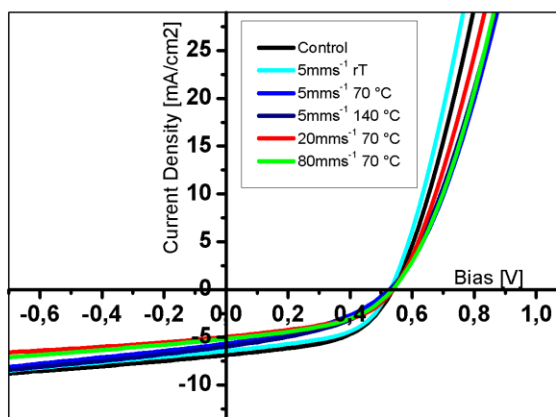


Figure 127: J-V curves of selected representative devices in which **PPC4** has been employed as interlayer between the active layer P3HT:PCBM and ZnO.

Further studies to explain this phenomenon are still ongoing, but we can make some conjectures: (i) it is possible that the annealing process badly affects the layer leading to poor electron transport properties of the interlayer; (ii) it may be that without annealing the material is actually easily removed by contact with xylene used during the deposition of the next layer in the device. Indeed, it is to be said, that the use of this novel class of polyfullerene as interlayer in solar cells can be complicated by the fact that it is not possible to process them with orthogonal solvents for multilayer fabrication.

3.2.3 Polyfulleropyrrolidine as an additive

In section 1.3.3 we have briefly detailed the different fullerene derivatives proposed in literature as additive in the active layer. As mentioned, the main objective is to limit one of the major problems with fullerene derivatives, and in particular with PCBM, which is their tendency to self-aggregate. The tendency to diffuse to the polymer matrix and self-aggregate into larger crystals or clusters with time, one of the major causes of the loss in performance of solar cells. The introduction of polyfullerenes as an additive in the active layer might have a plasticizing effect of the BHJ and thus limit the self-aggregation phenomenon. To verify either or not this was the case, **PPC4** has been employed in this role.

Additional fullerene content in the form of **PPC4** has been added to typical P3HT:PCBM blend solution in such a way as to have 1, 2, 5 or 10 wt%.

The J - V curves for selected representative devices are reported in **Figure 128** and show how the additive does not influence the device performance to any great extent.

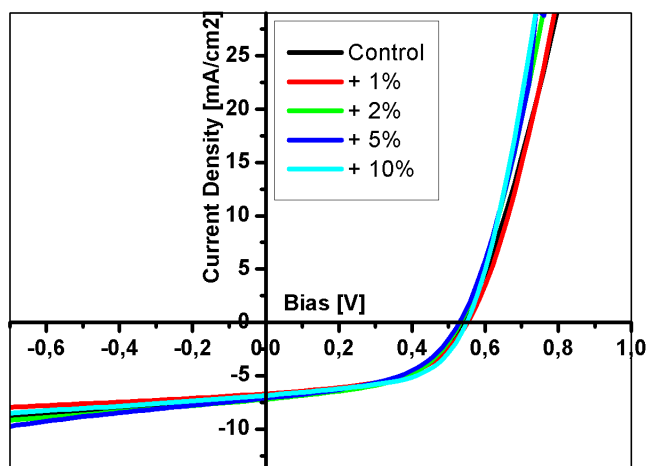


Figure 128: J - V curves of selected representative devices in which **PPC4** has been employed as additive (different % loading) in the active layer P3HT:PCBM.

This observation is confirmed when the different performance parameters are analysed. From the graphs reported in **Figure 129** a-d, one can conclude that the introduction of **PPC4** in devices as an additive in the BHJ does not have a strong influence on the device initial performance.

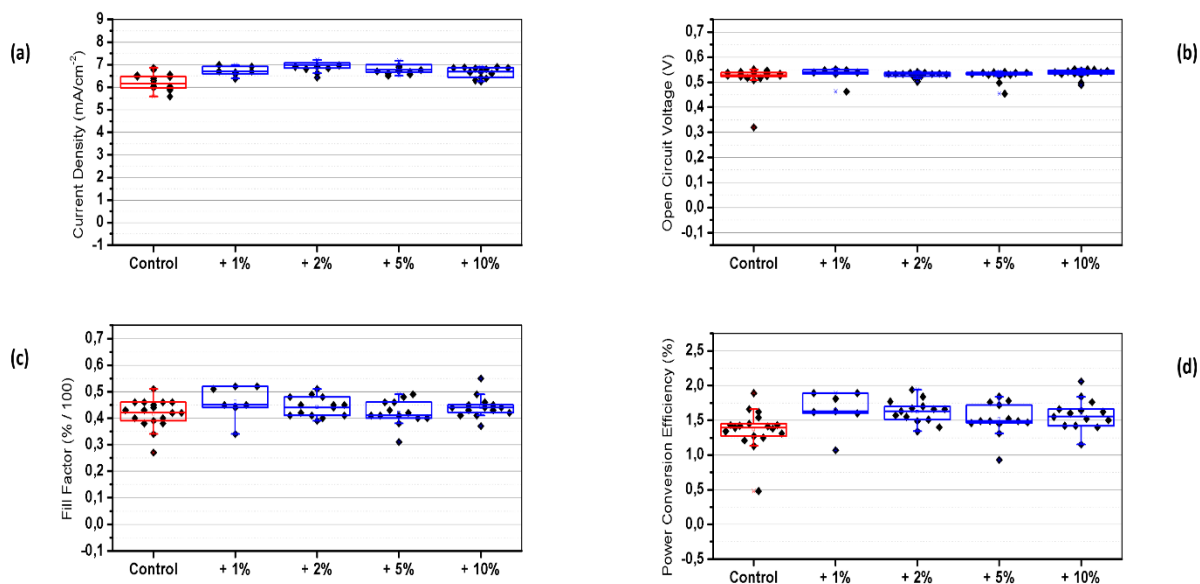


Figure 129: Performance parameters for P3HT:PCBM-based devices with **PPC4** as additive in the active layer as function of the % loading of the polymeric material.

Moreover, from the results it can be said that even a large amount of **PPC4** additive does not inhibit reasonable device performance.

The conclusions that arise from the conducted experiments would suggest that the introduction of **PPC4** in OPV devices does not result in the complete failure of the solar cell. However, analysing single cases, the polymeric material is not a good alternative to PCBM as acceptor in the active layer and, it worsens the device performance when used as an interlayer. The application that seems to be the most attractive is then the use of the polymeric material as an additive. Considering the results from the prior experiments, one can deduce that the use of **PPC4** as additive may actually improve the devices and certainly does not affect them negatively. To start exploring the potential of **PPC4** in the role of additive, accelerated thermal degradation studies have been carried out on devices. The experiments and results will be discussed in the next section.

3.2.4 Device thermal stability

Considering the results presented above, the effect of the introduction of **PPC4** as additive in the active layer of OPV solar cells on their thermal degradation have been tested. A first experiment has been carried out on inverted solar cells which have been prepared by employing **PPC4** at different load in the active layer and annealed in glove box at 140 °C. The inverted solar cells based on P3HT:PCBM blend is use as control. The improvement in the stability of the devices is clear for all the cases as one can notice from the parameters reported in **Figure 130 a-d**. In the graph, the variation of the PCE (**Figure 130a**), J_{sc} (**Figure 130b**), V_{oc} (**Figure 130c**) and, FF (**Figure 130d**) of devices with 2, 5 or 10% loading of **PPC4** additive are reported as a function of the annealing time.

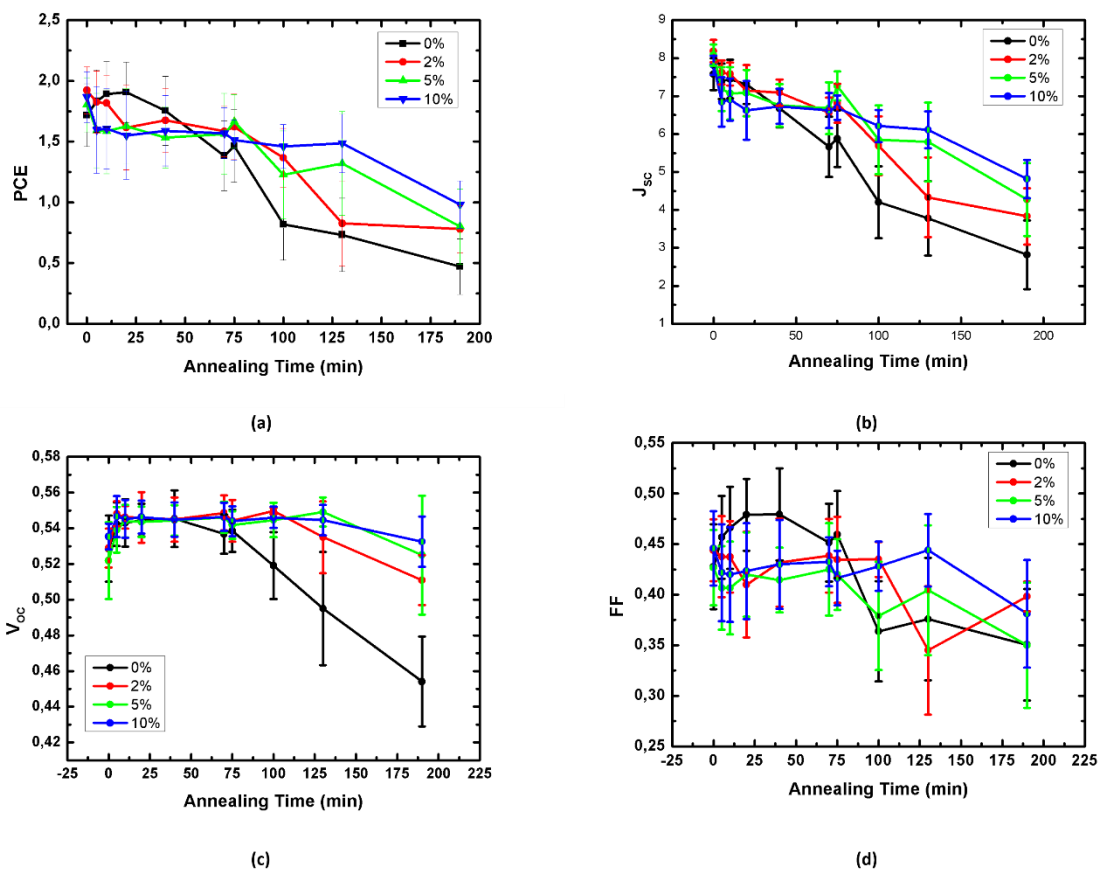


Figure 130: Performance parameters for P3HT:PCBM-based devices with different % loading of **PPC4** as additive in the active layer as function of the annealing time; temperature of annealing=140 °C.

From the values of J_{sc} (**Figure 131b**), it can be observed that **PPC4** improves device thermal stability through a mechanism that preserves this parameter or otherwise retards mechanisms that reduce it. It is an evidence that the greater is the **PPC4** loading in the blend, the larger is the stabilization effect upon annealing of the devices. A study on the influence of the annealing temperature in the stabilization capability of PCE additive has been carried out using devices with 10% load of **PPC4** in the BHJ. The P3HT:PCBM(10% **PPC4**) devices have been prepared and annealed at different time and different temperatures (100, 120 and 140 °C) in the glove box. The annealing temperature has been chosen in accordance with industrial interest.

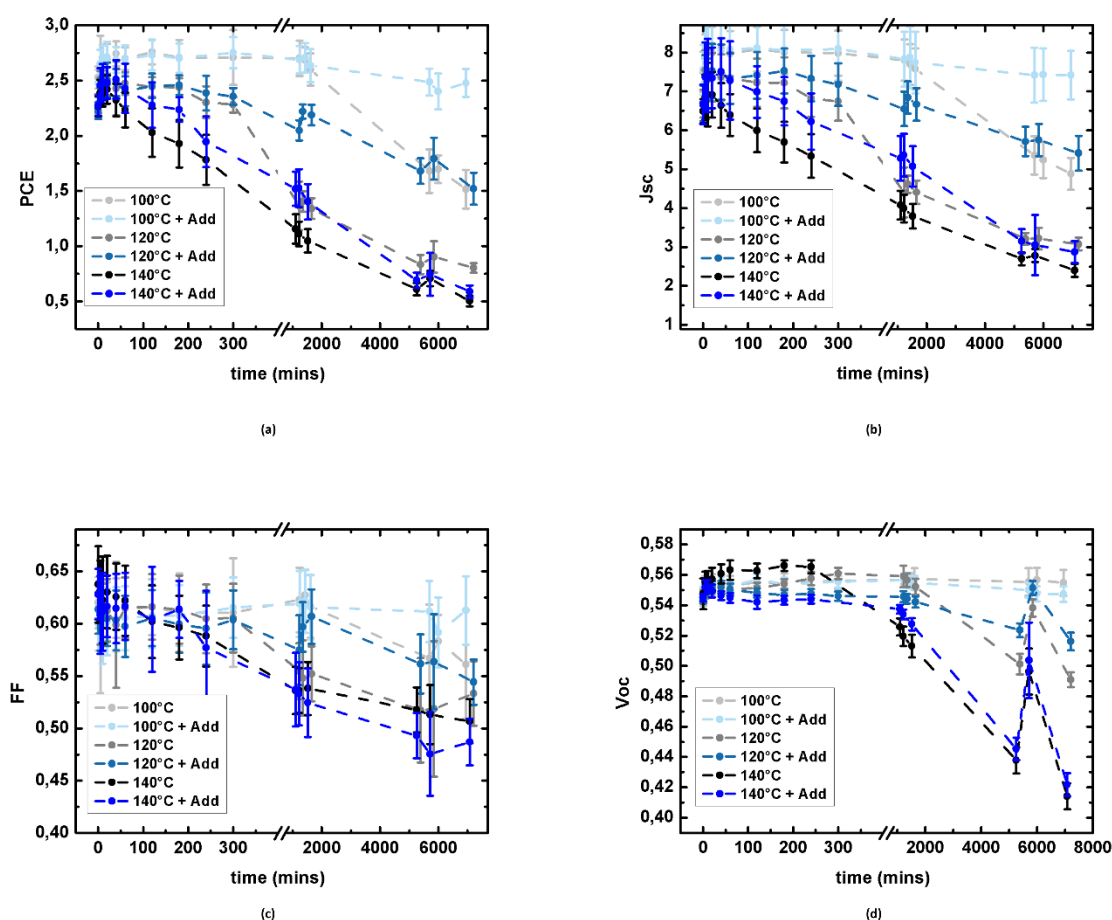


Figure 131: Performance parameters for P3HT:PCBM-based devices with and without 10% loading of **PPC4** as additive in the active layer as function of the annealing time; temperature of annealing=100, 120 and 140 °C.

As expected, the degradation occurs at different rates depending on temperature used. At the lower temperature used, the effect of **PPC4** is much more pronounced. It is to be said that 140

°C could be a too harsh condition to really observe stabilizing effect of potential additives. In time, a fluctuation of the performance can be observed that is coincident with the measurements taken as the first of the day after weekend. Indeed, the performance measured are lower than subsequent measurements. This fluctuation is a sign of a reversible degradation process that is unlikely to do with the thermal treatment. A hypothesis to justify this observation goes in the direction of a induced deactivation of the ZnO due to darkness. [326–329] The deactivation is then thought to be reduced after some small amount of light exposure (which occurs throughout the day when the light is on and the researchers work hard).

3.3 Comparison between polyPCBM and PPCs

From the results presented in the previous sections it is clear that the photovoltaic properties of the polyPCBM obtained by ATRAP polymerization and polyfullerenes obtained by using Prato chemistry, in a route we have called the sterically controlled azomethine ylide cycloaddition polymerization (SACAP), are quite different. In the last two sections we have focused our attention on the use of **PPC4**, and thus the poly(fulleropyrrolidines), as additive in the active layer as this is the application that seems to be the most attractive and promising one. Nonetheless, it is interesting also to compare the performance of these materials and polyPCBM, employed as acceptor material in the blend.

P3HT:PCBM, P3HT:polyPCBM and P3HT with the poly(fulleropyrrolidine) HHR63 blends have been processed at different ratio from neat xylene to fabricate inverted architecture solar cells. The PCE of the devices are reported in **Figure 132**.

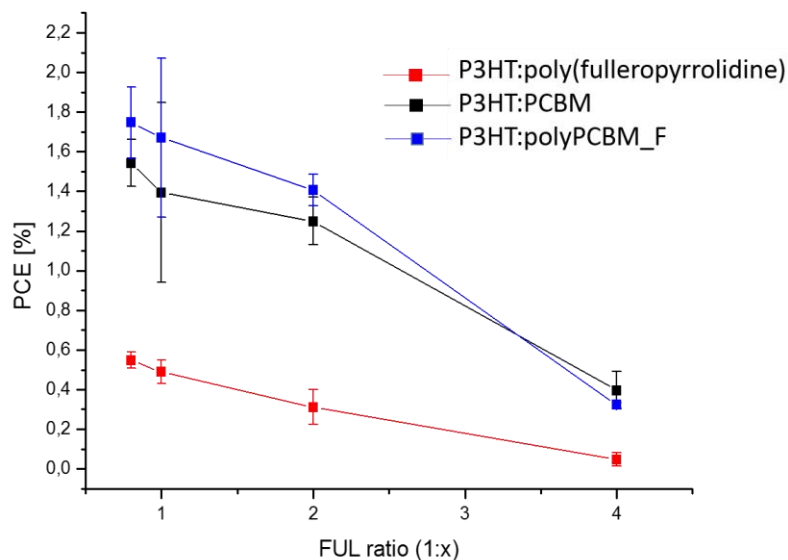


Figure 132: PCE for (black)P3HT/PCBM; (red) P3HT:HHR63 and (blue) P3HT:polyPCBM_F as function of the P3HT:fullerene ratio.

While the trend observed with increasing the fullerene content in the blend is similar to the three compounds, increasing the fullerene content, reduce the PCE of the devices, the differences in the PCE values are evident. Taking into account the properties of the materials it is expected that while the performances of PCBM and polyPCBM_F behave very similarly, the performance of HHR63 is relatively poor.

When the devices are subjected to thermal annealing at 120 °C in glovebox, the similarity in the performance of PCBM and polyPCBM_F are lost, as already showed in paragraph and again displayed in **Figure 133** .

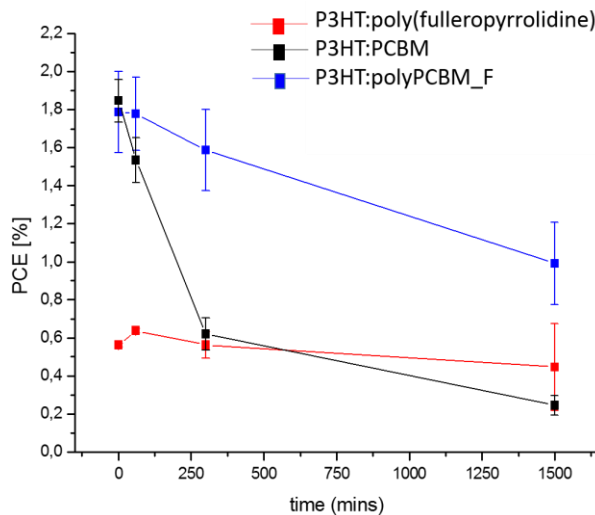


Figure 133: PCE for (black)P3HT:PCBM, (red) P3HT:HHR63 and (blue) P3HT:polyPCBM_F (1:0.8 ratio) as function of the annealing time; the annealing temperature being 120°C.

PCBM blends suffer from significant loss in performance over a short period of time (5 h) whereas both the polymeric compounds exhibit significantly improved stability relative to the PCBM control.

A first attempt to investigate the reason of these differences is here reported. These are preliminary experiments and further studies are to be planned to have a better understanding of these systems and their potential applications.

To perform a comparative study on the synthesized polymers, PCBM, polyPCBM and, poly(fulleropyrrolidine) (**Figure 134**) have been compared in their absorption and photoluminescence properties.

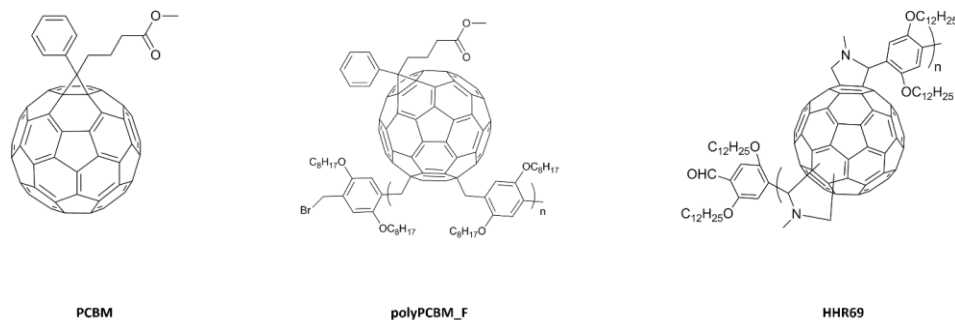


Figure 134: Chemical structure of PCBM, polyPCBM_F and poly(fulleropyrrolidine)

Thin films of the blends with different loading of the fullerene derivatives have been processed from xylene without additives. The absorption spectra of the different samples are shown in **Figure 135**. The film homogeneity of P3HT:PCBM blends is poor when these are cast from xylene. From the absorption spectra in **Figure 135a**, it is evident how the P3HT structure is lost with increasing PCBM loading and a blue shift of the maximum absorption is observed. Although the films obtained from P3HT:polyPCBM_F solution in xylene result with a quite good homogeneity, in the absorption spectra (**Figure 135b**) the P3HT band structure is lost in similar fashion to PCBM when increasing the fullerene derivative loading in the mixture. As in the prior case, a gradual blue shift of the P3HT maximum absorption wavelength is observed. In the case of poly(fulleropyrrolidine), the film homogeneity is superior to that of PCBM samples. Interestingly, the absorption spectra (**Figure 135c**) show a slight reduction of the P3HT absorption bands at low energy when the fullerene derivative is added to P3HT but an increasing of the same features when the loading of poly(fulleropyrrolidine) is increased. When the blends are constituted of a majority of fullerene, a sudden blue shift of the P3HT absorption maximum is observed as for the other analysed compound. For poly(fulleropyrrolidine) the shift is accompanied by the increasing of the low energy P3HT absorption features with increasing loading.

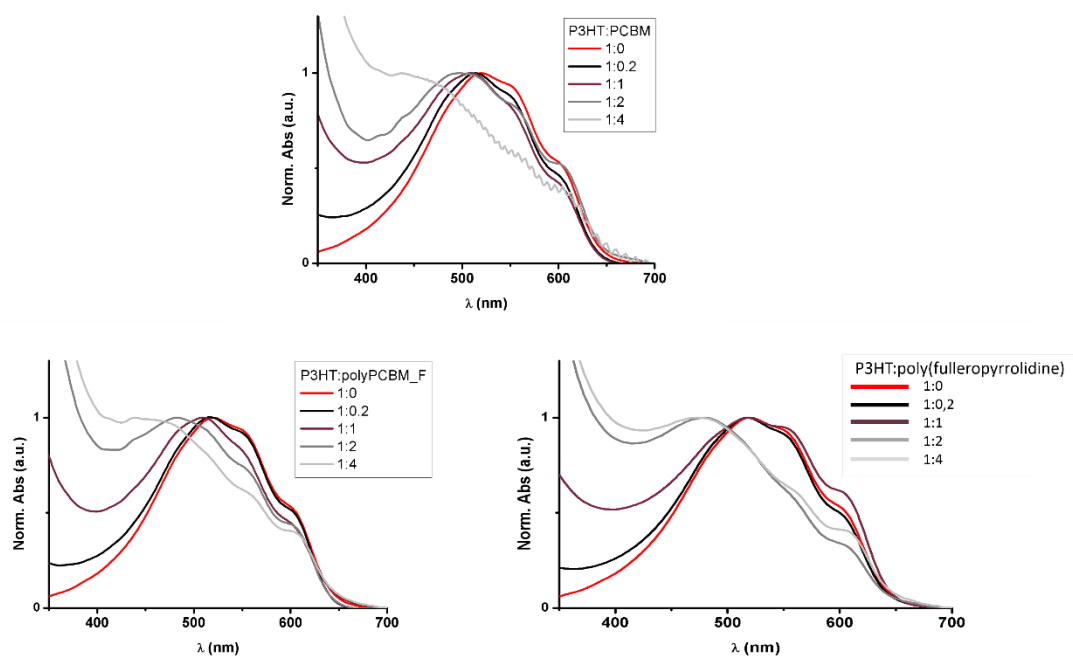
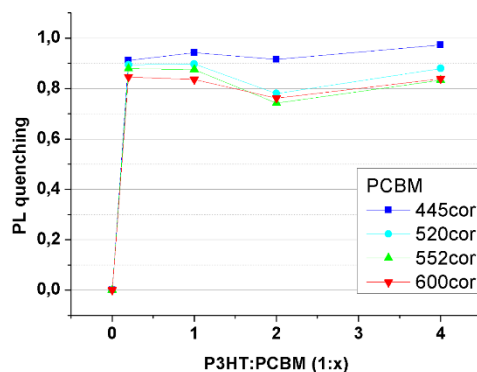
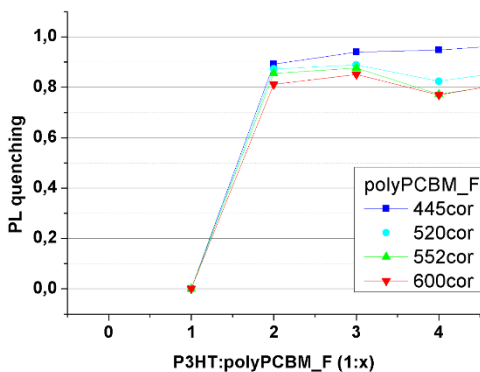


Figure 135: Absorption normalized to peak of P3HT absorption. NB: Films processed from xylene without additives.

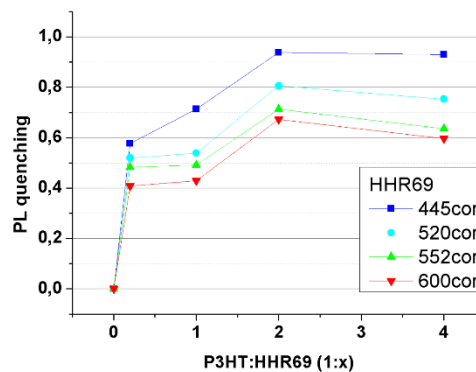
The differences in the optical properties of the compounds can also be observed by PL spectroscopy. Again, while PCBM (**Figure 136a**) and polyPCBM_F (**Figure 136b**) present similar behaviour suggesting a good intermixing with the donor polymer, poly(fulleropyrrolidine) (**Figure 136c**) presents a poor quenching ability at low loading and lower energy excitations that would suggest poor intermixing or the presence of pure P3HT domains within the blend morphology.



(a)



(b)



(c)

Figure 136: PL quenching of P3HT: (a) PCBM, (b) polyPCBM_F AND (c) poly(fulleropyrrolidine) at different excitation wavelengths as function of the donor:acceptor ratio.

Considering the structures of the polyPCBM_F and poly(fulleropyrrolidine), only two key differences are found. The first is the position of the site of polymerization. In the ATRAP polymerization, used to obtain polyPCBM_F, the sites of polymerization are linked to the same

hexagon on the fullerene cage. This is not the case of poly(fulleropyrrolidine) for which the sites of polymerization are most likely to be found at opposite ends of the fullerene. The second key difference is in the presence of the PCBM ester group in polyPCBM_F. To help picture the key differences, they are highlight in **Figure 137**.

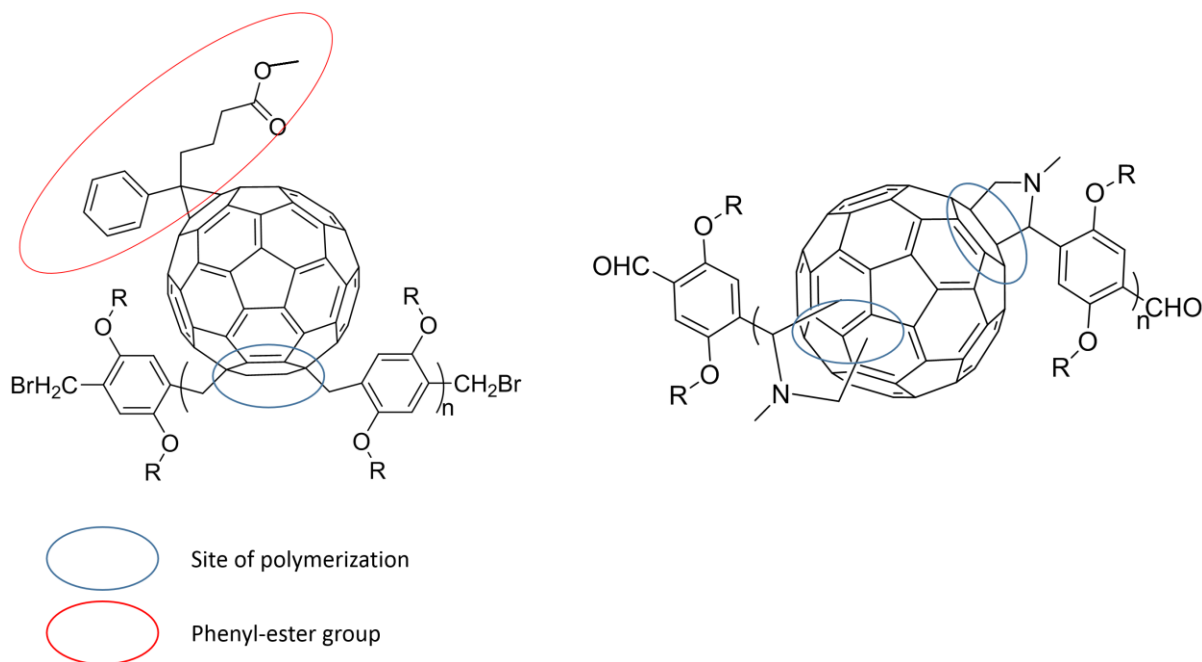


Figure 137: Chemical structures highlighting the key differences between (left) ATRAP-polyfullerene system and (right) SACAP poly(fulleropyrrolidine).

In conclusion of these studies it can be said that one or both of these factors appears to have a strong impact on the interaction of the main-chain polyfullerene with P3HT. No more detailed information are extrapolated from the measurements. With this in mind, further studies with the aim to explore the interactions between the blend components are planned.

In this chapter the results of the application of synthesized materials into inverted solar cells have been reported. In particular polyPCBM_F has been tested as an alternative acceptor to PCBM in the active layer and the novel poly(fulleropyrrolidine) materials have been tested (i) as electron acceptor material within the blend; (ii) as an interlayer between the active layer and the electron extraction layer and; (iii) as an additive to stabilize the morphology of the blend under thermal stress in inverted structure geometry solar cells.

Opto-electronic and charge-transfer properties of PCBM are found to be not influenced by the presence of polymer in polyPCBM_F. On the other hand, polyPCBM_F stabilizes device efficiency with T_{80} being 10 times longer than for the control when the devices are exposed to thermal treatment at 120 °C in the glovebox.

A study employing three different low band gap polymers demonstrate that polyPCBM_F is actually applicable to numerous systems. Results would also suggest that the material most likely requires an optimization specific to each partner low band gap polymer in order to improve device performance and stability.

*The introduction of the poly(fulleropyrrolidine) **PPC4** in OPV devices does not result in the complete failure of the solar cell. However, **PPC4** is not a good alternative to PCBM as acceptor in the active layer and it worsens the device performance when used as an interlayer. A promising and attractive application of poly(fulleropyrrolidines) in OPV is their use as an additive in the photoactive layer.*

4 Thermal degradation study on thin films

Abstract

*The causes of degradation for organic solar cells have been presented in paragraph 1.2.4 of this work. It is clear that the stability of the device is strongly related to the morphological stability of the active layer. In this chapter we focus on thin films of donor-acceptor blends in which the poly(fulleropyrrolidine) **PPC4** has been employed as an additive as a 10% load (with respect to the PCBM content) to stabilize the device performance against thermal degradation. The study addresses only the morphological degradation of the blends, a key factor in device performances. Using accelerated degradation conditions and evaluations by UV-visible spectroscopy and optical microscopy we attempt to give a rationale for the good stabilising properties of **PPC4**.*

*Thin films of P3HT, P3HT:PCBM blend and P3HT:PCBM (**PPC4** 10%) were prepared on glass substrates during a short visit at Belectric OPV and thermal degradation studies were conducted at Eberhard Karls Universität in Tübingen during the cotutelle secondment.*

This work has in part been presented at ESTABLIS STCs meetings:

1. FULLINC presentation at Tübingen University

Hasina H. Ramanitra

ESTABLIS MEETING, November 2014, Tübingen, Germany

The work herein presented is the result of a collaboration with Dr. Simon Dowland at Belectric OPV and Aurélien Tournebize at the University of Tübingen.

The research leading to these results has received funding from the French Region Aquitaine under the grant agreement FULLINC 2011 and from European Union Seventh Framework Program (FP7/2011) under grant agreement ESTABLIS no. 290022.

In the previous chapter, it was shown how the introduction of **PPC4** as an additive in the OPV active layer does not significantly affect the performance of the device and, moreover, how the material stabilizes the OPV performance against thermal stresses. These results are summarized here in **Figure 138** where the chemical structure of **PPC4** is also reported.

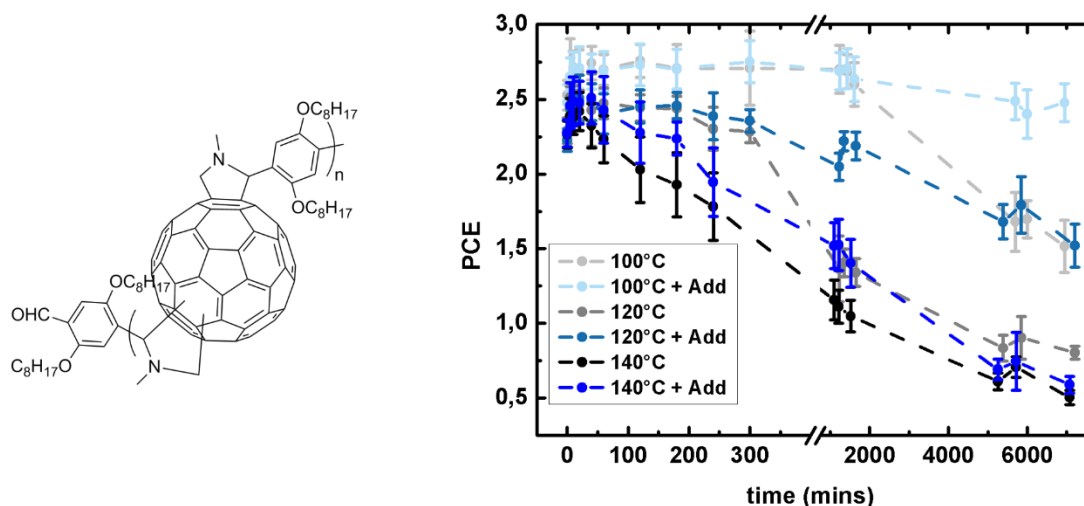


Figure 138: Chemical structure of **PPC4** and the variation of PCE with annealing time at 100, 120 and 140 °C of P3HT:PCBM devices with and without **PPC4** as an additive (10 wt% with respect to PCBM) to the active layer.

The optimization of the device morphology permits the nano-sized clusters necessary for a good charge extraction and that ensures the percolation paths towards the electrodes. It is now recognized that freezing the BHJ morphology in order to maintain these nano-scaled structures and avoid macro-sized clusters in the active layer is also necessary.[331,332] For instance, when PCBM is used as acceptor material in the active layer, once the pristine BHJ morphology is optimized, the fullerene-derivative molecules have the natural tendency to diffuse through the polymeric matrix, forming large domains and thus lead to the disruption of the optimized nanoscale morphology itself.[333, 334] Different approaches have been already proposed for the stabilization of the BHJ morphology and in particular, one of the most exploited is the idea to freeze the optimum morphology by creating chemical bonds via crosslinking moieties.[83,183,335–337]

A different approach, that is also the one proposed in this work, is the introduction of an additive in the blend. The use of fullerene derivatives as additives in the active layers count has

been variously exemplified in the literature (see paragraph 1.3.3). To recall two examples, Wang *et al.* demonstrated how the addition of a PCBM bis-adduct in the active layer blend (P3HT:PCBM) can stabilize the device performances against thermal annealing at 150 °C.[338] Moving to a different system, Schroeder and co-workers demonstrated that the use of a small amount of a dumbbell fullerene in a PCDTBT:PCBM-based OPV device leads to a morphological stabilization of blend when this is subjected to simulated operational conditions.[186]

4.1 Accelerated thermal degradation study on P3HT:PCBM based films with and without polyfullerene additive

Thin films of P3HT, P3HT:PCBM blend and P3HT:PCBM (**PPC4** 10%) were prepared from solution on glass substrates via blade deposition. Annealing of the films was used to simulate ageing of the active layer and thus to study the evolution of it with time. In accordance with the experiment carried out on the complete devices, three annealing temperatures, 100, 120 and 140 °C were chosen for the study. The various samples were annealed on a hotplate in glovebox at the chosen temperature and the evolution of the film morphology with time was monitored via UV-visible spectroscopy and optical microscopy. It is to be said that the measurements have been performed in ambient atmosphere.

In the next pages the results of the conducted experiments are reported and discussed. First, the UV-vis spectra of the samples are discussed. Then, the optical images of the samples that permit to observe the formation of PCBM aggregates are shown.

4.1.1 Study of the film morphology evolution via UV-visible spectroscopy

In the study of the morphological evolution of BHJ active layer of organic solar cell, UV-Visible spectroscopy is a valuable tool. In fact, it permits to investigate phenomena such as PCBM crystallization.[339,340]

PCBM molecules absorb mostly in the range of 300-400 nm of the electromagnetic spectrum. When crystallization occurs in PCBM samples, this results in a decrease of the characteristic absorption band at around 330 nm due to the scatter of the light. The evolution of this band, was

thus monitored during the different annealing processes as indicative of the crystallization of the fullerene derivative. Due to the formation of large crystals, transmittance is expected to be favoured resulting in a decrease of PCBM absorbance.

The spectra recorded at different annealing times of the film, annealed at 100, 120 and 140 °C are shown in **Figure 139**.

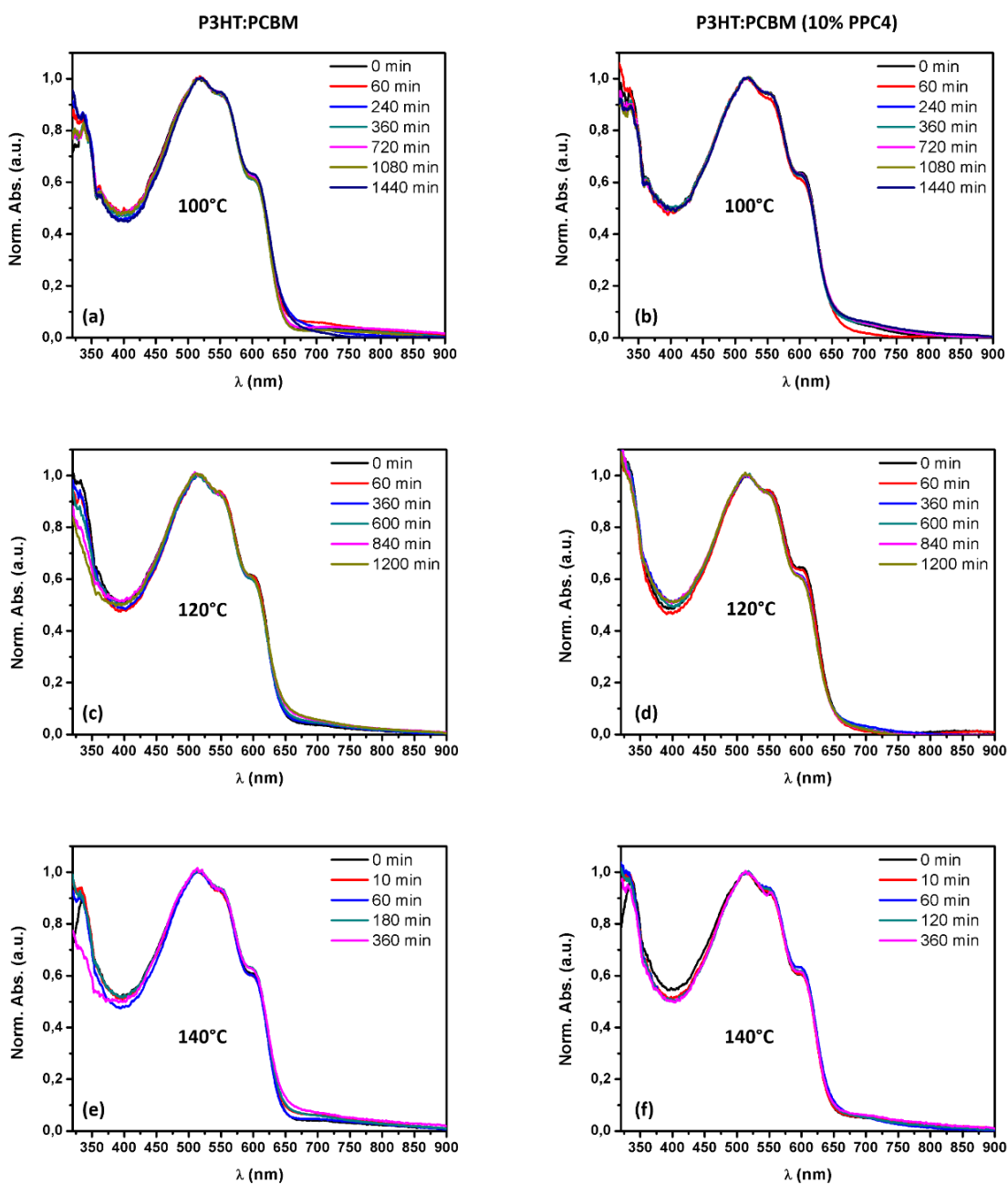


Figure 139: *left*- Absorption spectra at different annealing time of P3HT:PCBM (10% **PPC4**) films annealed at (a) 100 °C, (c) 120 °C and (e) 140 °C; *right* - Absorption spectra at different annealing time of P3HT:PCBM films annealed at (b) 100 °C, (d) 120 °C and (f) 140 °C.

The normalized spectra on the left side of **Figure 139** are those for P3HT:PCBM films. While the absorption band corresponding to the π - π^* transition of PCBM does not present significant changes when the films are annealed at 100°C (see **Figure 139a**), a reduction of this band is observed with time when the annealing temperature is raised to 120 °C (**Figure 139c**). This expected reduction with time is even more important when the temperature is further raised to 140 °C. Under this condition, more than 20% of the initial absorption of PCBM is lost after 360 min of annealing (**Figure 139e**).

The UV-visible spectra of the samples containing **PPC4** as additive in the blend (**Figure 139 b,d,f**) show how the films remain stable upon thermal aging at the chosen temperature. This suggests that **PPC4** acts as stabilizer in the blend affecting PCBM aggregation and thus, that the observed stabilization in the OPV performance of the devices (see paragraph 3.2.3) is likely to be correlated to the stabilization of the morphology of the active layer. To investigate how **PPC4** actually stabilize the blend, optical microscopy images of the unannealed and the annealed samples have been recorded. The results are discussed in the next paragraph.

4.1.2 Study of the film morphology evolution via optical microscopy

Herein, the optical microscopy images of P3HT:PCBM and P3HT:PCBM (10% **PPC4**) films, recorded at different annealing times, are discussed. The recorded images are in line with the UV-vis spectra of the samples. As expected, the thermal annealing of the samples induces, in all the cases, to the formation on microscale aggregates of the fullerene derivative. However, the images show that, when the **PPC4** additive is present in the blend, the fullerene clusters result smaller compared to the PCBM clusters in the correspondent blend sample. The effect of the temperature seems to be on the kinetics of the degradation. In particular, while at 140 °C the fullerene clusters are evident after 360 min of annealing (**Figure 140d**), they are not present at 1500 min when the temperature is lower to 100 °C (**Figure 142d**). From the results displayed in **Figure 140**, **Figure**

141 and Figure 142, it is evident that **PPC4** has two effects on the morphological degradation of the donor/acceptor blends.

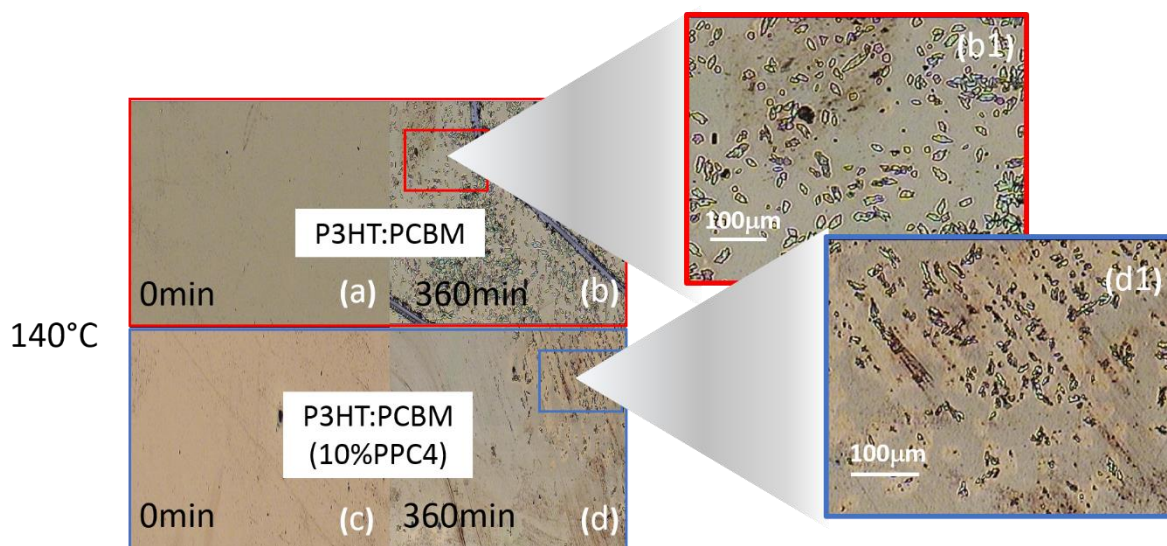


Figure 140: Optical images of (top) P3HT:PCBM films; and (bottom) P3HT:PCBM(10 wt% **PPC4**) films at different annealing times at 140 °C with (b1) and (d1) magnification showing fullerene clusters.

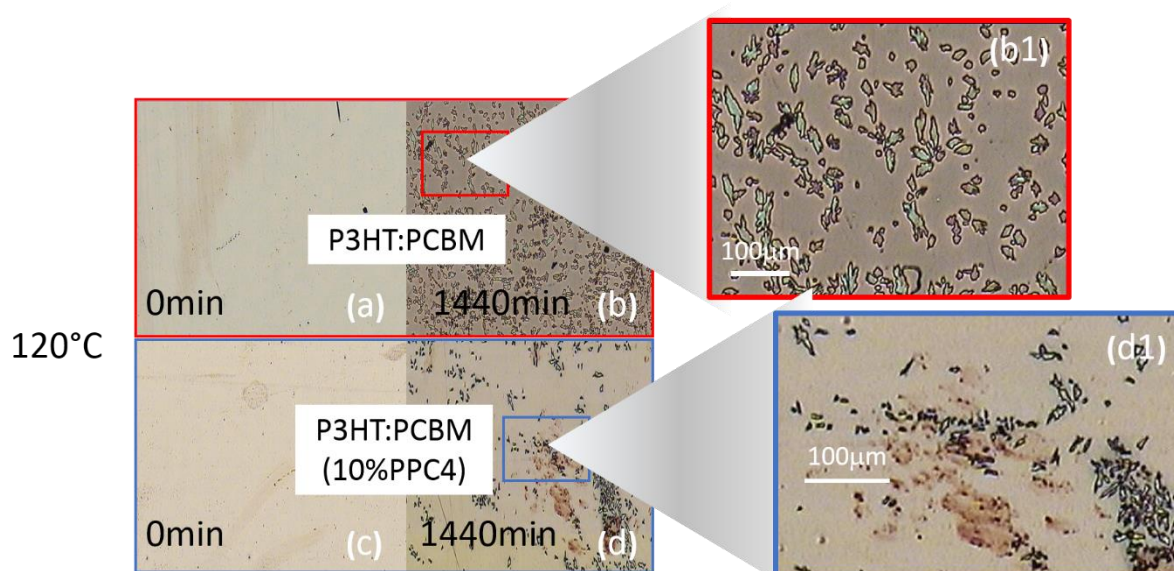


Figure 141: Optical images of (top) P3HT:PCBM films and (bottom) P3HT:PCBM(10 wt% **PPC4**) films at 0min and after 1440 min at 120 °C with (b1) and (d1) magnification showing fullerene clusters.

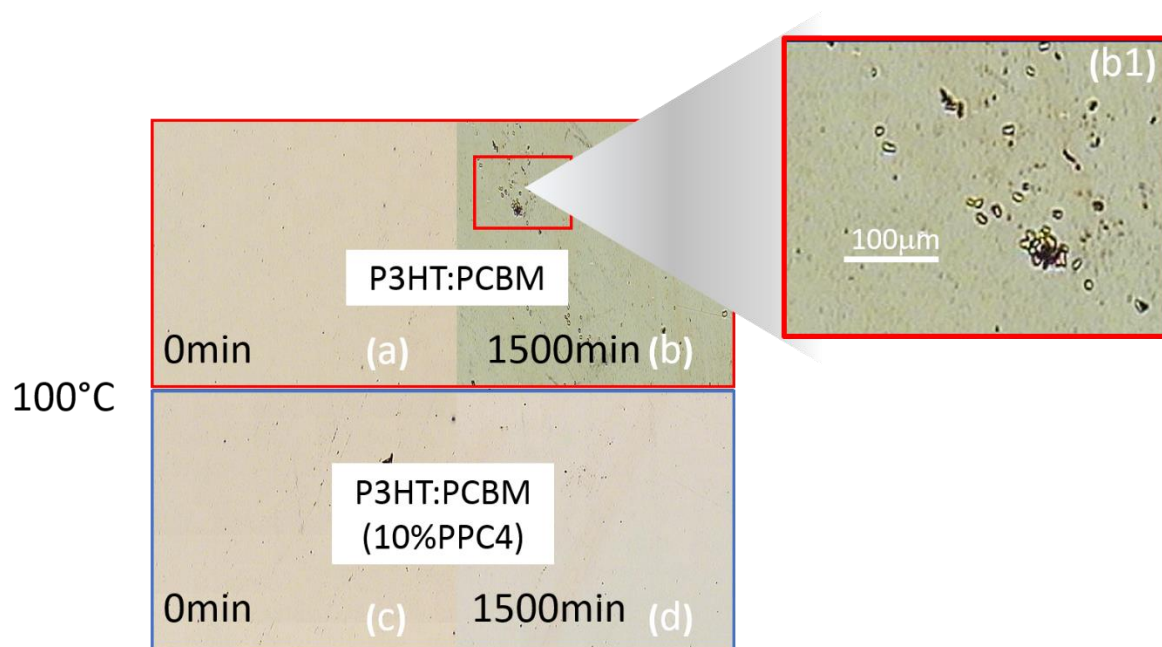


Figure 142: Optical images of (top) P3HT:PCBM films and (bottom) P3HT:PCBM (10 wt% **PPC4**) films at 0min and after 1500 min at 100 °C with (b1) and (d1) magnification showing fullerene clusters.

The first effect that one can observe in the images concerns the size of the PCBM clusters, and the second is the number of aggregates. In all cases the size of the fullerene derivative clusters are smaller when **PPC4** is present in the blend, and the number of clusters on the film surface is reduced with respect to the control blend without **PPC4**.

The two effects are both desired for the application of a compound as additive in the OPV donor/acceptor blend. In analogy of what was reported by Wang *et al.* when bis-PCBM is employed as an additive in P3HT:PCBM BHJ blends,[338] polymer **PPC4** acts as an aggregation inhibitor due to its steric hindrance that stops the PCBM molecules from coming in close contact. This behaviour also results in a reduction of the size of the fullerene acceptor clusters inside the P3HT matrix when the samples are exposed to thermal stresses. Also polystyrene-tethered fullerenes, reported by Moore, Ali and Berry, have shown similar ability when inserted in BHJ photoactive layers where they were found to slower the growth rate of the PCBM domains and to reduce the size of the clusters increasing thus both efficiency and lifetime of the OPV devices.[185] In the case of **PPC4**, no crucial increase on the initial performance of the devices are observed. However, the possibility of easily modifying the polymer by inserting different substituents on the fulleropyrrolidine ring gives great room for design improvements of this new class of compounds.

4.2 Investigating the use of poly(fulleropyrrolidine) additive in KP115:PCBM based BHJ blends

To investigate whether or not **PPC4** can be proposed as morphology-stabilizing additive in BHJ photoactive layers other than those based on P3HT:PCBM, we tested the additive for P3HT:PCBM (1:1) and KP115:PCBM (1:2) polymer blend films. The chemical structures of the donor materials are shown in **Figure 143**.

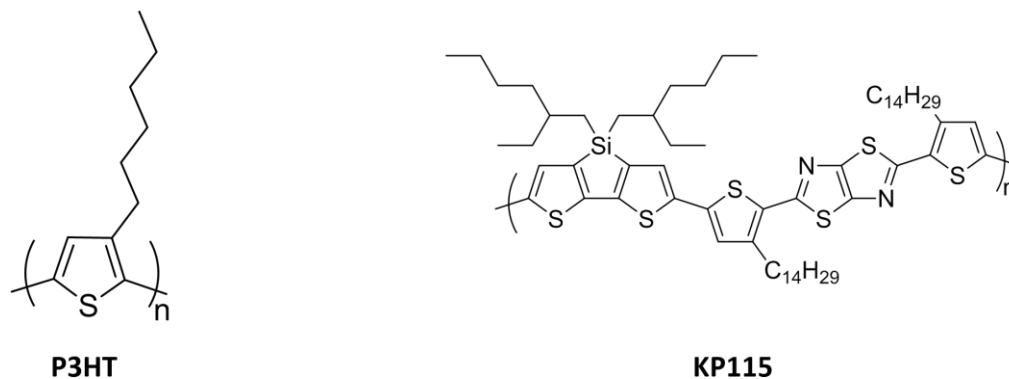


Figure 143: Chemical structure of the polymers employed as donor material in BHJ blends with PCBM: (left) P3HT and (right) KP115.

Films based on P3HT:PCBM (1:1) and KP115:PCBM (1:2) were prepared without (control sample) and with **PPC4** as an additive (10wt% with respect PCBM). Again, optical microscopy and UV-visible spectroscopy are used to investigate the systems.

4.2.1 Evolution of BHJ morphology with thermal stress using optical microscopy

The evolution of the film morphology with time when the samples are exposed to annealing treatment at 120 °C and 140 °C were observed first at the macroscopic scale by optical microscopy.

Considering the P3HT-based systems, when the films are annealed at 120 °C, no significant differences are found between the control and the blends incorporating **PPC4**. Indeed, it can be seen from **Figure 144(top)** where the optical images for P3HT:PCBM and P3HT:PCBM(10% **PPC4**) films are reported before and after 5 h thermal treatments at 120 °C, that few PCBM

clusters are present for both samples. Threshold color treatments (**Figure 144 bottom**) were used to help the visualization of the PCBM clusters. The use of this technique also helps to highlight the imperfections of the pristine film, which has been found crucial for the cluster formation behaviour when **PPC4** is present in the blend. This topic will be discussed later on in this work. Observing the pristine P3HT:PCBM sample (**Figure 144d**), 0.1% of the surface is found covered by imperfections from film fabrication. After 5 h at 120 °C, the black area, which is attributed to both imperfections in the film and PCBM clusters, increases to 0.6% and 0.7% when no additive is present (**Figure 144e**) and when **PPC4** is employed (**Figure 144f**) in the respective blends.

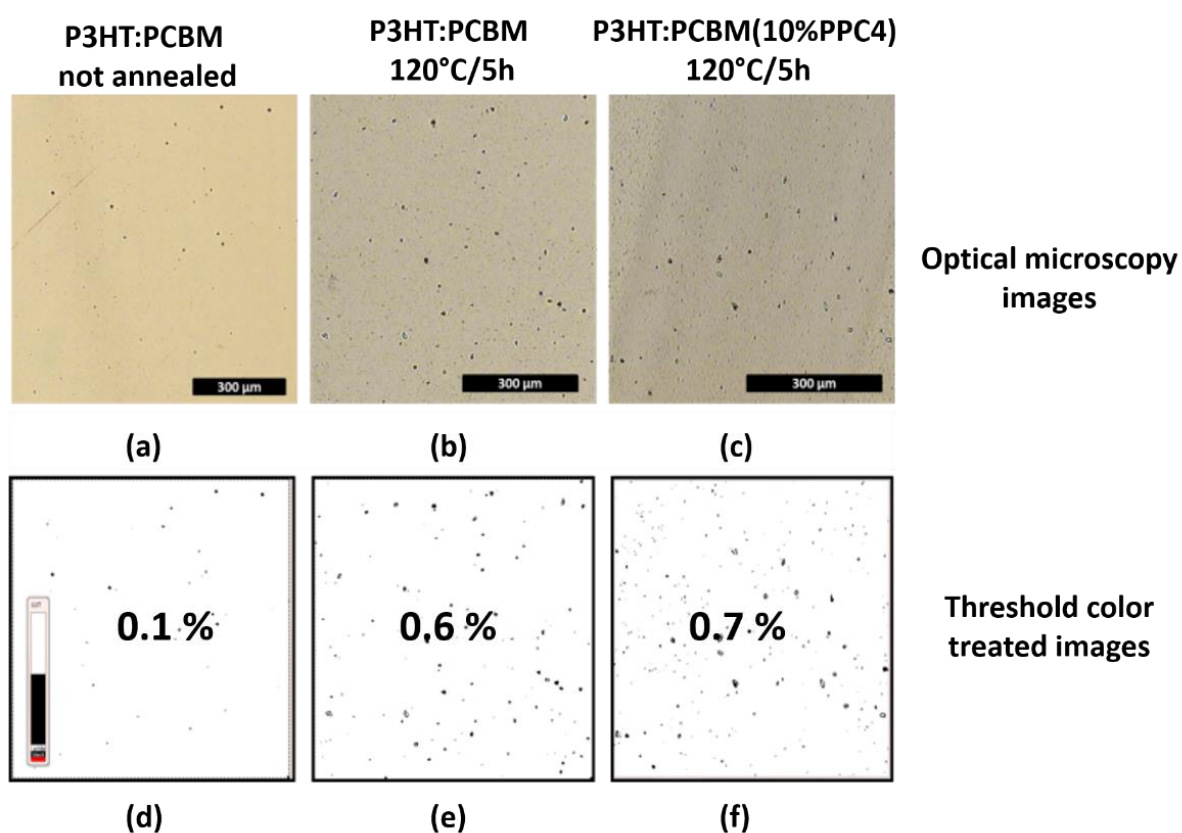


Figure 144: Optical microscopy images and the corresponding threshold color treated images of **(a, d)** P3HT:PCBM films before thermal annealing and after 5 h at 120 °C **(b, e)** without additive and **(c, f)** with **PPC4** as additive. The values indicate the percentage of black spots versus the white background.

Observing now the results for KP115-based films reported in **Figure 145**, it can be seen how the additive seems to have a greater effect on this system. A clear increase in the PCBM cluster density is observed for the KP115:PCBM film without additive after 5 h annealing at 120 °C (**Figure**

145b,e). From the threshold color treatment, this increase result is as much as 64 times the initial value. When **PPC4** is employed as additive in the blend (**Figure 145c,f**), the comparable increase of PCBM domains is not observed, suggesting that the poly(fulleropyrrolidine) acts as an efficient morphology stabilizer for the KP115:PCBM photoactive blend.

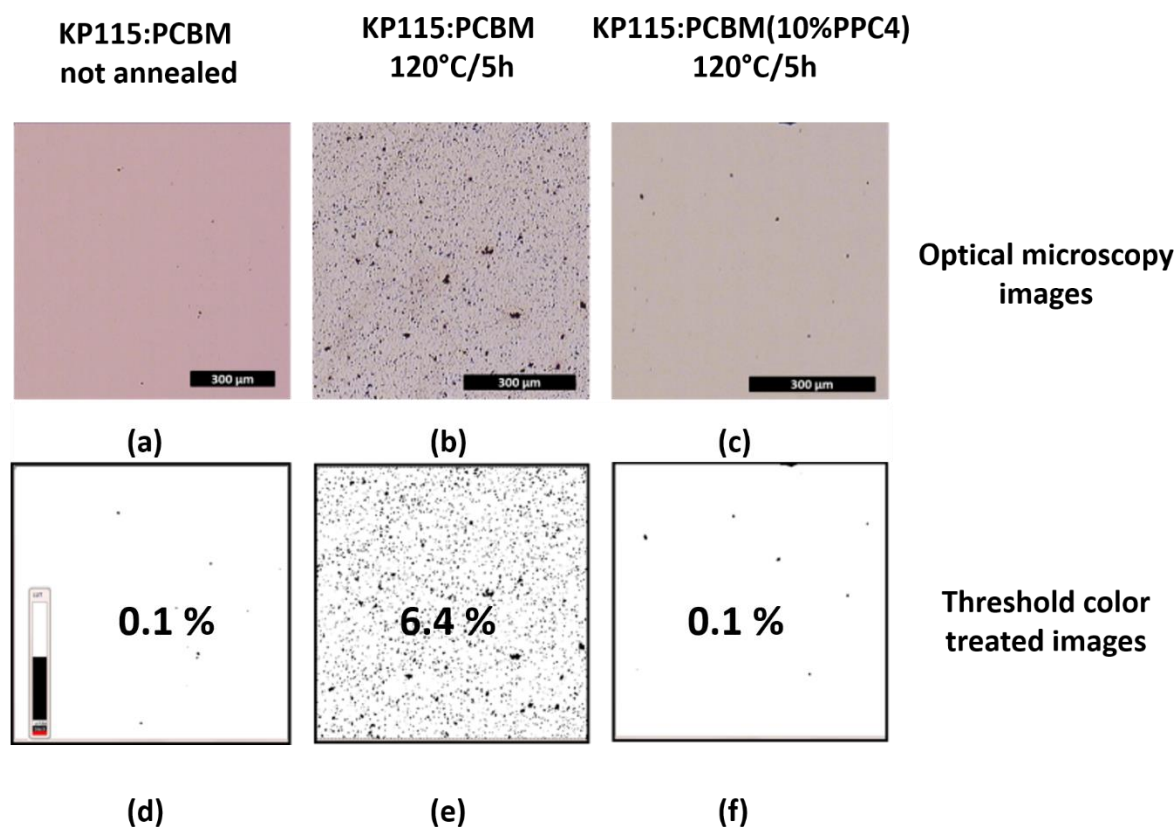


Figure 145: Optical microscopy images and the corresponding threshold color treated images of **(a, d)** KP115:PCBM films before thermal annealing and after 5 h at 120 °C **(b, e)** without additive and **(c, f)** with additive. The values indicate the percentage of black spots *versus* the white background.

More severe conditions were employed in order to obtain more information on the macroscopic differences between samples w/out additive when these are exposed to thermal stresses. A treatment at 120 °C for 5 h did not result in remarkable differences for the P3HT:PCBM films. Thus, experiments with thermal treatments at 140 °C for 10 h were performed to better observe the blends.

From the optical microscopy images reported in **Figure 146**, it is now possible to observe the typical needle-like crystal structure of PCBM after annealing of the P3HT:PCBM blends.[341] When the **PPC4** additive is added (**Figure 146c,f**), the fullerene clusters are smaller in agreement

what was observed in Section 4.1.2. Interestingly, the covered surface from the clusters is only slightly less important that observed with no additive (7.7 % and 8% respectively). This is indicative of a difference in the phase separation, or in the intermixing ability, in the blend due to the presence of **PPC4**. It is evident that when the additive is present, the nucleation points are more abundant crystal growth is limited. On the contrary, when **PPC4** is not present in the blend, while nucleation points are less abundant, the growing of the crystals is faster and can results in larger clusters.

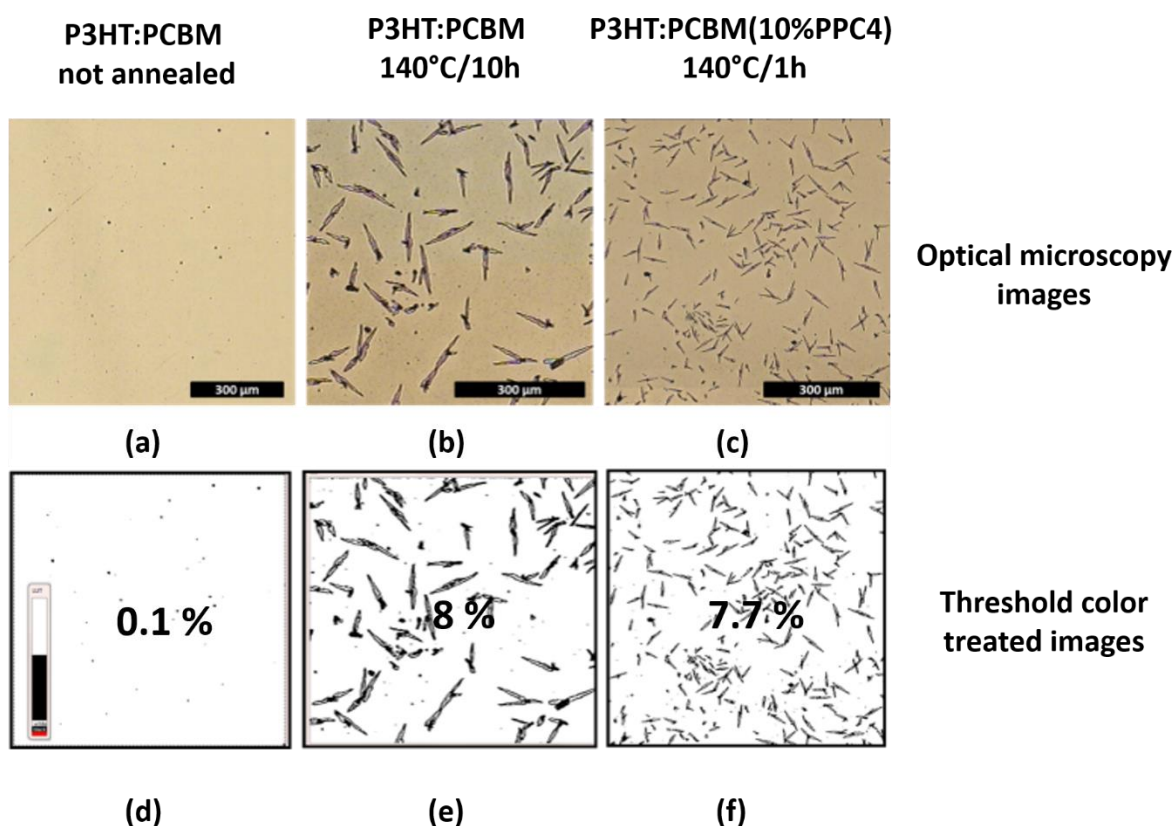


Figure 146: optical microscopy images and the corresponding threshold color treated images of (a, d) P3HT:PCBM films before thermal annealing and after 10 h at 140 °C (b, e) without additive and (c, f) with additive. The values indicate the percentage of black spots versus the white background.

Again, the stabilizing effect of **PPC4** is much more accentuated when the material is employed in KP115:PCBM blends as shown in **Figure 147**. While, the annealing treatment at 140 °C for 10 h without additive results in the formation of a large amount of PCBM aggregates (**Figure 147b,e**), this is not the case when the novel fullerene-polymer is added(**Figure 147d,f**). In fact, despite the fact that the PCBM crystallization is not suppressed when the additive is present, it is greatly

attenuated with respect to the blend without the additive. The surface covered by the PCBM clusters passes from about 31% for KP115:PCBM to only 7% for KP115:PCBM(10% PPC4).

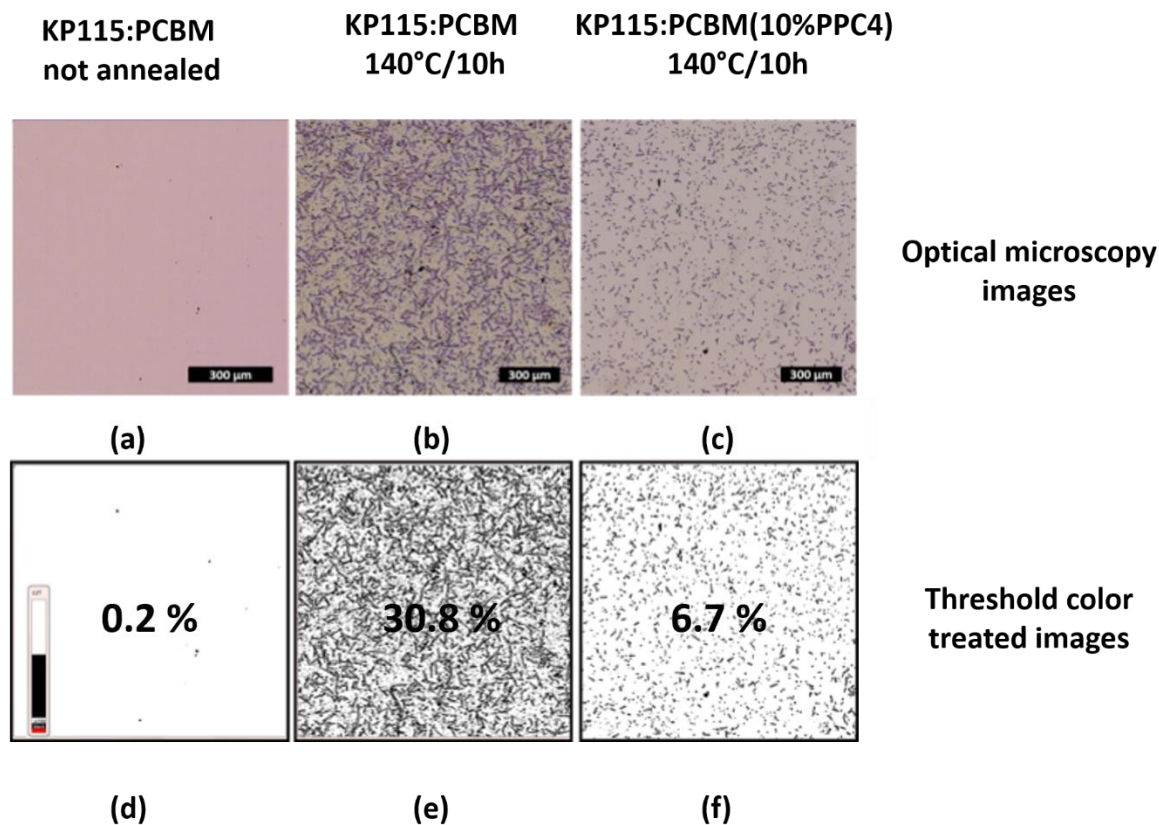


Figure 147: Optical microscopy images and the corresponding threshold color treated images of (a, d) KP115:PCBM films before thermal annealing and after 10 h at 140 °C (b, e) without additive and (c, f) with additive. The values indicate the percentage of black spots versus the white background.

Figure 148 summarizes the PCBM aggregation observed for the different samples. The stabilizing ability of the poly(fulleropyrrolidine) is clearly dependent on the choice of the donor material in the blend. In particular, the additive **PPC4**, is clearly more effective when employed in KP115-based blends than when used in P3HT-based blends.

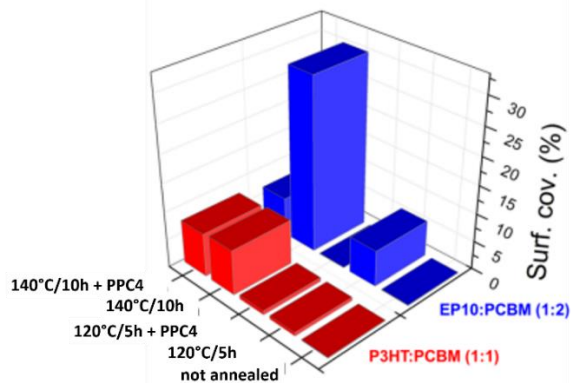


Figure 148: Summary diagram of the PCBM aggregates surface coverage of all the investigated blends in this work.

4.2.2 Evolution of BHJ morphology with thermal stress using UV-visible spectroscopy

In this section we discuss the results obtained by monitoring the evolution of the absorption spectra of the blends during the different annealing processes. As already discussed in paragraph 4.1.1, where the UV-vis spectra for P3HT:PCBM films with and without **PPC4** additive are discussed, this evolution is here used to investigate the morphological change in the BHJ blend.

In **Figure 149**, the absorption spectra of the pristine blends are reported. In the spectra two regions can be individuated: the first region at smaller wavelength, (300-400 nm) where the absorption for PCBM is present and, the absorption region for the donor materials (400 -700 nm).

For the discussion in this section, we will only focus on the PCBM absorbance.

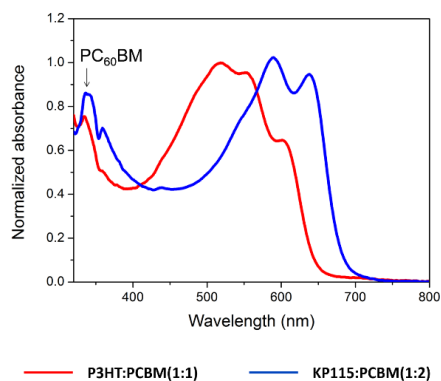


Figure 149: Absorption spectra of (red) P3HT:PCBM and (blue) KP115:PCBM pristine films.

The decreasing of the characteristic band for PCBM is observed for all the blends with annealing time. However, in line with what already observed with the optical images, when the **PPC4** additive is present, this decrease is reduced for both polymer blends. This result can be seen in **Figure 150**. In the figure, the absorption spectra of P3HT:PCBM after the different thermal treatments to show the effect of the crystallization on the absorption band at 334 nm.

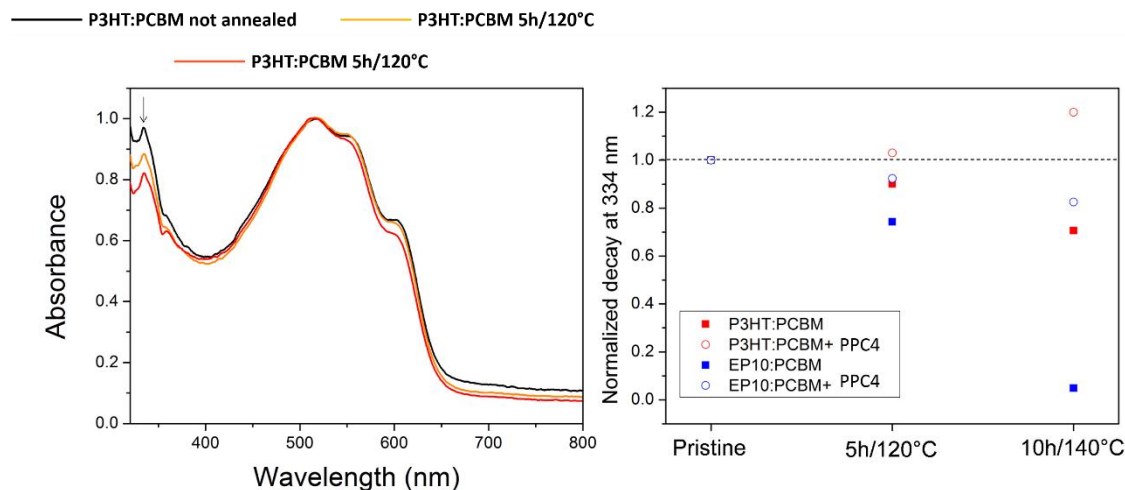


Figure 150: (left) UV-vis absorption spectra of P3HT:PCBM (1:1) films after 5h at 120°C and 10h at 140°C. (right) Evolution of the π - π^* band of PCBM (334 nm) after annealing for P3HT:PCBM (1:1) and KP115:PCBM (1:2) with and without **PPC4** additive.

From the graph in **Figure 150(right)**, it is evident how in the case of P3HT, no significant difference is observed when the sample is annealed at 120 °C for 5 h. The difference becomes significant when the harsher annealing conditions are employed. In the case of KP115-based samples, a clear difference in the absorption is already found for the sample annealed at 120 °C for 5 h and the difference becomes even more important upon the annealing treatment at 140 °C for 10 h.

4.3 Impact of the film quality on the morphological degradation behaviour

The quality of the BHJ active layer film has a great impact on the morphological degradation of the blend when it is exposed to accelerated degradation experiments. In this short section we report some observations on samples performed during various experiments to underline the importance of good film quality in the BHJ blend applications.

During the accelerated degradation studies conducted during this work, we noticed that film imperfections seemed to lead the shape of the fullerene derivative clusters when **PPC4** was used as an additive in P3HT:PCBM blends and when the high annealing temperature of 140 °C was used to conduct the experiments.

As shown in *Figure 151* the annealing at 140 °C of some of the samples induced the formation of quite regular, elongated fullerene derivatives clusters when **PPC4** is present, while the clusters seem to be more randomly distributed in simple P3HT:PCBM films. Moreover, in complete disagreement with what observed in the experiments discussed in previous sections, for these samples, the number of crystals is much higher in the presence of **PPC4**.

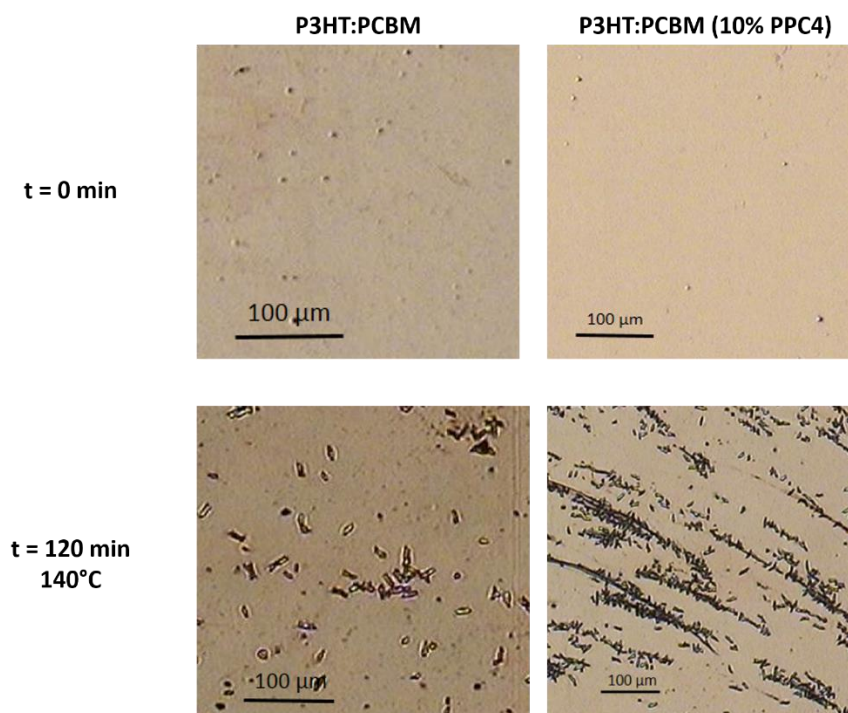


Figure 151: Optical microscopy images of P3HT:PCBM and P3HT:PCBM(10% **PPC4**) (*top*) before and, (*bottom*) after 120 min annealing at 140 °C.

Looking at the patterns followed by the crystals on the annealed films, one can notice that these correspond to defects on the films themselves as highlighted in **Figure 152**.

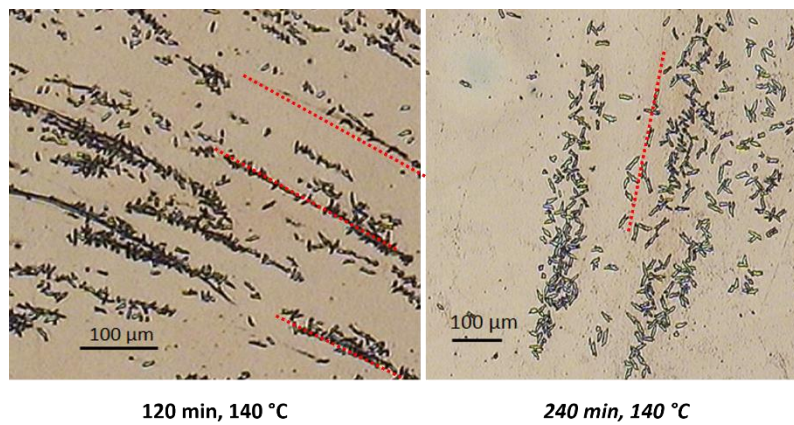


Figure 152: Optical microscopy images of P3HT:PCBM (10 wt% **PPC4**) films showing film defects driven by PCBM cluster shapes.

The defect-guided crystallization may represent a great challenge in the study and in the application of the materials. Indeed, when the P3HT:PCBM(10% **PPC4**) films with defects are annealed for 240 min at 140 °C, the described effects are strongly visible and the concentration of PCBM aggregates is very high in the film (**Figure 153**).

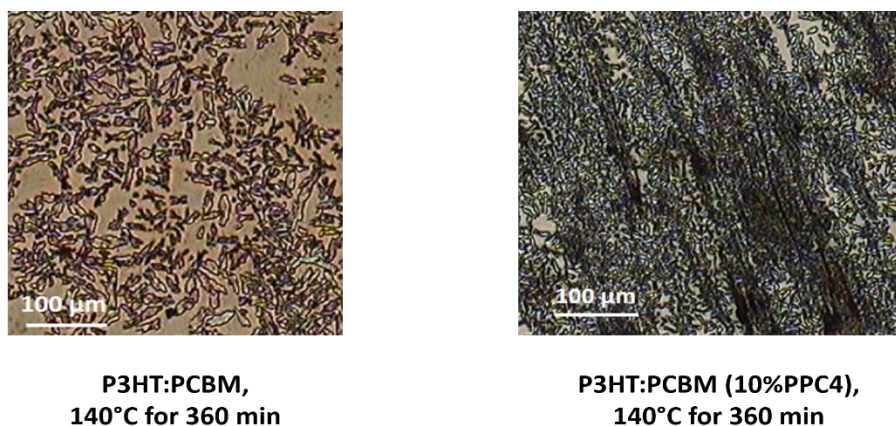


Figure 153: (left) P3HT:PCBM film annealed at 140 °C for 360 min; (right) P3HT:PCBM(10% **PPC4**) film presenting deposition defects and annealed at 140 °C for 360 min.

It was thought that these patterns could also result from stronger mechanical post-deposition disruptors on the films. To verify this hypothesis, we performed scratches on unannealed films prior to the thermal treatment at 140 °C. The scratches are intended to simulate eventual mechanical breaks in the blend during the device lifetime. As shown in **Figure 154**, discontinuity and defects caused post-deposition do not seem to influence the patterns of the PCBM self-aggregation.

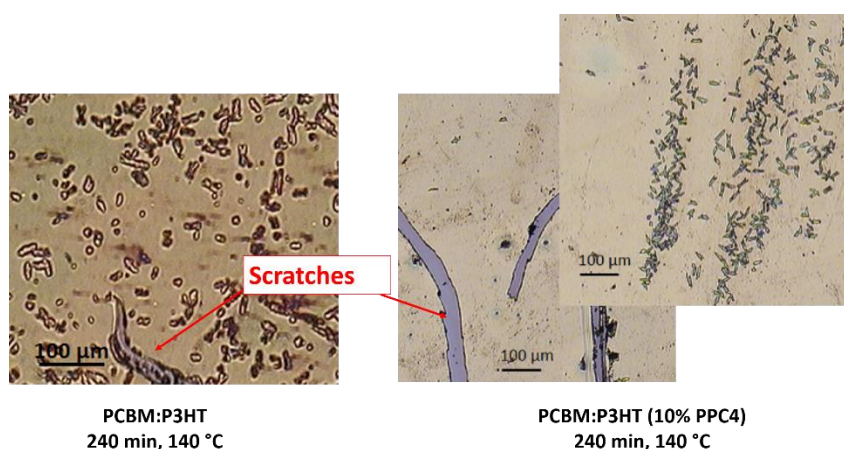


Figure 154: Optical microscopy images of (left) scratched P3HT:PCBM film and (right) scratched P3HT:PCBM(10 wt% **PPC4**) film after 240 min annealing at 140 °C.

From the presented results, it can be concluded that the quality of the BHJ active layer films is a key point for the morphological degradation of the P3HT:PCBM blend when a poly(fulleropyrrolidine) additive (such a **PPC4**) is employed probably because they represent a slight discontinuity in the films where the intermixing of the three materials in the blends are not optimized, and are thus good sites for nucleation seeds.

*To summarize the results discussed in this chapter, it can be said that **PPC4**, employed as additive at 10wt% with respect to PCBM content in BHJ blends, stabilizes the morphology of the film upon thermal treatment in the glovebox.*

*In this chapter we reported the study on thin films of P3HT:PCBM blend and P3HT:PCBM (**PPC4** 10 wt%) prepared from solution on glass substrates via blade deposition and annealing at different temperatures to simulate aging of the active layer and thus study their evolution with time. Three annealing temperatures, 100, 120 and 140 °C were used.*

*UV-visible spectroscopy and optical microscopy analyses suggest that **PPC4** acts as stabilizer in the blend affecting PCBM aggregation and thus, that the observed stabilization in the OPV performance of the devices discussed in Section 3 is likely to be correlated to the stabilization of the morphology of the active layer. The first effect observed in the optical images is on the size of the PCBM clusters. The second, is on the number of the aggregates. The size of the fullerene derivative clusters are smaller when **PPC4** is present in the blend and their number on the film surface is decreased.*

*The results corroborate the hypothesis that the polymer **PPC4** acts as an aggregation inhibitor due to its steric hindrance that does not allow the PCBM molecules to come in to close contact.*

*The stabilizing ability of the poly(fulleropyrrolidine) depend on the choice of the donor material in the blend. Films based on P3HT:PCBM (1:1) and KP115:PCBM (1:2) without (control sample) and with **PPC4** as additive (10% of PCBM mass content) were investigated. Again, optical microscopy and UV-visible spectroscopy show that the poly(fulleropyrrolidine) acts as an efficient morphology stabilizer for the systems and in particular, the additive **PPC4**, is clearly more effective when employed in the KP115-based blends.*

*Finally, the quality of the BHJ active layer films is found to be a key point for the morphological degradation of the P3HT:PCBM blend when the poly(fulleropyrrolidine) additive (**PPC4**) is employed. During the accelerated degradation studies conducted during this work, we have noticed that film imperfections seem to lead the shape of the fullerene derivative clusters when **PPC4** is used in P3HT:PCBM blends and when a high annealing temperature of 140 °C is used. This phenomenon is probably caused by the fact that defects represent a slight discontinuity in the films where the intermixing of the three different materials in the blends are not optimized, and can thus act as nucleation seeds.*

5 Experimental section

In this section a collection of experimental results are reported with the experimental conditions employed in the different studies.

5.1 Experimental conditions

In this section, experimental protocols, conditions and equipment used for experiments are listed.

Atomic Force Microscopy

AFM measurements were performed using a Multi Mode™ Scanning Probe Microscope (MM SPM) by Digital Instrument in tapping mode. Images were recorded using NanoScope software.

Differential Scanning Calorimetry DSC

Differential scanning calorimetry was performed either on a TA Instruments DSC Q100 or on a Perkin Elmer DSC8000 with solid samples in aluminium crucibles at a heating/cooling rate of 20 °C min⁻¹ unless otherwise noted under a flux of N₂ maintained at 20 mL min⁻¹. Data treatment was performed with a Pyris™ series DSC8000 software.

FTIR spectroscopy

FT-IR spectra were recorded using KCl pellet supports on a Bruker Vertex 70v spectrometer in transmission mode with a resolution of better than 1 cm⁻¹ connected to OPUS software. The base pressure of the vacuum spectrometer was better than 1 mbar.

Nuclear Magnetic Resonance

¹H (400.6 MHz), ¹³C (100.16 MHz), and 2-D NMRs were recorded on a Bruker® Avance 400 spectrometer using solvents and temperature as indicated.

Optical microscopy

Film morphology was observed by an optical microscope (OLYMPUS, BH) equipped with a CCD camera. The threshold color treatment was done by using Scion Image software.

Size-exclusion Chromatography in CB

SEC-CB measurements were performed in a Agilent Technologies 1260 Infinity equipment eluted at 1 mL/min with 50 °C HPLC grade chlorobenzene (Aldrich) through a PLgel 10 micrometer Mixed-B (300x7.5 mm) SEC column.

Size-exclusion Chromatography in THF

SEC-THF measurements were performed in a Viscotek set equipped with a VE 5200 GPC auto-sampler and a VE 3580 RI detector. The elution was performed at 1 mL min⁻¹ rate with 30 °C HPLC grade tetrahydrofuran (VWR) through a Viscotek styrene-divinyl benzene (300x8.0 mm) SEC column.

The calibration was done using polystyrene standards with known molecular weight and chromatogram signals were obtained from a UV-visible detector coupled with the SEC instrument.

Thermogravimetric Analysis TGA

DSC measurements were performed in a TA Instruments TGA Q50 piece of equipment.

UV-VIS spectroscopy

UV-VIS spectra were recorded in transmission mode using a homemade set up containing an optic fiber spectrometer from Ocean Optics (Maya2000 Pro). An UV-VIS-NIR Deuterium-Halogen DH-2000-BAL (Mikropack) light source was used as excitation.

XPS spectroscopy

XPS measurements were performed using a multi-chamber UHV-system (base pressure 10⁻¹⁰ mbar) equipped with a Phoibos 150 cylindrical hemispherical analyser (SPECS). The employed excitation X-rays have a monochromatic energy of 1486.7 eV, from an AlK α source.

Chemicals and Solvents

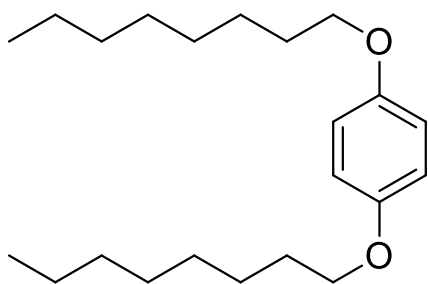
All starting materials, except for C₆₀ from MER Corp. and PCBM from Merck KGaA, were purchased from Sigma-Aldrich (France) in their analytical grades and used as received.

Toluene and THF were distilled from their respective drying agents, i.e., sodium or sodium and benzophenone, under dry nitrogen.

1,2-Dichlorobenzene (DCB) was degassed under reduced pressure and nitrogen-flushed prior to use. All technical solvents were acquired and used as received from VWR International.

5.2 Synthetic protocols and NMR analysis of comonomers

1,4-Bis(octyloxy)benzene (**2a**)



1,4-Hydroquinone (**1**) (10 g, 90.8 mmol), 1-bromooctane (47 mL, 272 mmol), and K₂CO₃ (37.70 g, 273 mmol) were stirred in acetonitrile (180 mL) at reflux for 2 days and dropped into water (1 L). The precipitates were collected by filtration, air dried, and twice dissolved in a minimum of hot hexane and reprecipitated in methanol (100 mL). Recovery

by filtration and drying at reduced pressure gave **2a** (25 g, 70 % yield) as a sand-like solid.

¹H NMR (400.6 MHz, CDCl₃) δ = 0.89 (t, 6H -OCH₂(CH₂)₆CH₃), 1.29-1.75 (m, 24H, -OCH₂(CH₂)₆CH₃), 3.90 (t, 4H, -OCH₂(CH₂)₆CH₃), 6.82 (s, 4H, aromatics) ppm.

¹³C NMR (100.16 MHz, CDCl₃): δ = 14.56 (s, O-CH₂(CH₂)₆CH₃), 23.13 (s, O-CH₂(CH₂)₅CH₂CH₃), 26.54 (s, O-CH₂CH₂CH₂(CH₂)₄CH₃), 29.72 - 29.86 (s, O-CH₂CH₂CH₂(CH₂)₂CH₂CH₂CH₃), 32.29 (s, O-CH₂(CH₂)₄CH₂CH₂CH₃), 69.13 (s, O-CH₂(CH₂)₆CH₃), 115.86 (s, aromatic), 153.67 (s, aromatic-OC₈H₁₇) ppm.

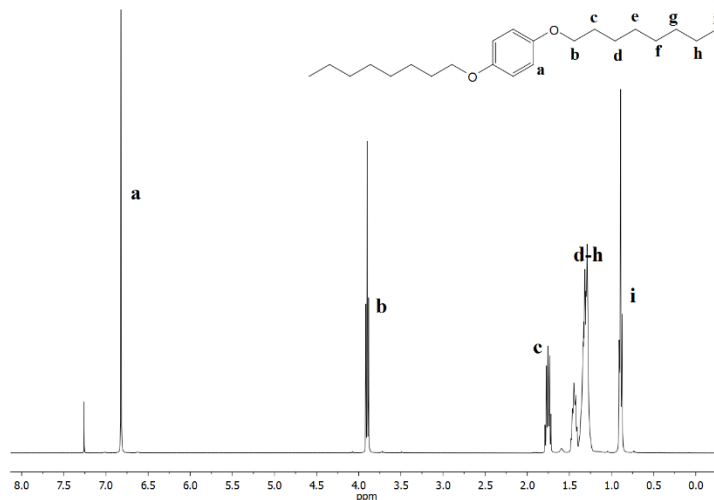


Figure 155: ¹H NMR spectrum (ambient temperature, CDCl₃) of 1,4-bis(octyloxy)benzene (**2a**).

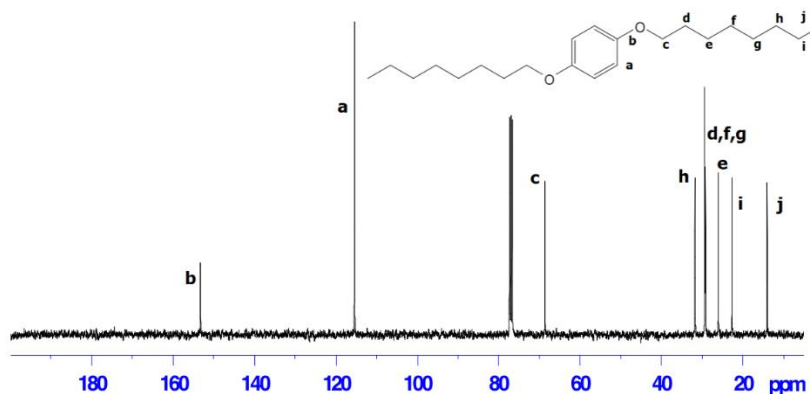
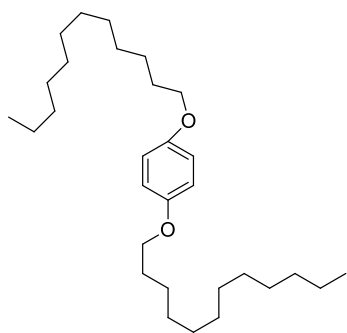


Figure 156: ¹³C NMR spectrum (ambient temperature, CDCl₃) of 1,4-bis(octyloxy)benzene (**2a**).

1,4-Bis(dodecyloxy)benzene (**2b**)



To a warmed suspension of **1** (3 g, 27.2 mmol) and K₂CO₃ (11.4 g, 82.5 mmol) in acetone (100 mL), was added n-dodecylbromide (17 g, 68.1 mmol) in one shot. The mixture was refluxed for 48 h without exclusion of air, the reaction quenched by dropping into cold water, and the product recovered by filtration. Three successive dissolutions in a minimum of hot chloroform and precipitation from cold methanol, and drying under reduced pressure gave the product **2b** in 60% yield.

^1H NMR, (400.6 MHz, CDCl_3) δ = 0.88 (t, 6H, $-\text{OCH}_2(\text{CH}_2)_{10}\text{CH}_3$), 1.01-1.52 (m, 36H, $-\text{OCH}_2\text{CH}_2(\text{CH}_2)_9\text{CH}_3$), 1.70-1.80 (m, 4H, $-\text{OCH}_2\text{CH}_2(\text{CH}_2)_9\text{CH}_3$), 3.90 (t, 4H, $-\text{OCH}_2(\text{CH}_2)_{10}\text{CH}_3$), 6.82 (s, 4H, aromatic).

^{13}C NMR (100.16 MHz, CDCl_3) δ = 14.27 (s, $\text{O}-\text{CH}_2(\text{CH}_2)_{10}\text{CH}_3$), 22.84 (s, $\text{O}-\text{CH}_2(\text{CH}_2)_9\text{CH}_2\text{CH}_3$), 26.22 (s, $\text{O}-\text{CH}_2\text{CH}_2\text{CH}_2(\text{CH}_2)_8\text{CH}_3$), 29.36-29.96 (m, $\text{O}-\text{CH}_2\text{CH}_2\text{CH}_2(\text{CH}_2)_6\text{CH}_2\text{CH}_2\text{CH}_3$), 32.07 (s, $\text{O}-\text{CH}_2(\text{CH}_2)_8\text{CH}_2\text{CH}_2\text{CH}_3$), 68.82 (s, $\text{O}-\text{CH}_2(\text{CH}_2)_{10}\text{CH}_3$), 115.54 (s, aromatic), 153.35 (s, aromatic- $\text{OC}_{12}\text{H}_{25}$) ppm.

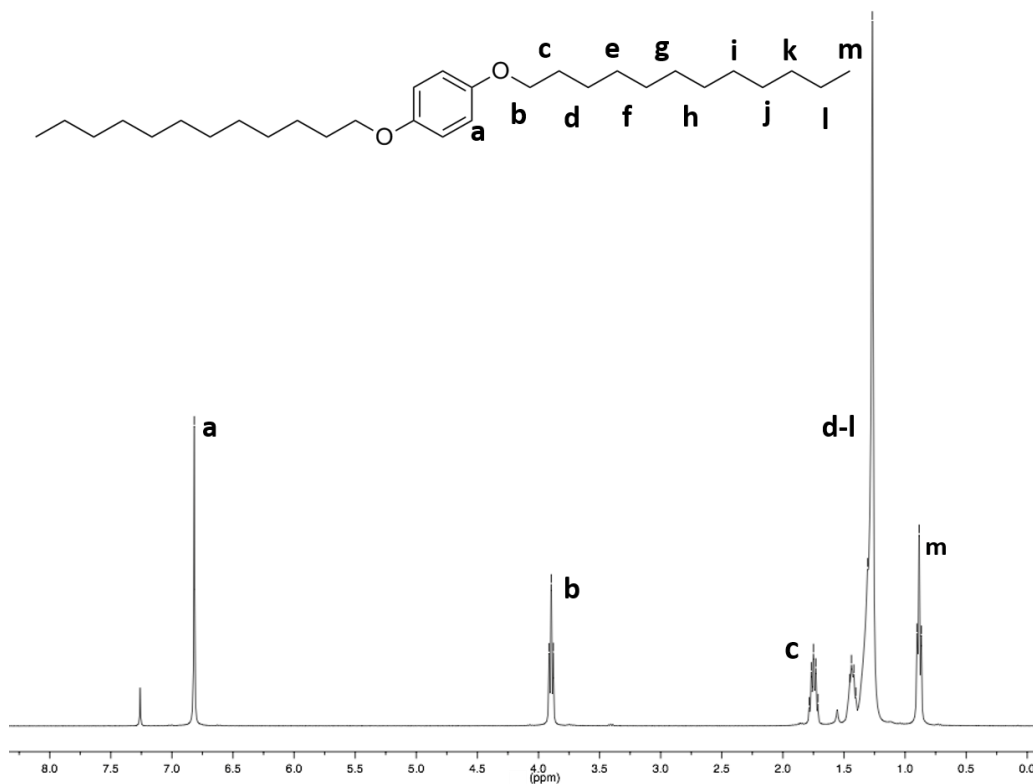


Figure 157: ^1H NMR spectrum (ambient temperature, CDCl_3) of **2b**.

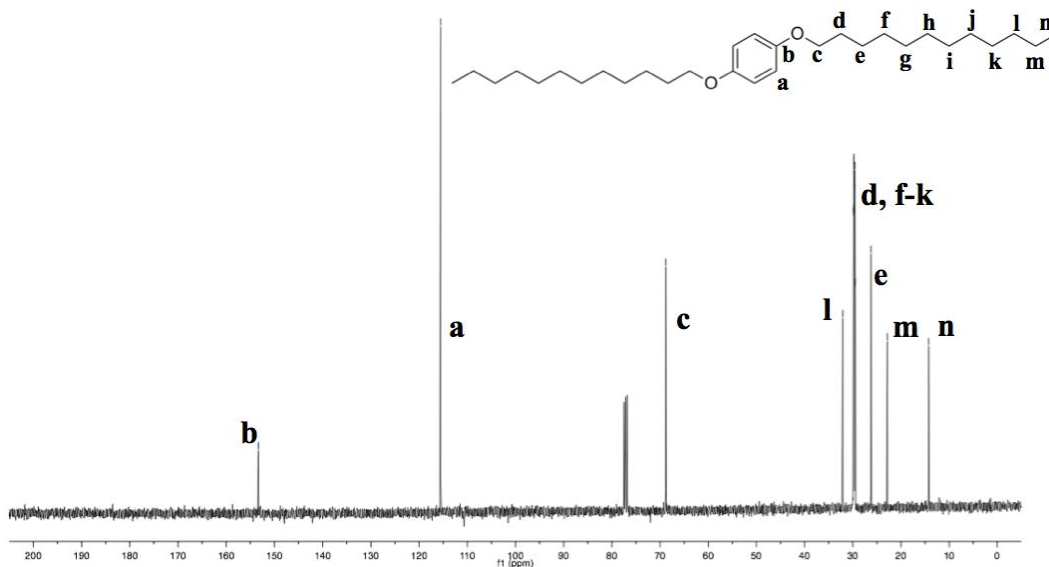
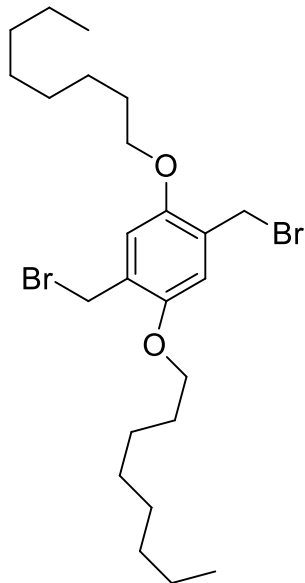


Figure 158: ^{13}C NMR spectrum (ambient temperature, CDCl_3) of **2b**.

2,5-Bis(bromomethyl)-1,4-bis(octyloxy)benzene (**3a**)



HBr (10 mL, 31 wt % in acetic acid) was added in one shot to a suspension of **2a** (7.48 g, 22.3 mmol) and paraformaldehyde (1.376 g, 45.8 mmol) in acetic acid (150 mL) and the mixture stirred at 70 °C for 2 h. Once cooled to room temperature, the solution was dropped into water (300 mL) to yield a white precipitate that was recovered by filtration in air, and three times dissolved in warm chloroform and precipitated from methanol. Drying overnight under reduced pressure yielded **3a** as a white, loose solid (8.51 g, 73% yield).

^1H NMR (400.6 MHz, CDCl_3) δ = 0.89 (t, 6H, $-\text{OCH}_2(\text{CH}_2)_6\text{CH}_3$), 1.28-1.83 (m, 24H, $-\text{OCH}_2(\text{CH}_2)_6\text{CH}_3$), 3.98 (t, 4H, $-\text{OCH}_2(\text{CH}_2)_6\text{CH}_3$), 4.53 (s, 4H, $-\text{CH}_2\text{Br}$), 6.85 (s, 2H, aromatic) ppm.

^{13}C NMR (100.16 MHz, CDCl_3) δ = 14.14 (s, $\text{O}-\text{CH}_2(\text{CH}_2)_6\text{CH}_3$), 22.69 (s, $\text{O}-\text{CH}_2(\text{CH}_2)_5\text{CH}_2\text{CH}_3$), 26.11 (s, $\text{O}-\text{CH}_2\text{CH}_2\text{CH}_2(\text{CH}_2)_4\text{CH}_3$), 28.77 (s, $-\text{CH}_2-\text{Br}$), 29.27 - 29.35 (m, $\text{O}-\text{CH}_2\text{CH}_2\text{CH}_2(\text{CH}_2)_2\text{CH}_2\text{CH}_2\text{CH}_3$), 31.84 (s, $\text{O}-\text{CH}_2(\text{CH}_2)_4\text{CH}_2\text{CH}_2\text{CH}_3$), 69.05 (s, $\text{O}-\text{CH}_2(\text{CH}_2)_6\text{CH}_3$), 114.69 (s, aromatic), 127.55 (s, aromatic- CH_2Br), 150.70 (s, aromatic- OC_8H_{17}) ppm.

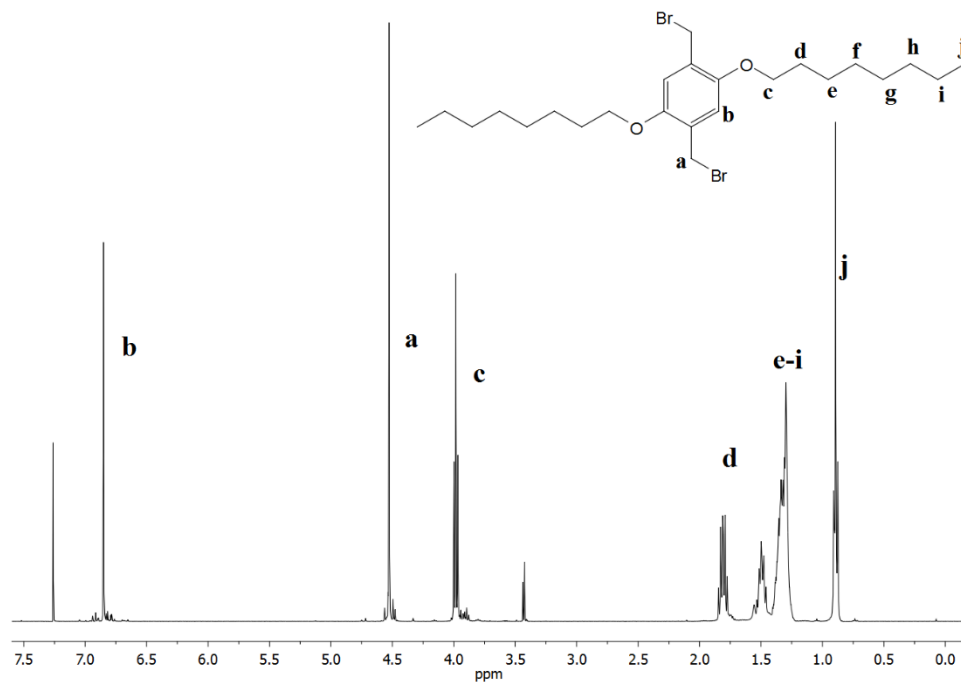


Figure 159: ^1H NMR spectrum (ambient temperature, CDCl_3) of 2,5-bis(bromomethyl)-1,4-bis(octyloxy)benzene (**3a**). Note peak at ca 3.4 ppm is due to methanol.

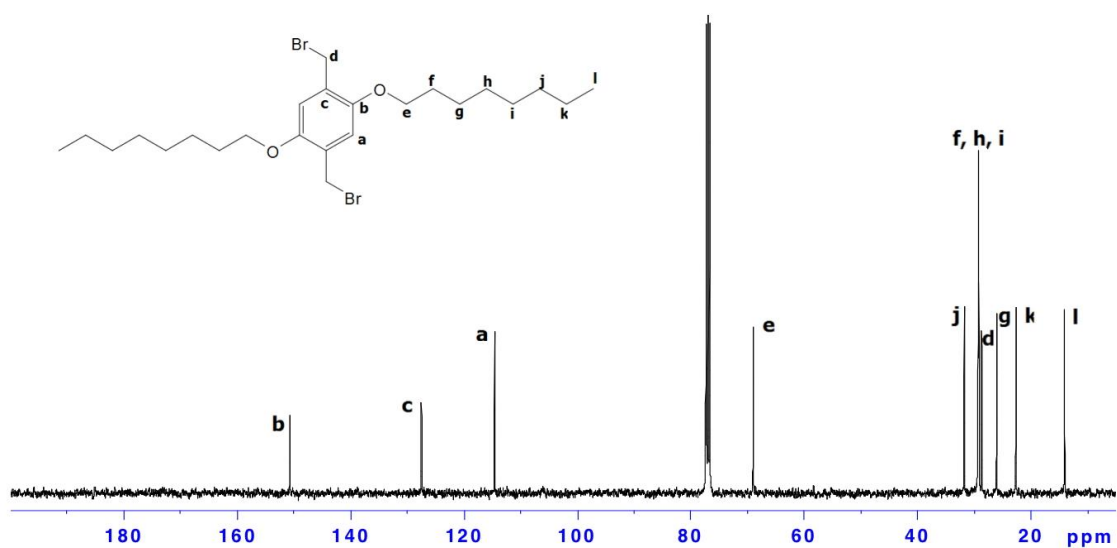
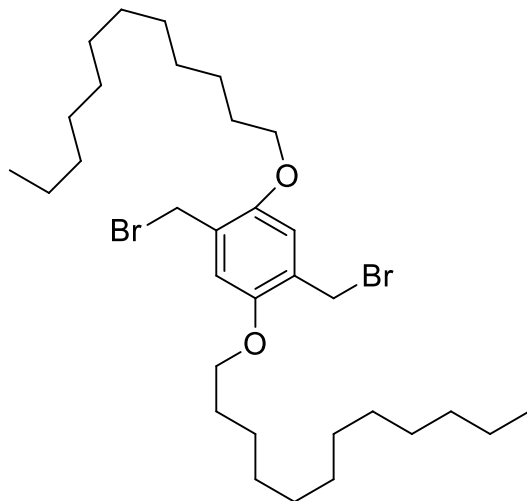


Figure 160: ^{13}C NMR spectrum (ambient temperature, CDCl_3) of 2,5-bis(bromomethyl)-1,4-bis(octyloxy)benzene (**3a**).

1,4-Bis(bromomethyl)-2,5-bis(dodecyloxy)benzene (**3b**)

To stirred solution of **2b** (5 g, 11.2 mmol) and paraformaldehyde (2 g, 67.2 mmol) in acetic acid (30 mL) and chloroform (70 mL) at 70 °C was added in one shot HBr (8 mL, 31 wt % in acetic acid). The reactor was sealed and left stirring for 48 h at 70 °C. The reaction was quenched by adding to excess cold water, and the product recovered by filtration. Thrice dissolution in the minimum of hot chloroform and precipitation from cold methanol, and drying under reduced pressure gave **3b** as a

white powder with yield 75%.

^1H NMR (400.6 MHz, CDCl_3) δ = 0.88 (t, 6H, $-\text{OCH}_2(\text{CH}_2)_{10}\text{CH}_3$), 1.21-1.41 (m, 32H, $-\text{OCH}_2\text{CH}_2(\text{CH}_2)_9\text{CH}_3$), 1.76-1.85 (m, 8H, $-\text{OCH}_2\text{CH}_2(\text{CH}_2)_9\text{CH}_3$), 3.98 (t, 4H, $-\text{OCH}_2(\text{CH}_2)_{10}\text{CH}_3$), 4.52 (s, 4H, $-\text{CH}_2\text{Br}$), 6.85 (s, 2H, *aromatic*).

^{13}C NMR (100.16 MHz, CDCl_3) δ = 14.27 (s, $\text{O}-\text{CH}_2(\text{CH}_2)_{10}\text{CH}_3$), 22.85 (s, $\text{O}-\text{CH}_2(\text{CH}_2)_9\text{CH}_2\text{CH}_3$), 26.23 (s, $\text{O}-\text{CH}_2\text{CH}_2\text{CH}_2(\text{CH}_2)_8\text{CH}_3$), 29.50 (d, J = 2.1 Hz, *aromatic*- CH_2Br), 29.65 - 29.93 (m, $\text{O}-\text{CH}_2\text{CH}_2\text{CH}_2(\text{CH}_2)_6\text{CH}_2\text{CH}_2\text{CH}_3$), 32.08 (s, $\text{O}-\text{CH}_2(\text{CH}_2)_8\text{CH}_2\text{CH}_2\text{CH}_3$), 69.18 (s, $\text{O}-\text{CH}_2(\text{CH}_2)_{10}\text{CH}_3$), 114.81 (s, *aromatic*), 127.68 (s, *aromatic*- CH_2Br), 150.82 (s, *aromatic*- $\text{OC}_{12}\text{H}_{25}$) ppm.

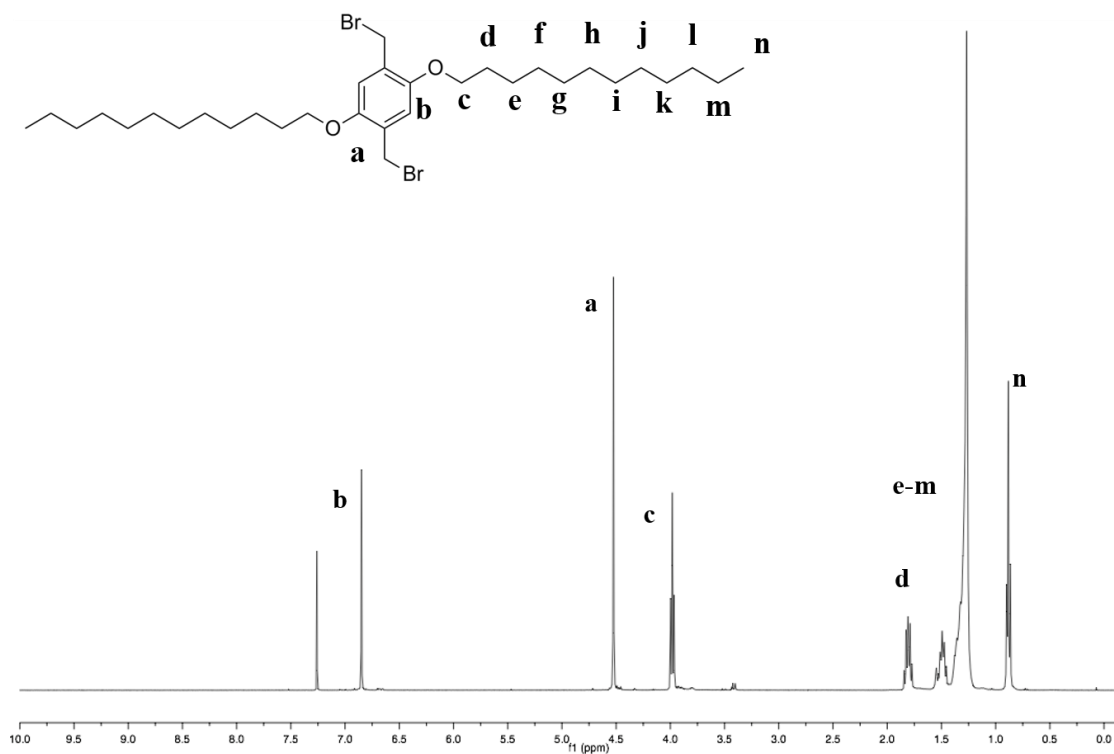


Figure 161: ¹H NMR spectrum (ambient temperature, CDCl₃) of **3b**.

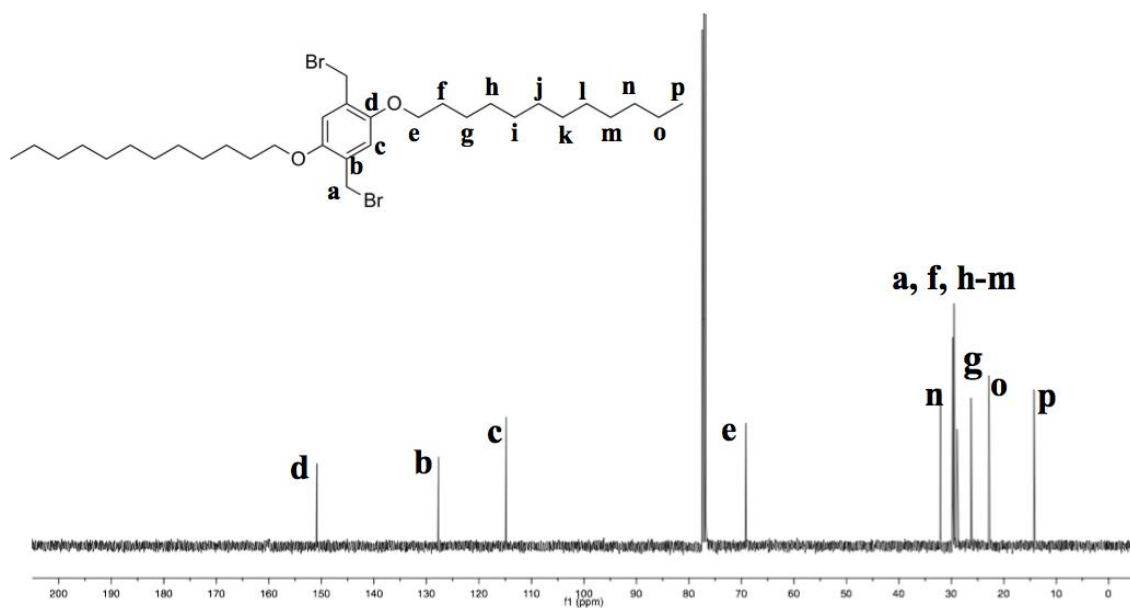
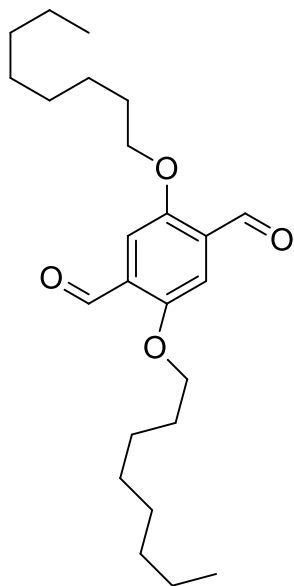


Figure 162: ¹³C NMR spectrum (ambient temperature, CDCl₃) of **3b**.

2,5-Bis(octyloxy)terephthalaldehyde (**5a**)

A mixture of **3a** (2 g, 3.8 mmol), NaHCO_3 (7.56 g, 90 mmol) and DMSO (100 mL) was stirred at 115 °C for 0.5 h and then dropped into water (2 L). Following filtration and air-drying, the product was purified using silica gel column chromatography with petroleum ether/ CHCl_3 (1/2, V/V) as eluent to give **5a** as a yellow solid (0.7 g, 47% yield).

^1H NMR (400.6 MHz, CDCl_3) δ = 0.89 (t, 6H, $-\text{OCH}_2(\text{CH}_2)_6\text{CH}_3$), 1.29-1.83 (m, 24H, $-\text{OCH}_2(\text{CH}_2)_6\text{CH}_3$), 4.08 (t, 4H, $-\text{OCH}_2(\text{CH}_2)_6\text{CH}_3$), 7.43 (s, 2H, aromatic), 10.52 (s, 2H, aldehyde).

^{13}C NMR (100.16 MHz, CDCl_3) δ = 14.24 (s, $\text{O}-\text{CH}_2(\text{CH}_2)_6\text{CH}_3$), 22.88 (s, $\text{O}-\text{CH}_2(\text{CH}_2)_5\text{CH}_2\text{CH}_3$), 26.32 (s, $\text{O}-\text{CH}_2\text{CH}_2\text{CH}_2(\text{CH}_2)_4\text{CH}_3$), 29.20 - 29.51 (m, $\text{O}-\text{CH}_2\text{CH}_2\text{CH}_2(\text{CH}_2)_2\text{CH}_2\text{CH}_2\text{CH}_3$), 31.75 (s, $\text{O}-\text{CH}_2(\text{CH}_2)_4\text{CH}_2\text{CH}_2\text{CH}_3$), 69.39 (s, $\text{O}-\text{CH}_2(\text{CH}_2)_6\text{CH}_3$), 111.85 (s, aromatic), 129.41 (s, aromatic-CHO), 155.24 (s, aromatic- OC_8H_{17}), 189.37 (s, $\text{C}=\text{O}$) ppm.

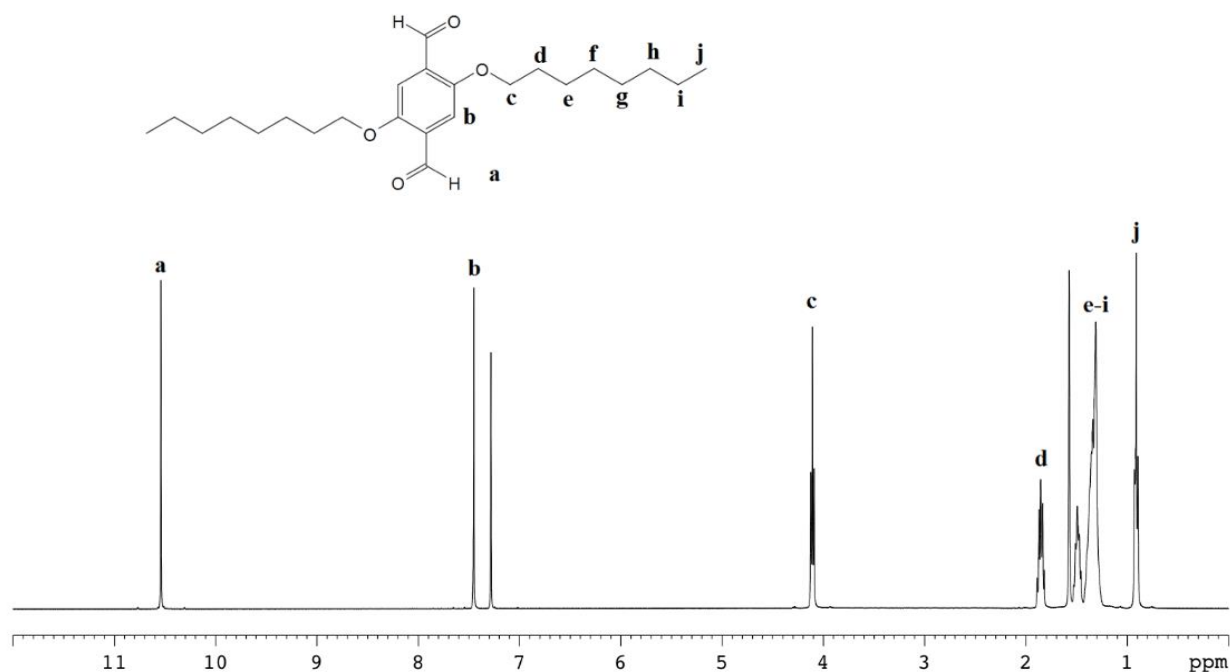


Figure 163: ^1H NMR spectrum (ambient temperature, CDCl_3) of **5a**. Note peak due to water at *ca* 1.57 ppm.

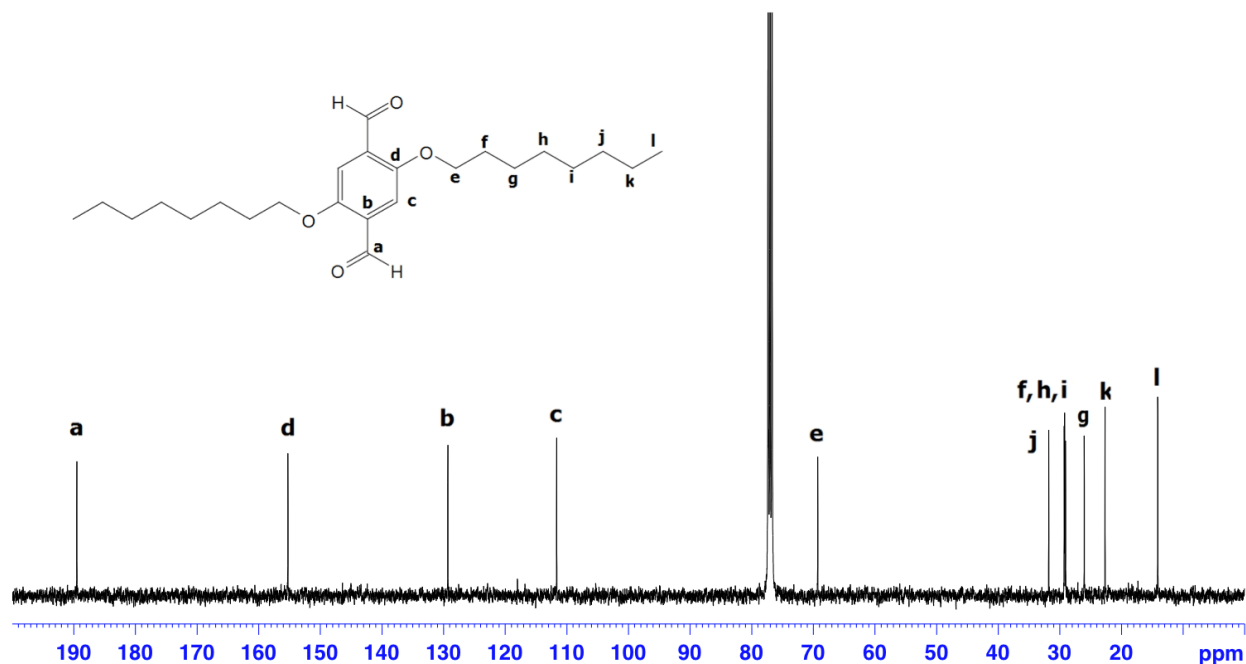
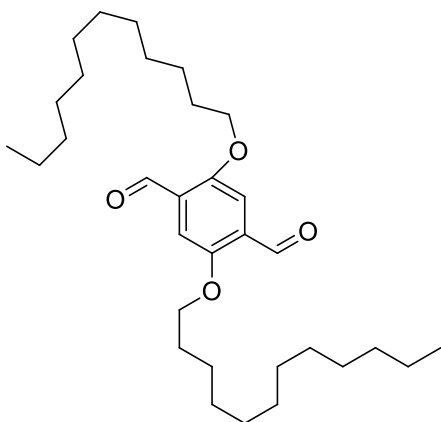


Figure 164: ¹³C NMR spectrum (ambient temperature, CDCl₃) of **5a**.

2,5-Bis(dodecyloxy)terephthalaldehyde (**5b**)



NaHCO₃ (2.39 g, 28.5 mmol) and **3b** (1.2 g, 1.9 mmol) were stirred in dimethyl sulfoxide (50 mL) at 115 °C for 2 h. The reaction mixture was poured into 500 mL of water. The precipitate was filtered and dried. Further purification was performed using silica gel column chromatography with petroleum ether/CHCl₃ (1/2, V/V) as the eluent to give **5b** as a slightly yellow solid (0.2 g, 21% yield).

¹H NMR (400.6 MHz, CDCl₃) δ = 0.88 (t, 6H, -OCH₂(CH₂)₁₀CH₃), 1.26 - 1.83 (m, 40H, -OCH₂(CH₂)₁₀CH₃), 4.8 (t, 4H, -OCH₂(CH₂)₁₀CH₃), 7.43 (s, 2H, aromatic), 10.52 (s, 2H, aldehyde) ppm.

¹³C NMR (100.16 MHz, CDCl₃) δ 14.27 (s, O-CH₂(CH₂)₁₀CH₃), 22.84 (s, O-CH₂(CH₂)₉CH₂CH₃), 26.17 (s, O-CH₂CH₂CH₂(CH₂)₈CH₃), 29.21 - 29.80 (m, O-CH₂CH₂CH₂(CH₂)₆CH₂CH₂CH₃), 32.07 (s, O-

$\text{CH}_2(\text{CH}_2)_8\text{CH}_2\text{CH}_2\text{CH}_3$), 69.41 (s, $\text{O}-\text{CH}_2(\text{CH}_2)_{10}\text{CH}_3$), 111.78 (s, aromatic), 129.44 (s, aromatic-CHO), 155.39 (s, aromatic- $\text{OC}_{12}\text{H}_{25}$), 189.60 (s, $\text{C}=\text{O}$) ppm.

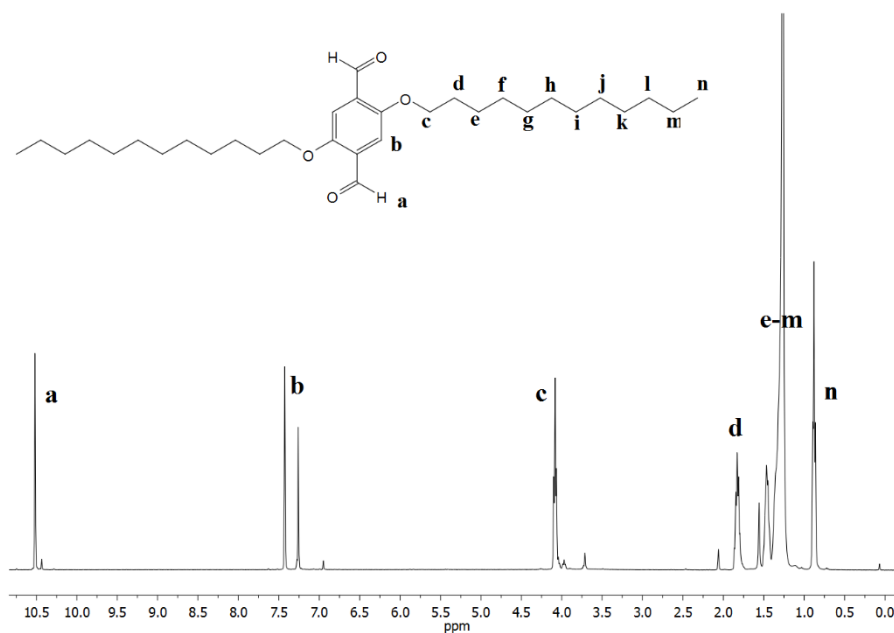


Figure 165: ^1H NMR spectrum (ambient temperature, CDCl_3) of **5b**. Note impurities at *ca* 3.7 and 2.1 ppm, and water at 1.57 ppm.

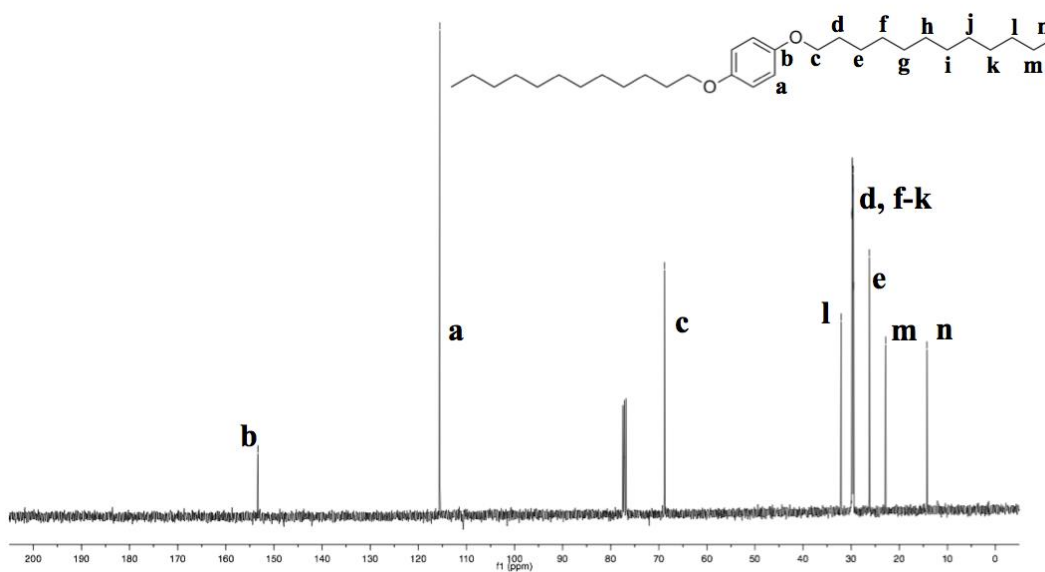


Figure 166: ^{13}C NMR spectrum (ambient temperature, CDCl_3) of **5b**.

5.3 Synthesis and NMR spectra of oligo- and poly-PCBM

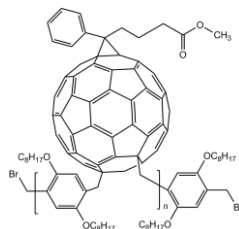


Figure 167: Chemical structure of oligo- and poly-PCBM

Synthesis of polyPCBM_A

Polymerizations were performed in flame-dried, dry-nitrogen flushed glass reactors. Where possible, air and light were excluded from handling of the polymers and their solutions. This is a representative procedure. PCBM (0.4 g, 0.44×10^{-3} mol) and 1,4-bis(bromomethyl)-2,5-bis(octyloxy)benzene (0.23 g, 0.44×10^{-3} mol) were dissolved in toluene (25 mL) at room temperature. CuBr (0.126 g, 0.88×10^{-3} mol) and bipyridine (0.27 g, 1.76×10^{-3} mol) were added and, with vigorous stirring, the temperature was slowly raised to 100 °C. After 16 h, and recovery by precipitation in methanol (500 mL), the product was Soxhlet washed with acetone for three days. Drying under reduced pressure yielded a dark brown powder (0.396 g, 70%).

SEC: M_n 2410 g mol⁻¹, M_w 4130 g mol⁻¹, M_p 3040 g mol⁻¹, M_z 6720 g mol⁻¹, D 1.7.

¹H NMR (400 MHz, C₆D₆) δ = 0.92 (s, -OC₇H₁₄-CH₃), 1.30-2.06 (m, broad, O-CH₂-C₆H₁₂-CH₃), 2.15-2.72 (m, -C₃H₆-C=OOCH₃), 3.33 (s, -O-CH₃), 3.39-4.06 (broad, C₆₀-CH₂-ph, O-CH₂-C₆H₁₂-CH₃), 4.46 (broad, -CH₂-Br), 7.22-7.68 (m, *aromatic*) ppm.

¹³C NMR (101 MHz, C₆D₆) δ = 14.13 (-OC₇H₁₄-CH₃), 22.27-33.27 (O-CH₂-C₆H₁₂-CH₃, CH₂-Br), 50.76-51.91 (-O-CH₃), 69.53 (O-CH₂-C₆H₁₂-CH₃), 114.69- 117.84 (*aromatic*), 131.95 (*aromatic*-PCBM), 136.82-148.82 (*fullerene cage*), 172.31 (C=O) ppm.

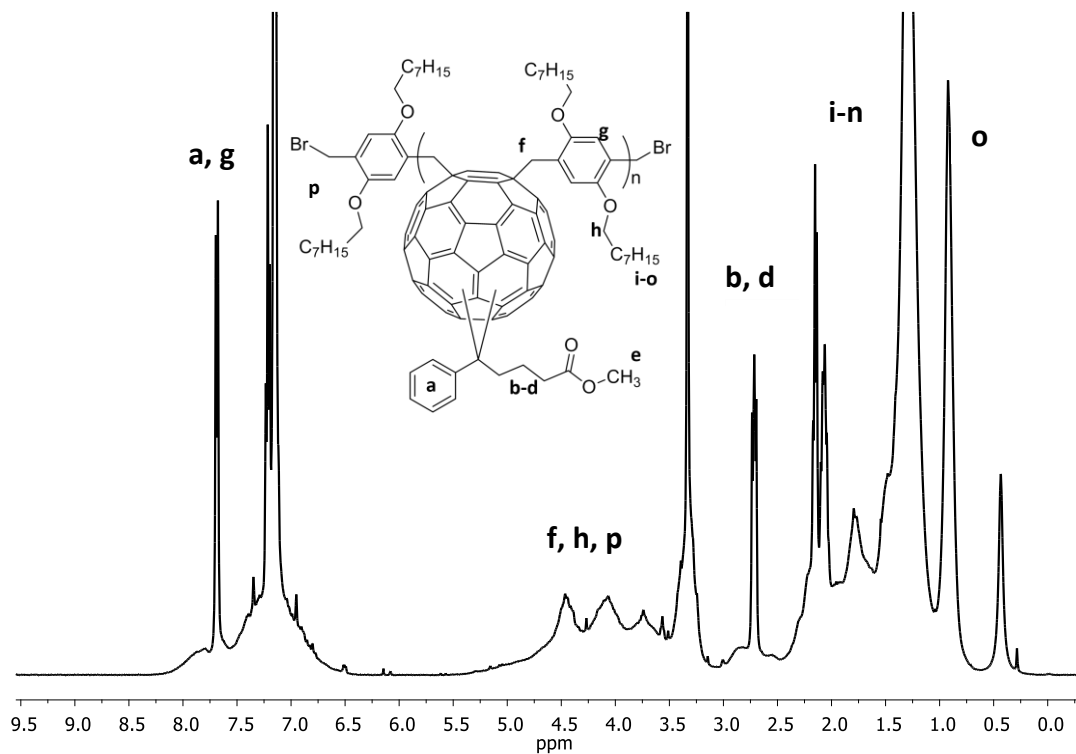


Figure 168: ^1H NMR spectrum (C_6D_6 , ambient temperature) of polyPCBM_A. Note peak due to water at 0.4 ppm.

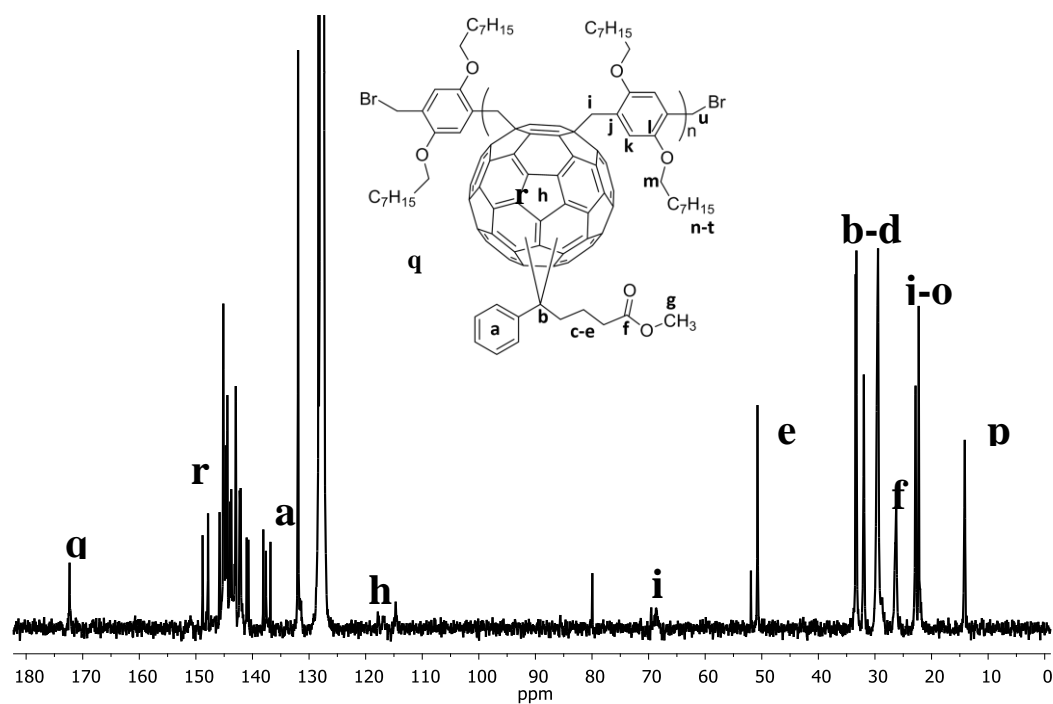


Figure 169: ^{13}C NMR spectrum of polyPCBM (C_6D_6 , ambient temperature).

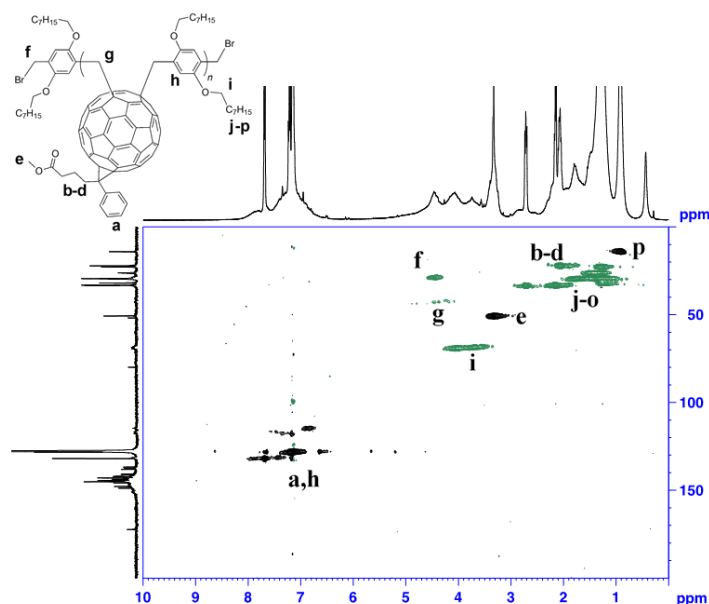


Figure 170: 2D HSQC NMR spectrum of polyPCBM_A (C_6D_6 , ambient temperature). Black indicates methyl and aromatic correlations, blue methylene.

Synthesis of polyPCBM_F

Polymerizations were performed in flame-dried, dry-nitrogen flushed glass reactors. Where possible, air and light were excluded from handling of the polymers and their solutions. This is a representative procedure. PCBM (3 g, 3.28×10^{-3} mol) and 1,4-bis(bromomethyl)-2,5-bis(octyloxy)benzene (1.71 g, 3.28×10^{-3} mol) were dissolved in toluene (150 mL) at room temperature. CuBr (0.158 g, 1×10^{-3} mol) and bipyridine (2.06 g, 13.2×10^{-3} mol) were added and, with vigorous stirring, the temperature was slowly raised to 100 °C. After 16 h, and recovery by precipitation in methanol (500 mL), the product was soxhlet washed with acetone for three days. Drying under reduced pressure yielded a dark brown powder (2.07 g, 49%). SEC: Mn 2410 g mol⁻¹, Mw 710 g mol⁻¹, Mp 980 g mol⁻¹, Mz 1270 g mol⁻¹, Đ 1.4.

¹H NMR (400 MHz, C_6D_6) δ = 0.92 (s, -OC₇H₁₄-CH₃), 1.30-2.06 (m, broad, O-CH₂-C₆H₁₂-CH₃), 2.15-2.72 (m, -C₃H₆-C=OOCH₃), 3.33 (s, -O-CH₃), 3.39-4.06 (broad, C₆₀-CH₂-ph, O-CH₂-C₆H₁₂-CH₃), 4.46 (broad, -CH₂-Br), 7.22-7.68 (m, aromatic) ppm.

^{13}C NMR (101 MHz, C_6D_6) δ = 14.13 (-OC $_7\text{H}_{14}$ -CH $_3$), 22.27-33.27 (O-CH $_2$ -C $_6\text{H}_{12}$ -CH $_3$, CH $_2$ -Br), 50.76-51.91 (-O-CH $_3$), 69.53 (O-CH $_2$ -C $_6\text{H}_{12}$ -CH $_3$), 114.69- 117.84 (aromatic), 131.95 (aromatic-PCBM), 136.82-148.82 (fullerene cage), 172.31 (C=O) ppm.

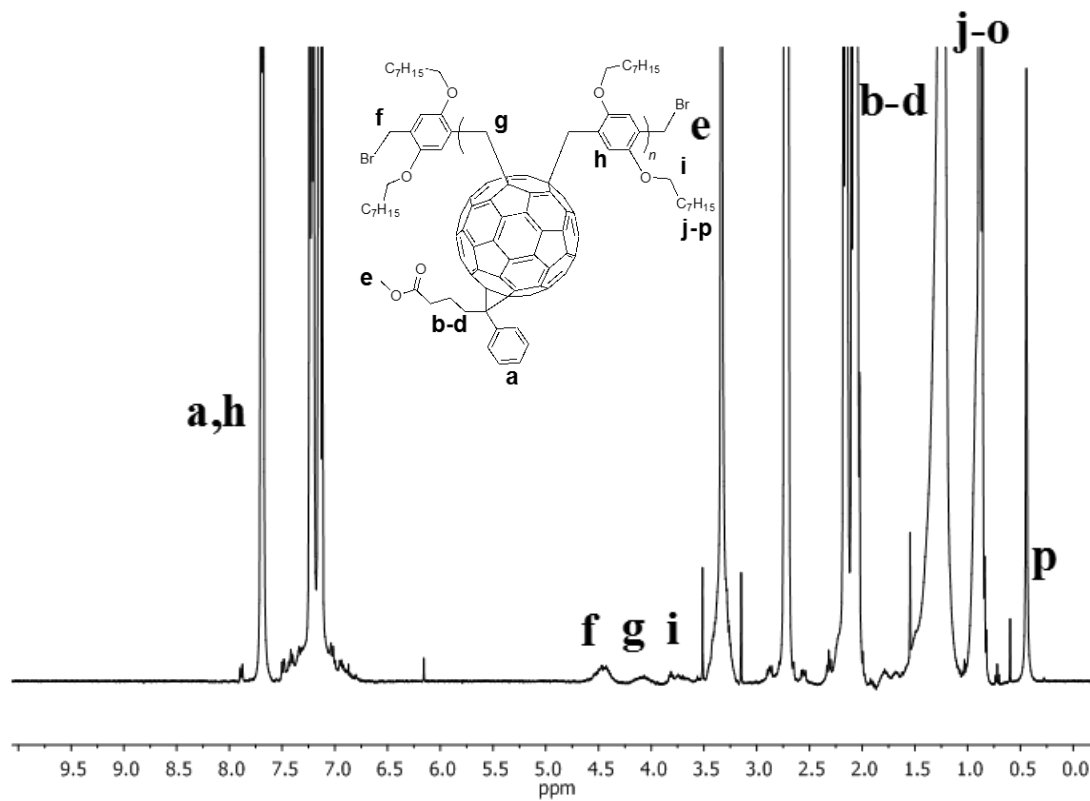


Figure 171: ^1H NMR spectrum of oligoPCBM (C_6D_6 , room temperature).

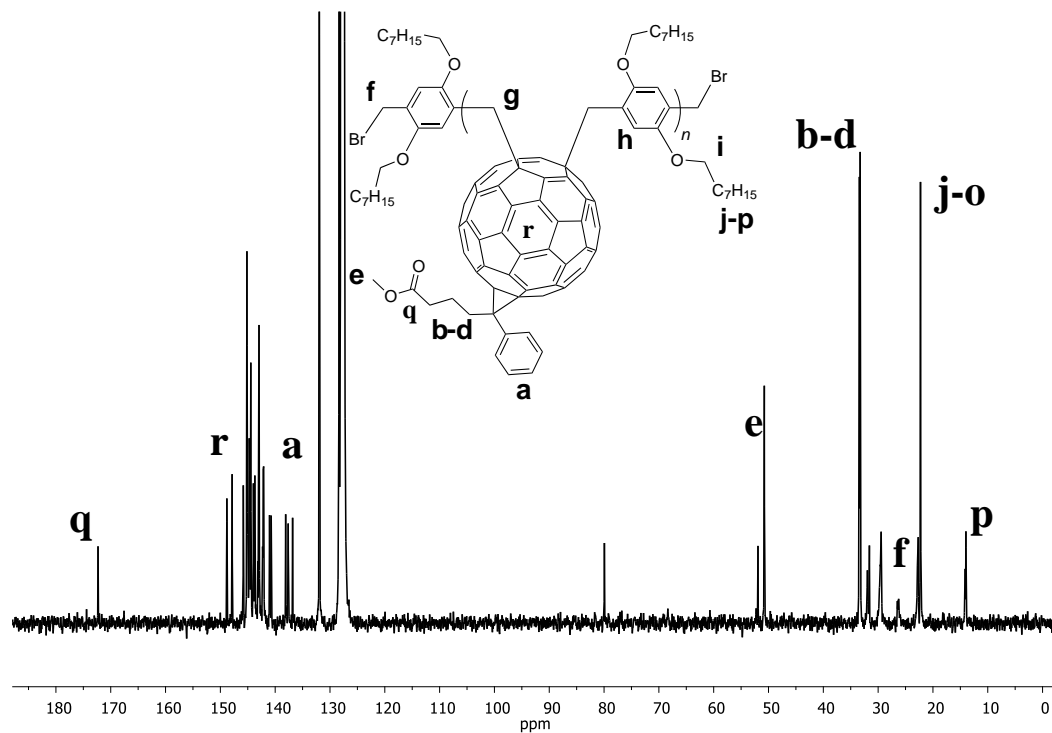


Figure 172: ^{13}C NMR spectrum of oligoPCBM (C_6D_6 , ambient temperature).

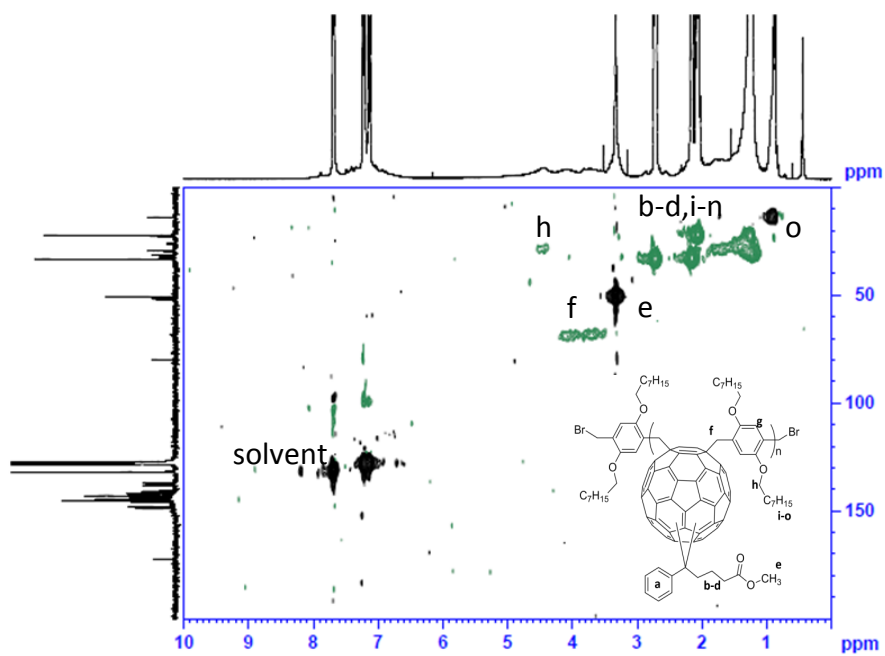


Figure 173: 2D HSQC NMR spectrum of polyPCBM_F (C_6D_6 , ambient temperature). Black indicates methyl and aromatic correlations, green methylene.

5.4 Synthesis and characterization of poly(fulleropyrrolidines)

Synthesis of **PPC1**

C_{60} (0.5 g, 6.94×10^{-4} mol), terephthalaldehyde (**2**, 0.093 g, 6.94×10^{-4} mol) and N-methylglycine (0.124 g, 1.39×10^{-3} mol) were dissolved in toluene (555 mL) and the solution heated at reflux for 18 h prior to dropping into methanol. The brut product precipitate, on recovery by filtration, was dried under reduced pressure. To remove C_{60} the solids were hexane washed overnight in a soxhlet, recovered and dried under reduced pressure at 40 °C for three days, to yield 0.236 g (37.5%) of a brown powder. SEC, THF eluent at 1 mL min⁻¹, 30 °C, UV = 300 nm: $M_n = 180$ g mol⁻¹; $M_p = 300$ g mol⁻¹; $\bar{D} = 4.4$. SEC, chlorobenzene eluent at 1 mL min⁻¹, 50 °C, refractive index: $M_n = 30700$ g mol⁻¹, $M_w = 62800$ g mol⁻¹, $\bar{D} = 2.00$

¹H NMR (400.6 MHz, 85°C, 1,4-DCB) $\delta = 2.72$ (s, 3H, -N-CH₃), 4.14-4.85 (dd, J = 272 Hz, J = 8 Hz, 2H, -CH₂-N-), 5.40 (s, 1H, -CH-N-), 7.76-7.94 (aromatics), 9.92 (s, 1H, C=O).

¹³C NMR (400 MHz, 85°C, 1,4-DCB) $\delta = 39.50$ (s, -N-CH₃), 69.13 (s, -CH₂-N-), 83.09 (s, -CH-N-), 132.43-152.48 (m, aromatics), 143.30 (unbound C_{60}), 189.91 (s, C=O) ppm. 2D-HMQC NMR (C_6D_6) 2.36, 39.50 (-N-CH₃); 3.74 and 4.42, 69.78 (-CH₂-N-); 4.59, 83.09 (-CH-N-); 143.30 (C_{60} impurity, no correlation with proton); 9.58, 190.76 (CH=O) ppm.

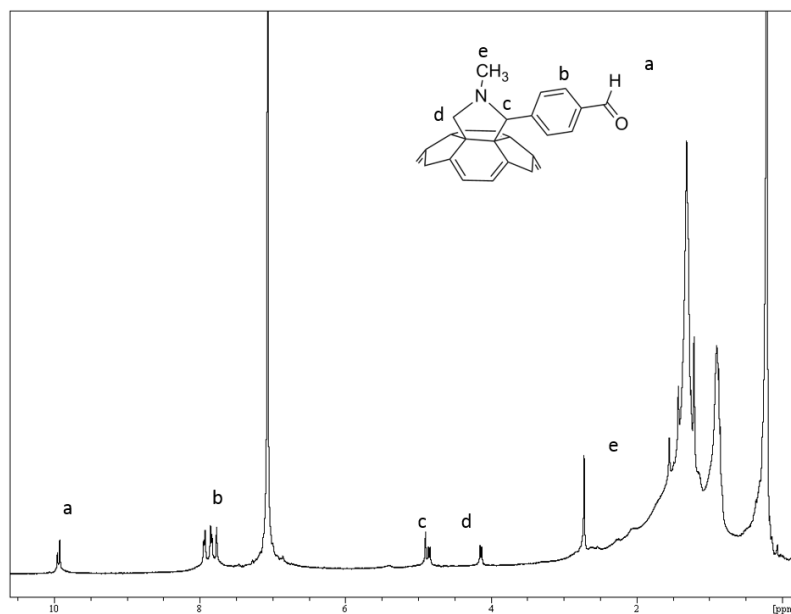


Figure 174: ¹H-NMR spectrum (1,4-DCB, 85°C) of **PPC1**.

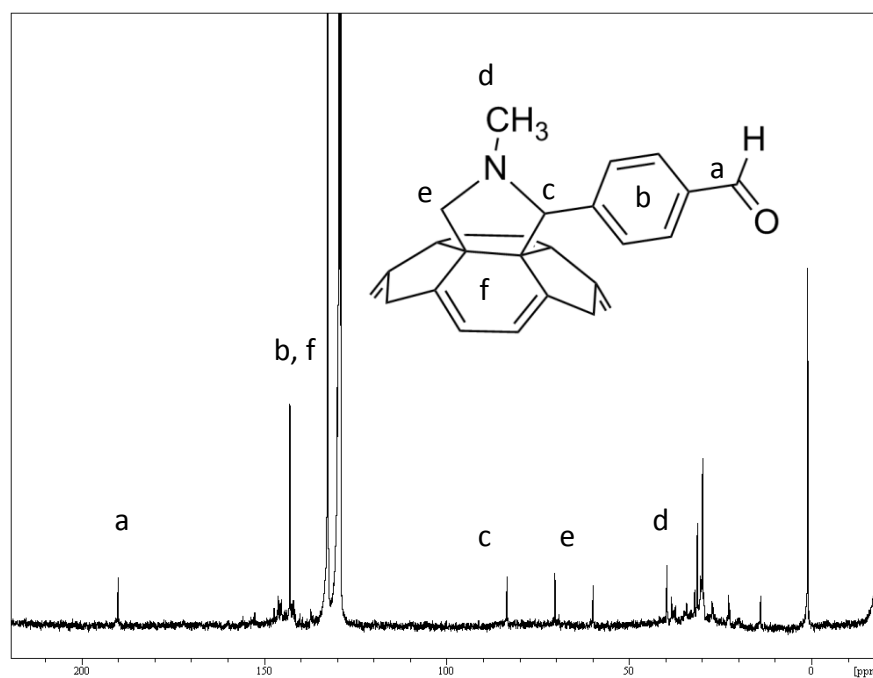


Figure 175: ^{13}C -NMR spectrum (1,4-DCB, 85°C) of PPC1. Note the numerous additional peaks due to trapped impurities such as C_{60} and hexane.

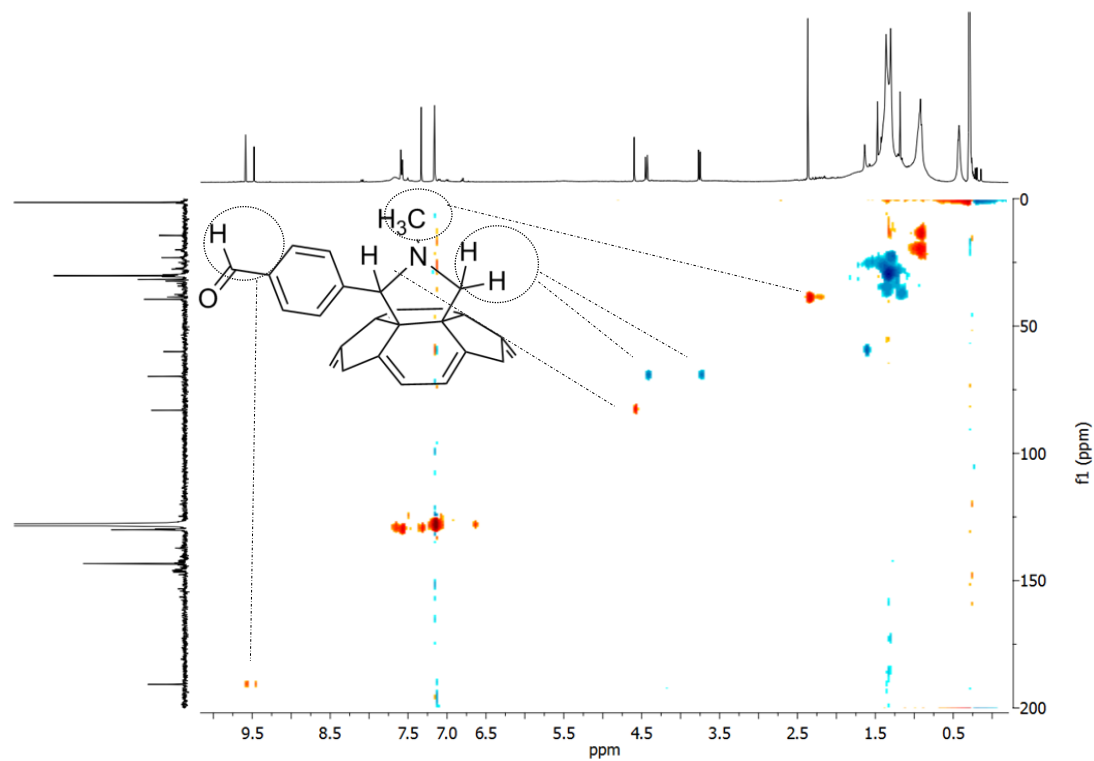


Figure 176: HSQC 2D NMR spectrum (C_6D_6 , ambient temperature) of PPC1.

Synthesis of **PPC2**

C₆₀ (0.1 g, 1.39 × 10⁻⁴ mol), terephthalaldehyde (**2**, 0.019 g, 1.39 × 10⁻⁴ mol) and *N*-methylglycine (0.025 g, 2.78 × 10⁻⁴ mol) were dissolved in 1,2-chlorobenzene (DCB, 5 mL) and the solution heated and stirred at 150 °C for 18 h prior to dropping into methanol. The brut product precipitate, on recovery by filtration, was dried under reduced pressure. To remove most of the C₆₀, the solids were hexane washed overnight in a soxhlet, recovered and dried under reduced pressure for three days, to yield 0.039 g (30%) of a brown powder. SEC (THF eluent at 1 mL min⁻¹, 30 °C, UV = 300 nm): $M_n = 190 \text{ g mol}^{-1}$; $M_p = 3060 \text{ g mol}^{-1}$ $\mathcal{D} = 9.8$.

No NMR due to low solubility.

Synthesis of **PPC3**

C₆₀ (0.5 g, 6.9 × 10⁻⁴ mol), **5** (0.271 g, 6.9 × 10⁻⁴ mol) and *N*-methylglycine (0.124 g, 1.3 × 10⁻³ mol) were dissolved in toluene (555 mL) and the solution heated at reflux for 18 h prior to dropping into methanol (3 L). The brut product precipitate, on recovery by filtration, was dried under reduced pressure. To remove most of the C₆₀, the solids were hexane washed overnight in a soxhlet, recovered and dried under reduced pressure for three days, to yield 0.328 g (40.6 %) a brown powder.

SEC, THF eluent at 1 mL min⁻¹, 30 °C, UV = 300 nm: $M_n = 3120 \text{ g mol}^{-1}$; $M_p = 3500 \text{ g mol}^{-1}$; $\mathcal{D} = 1.1$.
SEC, chlorobenzene eluent at 1 mL min⁻¹, 50 °C, refractive index: $M_n = 500 \text{ g mol}^{-1}$, $M_w = 550 \text{ g mol}^{-1}$, $\mathcal{D} = 1.1$.

¹H NMR (400.6 MHz, 1,4-DCB-*d*₄, 85 °C) δ (ppm): 0.84 (broad, -OCH₂(CH₂)₆CH₃), 1.27-1.75 (m, -OCH₂(CH₂)₆CH₃), 2.77 (N-CH₃), 3.74 – 4.81 (m, -OCH₂(CH₂)₆CH₃), -CH₂-N-), 5.65 (s, -CH-N-), 7.42 – 7.86 (s, *aromatics*), 10.67 (s, -CHO) ppm.

¹³C NMR (100.16 MHz, 1,4-DCB-*d*₄, 85 °C), δ : 13.42 (s, OCH₂(CH₂)₆CH₃), 22.24 (s, OCH₂(CH₂)₅CH₂CH₃), 25.73 (s, OCH₂CH₂CH₂(CH₂)₄CH₃), 28.91 (s, OCH₂CH₂CH₂(CH₂)₄CH₃), 31.43 (s, OCH₂(CH₂)₄CH₂CH₂CH₃), 39.25 (s, -N-CH₃), 68.54, 68.97, 69.62 (s, -OCH₂(CH₂)₆CH₃ and -CH₂-N-), 75.47, 76.12 (s, -CH-N-), 109.97, 115.64 (s, *aromatic*), 125.66 – 155.79 (m, *aromatic*, C₆₀, *aromatic*-OC₈H₁₇), 187.24 (C=O) ppm.

2D-HMQC NMR (1,4-DCB-*d*4, 85 °C), $d = \delta = 0.84, 13.42$ (-OCH₂(CH₂)₆CH₃); 1.27-1.75, 22.24-31.43 (-OCH₂(CH₂)₆CH₃); 2.77, 39.25 (-N-CH₃), 3.74-4.81, 68.54-69.62 (-OCH₂(CH₂)₆CH₃), -CH₂-N-); 5.65, 75.47-76.12 (-CH-N-), 7.42 - 7.86, 109.97 - 115.64 (*aromatics*); 10.55, 187.24 (CHO) ppm.

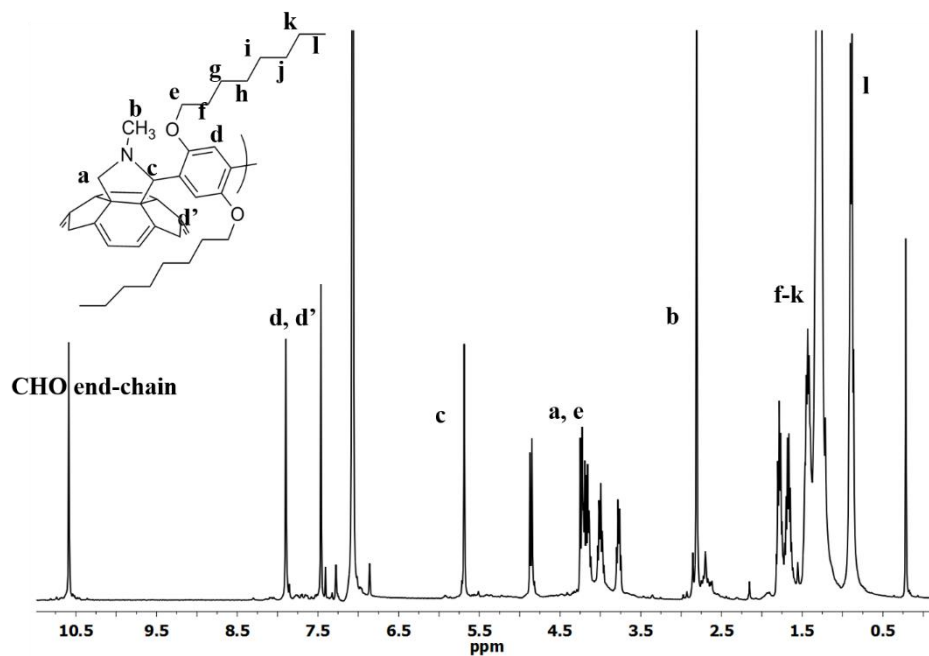


Figure 177: ¹H-NMR spectrum (1,4-DCB-*d*4, 85 °C) of PPC3.

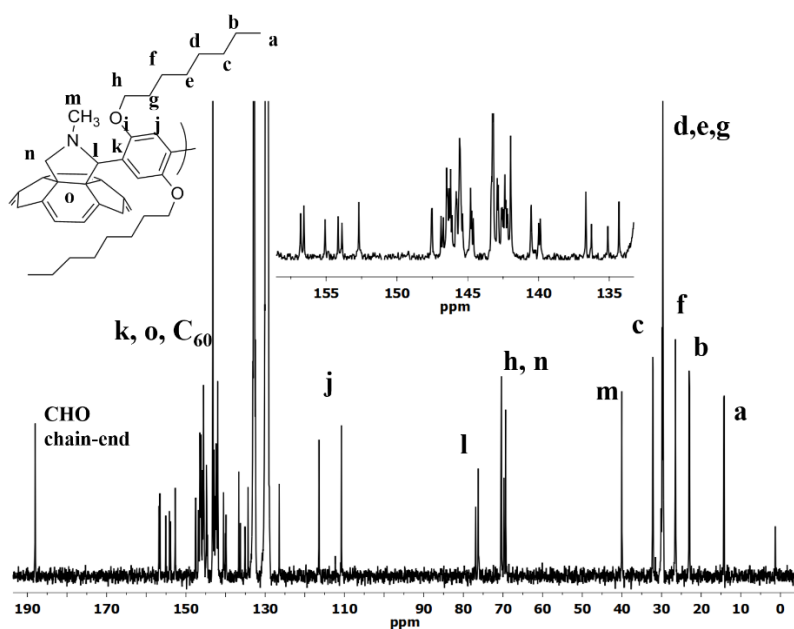


Figure 178: ¹³C-NMR spectra of PPC3 and the comonomer 5a (1,4-DCB-*d*4, 85 °C).

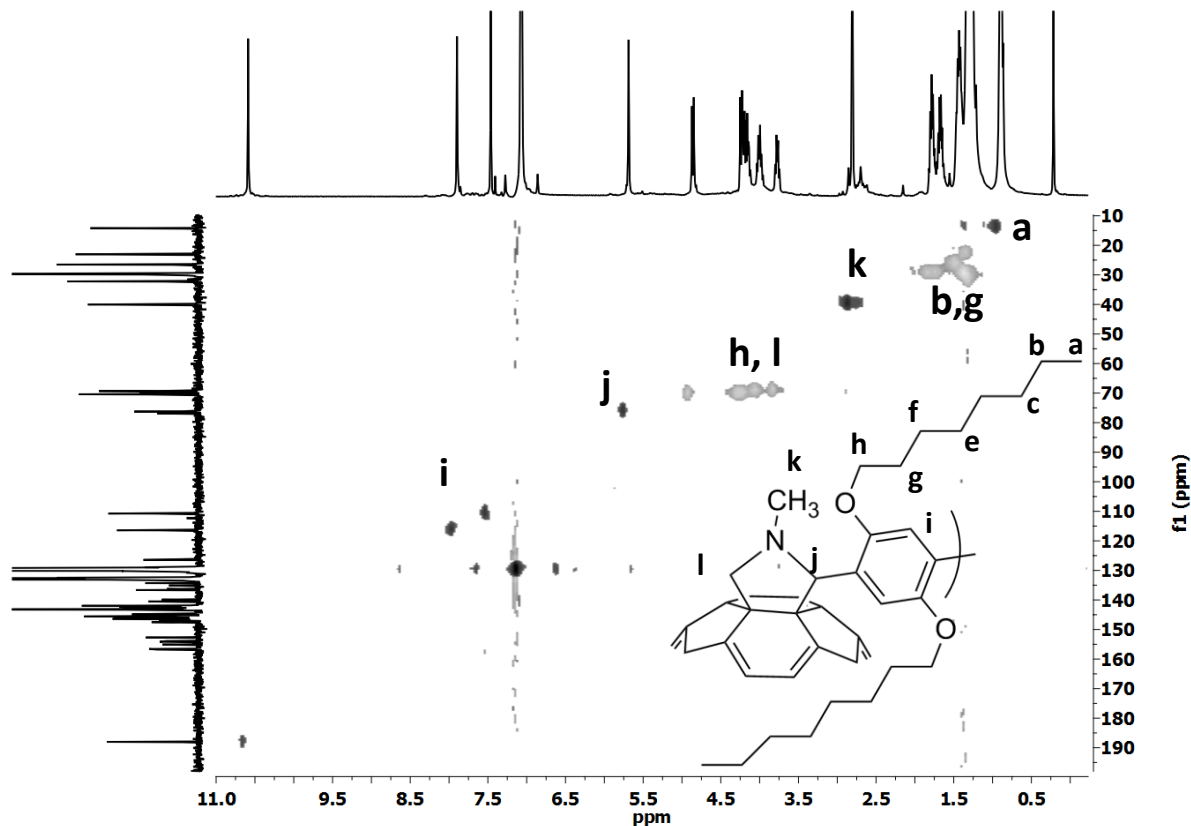


Figure 179: HSQC 2D NMR spectrum (1,4-DCB-*d*4, 85 °C) of **PPC3** where (above) light grey indicates methylene, and dark grey methyl or methine.

Synthesis of **PPC4**

C_{60} (0.5 g, 6.9×10^{-4} mol), **5** (0.272 g, 6.9×10^{-4} mol), and *N*-methylglycine (0.125 g, 1.3×10^{-3} mol) were dissolved in DCB (25 mL) and stirred at 150 °C for 18 h, then poured into methanol (250 mL). The purification of **PPC4** was as that of **PPC3**, and yielded (0.463 g, 57.5%) of a shiny black powder. SEC, THF eluent at 1 mL min⁻¹, 30 °C, UV = 300 nm: $M_n = 2064$ g mol⁻¹; $M_p = 4288$ g mol⁻¹; $\bar{D} = 2.2$. SEC, chlorobenzene eluent at 1 mL min⁻¹, 50 °C, refractive index: $M_n = 5800$ g mol⁻¹, $M_w = 20100$ g mol⁻¹, $\bar{D} = 3.5$.

¹H NMR (400.6 MHz, 1,4-DCB-*d*4, 85 °C) $\delta = 0.85$ (broad, -OCH₂(CH₂)₆CH₃), 1.26 (broad, -OCH₂(CH₂)₆CH₃), 2.11-2.81 (broad, -N-CH₃), 3.72 - 4.81 (m, broad, -OCH₂(CH₂)₆CH₃), -CH₂-N-), 5.67 (broad, -CH-N-), 7.53 - 7.81 (m, broad, *aromatics*) ppm.

¹³C NMR (100.16 MHz, 1,4-DCB-*d*4, 85 °C) $\delta = 13.57$ (s, OCH₂(CH₂)₆CH₃), 22.28 (s, OCH₂(CH₂)₅CH₂CH₃), 25.85 (s, OCH₂CH₂CH₂(CH₂)₄CH₃), 29.05 (s, OCH₂CH₂CH₂(CH₂)₄CH₃), 31.50

(s, $\text{OCH}_2(\text{CH}_2)_4\text{CH}_2\text{CH}_2\text{CH}_3$), 39.28 (s, -N- CH_3), 69.08 (broad, $-\text{OCH}_2(\text{CH}_2)_6\text{CH}_3$ and $-\text{CH}_2\text{-N-}$), 75.38 (broad, $-\text{CH-N-}$), 114.47 (broad, aromatic), 141.16 – 145.52 (m, aromatic, C_{60}), 152.43 (broad, aromatic- OC_8H_{17}) ppm.

2D-HMQC NMR (1,4- DCB-d_4 , 85 °C), $d = \delta = 0.85$, 13.57 ($-\text{OCH}_2(\text{CH}_2)_6\text{CH}_3$); 1.26, 22.28, -31.50 ($-\text{OCH}_2(\text{CH}_2)_6\text{CH}_3$); 2.81, 39.28 (-N- CH_3), 3.72 – 4.81, 69.08 ($-\text{OCH}_2(\text{CH}_2)_6\text{CH}_3$), $-\text{CH}_2\text{-N-}$); 5.67, 75.38 ($-\text{CH-N-}$), 7.53 – 7.81, 114.47 (aromatics) ppm.

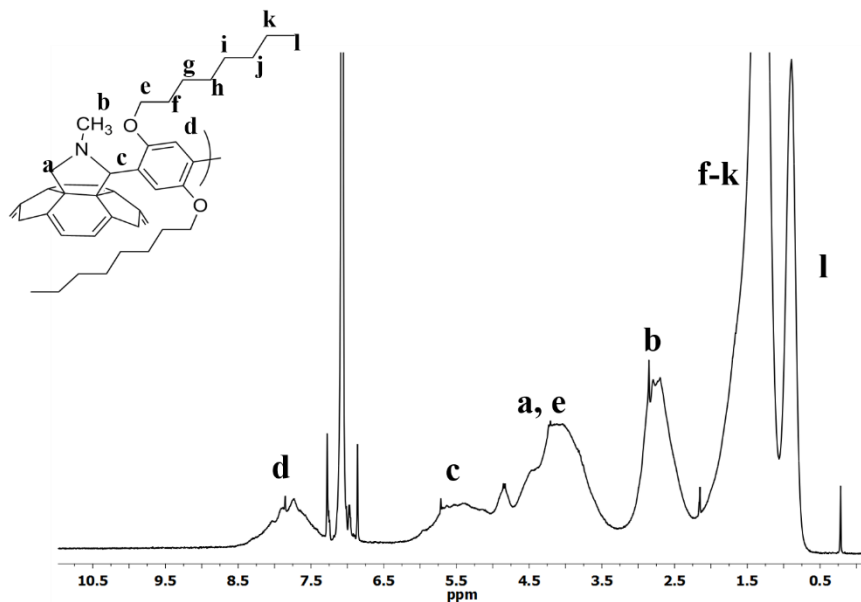


Figure 180: $^1\text{H-NMR}$ spectrum (1,4- DCB-d_4 , 85 °C) of PPC4.

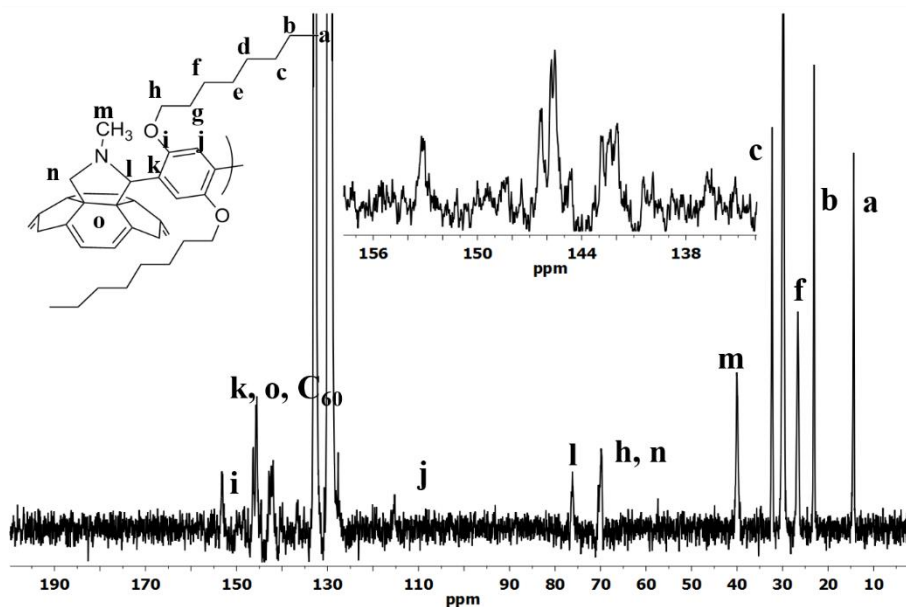


Figure 181: $^{13}\text{C-NMR}$ spectrum (1,4- DCB-d_4 , 85 °C) of PPC4.

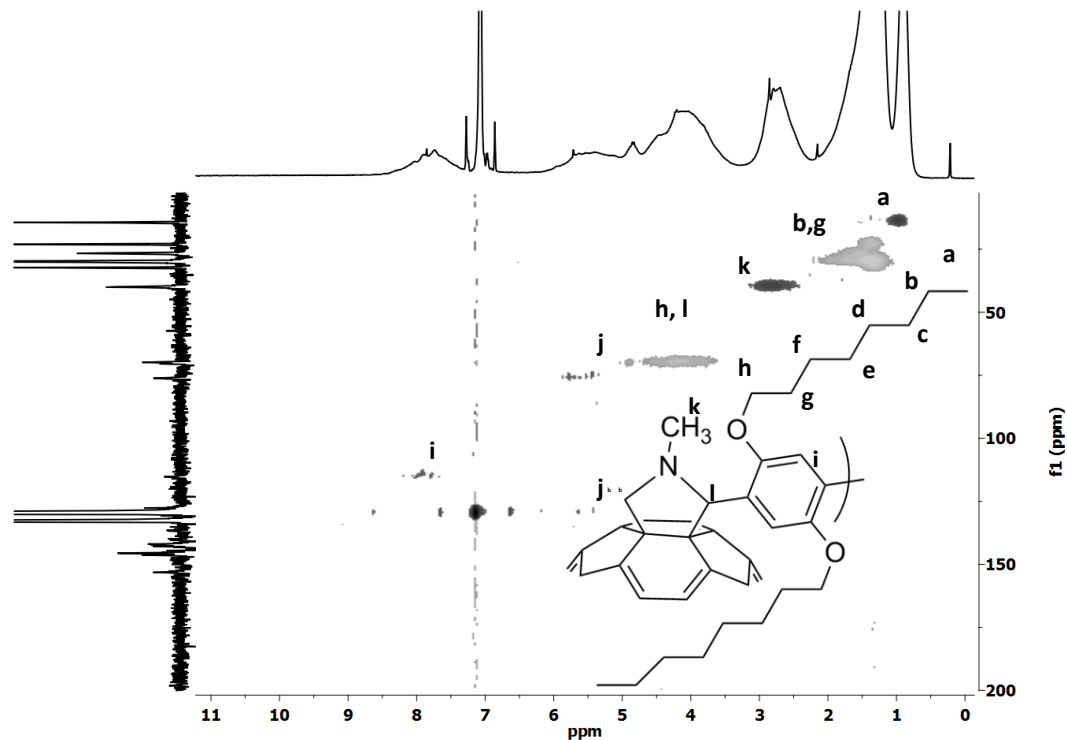


Figure 182: HSQC 2D NMR spectrum (1,4-DCB-*d*4, 85 °C) of **PPC4** where (above) light grey indicates methylene, and dark grey methyl or methine.

Synthesis of **PPC5**

C_{60} (0.05 g, 6.94×10^{-5} mol), **8** (0.035 g, 6.96×10^{-5} mol), and *N*-methylglycine (0.0124 g, 1.39×10^{-4} mol) were dissolved in toluene (55.5 mL) and heated at reflux for 18 h, then poured into methanol. The purification of **PPC5** was as that of **PPC4**, and yielded (0.038 g, 42.3%) of a shiny black powder. SEC, THF eluent at 1 mL min⁻¹, 30 °C, UV = 300 nm: $M_n = 2770$ g mol⁻¹; $M_p = 4260$ g mol⁻¹; $D = 1.7$.

¹H NMR (400.6 MHz, 1,4-DCB-*d*4, 85 °C) δ = 0.86 (broad, -OCH₂(CH₂)₁₀CH₃), 1.25 – 2.12 (broad, -OCH₂(CH₂)₁₀CH₃), 2.66-2.82 (broad, -N-CH₃), 3.39 – 4.80 (m, broad, -OCH₂(CH₂)₁₀CH₃), -CH₂-N-), 5.68 (broad, -CH-N-), 7.50– 7.82 (broad, *aromatics*).

¹³C NMR (100.16 MHz, 1,4-DCB-*d*4, 85 °C) δ = 13.51 (s, O-CH₂(CH₂)₁₀CH₃), 22.25 (s, O-CH₂(CH₂)₉CH₂CH₃), 25.90 (s, O-CH₂CH₂CH₂(CH₂)₈CH₃), 28.97 – 29.34 (m, O-CH₂CH₂CH₂(CH₂)₆CH₂CH₂CH₃), 31.52 (s, O-CH₂(CH₂)₈CH₂CH₂CH₃), 39.26 (s, -CH₃-N-), 69.08 (broad, O-CH₂(CH₂)₁₀CH₃), 75.37 (broad, -CH-N-), 114.56 (broad, *aromatic*), 135.83–147.62 (m, *aromatic*, C_{60}), 152.51 (broad, *aromatic*-OC₁₂H₂₅) ppm.

2D-HMQC NMR (1,4-DCB-*d*4, 85 °C), $d = \delta = 0.86$, 13.51 (-OCH₂(CH₂)₁₀CH₃); 1.25–2.12, 22.25–31.52 (-OCH₂(CH₂)₁₀CH₃); 2.82, 39.26 (-N-CH₃), 3.39–4.80, 69.08 (-OCH₂(CH₂)₁₀CH₃), -CH₂-N-); 5.68, 75.37 (-CH-N-), 7.50–7.82, 114.56 (aromatics) ppm.

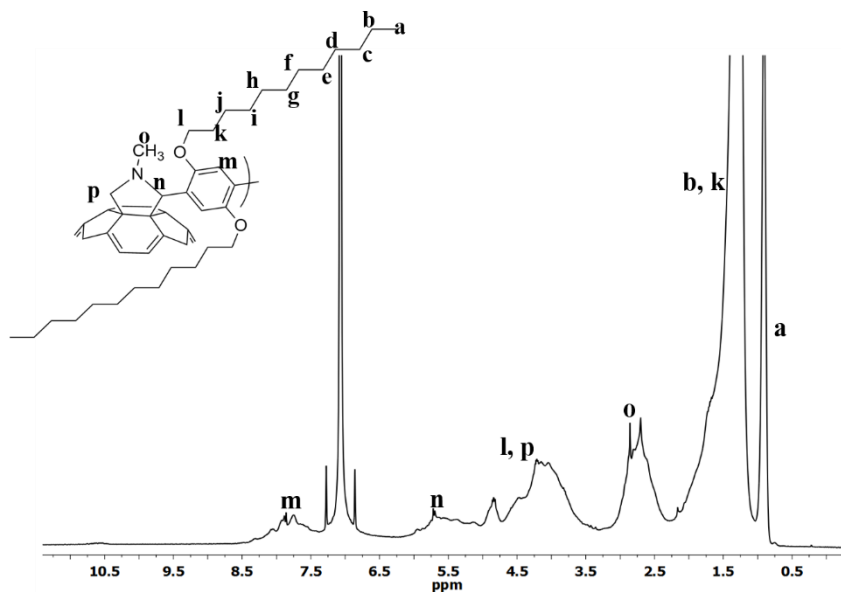


Figure 183: ¹H-NMR spectrum (1,4-DCB-*d*4, 85 °C) of PPC5.

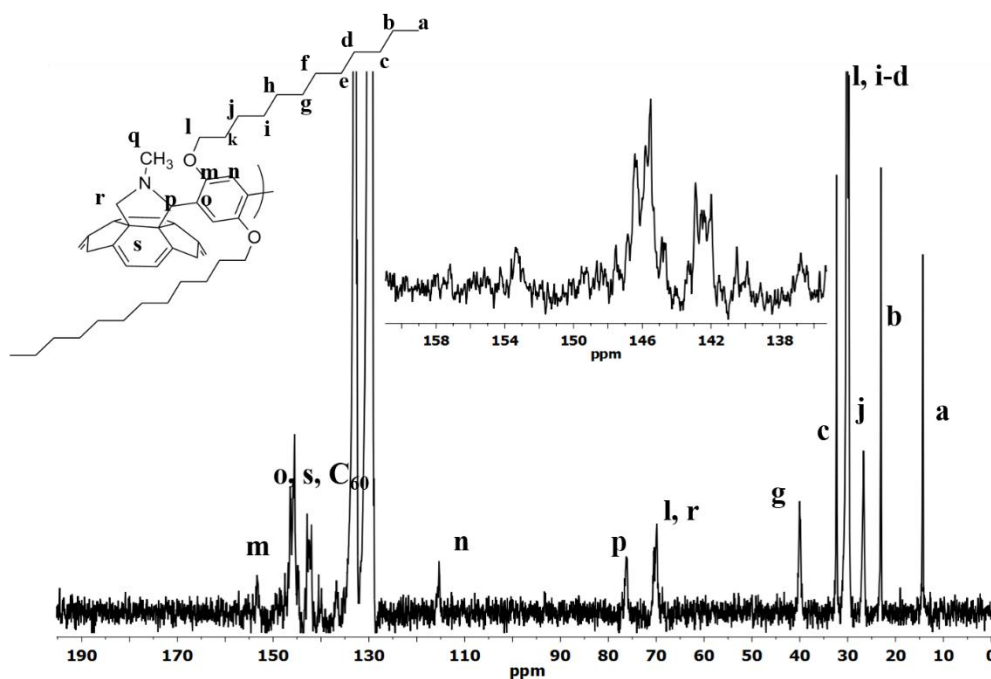


Figure 184: ¹³C-NMR spectrum (1,4-DCB-*d*4, 85 °C) of PPC5.

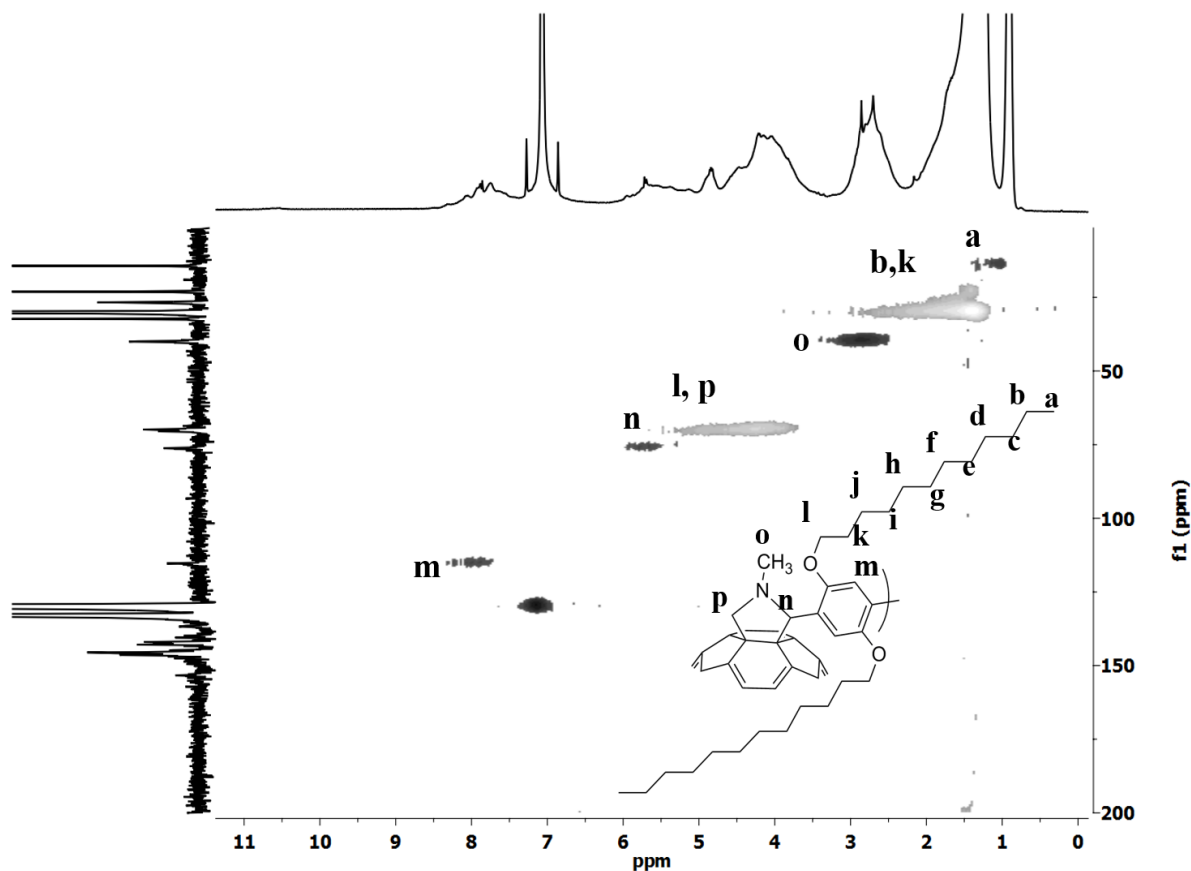


Figure 185: HMQC 2D NMR spectrum (1,4-DCB-*d*₄, 85 °C) of **PPC5**.

Synthesis of **PPC6**

C₆₀ (0.05 g, 6.94 × 10⁻⁵ mol), **8** (0.035 g, 6.94 × 10⁻⁵ mol), and *N*-methylglycine (0.0123 g, 1.38 × 10⁻⁴ mol) were dissolved in DCB (2.5 mL) and stirred at 150 °C for 18 h, then poured into methanol. The purification of **PPC6** was as that of **PPC5**, and yielded 0.031g (35%) of a shiny black powder. SEC, THF eluent at 1 mL min⁻¹, 30 °C, UV = 300 nm: *M*_n = 5710 g mol⁻¹; *M*_p = 8100 g mol⁻¹; *D* = 1.9. SEC, chlorobenzene eluent at 1 mL min⁻¹, 50 °C, refractive index: *M*_n = 6700 g mol⁻¹, *M*_w = 19100 g mol⁻¹, *D* = 2.9.

¹H NMR (400.6 MHz, 1,4-DCB-*d*₄, 85 °C) δ = 0.87 (broad, -OCH₂(CH₂)₁₀CH₃), 1.26 – 2.12 (broad, -OCH₂(CH₂)₁₀CH₃), 2.64-2.82 (broad, -N-CH₃), 3.81 – 4.82 (m, broad, -OCH₂(CH₂)₁₀CH₃), -CH₂-N-, 5.38 – 5.68 (broad, -CH-N-), 7.51 – 7.82 (broad, aromatics).

¹³C NMR (100.16 MHz, 1,4-DCB-*d*₄, 85 °C) δ = 13.52 (s, O-CH₂(CH₂)₁₀CH₃), 22.26 (s, O-

$\text{CH}_2(\text{CH}_2)_9\text{CH}_2\text{CH}_3$), 25.84 (s, $\text{O}-\text{CH}_2\text{CH}_2\text{CH}_2(\text{CH}_2)_8\text{CH}_3$), 28.98 - 29.34 (m, $\text{O}-\text{CH}_2\text{CH}_2\text{CH}_2(\text{CH}_2)_6\text{CH}_2\text{CH}_2\text{CH}_3$), 31.53 (s, $\text{O}-\text{CH}_2(\text{CH}_2)_8\text{CH}_2\text{CH}_2\text{CH}_3$), 39.28 (s, $-\text{CH}_3-\text{N}-$), 69.19 (broad, $\text{O}-\text{CH}_2(\text{CH}_2)_{10}\text{CH}_3$), 75.35 (broad, $-\text{CH}-\text{N}-$), 114.46 (broad, *aromatic*), 135.84 - 148.51 (m, *aromatic*, C_{60}), 152.38 (broad, *aromatic*- $\text{OC}_{12}\text{H}_{25}$) ppm.

2D-HMQC NMR (CDCl_3 , ambient temperature) $\delta = 0.87, 13.52$ ($-\text{OCH}_2(\text{CH}_2)_{10}\text{CH}_3$); 1.26 - 2.12, 22.26 - 31.53 ($-\text{OCH}_2(\text{CH}_2)_{10}\text{CH}_3$); 2.82, 39.28 ($-\text{N}-\text{CH}_3$), 3.81 - 4.82, 69.19 ($-\text{OCH}_2(\text{CH}_2)_{10}\text{CH}_3$, $-\text{CH}_2-\text{N}-$); 5.68, 75.35 ($-\text{CH}-\text{N}-$), 7.51 - 7.82, 114.46 (*aromatics*) ppm. 2D-HSQC NMR (1,4- $\text{DCB}-d_4$, 85 °C) $\delta = 0.86, 14.34$ ($-\text{OCH}_2(\text{CH}_2)_{10}\text{CH}_3$); 1.23, 22.89 - 32.11 ($-\text{OCH}_2(\text{CH}_2)_{10}\text{CH}_3$); 2.67, 40.37 ($-\text{N}-\text{CH}_3$), 3.90 - 4.96, 69.35 ($-\text{OCH}_2(\text{CH}_2)_{10}\text{CH}_3$, $-\text{CH}_2-\text{N}-$); 5.20 - 5.56, 75.74 ($-\text{CH}-\text{N}-$), 7.45 - 7.75, 114.29 (*aromatics*) ppm.

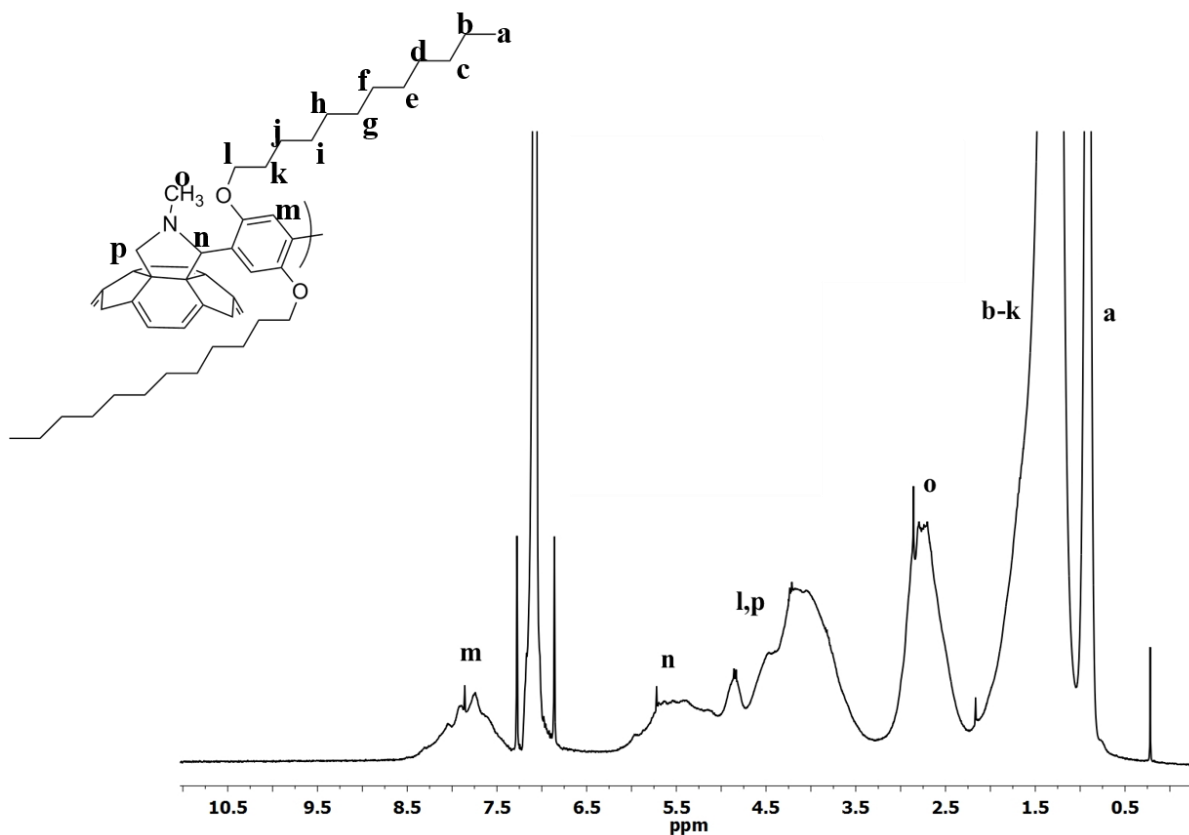


Figure 186: ^1H -NMR spectrum (1,4- $\text{DCB}-d_4$, 85 °C) of PPC6.

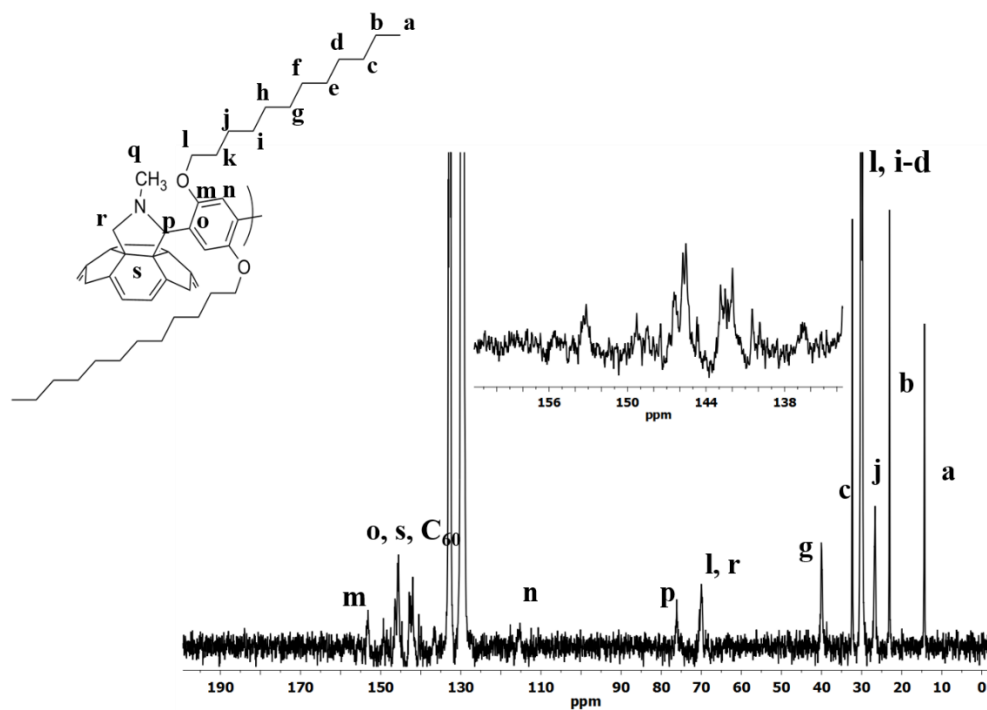


Figure 187: ^{13}C -NMR spectrum (1,4-DCB- d_4 , 85 °C) of PPC6.

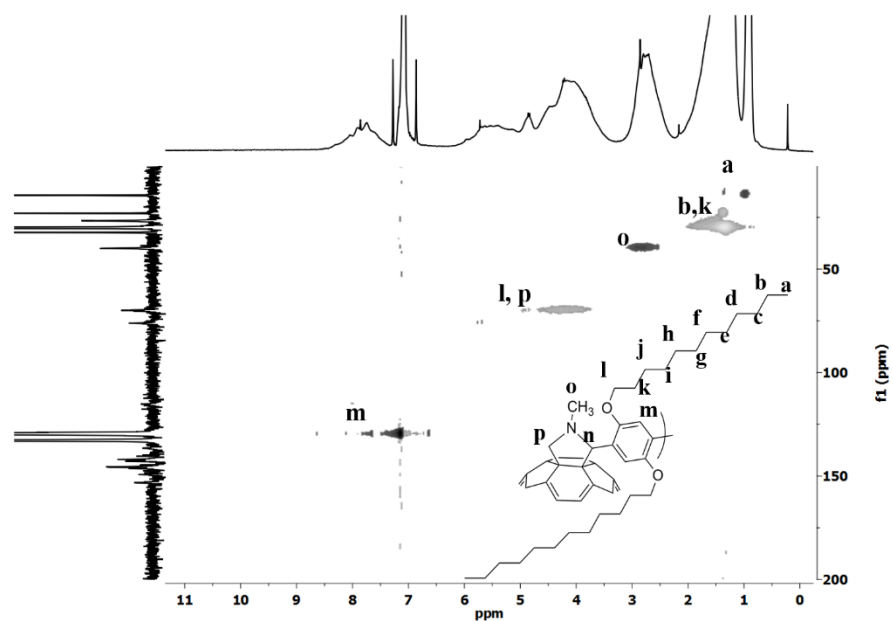


Figure 188: HMQC 2D NMR spectrum (1,4-DCB- d_4 , 85 °C) of PPC6.

5.5 Device fabrication and characterization

Glass/Flex substrates were cleaned by wiping with an IPA soaked tissue before being sonicated in acetone and IPA for 15 mins each. A suspension of ZnO nanoparticles (5 wt%) in EtOH was sonicated for 30 mins before being deposited on the substrates by doctor blading. The coater surface was set to 65 °C and the blade run 700 µm over the samples at a speed of 5 mm/s. The ZnO layer was subsequently annealed at 140 °C for 10 mins before deposition of the active layer. The active layer was coated at 65 °C at a speed of 35-40 mm/s with a blade height of 700 µm in all cases except where explicitly stated. Absorption spectra were taken here to ensure consistency of the active layer thickness between samples. A PEDOT:PSS solution was filtered using 0.45 µm hydrophilic filters before being deposited on the active layer at 65 °C, a speed of 20 mm/s and a blade height of 700 µm. Samples were then annealed for 5 min at 120 °C under nitrogen to drive off residual water before being placed in an evaporator. 150 nm of silver was then evaporated onto the samples under vacuum.

The current voltage characteristics of the devices were measured using a Keithley source meter both in the dark and under illumination by a Xenon lamp calibrated to approximately a 1 sun intensity using a silicon photodiode.

External quantum efficiency measurements were conducted using a Keithley source meter and chopped light focused onto the sample from a Xenon lamp attached to an Acton Spectrapro 2150i monochromator.

Conclusions

This thesis addresses the synthesis of main-chain polyfullerene for photovoltaic applications.

Due to its good electronic properties and high electron mobility, fullerene and its derivatives are widely used in organic solar cell as acceptor materials in the active layer. Moreover, various derivatives have been proposed in the role of third component in the active layer to stabilize the BHJ morphology as well as electron-selective interlayer to improve the interfaces and the charge extraction.

However, when used in the active layer, fullerene derivatives have the natural tendency to self-aggregation. Although this tendency permits first to obtain a good nanomorphology of the BHJ, the growth of the domain with time results in microscale clusters that inhibit the charge separation and the charge transfer within the active layer, and thus reduces the performance of the solar cell.

The merging of the electronic properties of fullerene and the mechanical and processibility of polymers, is thought to be a promising approach to minimize this tendency and obtain a good intermixing with the *p*-type polymer in the photoactive blend. In particular, main-chain polyfullerenes can give the possibility of a better control on the fullerene content and dispersion in the blend as fullerenes are present in the back-bone of the polymers.

In this work, two different polymerization routes have been exploited in order to obtain oligo- and polyfullerene with good solubility in common organic solvents and promising photovoltaic properties.

The first route is based on that of the atomic transfer addition polymerisation (ATRAP), which has used with PCBM as monomer to take advantage from its good solubility. This route, chosen because easy to implement, results in oligo- and polyPCBM materials with good solubilities. The ratio between the reagents was the same for all the reactions (PCBM: bis-bromo-comonomer: CuBr: bipyridine, 1:1:2:4). The synthesis is facile but highly sensitive to impurities. SEC chromatography analysis on different batches of materials suggest that particular care with handling of C₆₀ and PCBM with respect to oxygen and light, and great care with respect to the pre-cleaning of the CuBr are necessary to obtain a controlled reaction.

In particular, two materials have been studied. The first material, polyPCBM_A, has polymeric nature, while polyPCBM_F, the second compounds, has an oligomeric nature. The difference in the two materials could be attributed to the different scale of the reactions. While polyPCBM_A has been prepared using 0.4 g of PCBM as starting material, polyPCBM_F has been obtained from the reaction of 3 g of PCBM with equimolar amount of the comonomer. Temperature, concentration, as well as time of reaction were the same for the two reactions.

The structure and the nature of the two macromolecules, and the close similarity between polyPCBM_F and PCBM have been confirmed from the various characterisation techniques employed. In addition, it has been noticed that PCBM contributes to polyPCBM_A to the extent of 3% while the percentage drastically increases to 35% in polyPCBM_F after purification in Soxhlet apparatus with acetone.

The second route of polymerisation explored in this work is based on fulleropyrrolidine chemistry (Prato chemistry), which is, to our knowledge, exploited for the first time for the synthesis of main-chain polyfullerenes.

Three different co-monomers, namely, 2,5-bis(octyloxy)terephthaldehyde and, 2,5-bis(dodecyloxy)terephthaldehyde, have been employed in the reactions to study the role of the substituents on the polymerisation process. It has been found that the polymerisation is highly dependent on the steric hindrance of the comonomer. In particular, while the small terephthaldehyde results in a multi-substituted fullerene derivatives, the hindrance of the comonomers with longer side alkoxy-chain led to oligo- and polyfullerene.

The reaction has been found to be sensitive also to concentration and temperature. Despite the use of the same comonomer, higher temperatures (150 °C instead of 110 °C), and higher concentrations led to higher molecular weight macromolecules.

Kinetic studies suggest that the polymerization process occurs through three distinct regimes with time:

- A. a period of induction, where C₆₀ dissolution or ylide formation or both are rate determining up to the 180th minute;
- B. a period where the polymerisation proceeds in accordance with a typical step growth reaction to around 10 h;
- C. a period where the polymerisation is limited by product precipitation.

Comparing the calculated electronic transitions for a representative compound with the UV-vis spectrum of one of the polymers, we observed that the closest correlation was found for the *trans*-3 isomer. *Trans*-2 adduct was detected in smaller amount in the mixture and resulted very much reduced when larger $-OC_{12}H_{25}$ chains are used in the comonomer. This indicates that the larger comonomer are enforcing steric control over the product. An unexpected result is that *trans*-4 and equatorial products appear limited.

XPS and UPS analysis have been conducted on the synthesized materials which have been deposited on various substrates. According to the ICT model, a charge transfer from the substrate to the different fullerenes resulting in a pinning at the ICT- level can be expected if the work function of the substrate is lower as ICT- of the fullerene. In our case, a lowering of the ionization potential as a consequence of the polymerization is observed (6.03 eV for PCBM, 5.93 eV for **PPC4** and 5.8 eV for **PPC6**). At the interface to PEI substrate, interface dipoles of 0.5 eV and 0.4 eV were observed for **PPC4** and **PPC6**, respectively. The formation of such interface dipoles points to a pinning of the energy levels at the interface. The pinning level can be related to the ICT- level of the polymer. The value for E_{ICT} is 4.0 eV (**PPC4**) and 3.9 eV (**PPC6**) and thus significantly lower compared to PCBM.

PolyPCBM_F has been tested as an alternative acceptor to PCBM in the active layer. The novel poly(fulleropyrrolidine) materials have been tested for three applications: (i) as electron acceptor material within the blend; (ii) as an interlayer between the active layer and the electron extraction layer and; (iii) as an additive to stabilize the morphology of the blend under thermal stress in inverted structure geometry solar cells.

The obtained results indicate that both the opto-electronic and the charge-transfer properties of PCBM are not diminished by the presence of polymer in polyPCBM_F. However, polyPCBM_F stabilizes device efficiency with T_{80} being 10 times longer than for the control when the devices are exposed to thermal treatment at 120 °C in glovebox.

A study employing two different low band gap polymers demonstrate that while polyPCBM_F is actually applicable to numerous systems, it most likely requires an optimization specific to each partner low band gap polymer in order to improve the intermixing in the blend.

The introduction of the poly(fulleropyrrolidine) **PPC4** in OPV devices does not result in the complete failure of the solar cell. However, analysing single cases, the polymeric material is not a good alternative to PCBM as acceptor in the active layer and, it worsens the device

performance when used as an interlayer. The application that seems to be the most attractive is then the use of the polymeric material as an additive.

Accelerated thermal degradation studies on inverted solar cells devices incorporating **PPC4** as additive in the active layer demonstrate that the poly(fulleropyrrolidine) stabilizes the performance of the devices with time at different temperature (100, 120 and 140 °C).

The UV-visible spectra and the optical microscopy images of annealed thin films of the active layer blend with and without **PPC4** as additive shows how the films remain stable upon thermal aging at the chosen temperature. This suggests that **PPC4** acts as stabilizer in the blend affecting PCBM aggregation and thus, that the observed stabilization in the OPV performance of the devices is likely to be correlated to the stabilization of the morphology of the active layer.

Comparative study using P3HT:PCBM-based and KP115:PCBM based samples (films and devices) with and without **PPC4** as additive demonstrates that the stabilizing ability of the poly(fulleropyrrolidine) is dependent on the choice of the donor material in the blend. In particular, the additive **PPC4**, is clearly more effective when employed in KP115-based blends than when used in P3HT-based blends.

Finally observations during the films degradation studies show that the quality of the BHJ active layer films is found to be a key point for the morphological degradation of the P3HT:PCBM blend when the poly(fulleropyrrolidine) additive (**PPC4**) is employed.

Further study to understand the mechanisms behind the stabilisation abilities of the novel materials would help the insertion of these novel polyfullerenes in the industrial application for organic photovoltaic devices.

Moreover, due to the nature and the ease of the syntheses exploited in this thesis, great room of design development is possible in the near future.

Conclusions

Cette thèse traite de la synthèse de poly-fullerènes à chaîne principale pour des applications au photovoltaïque.

Grâce à ses bonnes propriétés électroniques et à leur haute mobilité d'électrons, le fullerène et ses dérivés sont largement utilisés dans les cellules solaires organiques comme matériaux accepteurs dans la couche active. En outre, divers dérivés sont étés proposés dans le rôle de troisième composant dans la couche active pour stabiliser la morphologie BHJ ainsi que les couches intercalaires pour améliorer les interfaces et l'extraction de charge. Toutefois, lorsqu'ils sont utilisés dans la couche active, les dérivés de fullerène ont une tendance naturelle à l'auto-agrégation. Bien que cette tendance permette d'abord d'obtenir une bonne nanomorphologie du BHJ, la croissance des domaines avec le temps résulte dans la formation de clusters microscopiques qui inhibent la séparation de charge et le transfert de charge à l'intérieur de la couche active, et réduit ainsi la performance de la cellule solaire.

La fusion des propriétés électroniques de fullerène et l'aptitude au traitement mécanique de polymères, est pensé pour être une approche prometteuse pour minimiser cette tendance à l'autoagrégation et obtenir un bon mélange avec le polymère de type-p dans la couche photosensible. En particulier, les polyfullerènes à chaîne principale peuvent donner la possibilité d'un meilleur contrôle sur le contenu du fullerène et sa dispersion dans le mélange parce que les fullerènes sont présents dans les squelettes des polymères.

Dans ce travail, deux voies de polymérisation différentes ont été exploitées afin d'obtenir des oligo- et polyfullerènes avec une bonne solubilité dans les solvants organiques communs et avec de prometteuses propriétés photovoltaïques.

La première voie est basée sur la polymérisation ATRAP, ici utilisée avec PCBM comme monomère pour profiter de sa bonne solubilité. Cette voie, choisie car facile à implémenter, procure des matériaux oligo- et polyPCBM avec de bonnes solubilités. Le rapport entre les réactifs a été la même pour toutes les réactions (PCBM: bis-brome-comonomère: CuBr: bipyridine, 1: 1: 2: 4). La synthèse est simple mais très sensible aux impuretés. Les analyses de chromatographie SEC sur différents lots de matériaux suggèrent qu'un soin particulier à la manipulation de C₆₀ et PCBM par rapport à l'oxygène et à la lumière, aussi qu'un grand soin par rapport à la pré-nettoyage de CuBr sont nécessaires pour obtenir une réaction contrôlée.

En particulier, deux matériaux ont été étudiés. Le premier, polyPCBM_A, possède nature polymérique, tandis que polyPCBM_F, le second composé, a une nature oligomère. La différence entre les deux matériaux pourrait être attribuée à différentes échelles des réactions. Alors que polyPCBM_A a été préparé en utilisant 0,4 g de PCBM comme matériau de départ, polyPCBM_F a été obtenue à partir de la réaction de 3 g de PCBM avec une quantité équimolaire du comonomère. La température, la concentration, ainsi que le temps de réaction étaient les mêmes pour les deux réactions.

La structure et la nature des deux macromolécules, et la similitude étroite entre polyPCBM_F et PCBM ont été confirmés par les différentes techniques de caractérisation employées. De plus, il a été remarqué que le PCBM contribue au polyPCBM_A à hauteur de 3% alors que le pourcentage augmente considérablement à 35% en polyPCBM_F après purification dans un appareil Soxhlet avec acétone.

La seconde voie de polymérisation explorée dans ce travail est basée sur la chimie du fulleropyrrolidine (chimie de Prato), qui est ici exploité pour la première fois pour la synthèse de polyfullerènes à chaîne principale.

Trois co-monomères différents, à savoir 2,5-bis (octyloxy) et le téréphtaldéhyde, le 2,5-bis (dodécyloxy) téréphtaldéhyde, ont été utilisés dans les réactions pour étudier le rôle des substituants dans le procédé de polymérisation. Il a été trouvé que la polymérisation est très dépendante de l'encombrement stérique du comonomère. En particulier, alors que le petit téréphtaldéhyde donne des dérivés multi-substitués du fullerène, l'encombrement des comonomères avec des chaînes latérales alcoxy conduit à des oligo- et polyfullerènes.

La réaction est également sensible à la concentration et à la température. Malgré l'utilisation du même comonomère, des températures plus élevées (150 °C au lieu de 110 °C), et des concentrations plus élevées conduisent à des macromolécules de poids moléculaire supérieur. Des études cinétiques suggèrent que le processus de polymérisation se fait par trois régimes distincts dans le temps :

- A. une période d'induction, où la dissolution du C₆₀, la formation d'ylure ou les deux déterminent le taux de la réaction ;
- B. Une période où la polymérisation se déroule comme une typique polymérisation par étapes jusqu'à environ 10 h ;

C. une période où la polymérisation est limitée par la précipitation du produit.

Une comparaison des transitions électroniques calculées sur un composé représentatif avec le spectre UV-visible d'un des polymères a révélé que la corrélation la plus proche a été trouvée pour l'isomère *trans*-3. Le produit d'addition *trans*-2 a été détecté dans une plus petite quantité et s'est révélé bien moindre lorsque de plus grandes chaînes $-OC_{12}H_{25}$ sont utilisées dans le comonomère. Ceci corrobore l'idée que les plus grands comonomères forcent le contrôle stérique sur le produit. Un résultat inattendu est que les produits *trans*-4 et équatoriaux apparaissent limités.

Des analyses XPS et UPS ont été conduites sur les matériaux synthétisés, lesquels ont été déposés sur divers substrats. Dans notre cas, un abaissement du potentiel d'ionisation : une conséquence de la polymérisation est observée (6.03 eV pour le PCBM, 5.93 eV pour le PPC4 et 5.8 eV pour le PPC6). A l'interface avec le substrat PEI, des dipôles d'interface de 0,5 eV et 0,4 eV ont été observés pour PPC4 et PPC6, respectivement. La formation de ces dipôles indique épingleage des niveaux d'énergie à l'interface. Le niveau de *pinning* peut être relié au niveau ICT du polymère. Les valeurs pour E_{ICT} sont 4.0 eV pour le PPC4 et 3.9 eV pour le PPC6 et sont ainsi significativement inférieures à celle du PCBM.

Le PolyPCBM_F a été testé comme un accepteur alternatif au PCBM dans la couche active. Les poly(fulleropyrrolidines) ont été testés pour trois applications: (i) comme matériau accepteur d'électrons dans le mélange; (ii) comme couche intermédiaire entre la couche active et la couche d'extraction des électrons et; (iii) comme additif pour stabiliser la morphologie du mélange soumis à un stress thermique dans les cellules solaires.

Les résultats obtenus indiquent que les propriétés opto-électroniques et le transfert de charge de PCBM ne sont pas diminuées par la présence de polymère dans polyPCBM_F. Cependant, polyPCBM_F stabilise l'efficacité de l'appareil avec un T_{80} 10 fois plus grand que pour le contrôle quand les appareils sont exposés à un traitement thermique à 120 ° C dans la glovebox.

Une étude employant deux polymères à faible largeur de bande différents démontre que polyPCBM_F est effectivement applicable à de nombreux systèmes. Les résultats suggèrent également que le matériau requiert très probablement une optimisation spécifique à chaque polymère à faible largeur de bande afin d'améliorer la performance et la stabilité du dispositif.

L'introduction du PPC4 poly (fulleropyrrolidine) dans les dispositifs de CSO ne conduit pas à l'échec complet de la cellule solaire. Cependant, le matériau polymère n'est pas une bonne alternative au PCBM comme accepteur dans la couche active et il baisse la performance de l'appareil lorsqu'il est utilisé comme couche intermédiaire. L'application qui semble être la plus prometteuse est alors l'utilisation du polymère comme additif.

Des études de dégradation thermique accélérée sur des dispositifs intégrant PPC4 comme additif dans la couche active démontrent que le poly(fulleropyrrolidine) stabilise la performance des dispositifs avec le temps à des températures différentes (100, 120 et 140 ° C). Les spectres UV-visible et les images de microscopie optique de films minces recuits du mélange de la couche active, avec ou sans PPC4 comme additif, montrent comment les films restent stables lors du vieillissement thermique à la température choisie. Ceci suggère que PPC4 agit comme stabilisateur en affectant l'agrégation de PCBM dans le mélange. La stabilisation observée dans les performances des dispositifs CSO est donc susceptible d'être corrélée à la stabilisation de la morphologie de la couche active.

Des études comparatives utilisant des échantillons basés sur les systèmes P3HT: PCBM et KP115: PCBM (films et appareils) avec et sans PPC4 comme additif, démontrent que la capacité de stabilisation du poly(fulleropyrrolidine) dépend du choix du matériau donneur dans le mélange. En particulier, le PPC4 est clairement plus efficace lorsqu'il est utilisé dans des mélanges à base de KP115 plutôt que dans des mélanges à base de P3HT.

Enfin des observations au cours des études de dégradation des films, montrent que la qualité initial des films de la couche actif est un point clé pour la dégradation morphologique du système P3HT: PCBM lorsque l'additif poly(fulleropyrrolidine) (PPC4) est employé.

Des travaux supplémentaires afin de comprendre les mécanismes derrière les aptitudes de stabilisation des nouveaux matériaux pourront aider à l'insertion de ces derniers dans des dispositifs photovoltaïques organiques à l'échelle industrielle.

De plus, grâce à leur nature et la facilité des synthèses utilisées dans ce mémoire, il existe dans un futur proche une large place à l'amélioration quant au design des molécules.

Appendix A : Modelling and UV-visible characterisation

The work presented in this section was performed by Dr. Hugo Santos-Silva and are here reported in order to have a more complete description of the properties of the novel polyfullerenes obtained in this work.

Modelling was explored to determine: first, what UV-spectra might be expected the possible isomers; and second, identify the most preferred isomer formed by the reaction.

The eight known attack positions for bisadducts formation in Prato synthesis were studied by Time Dependent Density Functional Theory (TDDFT). The geometries were full optimized within the B3LYP/6-31G** level of theory. 20 UV-VIS electronic transitions were calculated using the same formalism. The electronic transitions were enveloped with Gaussian functions having 0.125 eV at FWHM and shifted to have their highest-intensity maximum coincident with the experimental spectra. The experimental spectra were treated to remove non-resonant backgrounds due to scattering. Theoretical spectra were shifted in order to have their highest-intensity maximum coincident with the one of the experimental spectra. This thereby made it possible to eliminate any energy parameter and avoid discussions on the method-induced errors to energies. For all the calculations, the RIJCOSX approximation was used and all the calculations run in Orca 3.0.2 software.[342] Results are shown in **Figure 189** and **Figure 190**.

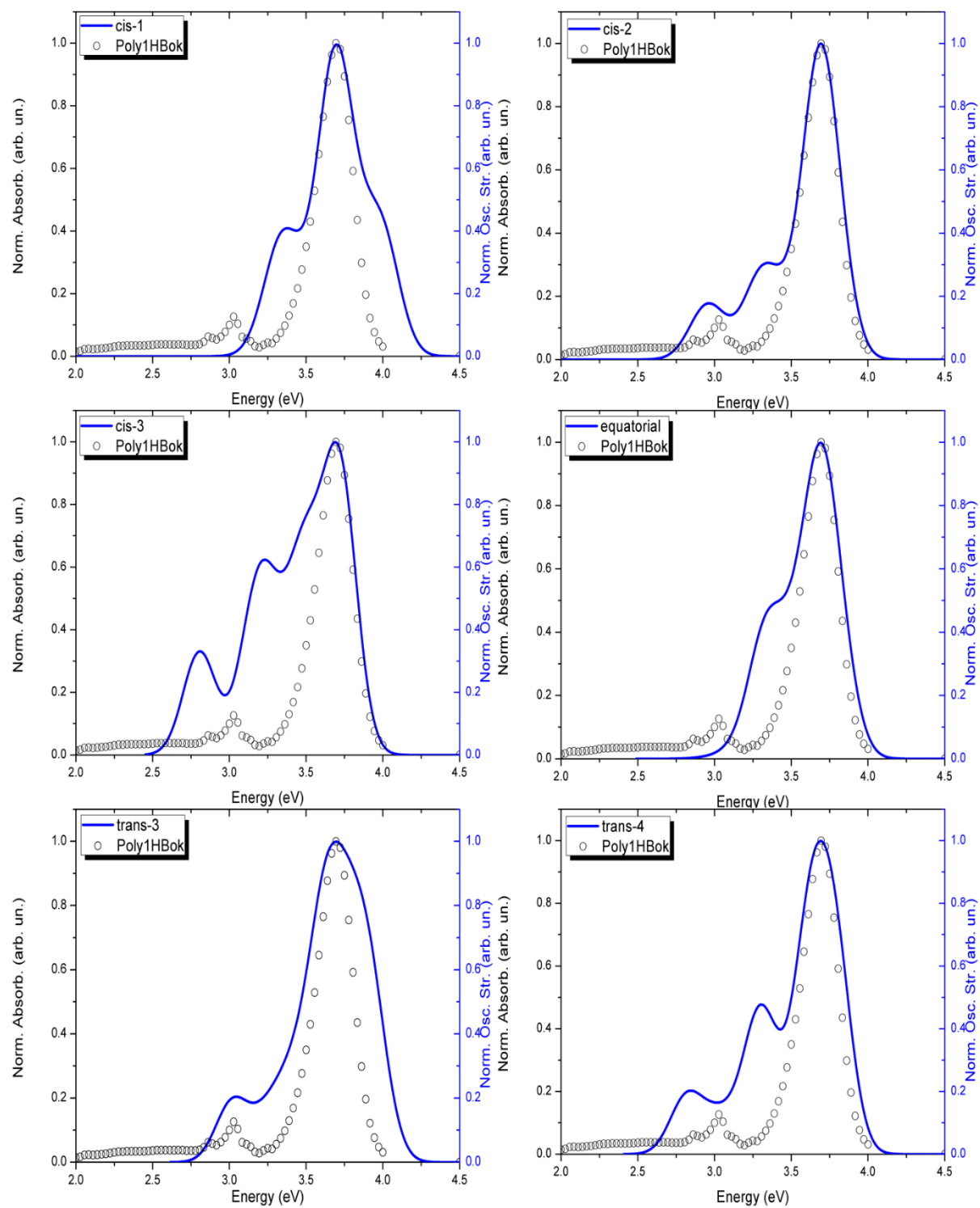


Figure 189: comparisons between the obtained spectra for the generic compound of **Figure 105a** and PPC1.

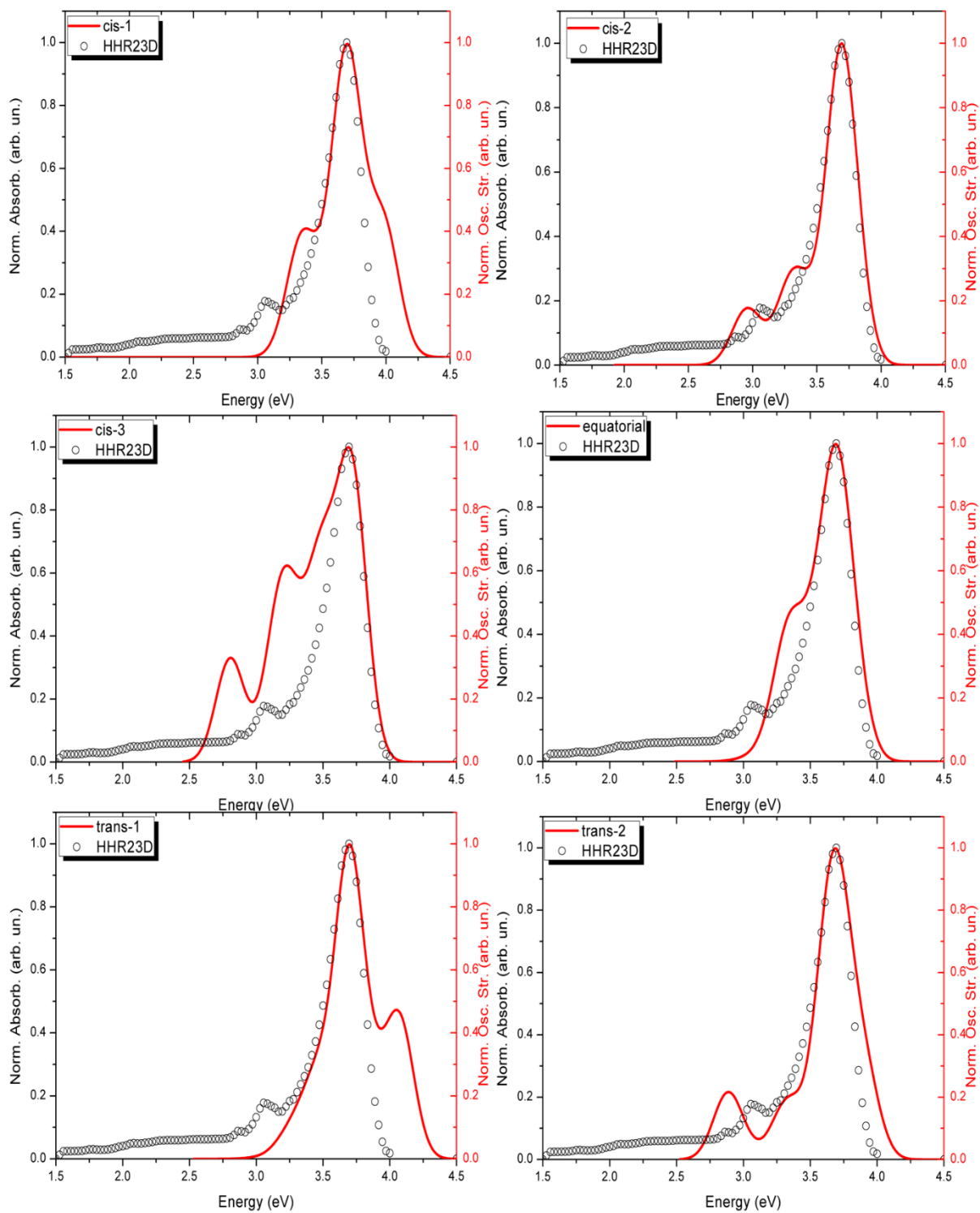


Figure 190: comparisons between the obtained spectra for the generic compound of **Figure 105a** and PPC3.

In an attempt to better understand the underlying process, the frontier molecular orbital-based mechanism of the 1,3-dipolar azomethine cycloaddition to C_{60} was considered. As a pericyclic reaction, Woodward-Hoffmann rules are followed and the frontier molecular orbitals of the 1,3-dipole and the dipolarophile overlap in allowed symmetry of $\pi^4s + \pi^2s$. Such orbital overlaps can be achieved in three ways: type I, II and III. The dominant pathway is the one which possesses the smallest HOMO-LUMO energy gap.[343] The C_{60} dipolarophile possesses a LUMO and therefore the orbital overlap occurs between the HOMO of the 1,3-dipole and the LUMO of the already modified C_{60} (i.e., C_{60} -mono-adduct). **Figure 192** shows the energy diagram in which the HOMO-LUMO gap for two possible configurations, indicated as blue and red, are 4.54 eV and only 0.43 eV, respectively. Thus any specific reaction site is not ruled out by the C_{60} HOMO but rather by its LUMO. Based on this analysis, and the information garnered from **Figure 191** showing frontier orbitals, it is clear that *equatorial* and *trans-1* bis-adducts are not favoured due to poor LUMO distributions. *Cis-1* and *cis-2* may occur but suffer from steric hindrance. *Cis-3* and *trans-4* may also occur but from TDDFT calculations are not apparent.

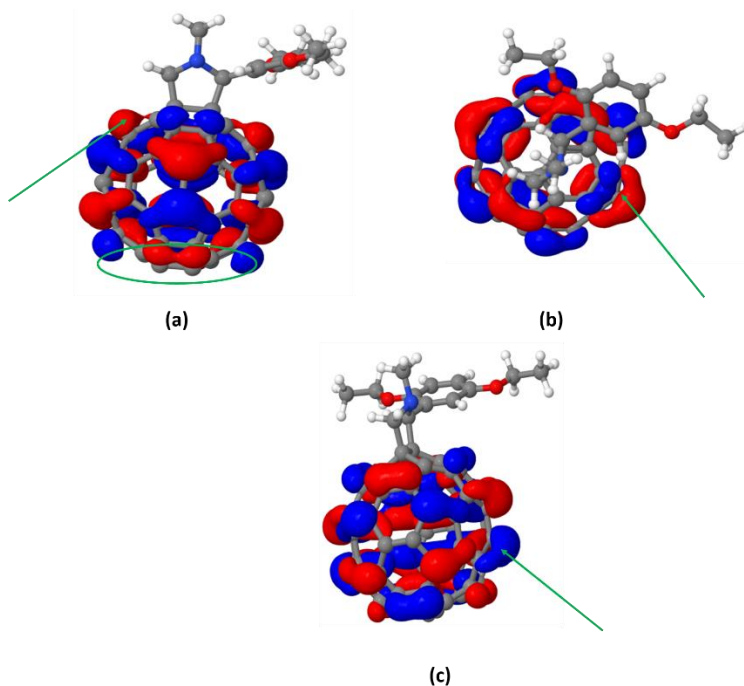


Figure 191: (a) The green arrow indicates the LUMO density of the lobe where the *cis-2* position is formed; and the circle on the bottom indicates the position where the *trans-1* structure would be formed. The LUMO density in this region is close to zero, which indicates that a linear symmetrically attacked C_{60} is not formed during the reaction. In (b) the green arrow indicates the same density where the following positions are formed: *cis-3*, *trans-3* and *trans-4*. This density is the most voluminous lobe on the LUMO of this molecule. In (c), this same lobe is indicated but we can also see the position of the *trans-2*, at the bottom.

In complete agreement with the above UV-visible work, *trans*-3 and *trans*-2 show the most favourable LUMO distributions, while the overall order found is *trans*-3 > *trans*-2 > *cis*-2 / *trans*-4 / *cis*-3 > *equatorial* / *trans*-1 >> *cis*-1. While these experiments were performed *in vacuo*, it is noted that 1,3-dipolarcycloadditions are only weakly solvent dependent. These results are not unfavourable in comparison with those of Kordatos *et al.*[287] although they found a greater presence of equatorial materials than we would expect, perhaps due to the different nature of their adduct.

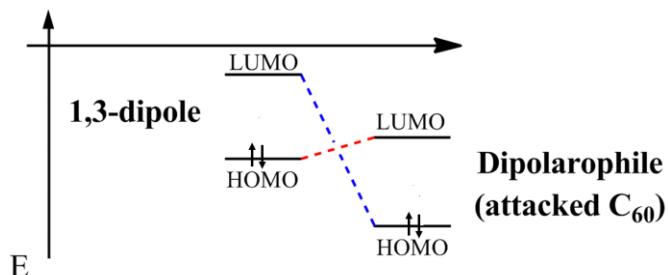


Figure 192: Energy diagram of the reaction between C_{60} and the 1,3-dipole azomethine.

Appendix B: UV-visible spectroscopy of P3HT:PCBM and P3HT:poly(fulleropyrrolidines)HHR63.

UV-visible spectroscopy have been performed on blends thin films of P3HT:PCBM and P3HT:poly(fulleropyrrolidines) HHR63. The films have been prepared using different P3HT/FULLERENE weight ratio, up to 1:4, from xylene with 5% vol 1-methylnaphthaline. The spectra are reported in **Figure 193**. A P3HT film has been used as a control.

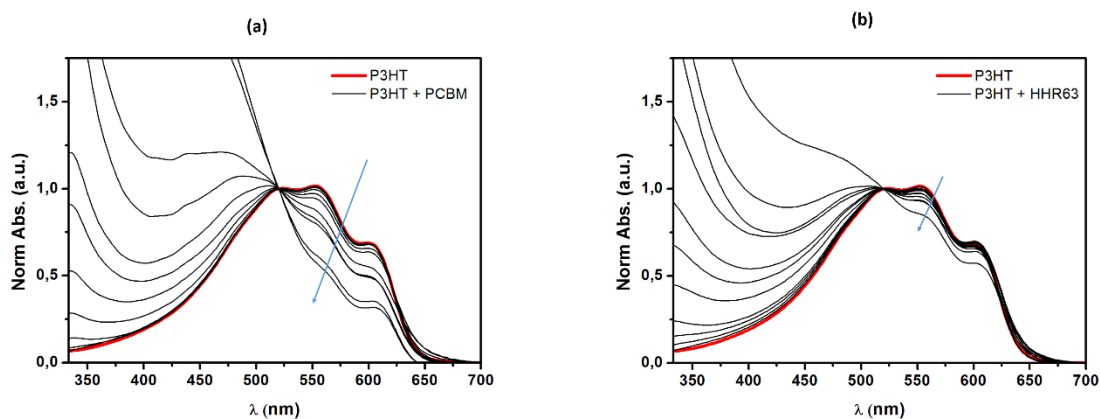


Figure 193: Normalized (to 520 nm) Absorption of blends up to 1:4 (P3HT:FULLERENE) by weight processed from xylene with 5%vol 1-Methylnaphthaline.

From the spectra it can be observed that the absorption profile of the P3HT:PCBM blends changes significantly as PCBM loading is increased. In contrast, only small deviation in shape (ratio) from the characteristic P3HT absorption peaks is observed when increasing loadings of HHR63 are added in the formulation. We attributed this lack of changing in the absorption as indicative of poor disruption of the P3HT phases. Possibly due to strong spinodal decomposition resulting in distinct phases and/or poor miscibility between the blend components.

Also photoluminescence measurements have been performed with increasing the loadings of HHR63 in the blends. As shown in **Figure 194**, the PL quenching of the films are lower respect to the correspondent PCBM-based sample and rises slowly at low concentrations. Moreover, a low quenching can be observed at high concentrations for this system. These again, would suggest a poor miscibility between the two components in the blend.

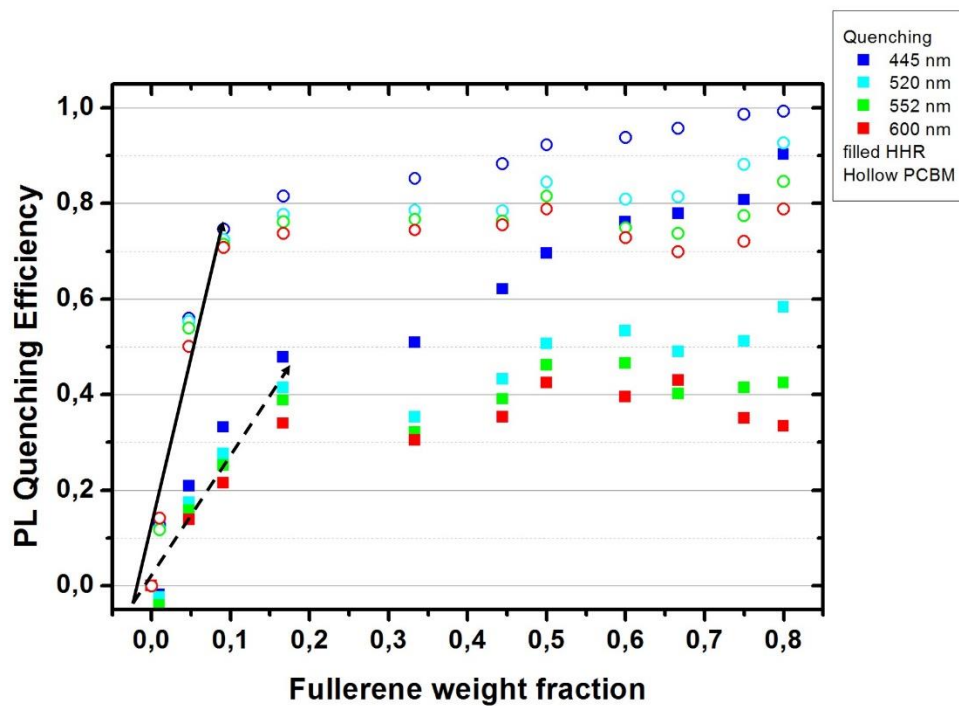


Figure 194: PL Quenching as a function of blend composition of P3HT:fullerene derivative processed from xylene with 5%vol 1-methylnaphthaline at different excitation wavelengths.

Appendix C: Summary

The photovoltaic technology (PV) allows to directly convert sunlight into electricity and it is seen as a very promising solution to the energy crisis. Although the PV market is currently dominated by inorganic-based devices, those systems present high production cost and environmental issues that limits their application. Polymer-based organic solar cells (OPVs) are promising sources of renewable energy due to their facile, low cost production, and formable nature. Due to its electronic properties and high electron mobility, small molecule fullerene C_{60} derivatives are widely used in large scale OPVs. However the morphological properties of C_{60} derivatives decrease device stability as C_{60} easily undergoes self-aggregation during OPV use. The processibility of C_{60} can be improved by incorporating it into a polymer. These systems are already described in literature but have in general a multistage synthesis that could affect the electronic properties of C_{60} as well as give insoluble products due to reticulation reaction.

This thesis is a part of the Region Aquitaine project FULLINC and the European Project ESTABLIS. The main objective of the project was to prepare innovative materials based on fullerene for photovoltaic and electronic devices using well-known and reliable routes.

The materials have been used in Establis' OPVs. ESTABLIS project has been created with the aim to provide different approaches to avoid organic solar cells performance loss caused by degradation over an extended period of time, see 10 to 15 years.

This thesis is a cotutelle between the Université de Pau et des Pays de l'Adour (UPPA), in France, and Eberhard Karls Universität Tübingen (EKTU), in Germany. A one-month secondment at Aston University, UK, to develop organic synthetic techniques has also been spent.

The thesis comprises five parts:

- (1) A general introduction to the scientific topics addressed in the dissertation.

In particular, a non-exhaustive review of the various classes of polyfullerenes is given in the last part of the first chapter. Moreover, the applications of polyfullerenes in organic photovoltaics are briefly discussed. Polyfullerenes are very versatile materials that remain relatively unexplored that can be potentially used in the OPV active layer as well as an interlayer to optimize the device interfaces and enhance the performances. Thanks to their polymeric natures, polyfullerenes are also good candidates for organic photovoltaics when the issue of stability is addressed. It is expected that all-polymers active layer can reach a better miscibility of the materials avoiding

the formation of macroscopic fullerene clusters with time. This effect is also expected in a ternary blend where, for example, a polyfullerene is mixed with donor:acceptor materials. However, in order to be used in industrial application, polyfullerenes must fulfill different requirements such as facile production, good solubility and easy processibility.

(2) A report on the synthesis of novel fullerene-based materials with discussions on the obtained results.

Preliminary studies to understand the effect of the reaction parameters (reagents, reagents concentration, temperature, time and solvent) and the kinetics of the polymerisation have been performed. Materials characterisation has been carried out via GPC chromatography, NMR spectroscopy, and UV-vis and IR spectroscopies. Thermal analyses (TGA and DSC) have also been ran to complete the characterisations.

In this work we present the synthesis of new classes of soluble main-chain polyfullerenes. The first type of materials are PCBM-based oligo- and poly-fullerenes synthesized using atom transfer addition polymerisation (ATRAP). This route, chosen because easy to implement, results in oligo- and polyPCBM materials with good solubility. The synthesis is facile but highly sensitive to impurities. SEC chromatography analysis on different batches of materials suggests that particular care with handling of C_{60} and PCBM with respect to oxygen and light, and great care with respect to the pre-cleaning of the CuBr are necessary to obtain a controlled reaction.

More details on the studies of two materials are reported. PolyPCBM_A, presents a polymeric nature, while polyPCBM_F, the second compounds, has an oligomeric nature. The difference in the two materials could be attributed to the different scale of the reactions while temperature, concentration, as well as time of reaction were the same for the two reactions. Different characterisation techniques show the close similarity between polyPCBM_F and PCBM. This was confirmed by the SEC analysis. Indeed, it has been noticed that PCBM contributes to polyPCBM_A to the extent of 3% while the percentage drastically increases to 35% in polyPCBM_F after purification in Soxhlet apparatus with acetone.

The second route of polymerisation employs C_{60} as monomer and yield to highly soluble main-chain polyfullerenes. This route is based on fulleropyrrolidine chemistry (Prato chemistry), which is, to our knowledge, exploited for the first time for the synthesis of main-chain polyfullerenes.

Three different co-monomers, namely terephthalaldehyde, 2,5-bis(octyloxy)terephthalaldehyde and, 2,5-bis(dodecyloxy)terephthalaldehyde, have been employed in the reactions to study the role of the substituents on the polymerisation process.

The polymerisation results highly dependent on the steric hindrance of the comonomer. In particular, while the small terephthalaldehyde results in a multi-substituted fullerene derivatives, the hindrance of the comonomers with longer side alkoxy-chain led to oligo- and polyfullerene.

Also concentration and temperature of reaction play a role in the polymerisation. In particular, despite the use of the same comonomer, higher temperature (150 °C instead of 110 °C), and higher concentration, led to higher molecular weight macromolecules.

Kinetic studies suggest that the polymerization process occurs through three distinct regimes with time:

- A. a period of induction, where C_{60} dissolution or glide formation or both are rate determining up to the 180th minute;
- B. a period where the polymerisation proceeds in accordance with a typical step growth reaction to around 10 h;
- C. a period where the polymerisation is limited by product precipitation.

Comparing the calculated electronic transitions for a representative compound with the UV-vis spectrum of one of the polymers, revealed that the closest correlation was found for the trans-3 isomer. Trans-2 adduct was detected in smaller amount in the mixture and resulted very much reduced when larger $-OC_{12}H_{25}$ chains are used in the comonomer. This corroborates the idea that the larger comonomer are enforcing steric control over the product.

XPS and UPS analysis have been conducted on the synthesized materials which have been deposited on various substrates. A lowering of the ionization potential as a consequence of the polymerization is observed (6.03 eV for PCBM, 5.93 eV for PPC4 and 5.8 eV for PPC6). At the interface to PEI substrate, interface dipoles of 0.5 eV and 0.4 eV were observed for PPC4 and PPC6, respectively, which suggest a pinning of the energy levels at the interface. The pinning level can be related to the ICT- level of the polymer. The value for E_{ICT-} is 4.0 eV (PPC4) and 3.9 eV (PPC6) and thus significantly lower compared to PCBM.

(3) A chapter reporting the applications of the synthesized materials into organic solar cells.

The study on the photovoltaic performance of representative synthesized oligo- and polyfullerene materials applied to devices is presented here. The material based on PCBM has been tested as an alternative acceptor in the active layer. The novel poly(fulleropyrrolidine) materials have been tested for three applications: (i) as electron acceptor material within the blend; (ii) as an interlayer between the active layer and the electron extraction layer and; (iii) as an additive to stabilize the morphology of the blend under thermal stress.

In particular polyPCBM_F has been tested as an alternative acceptor to PCBM in the active layer and the novel poly(fulleropyrrolidine) materials have been tested (i) as electron acceptor material within the blend; (ii) as an interlayer between the active layer and the electron extraction layer and; (iii) as an additive to stabilize the morphology of the blend under thermal stress in inverted structure geometry solar cells.

Opto-electronic and charge-transfer properties of PCBM are found to be not influenced by the presence of polymer in polyPCBM_F. On the other hand, polyPCBM_F stabilizes device efficiency with T_{80} being 10 times longer than for the control when the devices are exposed to thermal treatment at 120 °C in glovebox.

A study employing two different low band gap polymers demonstrate that polyPCBM_F is actually applicable to numerous systems. Results would also suggest that the material most likely requires an optimization specific to each partner low band gap polymer in order to improve device performance and stability.

The introduction of the poly(fulleropyrrolidine) PPC4 in OPV devices does not result in the complete failure of the solar cell. However, PPC4 is not a good alternative to PCBM as acceptor in the active layer and it worsens the device performance when used as an interlayer. A promising and attractive application of poly(fulleropyrrolidines) in OPV is their use as an additive in the photoactive layer.

(4) A chapter where thermal degradation study on active layer blends containing the novel materials is addressed.

The stability of the device is strongly related to the morphological stability of the active layer. A study addressing the morphological degradation of the blends, using accelerated degradation conditions and evaluations by UV-visible spectroscopy and optical microscopy have been

performed. The aim was to attempt to give a rationale for the good stabilising properties of the poly(fulleropyrrolidine)PPC4. The study has been carried on thin films of donor-acceptor blends in which the poly(fulleropyrrolidine) PPC4 has been employed as an additive as a 10% load (with respect to the PCBM content) in accordance to the devices. The three annealing temperatures, 100, 120 and 140 °C used in the case of the devices have been employed.

The thin films were prepared on glass substrates during a short visit at Belectric OPV and thermal degradation studies were conducted at Eberhard Karls Universität in Tübingen during the cotutelle secondment.

As expected, **PPC4** is found to stabilize the morphology of the film upon thermal treatment in the glovebox.

UV-visible spectroscopy and optical microscopy analyses suggest that **PPC4** acts as stabilizer in the blend affecting PCBM aggregation and thus, that the observed stabilization in the OPV performance of the devices is likely to be correlated to the stabilization of the morphology of the active layer. Two effects are observed in the recorded optical images. The first effect is on the size of the PCBM clusters. The second, is on the number of the aggregates. The size of the fullerene derivative clusters are smaller when **PPC4** is present in the blend and their number on the film surface is decreased.

The results corroborate the hypothesis that the polymer **PPC4** acts as an aggregation inhibitor due to its steric hindrance that does not allow the PCBM molecules to come in to close contact.

The stabilizing ability of the poly(fulleropyrrolidine) depends on the choice of the donor material in the blend. Films based on P3HT:PC₆₀BM (1:1) and KP115:PC₆₀BM (1:2) without (control sample) and with PPC4 as additive (10% of PC₆₀BM mass content) were investigated. Again, optical microscopy and UV-visible spectroscopy show that the poly(fulleropyrrolidine) acts as an efficient morphology stabilizer for the systems and in particular, the additive **PPC4**, is clearly more effective when employed in the KP115-based blends.

Finally, the quality of the BHJ active layer films is found to be a key point for the morphological degradation of the P3HT:PCBM blend when the poly(fulleropyrrolidine) additive (**PPC4**) is employed. During the accelerated degradation studies conducted during this work, we have noticed that film imperfections seem to lead the shape of the fullerene derivative clusters when PPC4 is used in P3HT:PCBM blends and when a high annealing temperature of 140 °C is used. This phenomenon is probably caused by the fact that defects represent a slight discontinuity in

the films where the intermixing of the three different materials in the blends are not optimized, and can thus act as nucleation seeds.

- (5) An experimental section where experimental protocols and conditions as well as experimental results are collected.

In this work, the synthesis of novel polyfullerenes have been presented. In particular, oligo- and polyPCBM prepared via ATRAP polymerisation, and poly(fulleropyrrolidine) prepared on the basis of Prato-chemistry have been presented. This latter route is exploited here for the first time to obtain main-chain polyfullerene.

The synthesized materials results attractive for photovoltaic application. The first type of materials, polyPCBMs, are interesting alternative to PCBM in the active layer of organic solar cell as they do not influence the initial performance of the devices, but improve the stabilization upon thermal stresses. The second kind of materials results very promising stabilizer for the active layer.

Further study to understand the mechanisms behind the stabilisation abilities of the novel material would help the insertion of these novel polyfullerenes in the industrial application for organic photovoltaic devices.

Moreover, due to the nature and the ease of the syntheses exploited in this thesis, great room of design development is possible in the near future.

Appendix D: Résumé détaillé

La technologie photovoltaïque (PV) permet de convertir directement la lumière du soleil en énergie électrique et elle semble être une solution très prometteuse à la crise de l'énergie. Bien que le marché du photovoltaïque soit actuellement dominé par des dispositifs à base de matériaux inorganiques, ces systèmes présentent un fort coût de production et soulèvent des questions environnementales qui limitent leurs applications. Les cellules solaires organiques à base de polymères (CSO) sont des sources prometteuses d'énergie renouvelable grâce à leur production facile et peu coûteuse ainsi qu'à leur nature malléable.

En raison des propriétés électroniques du C_{60} et de sa haute mobilité d'électrons, de petites molécules dérivées du fullerène sont largement utilisées dans les CSO à grande échelle. Cependant, les propriétés morphologiques des dérivés du C_{60} réduisent la stabilité des dispositifs. En effet, le C_{60} s'auto-agrège facilement lors de l'utilisation des CSO.

La processabilité du C_{60} peut néanmoins être améliorée en l'incorporant dans un polymère. De tels systèmes ont déjà été décrits dans la littérature mais ont en général une synthèse en plusieurs étapes qui pourrait autant affecter les propriétés électroniques du C_{60} que donner des produits insolubles à cause de la réaction de réticulation.

Cette thèse entre dans le cadre du projet de la région Aquitaine FULLINC et du projet européen ESTABLIS. L'objectif principal du projet FULLINC était de préparer des matériaux innovants basés sur le fullerène pour des dispositifs photovoltaïques et électroniques en utilisant des procédés fiables et bien connus. Ces matériaux ont été utilisés dans les cellules solaires organiques ESTABLIS. Ce projet a été créé dans le but d'apporter des approches différentes pour éviter les pertes de performance des cellules solaires organiques causées par leur dégradation sur une période de temps étendue, disons de 10 à 15 ans.

Cette thèse s'inscrit par ailleurs dans une cotutelle entre l'université de Pau et des Pays de l'Adour (UPPA) et l'université Eberhard Karls de Tübingen en Allemagne. Un séjour d'un mois à l'Université d'Aston au Royaume-Uni afin de développer des techniques de synthèse organique a également été effectué.

Le présent mémoire de thèse est divisé en cinq parties :

- (1) Une introduction générale des sujets scientifiques adressés dans ce mémoire.

En particulier, un état de l'art non-exhaustif des divers types de polyfullerène est donné dans la dernière partie de ce premier chapitre. De plus, les applications des polyfullerènes au photovoltaïque organique sont brièvement discutées.

Les polyfullerènes sont des matériaux versatiles qui restent relativement inexplorés mais qui peuvent potentiellement être aussi bien utilisés dans la couche active des CSO que dans l'intercouche afin d'optimiser les interfaces des dispositifs et augmenter leurs performances. Grâce à leur nature polymérique, les polyfullerènes sont également de bons candidats pour le photovoltaïque organique lorsqu'on se pose la question de la stabilité. Il est attendu qu'une couche active entièrement polymérique peut atteindre une meilleure miscibilité des matériaux évitant ainsi la formation avec le temps d'agglomérats macroscopiques de fullerènes. Cet effet est également attendu dans un mélange où par exemple, un polyfullerène est associé à des matériaux donneur/accepteur. Cependant afin d'être utilisés au niveau industriel, les polyfullerènes doivent satisfaire différents critères tels qu'une production et une processabilité faciles ou encore une bonne solubilité.

(2) Un rapport sur la synthèse de nouveaux matériaux à base de fullerènes et des discussions sur les résultats obtenus.

Des études préliminaires pour comprendre les effets des paramètres de réaction (les réactifs, leur concentration, la température, le temps et le solvant) et de la cinétique de polymérisation ont été effectuées. La caractérisation des matériaux a été menée via chromatographie GPC, spectroscopies NMR, UV-visible et IR. Des analyses thermiques (TGA et DSC) complètent ces caractérisations.

Dans ce travail, nous présentons la synthèse de nouvelles classes de polyfullerènes à chaîne principale solubles. Les premiers matériaux sont des oligo- et polyfullerène synthétisés en utilisant la polymérisation « atom transfer radical addition polymerisation » (ATRAP) avec PCBM. Ce procédé, choisi car aisé à mettre en place, donne des matériaux oligo- et polyPCBM possédant une bonne solubilité. La synthèse, certes facile, est cependant fortement sensible aux impuretés. L'analyse par chromatographie SEC sur les différents lots de matériaux suggère qu'une attention particulière en manipulant le C₆₀ et le PCBM en présence d'oxygène et de lumière et une extrême attention quant au nettoyage préalable du CuBr sont nécessaires pour obtenir une solution contrôlée.

Nous donnons également davantage de détails concernant deux matériaux : le polyPCBM_A et polyPCBM_F.

Le polyPCBM_A présente une nature polymérique tandis que le polyPCBM_F a une nature oligomérique. Cette différence entre les deux matériaux peut être attribuée à l'échelle différente des réactions bien que la température, la concentration et le temps de réaction soient les mêmes dans les deux cas.

Différentes méthodes de caractérisation montrent les similitudes entre polyPCBM_F et PCBM. Ceci a été confirmé par l'analyse SEC. En effet, nous avons noté la présence de 3% de PCBM dans le polyPCBM_A et ce pourcentage augmente drastiquement à hauteur de 35% pour le polyPCBM_F après purification dans l'appareil Soxhlet avec acétone.

Le second procédé de polymérisation emploie le C_{60} comme monomère et mène à des polyfullerènes à chaîne principale très solubles. Ce procédé est basé sur la chimie du fulleropyrrolidine (chimie de Prato) qui est, à notre connaissance, pour la première fois exploitée pour la synthèse de polyfullerènes à chaîne principale.

Trois comonomères différents, à savoir le terephthalaldehyde, le 2,5-bis(octyloxy)terephthalaldehyde et le 2,5-bis(dodecyloxy)terephthalaldehyde, ont été utilisés dans les réactions pour étudier les rôles des substituants dans le processus de polymérisation.

La polymérisation est fortement dépendante de l'encombrement stérique du comonomère. En particulier, tandis que le petit terphthalaldehyde donne des dérivés de fullerène multi-substitués, l'encombrement des comonomères ayant une plus grande chaîne latérale alcoxy mène à des oligo- et polyfullerènes.

Aussi, la concentration et la température de la réaction jouent un rôle dans la polymérisation. En particulier, malgré l'utilisation du même comonomère, une température plus importante (150 °C au lieu de 110 °C) et une plus forte concentration mènent à des macromolécules avec un plus grand poids moléculaires.

Les études cinétiques suggèrent que le processus de polymérisation se produit à travers trois périodes distinctes :

- A. Une période d'induction, où la dissolution du C_{60} et/ou la formation d'ylide déterminent la vitesse à partir de la 180^{ème} minute.
- B. Une période où la polymérisation se déroule comme une typique polymérisation par étapes jusqu'à environ 10 h.
- C. Une période à laquelle la polymérisation est limitée par la précipitation du produit.

Une comparaison des transitions électroniques calculées sur un composé représentatif avec le spectre UV-visible d'un des polymères a révélé que la corrélation la plus proche se situe au niveau de l'isomère *trans*-3. Le produit *trans*-2 a été détecté dans une plus petite quantité du mélange et s'est révélé bien moindre quand de plus grandes chaînes $-OC_{12}H_{25}$ sont utilisées dans le comonomère. Ceci corrobore l'idée que les plus grands comonomères forcent le contrôle stérique sur le produit.

Des analyses XPS et UPS ont été conduites sur les matériaux synthétisés, lesquels ont été déposés sur divers substrats. Nous observons une baisse du potentiel d'ionisation qui est une conséquence de la polymérisation (6.03 eV pour le PCBM, 5.93 eV pour le PPC4 et 5.8 eV pour le PPC6).

A l'interface du substrat PEI, nous avons observés des dipôles de 0.5 eV et 0.4 eV pour le PPC4 et PPC6 respectivement, ce qui suggère un pinning des niveaux d'énergie à l'interface. Le niveau de pinning peut être relié au niveau ICT du polymère. Les valeurs pour E_{ICT} sont 4.0 eV pour le PPC4 et 3.9 eV pour le PPC6 et sont ainsi significativement inférieures à celle du PCBM.

(3) Un chapitre rapportant les applications des matériaux synthétisés dans les cellules solaires organiques.

Une étude des performances photovoltaïques des oligo- et polyfullerènes représentatifs synthétisés est présentée dans ce chapitre. En particulier, le polyPCBM_F a été testé comme un accepteur alternatif au PCBM dans la couche active. Les nouveaux matériaux poly(fulleropyrrolidine) ont été testés pour trois applications :

- (i) Comme un matériau accepteur d'électrons dans le mélange ;
- (ii) Comme intercouche entre la couche active et la couche d'extraction d'électrons ;
- (iii) Comme additif pour stabiliser la morphologie du mélange soumis à un stress thermique dans les cellules solaires à l'architecture inversée.

D'une part, les propriétés de charge-transfert et optoélectroniques restent inchangées par la présence de polymères dans polyPCBM_F. D'autre part, quand le dispositif est exposé à un traitement thermique à 120 °C dans une glovebox, le polyPCBM_F stabilise l'efficacité de celui-ci avec un T_{80} dix fois plus long que celui du contrôle.

Une étude employant deux différents polymères à faible largeur de bande a démontré que le polyPCBM_F est en fait applicable à de nombreux systèmes. Les résultats suggèrent également que le matériau requiert très probablement une optimisation spécifique à chaque polymère à faible largeur de bande afin d'améliorer la performance et la stabilité du dispositif.

L'introduction de poly(fulleropyrrolidine) PPC4 dans des dispositifs CSO n'entraîne pas la défaillance totale des cellules solaires. Cependant, le PPC4 n'est pas une bonne alternative au PCBM en tant qu'accepteur dans la couche active. De plus, il abaisse la performance du dispositif lorsqu'il est utilisé comme intercouche. Une application prometteuse et intéressante des poly(fulleropyrrolidines) dans les CSO est leur utilisation comme additif dans la couche photoactive.

(4) Un chapitre où est menée une étude de dégradation thermique sur les mélanges des couches actives contenant les nouveaux matériaux.

La stabilité du dispositif est fortement liée à la stabilité morphologique de la couche active. Nous avons réalisé une étude concernant la dégradation morphologique des mélanges. Pour cela, nous avons imposé des conditions de dégradation accélérée aux différents mélanges. De plus, afin de justifier les bonnes propriétés des poly(fulleropyrrolidine) PPC4, nous avons effectués des mesures par spectroscopie UV-visible et microscopie optique. L'étude a été menée sur des films minces de mélanges donneur/accepteur dans lesquelles le poly(fulleropyrrolidine) PPC4 a été utilisé comme additif dans les dispositifs à hauteur de 10% (par rapport à la quantité de PCBM). Trois températures de recuit ont été testées : 100, 120, 140°C.

Les films minces ont été déposés sur du verre lors d'un court séjour à Belectric OPV. Aussi, les études de dégradation thermique ont été réalisées à l'université Eberhard Karls de Tübingen (Allemagne).

Comme attendu, le PPC4 stabilise la morphologie de la couche sous traitement thermique dans une glovebox.

Les analyses par spectroscopie UV-visible et microscopie optique suggèrent que le PPC4 agit comme stabilisateur dans le mélange affectant ainsi l'agrégation de PCBM. Ainsi, nous notons que la stabilisation observée de la performance OPV des dispositifs est probablement corrélée à la stabilisation de la morphologie de la couche active. En effet, nous observons deux effets notables sur les images optiques obtenues. Le premier repose sur la taille des agrégats de PCBM. Le second

concerne leur nombre. Ils sont plus petits quand il y a du PPC4 dans le mélange et leur nombre sur la surface de la couche diminue.

Les résultats corroborent l'hypothèse que le PPC4 agit comme un inhibiteur d'agrégation grâce à son encombrement stérique qui empêche les molécules de PCBM de s'approcher de trop près.

Le potentiel de stabilisation du poly(fulleropyrrolidine) dépend du choix du matériau accepteur dans le mélange. Des films minces basées sur le P3HT :PCBM(1:1) et KP115 :PCBM(1 :2) avec (échantillon témoin) et sans addition de PPC4 (10% de la masse de PCBM présente) ont été étudiées. Une nouvelle fois, la microscopie optique et la spectrographie UV-visible montre que le poly(fulleropyrrolidine) agit comme un stabilisateur de morphologie efficace pour la couche photoactive et en particulier, le PPC4 est clairement plus efficace lorsqu'il est utilisé comme additif dans des mélanges à base de KP115.

Enfin, la qualité des films de couche active à hétérojonction de masse est un point clé dans la dégradation morphologique du mélange de P3HT :PCBM quand le poly(fulleropyrrolidine) PPC4 est utilisé comme additif. Au cours des études de dégradation accélérée conduites dans ce mémoire, nous avons remarqué que les imperfections des films semblent dicter la forme des agrégats de dérivés de fullerène quand le PPC4 est utilisé dans les mélanges de P3HT :PCBM et quand une forte température de recuit est utilisée (140 °C). Ce phénomène est probablement dû au fait que des défauts peuvent entraîner de légères discontinuités sur les films là où l'association de trois différents matériaux dans le mélange n'est pas optimisée. Ces défauts peuvent alors agir comme des points de nucléation.

(5) Une partie expérimentale où les protocoles, les conditions et les résultats expérimentaux sont rassemblés.

En conclusion, dans ce mémoire, nous présentons des synthèses de nouveaux polyfullerènes, en particulier des oligo- et polyPCBM préparés par polymérisation ATRAP et des poly(fulleropyrrodine) préparés sur la base de la chimie de Prato.

Le premier type de matériaux est une bonne alternative au PCBM dans la couche active des cellules solaires organiques puisqu'ils n'affectent pas la performance initiale des dispositifs et ils améliorent la stabilisation lors de stress thermique.

Le second type de matériaux est, à notre connaissance, appliqué pour la première fois ici pour obtenir des polyfullerènes à chaîne principale. Nous avons montré dans ce mémoire qu'ils sont des stabilisateurs très prometteurs dans la couche active.

Des travaux supplémentaires afin de comprendre les mécanismes derrière les aptitudes de stabilisation des nouveaux matériaux pourront aider à l'insertion de ces derniers dans des dispositifs photovoltaïques organiques à l'échelle industrielle.

De plus, grâce à leur nature et la facilité des synthèses utilisées dans ce mémoire, il existe dans un futur proche une large place à l'amélioration quant au design des molécules.

Appendix E: Summary – German

Die Photovoltaik (PV) erlaubt die direkte Umwandlung von Sonnenlicht in Elektrizität, diese Technologie ist deshalb sehr vielversprechend für die Lösung der gegenwärtigen Energiekrise. Der PV Markt ist durch anorganische Solarzellen dominiert, obwohl hohe Produktionskosten und ein Aufwand für Entwicklungen die Anwendung dieser Systeme limitiert. Eine auf Polymeren basierte, organische Photovoltaik (OPV) zeichnet sich im Gegensatz dazu durch eine einfache und preiswerte Produktion, sowie durch hohe Flexibilität aus und stellt deshalb eine vielversprechende erneuerbare Energiequelle dar. Fulleren(C_{60})- Derivate sind aufgrund der elektronischen Eigenschaften und der hohen Mobilität für Elektronen in großflächigen OPV Anwendungen weit verbreitet. Die morphologischen Eigenschaften der Fulleren(C_{60})- Derivate führen jedoch zu einer Aggregation dieser Moleküle und somit zu einer geringen Stabilität der Bauelemente. Die Verarbeitbarkeit von C_{60} kann jedoch durch Einbindung in polymere Strukturen verbessert werden. Solche Verbindungen wurden bereits in der Literatur beschrieben, sie werden generell in einer mehrstufigen Synthese hergestellt, die die elektronischen Eigenschaften von C_{60} verändert und auch zu unlöslichen Produkten durch Vernetzungsreaktionen führen kann.

Diese Dissertation wurde gefördert durch ein Projekt der Region Aquitaine (FULLINC) und ein EU Projekt (ESTABLIS). Das Hauptziel des FULLINC Projektes war die Präparation innovativer Fulleren-basierter Materialien für photovoltaische und elektronische Bauelemente unter Anwendung bekannter und zuverlässiger Synthesewege.

Die Materialien wurden in OPV Bauelementen verwendet, die im Rahmen des Projektes ESTABLIS hergestellt wurden. Das Ziel des ESTABLIS Projektes war, unterschiedliche Lösungsansätze zu liefern um der Verlust der Performance von organischen Solarzellen durch Degradation innerhalb der ersten 10-15 Jahre zu vermeiden.

Die Doktorarbeit ist ein Cotutelle zwischen der Université de Pau et des Pays de l'Adour (UPPA), in Frankreich, und der Eberhard Karls Universität Tübingen (EKUT), in Deutschland. Zusätzlich wurde ein einmonatiger Forschungsaufenthalt an der Aston University, UK, durchgeführt, um organische Synthesetechniken zu entwickeln

Die Dissertation umfasst 5 Teile:

- (1) Allgemeine Einleitung zu wissenschaftlichen Themengebieten der Dissertation.

Insbesondere wird am Ende dieses Kapitels ein teilweiser Überblick über verschiedene Klassen von Polyfullerenen gegeben. Weiterhin werden Anwendungen von Polyfullerenen in der organischen Photovoltaik kurz diskutiert. Polyfullerene sind sehr vielseitige Materialien. Ihre potentielle Anwendung in OPV als aktive Schicht oder Zwischenschicht um Grenzflächen zu optimieren und die Performance zu erhöhen ist immer noch vergleichsweise wenig untersucht. Durch die polymere Struktur eignen sich Polyfullerene auch sehr gut für OPV, wenn die Stabilität der Bauelemente betrachtet wird. Es kann erwartet werden, dass aktive Schichten, die nur aus polymeren Materialien bestehen, eine bessere Mischbarkeit aufweisen da die nach einiger Zeit beobachtete Bildung von makroskopischen Fulleren Clustern vermieden wird. Dieser Effekt wird auch für eine ternäre Mischung erwartet, in welcher beispielsweise ein Polyfulleren mit Donor:Akzeptor Materialien gemischt wird. Für die industrielle Anwendung müssen Polyfullerene jedoch eine Anzahl von unterschiedlichen Voraussetzungen erfüllen, wie z. B. einfache Herstellung, gute Löslichkeit und leichte Verarbeitbarkeit.

(2) Beschreibung der Synthese von neuartigen Fulleren-basierten Materialien und Diskussion der Ergebnisse.

Vorbereitende Studien wurden durchgeführt, um Reaktionsparameter (Reagenzien und deren Konzentration, Temperatur, Lösungsmittel und Reaktionsdauer) und die Kinetik der Polymerisation zu verstehen. Die Reaktionsprodukte wurden mit Gel-Permeations-Chromatographie (GPC), NMR Spektroskopie sowie UV/vis und IR Spektroskopie charakterisiert. Zusätzlich wurden thermogravimetrische Analyse (TGA) und dynamische Differenzkalorimetrie (differential scanning calorimetry, DSC) angewandt.

In dieser Arbeit wird die Synthese von neuen Klassen löslicher Hauptketten-Polyfullerene vorgestellt. Die erste Serie von Materialien bilden PCBM-basierte Oligo- und Polyfullerene, die mit Hilfe der Atom Transfer Radical Additions polymerisation (ATRAP) synthetisiert wurden. Dieser Syntheseweg wurde gewählt, weil er einfach zu implementieren ist. Es wurden Oligo- und polyPCBM Verbindungen mit guter Löslichkeit erhalten. Die Synthese ist einfach, aber sehr empfindlich auf Verunreinigungen. Die SEC Chromatographie Analyse von verschiedenen Batches der Verbindungen legt nahe, dass bei der Arbeit mit C₆₀ and PCBM speziell auf Sauerstoff und Licht geachtet werden muss und insbesondere ist eine gründliche Vorreinigung von CuBr erforderlich um eine kontrollierte Reaktion zu erhalten

Zwei Materialien wurden detaillierter untersucht: PolyPCBM_A als polymere und polyPCBM_F als oligomere Verbindung. Der Unterschied der beiden Materialien kann dem unterschiedlichen

Ausmaß der Reaktion zugeschrieben werden, während Temperatur, Konzentration, und Reaktionszeit für die zwei Reaktionen gleich waren. Verschiedene Charakterisierungsmethoden zeigen eine deutliche Ähnlichkeit von polyPCBM_F und PCBM. Das wurde auch durch die SEC Analyse bestätigt. Es muss angemerkt werden, dass polyPCBM_A etwa 3% PCBM enthält, während der PCBM sich deutlich auf 35% erhöht in polyPCBM_F nach Reinigung in einer Soxhlet Apparatur mit Aceton.

In der zweiten Polymerisationsroute wird C_{60} als Monomer verwendet; es werden sehr gut lösliche Hauptketten-Polyfullerene erhalten. Dieser Weg basiert auf der Fulleropyrrolidine Chemie (Prato chemistry), welche nach unserem Wissen erstmalig zur Synthese von Hauptketten-Polyfullerenen angewandt wird. Drei verschieden Comonomere (Terephthaldehyd, 2,5-bis(octyloxy)terephthaldehyd and, 2,5-bis(dodecyloxy)terephthaldehyd) wurden in den Reaktionen verwendet um die Rolle der Substituenten in den Reaktionen zu untersuchen. Die Polymerisation ist stark beeinflusst von der sterischen Hinderung des Comonomers. Während der kleine Terephthaldehyd Substituent zu mehrfach-substituten Fullerene Derivaten führt, werden durch die Hinderung von Comonomeren mit längeren Seitenketten Oligo- und Polyfullerene erhalten.

Die Konzentration und Temperatur der Reaktion beeinflusst ebenfalls die Polymerisationsreaktion. Speziell führt eine höhere Temperatur (150 °C anstelle 110 °C) und eine höhere Konzentration bei gleichem Comonomer zu Makromolekülen mit höherem Molekulargewicht.

Kinetische Untersuchungen legen nahe, dass der Polymerisationsprozess in drei zeitlich getrennte Phasen unterteilt werden kann:

- A. Eine Periode der Vorbereitung, in welcher die C_{60} Auflösung oder Produktbildung (oder beides) geschwindigkeitsbestimmend ist, bis etwa 180 min.
- B. Eine Periode, in welcher die Polymerisation stattfindet verbunden mit einer typischen stufenweisen Reaktion bis zu etwa 10 h.
- C. Eine Periode, in welcher Polymerisation begrenzt wird durch die Fällung des Produktes.

Der Vergleich der berechneten elektronischen Übergänge für eine repräsentative Verbindung mit dem UV-vis Spektrum des Polymers zeigt, dass die beste Übereinstimmung für das trans-3 Isomer erhalten wird. Das Trans-2 Addukt wurde in geringer Menge im Gemisch nachgewiesen, die Menge war stark reduziert, wenn größere $-OC_{12}H_{25}$ im Comonomer vorhanden waren. Das

bestätigt die Vermutung, dass das Comonomer mit größeren Seitenketten eine sterische Kontrolle über das Produkt erzwingt.

XPS und UPS Untersuchungen wurden an den synthetisierten Materialien durchgeführt, diese wurden dazu auf einer Auswahl an verschiedenen Substraten aufgebracht. Es wurde eine Verringerung des Ionisationspotentials als Folge der Polymerisation beobachtet (6.03 eV für PCBM, 5.93 eV für PPC4 und 5.8 eV für PPC6). An der Grenzfläche zu einem Substrat mit niedriger Austrittsarbeit wurden Grenzflächendipole für PPC4 und PPC6 beobachtet (0.5 eV bzw. 0.4 eV), welche ein Pinning der Energieniveaus an der Grenzfläche suggerieren. Das Pinning-Niveau kann im Rahmen des „integer charge transfer“ Modells als sogenanntes ICT- Niveau interpretiert werden. Der Wert von E_{ICT} ist 4.0 eV (PPC4) und 3.9 eV (PPC6) und somit deutlich geringer im Vergleich zu PCBM.

(3) Kapitel: Anwendungen der synthetisierten Materialien in organischen Solarzellen.

Hier wird die Untersuchung der photovoltaischen Performance von repräsentativen Oligo- und Polyfullerenen in Bauelementen behandelt. Die PCBM-basierten Materialien als ein alternativer Elektronenakzeptor getestet. Die neuartigen Poly(fulleropyrrolidine) wurde für drei unterschiedliche Anwendungen getestet: (i) als Elektronenakzeptor in der aktiven Schicht (Blend); (ii) als Zwischenschicht zwischen der Aktiven Schicht und der elektronenleitenden Schicht, und (iii) als Additive in dem Blend-Material, um die Morphologie unter thermischem Stress zu stabilisieren.

Es wurde gezeigt, dass sowohl opto-electronische als auch den Ladungstransfer betreffende Eigenschaften des PCBM nicht durch die Anwesenheit von polyPCBM_F beeinflusst werden. Andererseits stabilisiert polyPCBM_F die Effizienz der Bauelemente, der sogenannte T_{80} Wert ist zehnfach länger im Vergleich zu einer Kontrollprobe, wenn die Bauelemente thermisch bei 120 °C in einer Glovebox behandelt werden.

Die Studien mit zwei verschiedenen low-band-gap Polymeren zeigen, dass polyPCBM_F in einer Vielzahl von Systemen eingesetzt werden kann. Die Resultate legen auch nahe, dass die Materialien höchstwahrscheinlich optimiert werden müssen, spezifisch für das jeweilige low band gap Polymer, um die Performance und Stabilität der Bauelemente zu verbessern.

Die Einbindung des poly(fulleropyrrolidine) PPC4 in OPV Bauelemente hatte nicht den vollständigen Ausfall des Bauelementes zu Folge. Es zeigte sich jedoch, dass PPC4 keine gute Alternative zu PCBM als Akzeptor in der aktiven Schicht ist und außerdem verschlechtert sich die

Performance, wenn es als Zwischenschicht verwendet wird. Eine vielversprechende und attraktive OPV-Anwendung der poly(fulleropyrrolidines) ist dagegen die Nutzung als Additiv in der photo-aktiven Schicht.

(4) Kapitel: Thermische Degradation der aktiven Schicht mit neuartigen Polyfullerenen

Die Stabilität der Bauelemente ist stark verbunden mit der morphologischen Stabilität der aktiven Schicht (Blend). Es wurden Untersuchungen mittels UV/vis Spektroskopie und optischer Mikroskopie durchgeführt, die die morphologische Degradation der Blends unter Verwendung von beschleunigten Degradationsbedingungen adressieren. Das Ziel war die Untersuchung der Ursachen für die guten stabilisierenden Eigenschaften des poly(fulleropyrrolidines) PPC4. Die Studien wurden an dünnen Donor/Akzeptorfilmen (Blends) durchgeführt, welche poly(fulleropyrrolidines) PPC4 als ein Additiv enthalten (10% bezüglich PCBM – in Übereinstimmung mit den untersuchten Bauelementen). Die Proben wurden auf drei Temperaturen geheizt (100, 120 und 140 °C), ebenfalls in Analogie zu den Bauelementen.

Die dünnen Schichten wurden während eines Kurzaufenthaltes bei der BELECTRIC OPV GmbH auf Glassubstrate aufgebracht, die Studien zur thermischen Degradation wurden an der Eberhard-Karls-Universität Tübingen im Rahmen des Co-tutelle Aufenthaltes durchgeführt.

Wie erwartet wurde gefunden, dass **PPC4** die Morphologie während der thermischen Behandlung in der Glovebox stabilisiert.

Die Analyse mit UV/vis Spektroskopie und optischer Mikroskopie legen nahe, dass **PPC4** als Stabilisator in der Blend wirkt indem es die Aggregation von PCBM beeinflusst. Das bedeutet auch, dass die beobachtete Stabilisierung der OPV Performance vermutlich verbunden ist mit der Stabilisierung der Morphologie der aktiven Schicht. Zwei Effekte sind aus den optischen Bildern erkennbar. Der erste Effekt bezieht sich auf die Größe der PCBM Cluster, der zweite auf die Anzahl der Aggregate. Die Größe der Cluster der Fulleren- Derivate ist kleiner, wenn **PPC4** in der Blend vorhanden ist und deren Anzahl auf der Schichtoberfläche ist reduziert.

Die Ergebnisse bestätigen die Hypothese, dass das Polymer **PPC4** aufgrund der sterischen Hinderung als ein Aggregationshemmer wirkt, welche den engeren Kontakt von PCBM Molekülen verhindert.

Die Fähigkeit zur Stabilisierung der poly(fulleropyrrolidines) hängt von der Wahl der Donorkomponente im Blend ab. Filme bestehend aus P3HT:PC₆₀BM (1:1) und KP115:PC₆₀BM

(1:2) ohne (Kontrollprobe) und mit PPC4 als Additiv (10% Masse% bezüglich PC₆₀BM) wurden untersucht. Optische Mikroskopie und UV/vis Spektroskopie zeigen wiederum, dass das poly(fulleropyrrolidine) als sein effektiver Morphologiestabilisator für diese Systeme wirkt. Das Additiv **PPC4** ist jedoch deutlich effektiver in Verbindung mit KP115-basierten Blends.

Schließlich wird gezeigt, dass die Qualität der aktiven Schicht in BHJ Solarzellen eine Schlüsselrolle in der morphologischen Degradation der P3HT:PCBM Blend darstellt; sie kann erhöht werden, wenn poly(fulleropyrrolidine) (**PPC4**) als Additiv zugefügt wird. Während der beschleunigten Degradationsstudien, die in dieser Arbeit durchgeführt wurden, haben wir bemerkt, dass scheinbar Unregelmäßigkeiten in der Schicht die Form der Cluster der Fulleren-Derivate beeinflussen wenn PPC4 als Additiv in P3HT:PCBM Blends verwendet wird und wenn hohe Temperaturen von 140 °C eingesetzt werden. Dieses Phänomen kann vermutlich dadurch verstanden werden, dass Defekte kleinere Diskontinuitäten darstellen in welchen die Durchmischung der drei Materialien nicht optimal ist – diese können somit wie Nukleationsstellen wirken.

(5) Experimenteller Abschnitt, in welchem experimentelle Protokolle und Bedingungen sowie auch experimentelle Resultate zusammengefasst sind.

In dieser Arbeit wurde die Synthese neuartiger Polyfullerene vorgestellt. Genauer wurden Oligo- and polyPCBM über die ATRAP Polymerisation dargestellt, und poly(fulleropyrrolidine) wurde synthetisiert auf Grundlage der "Prato-Chemie". Der letztere Syntheseweg hier erstmalig angewandt, um Hauptketten-Polyfullerene herzustellen.

Die synthetisierten Materialien sind vielversprechend für photovoltaische Anwendungen. Die erste Serie von Materialien, polyPCBMs, sind interessant als Alternative für PCBM in der aktiven Schicht der Solarzelle, da sie nicht die anfängliche Performance der Bauelemente beeinflussen und gleichzeitig die Stabilität gegen thermisches Stress verbessern. Die zweite Serie von Materialien erscheint als sehr aussichtsreich als Stabilisator für die aktive Schicht.

Weitere Untersuchungen zum Verständnis des Mechanismus, der der Fähigkeit zur Stabilisierung dieser neuartigen Materialien zugrunde liegt, würden den industriellen Einsatz dieser neuartigen Polyfullerene in organischen photovoltaischen Bauelementen unterstützen.

Darüber hinaus, aufgrund der Natur und der Einfachheit der in dieser Arbeit angewandten Synthesen, besteht ein weiter Raum für mögliche Entwicklungen in naher Zukunft.

Bibliography

- 1 C. Piskoti, J. Yarger and A. Zettl, *Nature*, 1998, **393**, 771–774.
- 2 H. W. Kroto, J. R. Heath, S. C. O'Brien, R. F. Curl and R. E. Smalley, *Nature*, 1985, **318**, 162–163.
- 3 W. Krätschmer, L. D. Lamb, K. Fostiropoulos and D. R. Huffman, *Nature*, 1990, **347**, 354–358.
- 4 Y.-Y. Lai, Y.-J. Cheng and C. S. Hsu, *Energy & Environmental Science*, 2014.
- 5 R. Bakry, R. M. Vallant, M. Najam-ul-Haq, M. Rainer, Z. Szabo, C. W. Huck and G. K. Bonn, *International journal of nanomedicine*, 2007, **2**, 639.
- 6 P. P. Shanbogh and N. G. Sundaram, *Resonance*, 2015.
- 7 H. Kroto, *Nature*, 1987, **329**, 529–531.
- 8 W. I. David, R. M. Ibberson, J. C. Matthewman, K. Prassides, T. J. S. Dennis, J. P. Hare, H. W. Kroto, R. Taylor and D. R. Walton, *Nature*, 1991, **353**, 147–149.
- 9 W. A. Scrivens and J. M. Tour, *J. Chem. Soc., Chem. Commun.*, 1993, 1207–1209.
- 10 R. Haddon, *Science*, 1993, **261**, 1545–1550.
- 11 R. S. Ruoff, D. S. Tse, R. Malhotra and D. C. Lorents, *The Journal of Physical Chemistry*, 1993, **97**, 3379–3383.
- 12 W. A. Scrivens and J. M. Tour, *Journal of the Chemical Society, Chemical Communications*, 1993, 1207.
- 13 M. T. Beck and G. Mándi, *Fullerenes, Nanotubes, and Carbon Nanostructures*, 1997, **5**, 291–310.
- 14 X. Zhou, J. Liu, Z. Jin, Z. Gu, Y. Wu and Y. Sun, *Fullerenes, Nanotubes, and Carbon Nanostructures*, 1997, **5**, 285–290.
- 15 R. Taylor and D. R. M. Walton, *Nature*, 1993, **363**, 685–693.
- 16 M. Prato, *J. Mater. Chem.*, 1997, **7**, 1097–1109.
- 17 X. Lu, L. Feng, T. Akasaka and S. Nagase, *Chemical Society Reviews*, 2012, **41**, 7723.
- 18 A. A. Popov, S. Yang and L. Dunsch, *Chem. Rev.*, 2013, **113**, 5989–6113.
- 19 F. Diederich, L. Isaacs and D. Philp, *Chemical Society Reviews*, 1994, **23**, 243–255.
- 20 R. Caballero, P. De La Cruz and F. Langa, *ChemInform*, 2012, **43**.
- 21 C. Bingel, *Chemische Berichte*, 1993, **126**, 1957–1959.
- 22 N. Camaioni, G. Fabbrini, E. Menna, M. Maggini, G. Ridolfi and A. Zanelli, *New Journal of Chemistry*, 2006, **30**, 335.
- 23 J. López-Andarias, A. Bolag, C. Nançoz, E. Vauthey, C. Atienza, N. Sakai, N. Martín and S. Matile, *Chem. Commun.*, 2015, **51**, 7543–7545.
- 24 S. H. Friedman, D. L. DeCamp, R. P. Sijbesma, G. Srdanov, F. Wudl and G. L. Kenyon, *Journal of the American Chemical Society*, 1993, **115**, 6506–6509.

- 25 S. Marchesan, T. Da Ros, G. Spalluto, J. Balzarini and M. Prato, *Bioorganic & Medicinal Chemistry Letters*, 2005, **15**, 3615–3618.
- 26 R. Kessinger, J. Crassous, A. Herrmann, M. Rüttimann, L. Echegoyen and F. Diederich, *Angewandte Chemie International Edition*, 1998, **37**, 1919–1922.
- 27 N. N. P. Moonen, C. Thilgen, F. Diederich and L. Echegoyen, *Chemical Communications*, 2000, 335–336.
- 28 R. Kessinger, N. S. Fender, L. E. Echegoyen, C. Thilgen, L. Echegoyen and F. Diederich, *Chem. Eur. J.*, 2000, **6**, 2184–2192.
- 29 P. Hudhomme, *Comptes Rendus Chimie*, 2006, **9**, 881–891.
- 30 V. M. Rotello, J. B. Howard, T. Yadav, M. M. Conn, E. Viani, L. M. Giovane and A. L. Lafleur, *Tetrahedron Letters*, 1993, **34**, 1561–1562.
- 31 J. K. Lee, Y.-M. Wang, S. Cho, F. Wudl and A. J. Heeger, *Organic Electronics*, 2009, **10**, 1223–1227.
- 32 U. M. Fernández-Paniagua, B. Illescas, N. Martín, C. Seoane, P. de la Cruz, A. de la Hoz and F. Langa, *The Journal of Organic Chemistry*, 1997, **62**, 3705–3710.
- 33 L. Lu, S. S. Yang, Z. Wang, R. G. Cooks and M. N. Eberlin, *Journal of Mass Spectrometry*, 1995, **30**, 581–594.
- 34 M. Maggini, G. Scorrano and M. Prato, *Journal of the American Chemical Society*, 1993, **115**, 9798–9799.
- 35 M. Prato and M. Maggini, *Accounts of chemical research*, 1998, **31**, 519–526.
- 36 N. Martín, M. Altable, S. Filippone, A. Martín-Domenech, L. Echegoyen and C. M. Cardona, *Angewandte Chemie*, 2006, **118**, 116–120.
- 37 S. Filippone, M. I. Barroso, Á. Martín-Domenech, S. Osuna, M. Solà and N. Martín, *Chemistry - A European Journal*, 2008, **14**, 5198–5206.
- 38 O. Lukoyanova, C. M. Cardona, M. Altable, S. Filippone, Á. Martín Domenech, N. Martín and L. Echegoyen, *Angewandte Chemie International Edition*, 2006, **45**, 7430–7433.
- 39 A. Hirsch, *Hirsch - 1999 - Principles of Fullerene Reactivity.pdf*, 1999.
- 40 P. J. Krusic, E. Wasserman, P. N. Keizer, J. R. Morton and K. F. Preston, *Science*, 1991, **254**, 1183–1185.
- 41 M. D. Tzirakis and M. Orfanopoulos, *Chem. Rev.*, 2013, **113**, 5262–5321.
- 42 G. P. Miller, *Comptes Rendus Chimie*, 2006, **9**, 952–959.
- 43 E. B. Zeynalov, N. S. Allen and N. I. Salmanova, *Polymer Degradation and Stability*, 2009, **94**, 1183–1189.
- 44 E. R. Badamshina and M. P. Gafurova, *Polymer Science Series B*, 2008, **50**, 215–225.
- 45 L. A. Shibaev, T. A. Antonova, L. V. Vinogradova, B. M. Ginzburg, V. G. Ginzburg, V. N. Zgonnik and E. Y. Melenevskaya, *Technical Physics Letters*, 1997, **23**, 730–731.
- 46 Z. Markovic and V. Trajkovic, *Biomaterials*, 2008, **29**, 3561–3573.
- 47 H. Shinohara, *Sci. Rep. RITU*, 1997, 47.
- 48 X. Lu, T. Akasaka and S. Nagase, *Chemical Communications*, 2011, **47**, 5942.

- 49 T. Wakahara, H. Nikawa, T. Kikuchi, T. Nakahodo, G. M. A. Rahman, T. Tsuchiya, Y. Maeda, T. Akasaka, K. Yoza, E. Horn, K. Yamamoto, N. Mizorogi, Z. Slanina and S. Nagase, *Journal of the American Chemical Society*, 2006, **128**, 14228–14229.
- 50 M. M. Olmstead, A. de Bettencourt-Dias, S. Stevenson, H. C. Dorn and A. L. Balch, *Journal of the American Chemical Society*, 2002, **124**, 4172–4173.
- 51 B. Cao, H. Nikawa, T. Nakahodo, T. Tsuchiya, Y. Maeda, T. Akasaka, H. Sawa, Z. Slanina, N. Mizorogi and S. Nagase, *Journal of the American Chemical Society*, 2008, **130**, 983–989.
- 52 C. M. Beavers, H. Jin, H. Yang, Z. Wang, X. Wang, H. Ge, Z. Liu, B. Q. Mercado, M. M. Olmstead and A. L. Balch, *Journal of the American Chemical Society*, 2011, **133**, 15338–15341.
- 53 E. N. Karaulova and E. I. Bagrii, *Russian Chemical Reviews*, 1999, **68**, 889.
- 54 Z. Ge, J. C. Duchamp, T. Cai, H. W. Gibson and H. C. Dorn, *Journal of the American Chemical Society*, 2005, **127**, 16292–16298.
- 55 S. Stevenson, K. Harich, H. Yu, R. R. Stephen, D. Heaps, C. Coumbe and J. P. Phillips, *Journal of the American Chemical Society*, 2006, **128**, 8829–8835.
- 56 R. B. Ross, C. M. Cardona, D. M. Guldi, S. G. Sankaranarayanan, M. O. Reese, N. Kopidakis, J. Peet, B. Walker, G. C. Bazan, E. Van Keuren, B. C. Holloway and M. Drees, *Nat Mater*, 2009, **8**, 208–212.
- 57 R. B. Ross, C. M. Cardona, F. B. Swain, D. M. Guldi, S. G. Sankaranarayanan, E. Van Keuren, B. C. Holloway and M. Drees, *Advanced Functional Materials*, 2009, **19**, 2332–2337.
- 58 A. Becquerel, *Comptes Rendus de L'Académie des Sciences*, 1839, **9**, 145–149.
- 59 A. Pochettino and A. Sella, *Acad. Lincei Rend*, 1906, **15**, 355–363.
- 60 G. A. Chamberlain, *Solar Cells*, 1983, **8**, 47–83.
- 61 D. M. Chapin, C. S. Fuller and G. L. Pearson, *Journal of Applied Physics*, 1954, **25**, 676.
- 62 *efficiency_chart.jpg (Image PNG, 4190 × 2456 pixels) - Redimensionnée (19%), .*
- 63 B. O'Regan and M. Grätzel, *Nature*, 1991, **353**, 737–740.
- 64 M. Grätzel, *Nature*, 2001, **414**, 338–344.
- 65 F. Dimroth and S. Kurtz, *MRS bulletin*, 2007, **32**, 230–235.
- 66
- 67 C. J. Brabec, *Solar Energy Materials and Solar Cells*, 2004, **83**, 273–292.
- 68 J.-L. Brédas, J. E. Norton, J. Cornil and V. Coropceanu, *Accounts of Chemical Research*, 2009, **42**, 1691–1699.
- 69 V. Coropceanu, J. Cornil, D. A. da Silva Filho, Y. Olivier, R. Silbey and J.-L. Brédas, *Chemical Reviews*, 2007, **107**, 926–952.
- 70 H. Hoppe and N. S. Sariciftci, *Journal of Materials Research*, 2011, **19**, 1924–1945.
- 71 C. W. Tang, *Applied Physics Letters*, 1986, **48**, 183.
- 72 G. Yu, K. Pakbaz and A. J. Heeger, *Applied Physics Letters*, 1994, **64**, 3422.
- 73 Y. Şahin, S. Alem, R. de Bettignies and J.-M. Nunzi, *Thin Solid Films*, 2005, **476**, 340–343.
- 74 <http://optics.org/news/4/1/36>.

- 75 P. K. Watkins, A. B. Walker and G. L. B. Verschoor, *Nano Letters*, 2005, **5**, 1814–1818.
- 76 S. Günes, H. Neugebauer and N. S. Sariciftci, *Chemical Reviews*, 2007, **107**, 1324–1338.
- 77 T. L. Benanti and D. Venkataraman, *Photosynthesis Research*, 2006, **87**, 73–81.
- 78 S. Rajaram, P. B. Armstrong, B. J. Kim and J. M. J. Fréchet, *Chemistry of Materials*, 2009, **21**, 1775–1777.
- 79 P. Heremans, D. Cheyns and B. P. Rand, *Accounts of Chemical Research*, 2009, **42**, 1740–1747.
- 80 B. Ray, P. R. Nair and M. A. Alam, *Solar Energy Materials and Solar Cells*, 2011, **95**, 3287–3294.
- 81 Z. Yi, W. Ni, Q. Zhang, M. Li, B. Kan, X. Wan and Y. Chen, *Journal of Materials Chemistry C*, 2014, **2**, 7247.
- 82 M. A. Ruderer, S. Guo, R. Meier, H.-Y. Chiang, V. Körstgens, J. Wiedersich, J. Perlich, S. V. Roth and P. Müller-Buschbaum, *Advanced Functional Materials*, 2011, **21**, 3382–3391.
- 83 B. J. Kim, Y. Miyamoto, B. Ma and J. M. J. Fréchet, *Advanced Functional Materials*, 2009, **19**, 2273–2281.
- 84 S. Miyanishi, K. Tajima and K. Hashimoto, *Macromolecules*, 2009, **42**, 1610–1618.
- 85 K. M. Coakley, Y. Liu, M. D. McGehee, K. L. Frindell and G. D. Stucky, *Advanced Functional Materials*, 2003, **13**, 301–306.
- 86 K. M. Coakley and M. D. McGehee, *Applied Physics Letters*, 2003, **83**, 3380.
- 87 H. Wu, J. Yang, S. Cao, L. Huang and L. Chen, *Macromolecular Chemistry and Physics*, 2014, **215**, 584–596.
- 88 P. D. Topham, A. J. Parnell and R. C. Hiorns, *Journal of Polymer Science Part B: Polymer Physics*, 2011, **49**, 1131–1156.
- 89 J. Wang and T. Higashihara, *Polymer Chemistry*, 2013, **4**, 5518.
- 90 K. Nakabayashi and H. Mori, *Materials*, 2014, **7**, 3274–3290.
- 91 A. M. Ramos, M. T. Rispens, J. K. J. van Duren, J. C. Hummelen and R. A. J. Janssen, *Journal of the American Chemical Society*, 2001, **123**, 6714–6715.
- 92 A. Cravino, *Polymer International*, 2007, **56**, 943–956.
- 93 B. Kippelen and J.-L. Brédas, *Energy & Environmental Science*, 2009, **2**, 251.
- 94 M. C. Scharber, D. Mühlbacher, M. Koppe, P. Denk, C. Waldauf, A. J. Heeger and C. J. Brabec, *Advanced Materials*, 2006, **18**, 789–794.
- 95 P. M. Sommeling, H. C. Rieffe, J. A. M. van Roosmalen, A. Schönecker, J. M. Kroon, J. A. Wienke and A. Hinsch, *Solar Energy Materials and Solar Cells*, 2000, **62**, 399–410.
- 96 V. Shrotriya, G. Li, Y. Yao, T. Moriarty, K. Emery and Y. Yang, *Adv. Funct. Mater.*, 2006, **16**, 2016–2023.
- 97 H. Cao, W. He, Y. Mao, X. Lin, K. Ishikawa, J. H. Dickerson and W. P. Hess, *Journal of Power Sources*, 2014, **264**, 168–183.
- 98 M. Jørgensen, K. Norrman and F. C. Krebs, *Solar Energy Materials and Solar Cells*, 2008, **92**, 686–714.

- 99 H. Habuchi, S. Nitta, D. Han and S. Nonomura, *Journal of Applied Physics*, 2000, **87**, 8580.
- 100 H. Ishii and K. Seki, *Electron Devices, IEEE Transactions on*, 1997, **44**, 1295–1301.
- 101 M. T. Lloyd, D. C. Olson, P. Lu, E. Fang, D. L. Moore, M. S. White, M. O. Reese, D. S. Ginley and J. W. P. Hsu, *Journal of Materials Chemistry*, 2009, **19**, 7638.
- 102 S. Chambon, A. Rivaton, J.-L. Gardette, M. Firon and L. Lutsen, *Journal of Polymer Science Part A: Polymer Chemistry*, 2007, **45**, 317–331.
- 103 K. Norrman, J. Alstrup, M. Jørgensen and F. C. Krebs, *Surface and Interface Analysis*, 2006, **38**, 1302–1310.
- 104 C. C. Eloi, D. J. Robertson, A. M. Rao, P. Zhou, K. A. Wang and P. C. Eklund, *Journal of materials research*, 1993, **8**, 3085–3089.
- 105 K. Norrman, N. B. Larsen and F. C. Krebs, *Solar Energy Materials and Solar Cells*, 2006, **90**, 2793–2814.
- 106 E. Voroshazi, B. Verreet, A. Buri, R. Müller, D. Di Nuzzo and P. Heremans, *Organic Electronics*, 2011, **12**, 736–744.
- 107 H. Cao and K. Ishikawa, *Solar Energy Materials and Solar Cells*, 2013, **109**, 215–219.
- 108 T. Tromholt, A. Manor, E. A. Katz and F. C. Krebs, *Nanotechnology*, 2011, **22**, 225401.
- 109 E. A. Katz, S. Gevorgyan, M. S. Orynbayev and F. C. Krebs, *The European Physical Journal Applied Physics*, 2006, **36**, 307–311.
- 110 M. Hermenau, S. Schubert, H. Klumbies, J. Fahlteich, L. Müller-Meskamp, K. Leo and M. Riede, *Solar Energy Materials and Solar Cells*, 2012, **97**, 102–108.
- 111 C. L. Chochos, N. Tagmatarchis and V. G. Gregoriou, *RSC Advances*, 2013, **3**, 7160.
- 112 P.-L. T. Boudreaault, A. Najari and M. Leclerc, *Chemistry of Materials*, 2011, **23**, 456–469.
- 113 X. Sun, Y. Zhou, W. Wu, Y. Liu, W. Tian, G. Yu, W. Qiu, S. Chen and D. Zhu, *The Journal of Physical Chemistry B*, 2006, **110**, 7702–7707.
- 114 H. Shang, H. Fan, Y. Liu, W. Hu, Y. Li and X. Zhan, *Advanced Materials*, 2011, **23**, 1554–1557.
- 115 D. Demeter, T. Rousseau and J. Roncali, *RSC Adv.*, 2013, **3**, 704–707.
- 116 A. B. Tamayo, M. Tantiwiwat, B. Walker and T.-Q. Nguyen, *The Journal of Physical Chemistry C*, 2008, **112**, 15543–15552.
- 117 L. Xue, J. He, X. Gu, Z. Yang, B. Xu and W. Tian, *The Journal of Physical Chemistry C*, 2009, **113**, 12911–12917.
- 118 V. Steinmann, N. M. Kronenberg, M. R. Lenze, S. M. Graf, D. Hertel, H. Bürckstümmer, F. Würthner and K. Meerholz, *Applied Physics Letters*, 2011, **99**, 193306.
- 119 K. N. Winzenberg, P. Kemppinen, G. Fanchini, M. Bown, G. E. Collis, C. M. Forsyth, K. Hegedus, T. B. Singh and S. E. Watkins, *Chemistry of Materials*, 2009, **21**, 5701–5703.
- 120 J. Mei, K. R. Graham, R. Stalder and J. R. Reynolds, *Organic Letters*, 2010, **12**, 660–663.
- 121 C. K. Chiang, C. R. Fincher Jr, Y. W. Park, A. J. Heeger, H. Shirakawa, E. J. Louis, S. C. Gau and A. G. MacDiarmid, *Physical Review Letters*, 1977, **39**, 1098.

- 122 J. Burroughes, D. Bradley, A. Brown, R. Marks, K. Mackay, R. Friend, P. Burns and A. Holmes, *nature*, 1990, **347**, 539–541.
- 123 M. M. Alam and S. A. Jenekhe, *Chemistry of Materials*, 2002, **14**, 4775–4780.
- 124 A. J. Heeger, .
- 125 S. E. Shaheen, C. J. Brabec, N. S. Sariciftci, F. Padinger, T. Fromherz and J. C. Hummelen, *Applied Physics Letters*, 2001, **78**, 841.
- 126 C. J. Brabec, S. E. Shaheen, C. Winder, N. S. Sariciftci and P. Denk, *Applied Physics Letters*, 2002, **80**, 1288.
- 127 C. Melzer, E. J. Koop, V. D. Mihailetschi and P. W. M. Blom, *Advanced Functional Materials*, 2004, **14**, 865–870.
- 128 E. Bundgaard and F. Krebs, *Solar Energy Materials and Solar Cells*, 2007, **91**, 954–985.
- 129 J. Nelson, *Current Opinion in Solid State and Materials Science*, 2002, **6**, 87–95.
- 130 H. Neugebauer, C. Kvarnström, C. Brabec, N. S. Sariciftci, R. Kiebooms, F. Wudl and S. Luzzati, *The Journal of chemical physics*, 1999, **110**, 12108–12115.
- 131 C. J. Brabec, C. Winder, N. S. Sariciftci, J. C. Hummelen, A. Dhanabalan, P. A. van Hal and R. A. Janssen, *Advanced Functional Materials*, 2002, **12**, 709–712.
- 132 http://www.pv-magazine.com/news/details/beitrag/organic-polymer-tandem-cell-reaches-record-115-efficiency_100015832/#axzz3jfljOp89.
- 133 A. J. Heeger, *Chemical Society Reviews*, 2010, **39**, 2354.
- 134 B. Tieke, A. R. Rabindranath, K. Zhang and Y. Zhu, *Beilstein Journal of Organic Chemistry*, 2010, **6**, 830–845.
- 135 J. E. Anthony, A. Facchetti, M. Heeney, S. R. Marder and X. Zhan, *Advanced Materials*, 2010, **22**, 3876–3892.
- 136 H. Murata, Z. H. Kafafi and M. Uchida, *Applied Physics Letters*, 2002, **80**, 189.
- 137 J. E. Anthony, *Angewandte Chemie International Edition*, 2008, **47**, 452–483.
- 138 B. A. Jones, A. Facchetti, T. J. Marks and M. R. Wasielewski, *Chemistry of Materials*, 2007, **19**, 2703–2705.
- 139 Z. Wang, C. Kim, A. Facchetti and T. J. Marks, *Journal of the American Chemical Society*, 2007, **129**, 13362–13363.
- 140 S. Ando, J. Nishida, E. Fujiwara, H. Tada, Y. Inoue, S. Tokito and Y. Yamashita, *Chemistry of Materials*, 2005, **17**, 1261–1264.
- 141 B. P. Karsten, J. C. Bijleveld and R. A. J. Janssen, *Macromolecular Rapid Communications*, 2010, **31**, 1554–1559.
- 142 P. Sonar, S. P. Singh, Y. Li, M. S. Soh and A. Dodabalapur, *Advanced Materials*, 2010, **22**, 5409–5413.
- 143 C. R. McNeill, *Energy & Environmental Science*, 2012, **5**, 5653.
- 144 E. Zhou, J. Cong, Q. Wei, K. Tajima, C. Yang and K. Hashimoto, *Angewandte Chemie International Edition*, 2011, **50**, 2799–2803.

- 145 T. W. Holcombe, J. E. Norton, J. Rivnay, C. H. Woo, L. Goris, C. Piliago, G. Griffini, A. Sellinger, J.-L. Brédas, A. Salleo and J. M. J. Fréchet, *Journal of the American Chemical Society*, 2011, **133**, 12106–12114.
- 146 D. Mori, H. Benten, H. Ohkita, S. Ito and K. Miyake, *ACS Applied Materials & Interfaces*, 2012, **4**, 3325–3329.
- 147 Y. Zhou, Q. Yan, Y.-Q. Zheng, J.-Y. Wang, D. Zhao and J. Pei, *Journal of Materials Chemistry A*, 2013, **1**, 6609.
- 148 T. Earmme, Y.-J. Hwang, S. Subramaniyan and S. A. Jenekhe, *Advanced Materials*, 2014, **26**, 6080–6085.
- 149 Y. Zhou, T. Kurosawa, W. Ma, Y. Guo, L. Fang, K. Vandewal, Y. Diao, C. Wang, Q. Yan, J. Reinspach, J. Mei, A. L. Appleton, G. I. Koleilat, Y. Gao, S. C. B. Mannsfeld, A. Salleo, H. Ade, D. Zhao and Z. Bao, *Advanced Materials*, 2014, **26**, 3767–3772.
- 150 K. D. Deshmukh, T. Qin, J. K. Gallaher, A. C. Y. Liu, E. Gann, K. O'Donnell, L. Thomsen, J. M. Hodgkiss, S. E. Watkins and C. R. McNeill, *Energy Environ. Sci.*, 2015, **8**, 332–342.
- 151 A. Facchetti, *Materials Today*, 2013, **16**, 123–132.
- 152 Y.-J. Hwang, B. A. E. Courtright, A. S. Ferreira, S. H. Tolbert and S. A. Jenekhe, *Advanced Materials*, 2015, **27**, 4578–4584.
- 153 A. Facchetti, *Materials Today*, 2013, **16**, 123–132.
- 154 G. Moretti, *Journal of electron spectroscopy and related phenomena*, 1998, **95**, 95–144.
- 155 H. Peisert, D. Kolacyak and T. Chassé, *The Journal of Physical Chemistry C*, 2009, **113**, 19244–19250.
- 156 S. Braun, W. R. Salaneck and M. Fahlman, *Advanced Materials*, 2009, **21**, 1450–1472.
- 157 M. Knapfer and H. Peisert, *physica status solidi (a)*, 2004, **201**, 1055–1074.
- 158 H. Vázquez, F. Flores and A. Kahn, *Organic Electronics*, 2007, **8**, 241–248.
- 159 J. Hwang, A. Wan and A. Kahn, *Materials Science and Engineering: R: Reports*, 2009, **64**, 1–31.
- 160 U. Aygül, H. Peisert, J. Frisch, A. Vollmer, N. Koch and T. Chassé, *ChemPhysChem*, 2011, **12**, 2345–2351.
- 161 M. Oehzelt, N. Koch and G. Heimel, *Nature Communications*, 2014, **5**.
- 162 M. Fahlman, P. Sehati, W. Osikowicz, S. Braun, M. P. de Jong and G. Brocks, *Journal of Electron Spectroscopy and Related Phenomena*, 2013, **190**, 33–41.
- 163 Q. Bao, O. Sandberg, D. Dagnelund, S. Sandén, S. Braun, H. Aarnio, X. Liu, W. M. Chen, R. Österbacka and M. Fahlman, *Advanced Functional Materials*, 2014, **24**, 6309–6316.
- 164 D. Çakir, M. Bokdam, M. P. de Jong, M. Fahlman and G. Brocks, *Applied Physics Letters*, 2012, **100**, 203302.
- 165 M. Fahlman, P. Sehati, W. Osikowicz, S. Braun, M. P. de Jong and G. Brocks, *Journal of Electron Spectroscopy and Related Phenomena*, 2013, **190**, 33–41.
- 166 J. C. Hummelen, B. W. Knight, F. LePeq, F. Wudl, J. Yao and C. L. Wilkins, *The Journal of Organic Chemistry*, 1995, **60**, 532–538.

- 167 B. Kraabel, J. C. Hummelen, D. Vacar, D. Moses, N. S. Sariciftci, A. J. Heeger and F. Wudl, *The Journal of chemical physics*, 1996, **104**, 4267–4273.
- 168 G. Yu, J. Gao, J. C. Hummelen, F. Wudl and A. J. Heeger, *Science-AAAS-Weekly Paper Edition*, 1995, **270**, 1789–1790.
- 169 R. Pacios, J. Nelson, D. D. C. Bradley and C. J. Brabec, *Applied Physics Letters*, 2003, **83**, 4764.
- 170 L. J. A. Koster, V. D. Mihailetschi and P. W. M. Blom, *Applied Physics Letters*, 2006, **88**, 093511.
- 171 F. B. Kooistra, J. Knol, F. Kastenberg, L. M. Popescu, W. J. H. Verhees, J. M. Kroon and J. C. Hummelen, *Organic Letters*, 2007, **9**, 551–554.
- 172 L. Echegoyen and L. E. Echegoyen, *Accounts of chemical research*, 1998, **31**, 593–601.
- 173 Y. He, H.-Y. Chen, J. Hou and Y. Li, *Journal of the American Chemical Society*, 2010, **132**, 1377–1382.
- 174 Y. He and Y. Li, *Physical Chemistry Chemical Physics*, 2011, **13**, 1970.
- 175 D. Mi, J.-H. Kim, H. U. Kim, F. Xu and D.-H. Hwang, *Journal of Nanoscience and Nanotechnology*, 2014, **14**, 1064–1084.
- 176 A. J. Ferguson, J. L. Blackburn and N. Kopidakis, *Materials Letters*, 2013, **90**, 115–125.
- 177 L. Zheng, Q. Zhou, X. Deng, M. Yuan, G. Yu and Y. Cao, *The Journal of Physical Chemistry B*, 2004, **108**, 11921–11926.
- 178 L. M. Popescu, P. van 't Hof, A. B. Sieval, H. T. Jonkman and J. C. Hummelen, *Applied Physics Letters*, 2006, **89**, 213507.
- 179 M. M. Wienk, J. M. Kroon, W. J. Verhees, J. Knol, J. C. Hummelen, P. A. van Hal and R. A. Janssen, *Angewandte Chemie*, 2003, **115**, 3493–3497.
- 180 B. A. Collins, Z. Li, J. R. Tumbleston, E. Gann, C. R. McNeill and H. Ade, *Adv. Energy Mater.*, 2013, **3**, 65–74.
- 181 Y. Yao, C. Shi, G. Li, V. Shrotriya, Q. Pei and Y. Yang, *Applied Physics Letters*, 2006, **89**, 153507.
- 182 Y.-Y. Lai, Y.-J. Cheng and C.-S. Hsu, *Energy & Environmental Science*, 2014, **7**, 1866.
- 183 G. Wantz, L. Derue, O. Dautel, A. Rivaton, P. Hudhomme and C. Dagron-Lartigau, *Polymer International*, 2014, **63**, 1346–1361.
- 184 Q. Tai, J. Li, Z. Liu, Z. Sun, X. Zhao and F. Yan, *Journal of Materials Chemistry*, 2011, **21**, 6848.
- 185 J. A. Moore, S. Ali and B. C. Berry, *Solar Energy Materials and Solar Cells*, 2013, **118**, 96–101.
- 186 B. C. Schroeder, Z. Li, M. A. Brady, G. C. Faria, R. S. Ashraf, C. J. Takacs, J. S. Cowart, D. T. Duong, K. H. Chiu, C.-H. Tan, J. T. Cabral, A. Salleo, M. L. Chabinyc, J. R. Durrant and I. McCulloch, *Angewandte Chemie International Edition*, 2014, **53**, 12870–12875.
- 187 C. Melzer, E. J. Koop, V. D. Mihailetschi and P. W. M. Blom, *Advanced Functional Materials*, 2004, **14**, 865–870.
- 188 S. M. Tuladhar, D. Poplavskyy, S. A. Choulis, J. R. Durrant, D. D. C. Bradley and J. Nelson, *Advanced Functional Materials*, 2005, **15**, 1171–1182.

- 189 T. Zhuang, X.-F. Wang, T. Sano, Z. Hong, Y. Yang and J. Kido, *Applied Physics Letters*, 2013, **103**, 203301.
- 190 Y. Ie, M. Karakawa, S. Jinnai, H. Yoshida, A. Saeki, S. Seki, S. Yamamoto, H. Ohkita and Y. Aso, *Chem. Commun.*, 2014, **50**, 4123–4125.
- 191 Y. Ie, K. Nishida, M. Karakawa, H. Tada, A. Asano, A. Saeki, S. Seki and Y. Aso, *Chemistry - A European Journal*, 2011, **17**, 4750–4758.
- 192 T. Zhuang, X.-F. Wang, T. Sano, Z. Hong, G. Li, Y. Yang and J. Kido, *Applied Physics Letters*, 2014, **105**, 093301.
- 193 J. L. Yang, P. Sullivan, S. Schumann, I. Hancox and T. S. Jones, *Applied Physics Letters*, 2012, **100**, 023307.
- 194 M. Kubo, K. Iketaki, T. Kaji and M. Hiramoto, *Applied Physics Letters*, 2011, **98**, 073311.
- 195 M. Kubo, T. Kaji and M. Hiramoto, *AIP Advances*, 2011, **1**, 032177.
- 196 G. A. Olah, I. Bucsi, C. Lambert, R. Aniszfeld, N. J. Trivedi, D. K. Sensharma and G. K. S. Prakash, *J. Am. Chem. Soc.*, 1991, **113**, 9387–9388.
- 197 E. Cloutet, J.-L. Fillaut, Y. Gnanou and D. Astruc, *J. Chem. Soc., Chem. Commun.*, 1994, 2433–2434.
- 198 M. Fedurco, D. A. Costa, A. L. Balch and W. R. Fawcett, *Angew. Chem. Int. Ed. Engl.*, 1995, **34**, 194–196.
- 199 X. Chen, B. Gholamkhash, X. Han, G. Vamvounis and S. Holdcroft, *Macromol. Rapid Commun.*, 2007, **28**, 1792–1797.
- 200 M. Nanjo, P. W. Cyr, K. Liu, E. H. Sargent and I. Manners, *Advanced Functional Materials*, 2008, **18**, 470–477.
- 201 Q.-D. Ling, S.-L. Lim, Y. Song, C.-X. Zhu, D. S.-H. Chan, E.-T. Kang and K.-G. Neoh, *Langmuir*, 2007, **23**, 312–319.
- 202 A. Rao, P. Zhou, K.-A. Wang, G. Hager, J. Holden, Y. Wang, W.-T. Lee, X.-X. Bi, P. Ecklund and D. Cornett, *Science*, 1993, **259**, 955–957.
- 203 M. Nunez-Regueiro, L. Marques, J.-L. Hodeau, O. Béthoux and M. Perroux, *Physical review letters*, 1995, **74**, 278.
- 204 F. Giacalone and N. Martín, *Chemical Reviews*, 2006, **106**, 5136–5190.
- 205 H. Nagashima, A. Nakaoka, Y. Saito, M. Kato, T. Kawanishi and K. Itoh, *Journal of the Chemical Society, Chemical Communications*, 1992, 377–379.
- 206 M. Drees, H. Hoppe, C. Winder, H. Neugebauer, N. S. Sariciftci, W. Schwinger, F. Schäffler, C. Topf, M. C. Scharber, Z. Zhu and R. Gaudiana, *Journal of Materials Chemistry*, 2005, **15**, 5158.
- 207 Y.-J. Cheng, C.-H. Hsieh, P.-J. Li and C.-S. Hsu, *Advanced Functional Materials*, 2011, **21**, 1723–1732.
- 208 F. GIACALONE, .
- 209 H. W. Goh, S. H. Goh and G. Q. Xu, *Journal of Polymer Science Part A: Polymer Chemistry*, 2002, **40**, 1157–1166.
- 210 X.-D. Huang, S. H. Goh and S. Y. Lee, *Macromol. Chem. Phys.*, 2000, **201**, 2660–2665.
- 211 T. Song, S. H. Goh and S. Y. Lee, *Macromolecules*, 2002, **35**, 4133–4137.

- 212 C. Weis, C. Friedrich, R. Muelhaupt and H. Frey, *Macromolecules*, 1995, **28**, 403–405.
- 213 W. T. Ford, A. L. Lary and T. H. Mourey, *Macromolecules*, 2001, **34**, 5819–5826.
- 214 C. Wang, J. He, S. Fu, K. Jiang, H. Cheng and M. Wang, *Polymer Bulletin*, 1996, **37**, 305–311.
- 215 Y. Ederle and C. Mathis, *Macromolecules*, 1997, **30**, 2546–2555.
- 216 Y. Ederlé and C. Mathis, *Macromolecules*, 1997, **30**, 4262–4267.
- 217 E. Mignard, R. C. Hiorns and B. François, *Macromolecules*, 2002, **35**, 6132–6141.
- 218 Y. Chen, J. Wang, Y. Lin, R. Cai and Z.-E. Huang, *Polymer*, 2000, **41**, 1233–1236.
- 219 T. . Goswami, B. Nandan, S. Alam and G. . Mathur, *Polymer*, 2003, **44**, 3209–3214.
- 220 K. L. Wooley, C. J. Hawker, J. M. J. Fréchet, F. Wudl, G. Srdanov, S. Shi, C. Li and M. Kao, *Journal of the American Chemical Society*, 1993, **115**, 9836–9837.
- 221 E. Allard, F. Oswald, B. Donnio, D. Guillon, J. L. Delgado, F. Langa and R. Deschenaux, *Organic Letters*, 2005, **7**, 383–386.
- 222 S. Campidelli, R. Deschenaux, J.-F. Eckert, D. Guillon and J.-F. Nierengarten, *Chemical Communications*, 2002, 656–657.
- 223 S. Campidelli, E. Vázquez, D. Milic, M. Prato, J. Barberá, D. M. Guldi, M. Marcaccio, D. Paolucci, F. Paolucci and R. Deschenaux, *Journal of Materials Chemistry*, 2004, **14**, 1266.
- 224 S. Campidelli, L. Pérez, J. Rodríguez-López, J. Barberá, F. Langa and R. Deschenaux, *Tetrahedron*, 2006, **62**, 2115–2122.
- 225 S. Campidelli, M. Séverac, D. Scanu, R. Deschenaux, E. Vázquez, D. Milic, M. Prato, M. Carano, M. Marcaccio, F. Paolucci, G. M. A. Rahman and D. M. Guldi, *Journal of Materials Chemistry*, 2008, **18**, 1504.
- 226 J.-F. Nierengarten, D. Felder and J.-F. Nicoud, *Tetrahedron Letters*, 1999, **40**, 269–272.
- 227 J.-F. Nierengarten, D. Felder and J.-F. Nicoud, *Tetrahedron Letters*, 2000, **41**, 41–44.
- 228 D. Felder, H. Nierengarten, J.-P. Gisselbrecht, C. Boudon, E. Leize, J.-F. Nicoud, M. Gross, A. Van Dorsselaer and J.-F. Nierengarten, *New Journal of Chemistry*, 2000, **24**, 687–695.
- 229 U. Hahn, F. Vögtle and J.-F. Nierengarten, *Polymers*, 2012, **4**, 501–538.
- 230 U. Hahn, J.-F. Nierengarten, F. Vögtle, A. Listorti, F. Monti and N. Armaroli, *New J. Chem.*, 2009, **33**, 337–344.
- 231 C. J. Hawker and J. M. Frechet, *Journal of the American Chemical Society*, 1990, **112**, 7638–7647.
- 232 U. Hahn, E. Maisonhaute, C. Amatore and J.-F. Nierengarten, *Angewandte Chemie International Edition*, 2007, **46**, 951–954.
- 233 B. Nie and V. M. Rotello, *Macromolecules*, 1997, **30**, 3949–3951.
- 234 R. C. Hiorns, E. Cloutet, E. Ibarboure, L. Vignau, N. Lemaitre, S. Guillerez, C. Absalon and H. Cramail, *Macromolecules*, 2009, **42**, 3549–3558.
- 235 C. Mathis, B. Schmaltz and M. Brinkmann, *Comptes Rendus Chimie*, 2006, **9**, 1075–1084.
- 236 F. Audouin, R. Nuffer and C. Mathis, *Journal of Polymer Science Part A: Polymer Chemistry*, 2004, **42**, 3456–3463.

- 237 S. Samal, B.-J. Choi and K. E. Geckeler, *Chemical Communications*, 2000, 1373–1374.
- 238 M. Taki, S. Sugita, Y. Nakamura, E. Kasashima, E. Yashima, Y. Okamoto and J. Nishimura, *Journal of the American Chemical Society*, 1997, **119**, 926–932.
- 239 M. Taki, S. Takigami, Y. Watanabe, Y. Nakamura and J. Nishimura, *Polym J*, 1997, **29**, 1020–1022.
- 240 A. Gügel, P. Belik, M. Walter, A. Kraus, E. Harth, M. Wagner, J. Spickermann and K. Müllen, *Tetrahedron*, 1996, **52**, 5007–5014.
- 241 A. Kraus and K. Müllen, *Macromolecules*, 1999, **32**, 4214–4219.
- 242 E. Scamporrino, D. Vitalini and P. Mineo, *Macromolecules*, 1999, **32**, 4247–4253.
- 243 M. Ozawa, J. Li, K. Nakahara, L. Xiao, H. Sugawara, K. Kitazawa, K. Kinbara and K. Saigo, *J. Polym. Sci. A Polym. Chem.*, 1998, **36**, 3139–3146.
- 244 H. Ito, Y. Ishida and K. Saigo, *Tetrahedron Letters*, 2006, **47**, 3095–3098.
- 245 L. Xiao, H. Shimotani, M. Ozawa, J. Li, N. Dragoe, K. Saigo and K. Kitazawa, *Journal of Polymer Science Part A Polymer Chemistry*, 1999, **37**, 3632–3637.
- 246 C. J. Hawker, *Macromolecules*, 1994, **27**, 4836–4837.
- 247 G. Adamopoulos, T. Heiser, U. Giovanella, S. Ould-Saad, K. I. van de Wetering, C. Brochon, T. Zorba, K. M. Paraskevopoulos and G. Hadziioannou, *Thin Solid Films*, 2006, **511-512**, 371–376.
- 248 Y. Chen, R.-F. Cai, Z.-E. Huang and S.-Q. Kong, *Polymer Bulletin*, 1995, **35**, 705–710.
- 249 H. Sato, D. Matsuda and K. Ogino, *Polym J*, 1998, **30**, 904–909.
- 250 J. Zheng, S. H. Goh and S. Y. Lee, *Polymer bulletin*, 1997, **39**, 79–84.
- 251 Z. & 114 H. Lu, S. & 114 H. Goh and S. & 114 Y. Lee, *Polymer bulletin*, 1997, **39**, 661–667.
- 252 F. Li, Y. Li, Z. Ge, D. Zhu, Y. Song and G. Fang, *Journal of Physics and Chemistry of Solids*, 2000, **61**, 1101–1103.
- 253 B. Z. Tang, H. Peng, S. M. Leung, C. F. Au, W. H. Poon, H. Chen, X. Wu, M. W. Fok, N.-T. Yu, H. Hiraoka and others, *Macromolecules*, 1998, **31**, 103–108.
- 254 Y. Chen, Z.-E. Huang and R.-F. Cai, *J. Polym. Sci. B Polym. Phys.*, 1996, **34**, 631–640.
- 255 Z. Li and J. Qin, *Journal of Polymer Science Part A: Polymer Chemistry*, 2004, **42**, 194–199.
- 256 Z. Li and J. Qin, *Journal of applied polymer science*, 2003, **89**, 2068–2071.
- 257 H. Okamura, K. Miyazono, M. Minoda and T. Miyamoto, *Macromol. Rapid Commun.*, 1999, **20**, 41–45.
- 258 A. O. Patil and G. W. Schriver, in *Macromolecular Symposia*, Wiley Online Library, 1995, vol. 91, pp. 73–79.
- 259 A. Cravino and N. S. Sariciftci, *Journal of Materials Chemistry*, 2002, **12**, 1931–1943.
- 260 G. Sonmez, C. K. F. Shen, Y. Rubin and F. Wudl, *Advanced Materials*, 2005, **17**, 897–900.
- 261 Z. Lu, C. He and T.-S. Chung, *Polymer*, 2001, **42**, 5233–5237.
- 262 L. Brunsveld, B. J. B. Folmer, E. W. Meijer and R. P. Sijbesma, *Chemical Reviews*, 2001, **101**, 4071–4098.

- 263 C. Wang, Z.-X. Guo, S. Fu, W. Wu and D. Zhu, *Progress in Polymer Science*, 2004, **29**, 1079–1141.
- 264 A. Cravino, G. Zerza, H. Neugebauer, N. S. Sariciftci, M. Maggini, S. Bucella, M. Svensson and M. R. Andersson, *Chemical Communications*, 2000, 2487–2488.
- 265 A. Cravino, G. Zerza, H. Neugebauer, M. Maggini, S. Bucella, E. Menna, M. Svensson, M. R. Andersson, C. J. Brabec and N. S. Sariciftci, *The Journal of Physical Chemistry B*, 2002, **106**, 70–76.
- 266 Z. 'ao Tan, J. Hou, Y. He, E. Zhou, C. Yang and Y. Li, *Macromolecules*, 2007, **40**, 1868–1873.
- 267 J. L. Delgado, P.-A. Bouit, S. Filippone, M. Herranz and N. Martín, *Chemical Communications*, 2010, **46**, 4853.
- 268 Y.-J. Cheng, F.-Y. Cao, W.-C. Lin, C.-H. Chen and C.-H. Hsieh, *Chemistry of Materials*, 2011, **23**, 1512–1518.
- 269 Y.-J. Cheng, F.-Y. Cao, W.-C. Lin, C.-H. Chen and C.-H. Hsieh, *Chemistry of Materials*, 2011, **23**, 1512–1518.
- 270 C. Yang, J. K. Lee, A. J. Heeger and F. Wudl, *Journal of Materials Chemistry*, 2009, **19**, 5416.
- 271 B. Gholamkhash and S. Holdcroft, *Chemistry of Materials*, 2010, **22**, 5371–5376.
- 272 H. S. Silva, A. Tournebize, D. Bégué, H. Peisert, T. Chassé, J.-L. Gardette, S. Therias, A. Rivaton and R. C. Hiorns, *RSC Adv.*, 2014, **4**, 54919–54923.
- 273 B. Wang and M. R. Wasielewski, *J. Am. Chem. Soc.*, 1997, **119**, 12–21.
- 274 A. W. Van der Made and R. H. Van der Made, *The Journal of Organic Chemistry*, 1993, **58**, 1262–1263.
- 275 N. Kornblum, W. J. Jones and G. J. Anderson, *Journal of the American Chemical Society*, 1959, **81**, 4113–4114.
- 276 P. Shao, Z. Li, J. Luo, H. Wang and J. Qin, *Synthetic Communications*, 2005, **35**, 49–53.
- 277 M. Lenes, G.-J. A. H. Wetzelaer, F. B. Kooistra, S. C. Veenstra, J. C. Hummelen and P. W. M. Blom, *Advanced Materials*, 2008, **20**, 2116–2119.
- 278 M. Lenes, S. W. Shelton, A. B. Sieval, D. F. Kronholm, J. C. (Kees) Hummelen and P. W. M. Blom, *Advanced Functional Materials*, 2009, **19**, 3002–3007.
- 279 H. Okamura, T. Terauchi, M. Minoda, T. Fukuda and K. Komatsu, *Macromolecules*, 1997, **30**, 5279–5284.
- 280 F. Audouin, R. Nuffer and C. Mathis, *Journal of Polymer Science Part A: Polymer Chemistry*, 2004, **42**, 3456–3463.
- 281
- 282 N. T. Tung, H. Lee, Y. Song, N. D. Nghia and D. Sohn, *Synthetic Metals*, 2010, **160**, 1303–1306.
- 283 O. F. Pozdnyakov, A. O. Pozdnyakov, B. Schmaltz and C. Mathis, *Polymer*, 2006, **47**, 1028–1035.
- 284 C. Mathis, S. Nunige, F. Audouin and R. Nuffer, *Synthetic Metals*, 2001, **121**, 1153–1154.
- 285 F. Audouin, R. Nuffer and C. Mathis, *Journal of Polymer Science Part A: Polymer Chemistry*, 2004, **42**, 4820–4829.

- 286 T. T. Ngo, D. N. Nguyen and V. T. Nguyen, *Advances in Natural Sciences: Nanoscience and Nanotechnology*, 2012, **3**, 045001.
- 287 K. Kordatos, S. Bosi, T. Da Ros, A. Zambon, V. Lucchini and M. Prato, *The Journal of Organic Chemistry*, 2001, **66**, 2802–2808.
- 288 J. Liu, X. Guo, Y. Qin, S. Liang, Z.-X. Guo and Y. Li, *J. Mater. Chem.*, 2012, **22**, 1758–1761.
- 289 G. Bottari, C. Dammann, T. Torres and T. Drewello, *Journal of The American Society for Mass Spectrometry*, 2013, **24**, 1413–1419.
- 290 A. Jenkins, P. Kratochvil, R. Stepto and U. Suter, *Pure and applied chemistry*, 1996, **68**, 2287–2311.
- 291 P. J. Flory, *Journal of the American Chemical Society*, 1936, **58**, 1877–1885.
- 292 P. J. Flory, 1953.
- 293 G. Odian, *Principles of polymerization*, John Wiley & Sons, 2004.
- 294 C.-H. Andersson, G. Berggren, S. Ott and H. Grennberg, *European Journal of Inorganic Chemistry*, 2011, **2011**, 1744–1749.
- 295 M. A. Tanatar, A. Graja, D. B. Zhu and Y. L. Li, *Synthetic Metals*, 1998, **94**, 83–86.
- 296 R. C. Hiorns, P. Iratçabal, D. Bégué, A. Khoukh, R. De Bettignies, J. Leroy, M. Firon, C. Sentein, H. Martinez, H. Preud'homme and C. Dagron-Lartigau, *Journal of Polymer Science Part A: Polymer Chemistry*, 2009, **47**, 2304–2317.
- 297 Y. Zhou, C. Fuentes-Hernandez, J. Shim, J. Meyer, A. J. Giordano, H. Li, P. Winget, T. Papadopoulos, H. Cheun, J. Kim, M. Fenoll, A. Dindar, W. Haske, E. Najafabadi, T. M. Khan, H. Sojoudi, S. Barlow, S. Graham, J.-L. Brédas, S. R. Marder, A. Kahn and B. Kippelen, *Science*, 2012, **336**, 327–332.
- 298 K. Sugiyama, H. Ishii, Y. Ouchi and K. Seki, *Journal of Applied Physics*, 2000, **87**, 295.
- 299 J. R. Vig, *Journal of Vacuum Science & Technology A*, 1985, **3**, 1027–1034.
- 300 S. Y. Kim, *Journal of Applied Physics*, 2004, **95**, 2560.
- 301 Q. Bao, O. Sandberg, D. Dagnelund, S. Sandén, S. Braun, H. Aarnio, X. Liu, W. M. Chen, R. Österbacka and M. Fahlman, *Advanced Functional Materials*, 2014, **24**, 6309–6316.
- 302 H. Peisert, A. Petr, L. Dunsch, T. Chassé and M. Knupfer, *ChemPhysChem*, 2007, **8**, 386–390.
- 303 S. Duhm, G. Heimel, I. Salzmann, H. Glowatzki, R. L. Johnson, A. Vollmer, J. P. Rabe and N. Koch, *Nature Materials*, 2008, **7**, 326–332.
- 304 M. T. Dang, L. Hirsch and G. Wantz, *Advanced Materials*, 2011, **23**, 3597–3602.
- 305 A. Marrocchi, D. Lanari, A. Facchetti and L. Vaccaro, *Energy & Environmental Science*, 2012, **5**, 8457.
- 306 T. Xu and L. Yu, *Materials Today*, 2014, **17**, 11–15.
- 307 M. A. Green, K. Emery, Y. Hishikawa, W. Warta and E. D. Dunlop, *Progress in Photovoltaics: Research and Applications*, 2015, **23**, 1–9.
- 308 L. Ye, C. Zhou, H. Meng, H.-H. Wu, C.-C. Lin, H.-H. Liao, S. Zhang and J. Hou, *J. Mater. Chem. C*, 2015, **3**, 564–569.

- 309 P. Hudhomme, *EPJ Photovoltaics*, 2013, **4**, 40401.
- 310 M. Karakawa, T. Nagai, K. Adachi, Y. Ie and Y. Aso, *J. Mater. Chem. A*, 2014, **2**, 20889–20895.
- 311 A. B. Sieval, N. D. Treat, D. Rozema, J. C. Hummelen and N. Stingelin, *Chem. Commun.*, 2015, **51**, 8126–8129.
- 312 M. Raïssi, H. Erothu, E. Ibarboure, H. Cramail, L. Vignau, E. Cloutet and R. C. Hiorns, *J. Mater. Chem. A*, 2015, **3**, 18207–18221.
- 313 A. A. Virkar, S. Mannsfeld, Z. Bao and N. Stingelin, *Advanced Materials*, 2010, **22**, 3857–3875.
- 314 J.-K. Lee, K. Fujida, T. Tsutsui and M.-R. Kim, *Solar Energy Materials and Solar Cells*, 2007, **91**, 892–896.
- 315 K. Matsumoto, K. Hashimoto, M. Kamo, Y. Uetani, S. Hayase, M. Kawatsura and T. Itoh, *Journal of Materials Chemistry*, 2010, **20**, 9226.
- 316 P. Wang, K. Yao, L. Chen, Y. Chen, F. Li, H. Wang and S. Yu, *Solar Energy Materials and Solar Cells*, 2012, **97**, 34–42.
- 317 B.-Y. Ren, C.-J. Ou, C. Zhang, Y.-Z. Chang, M.-D. Yi, J.-Q. Liu, L.-H. Xie, G.-W. Zhang, X.-Y. Deng, S.-B. Li, W. Wei and W. Huang, *The Journal of Physical Chemistry C*, 2012, **116**, 8881–8887.
- 318 D. Mi, H.-U. Kim, J.-H. Kim, F. Xu, S.-H. Jin and D.-H. Hwang, *Synthetic Metals*, 2012, **162**, 483–489.
- 319 K. Yoshimura, K. Matsumoto, Y. Uetani, S. Sakumichi, S. Hayase, M. Kawatsura and T. Itoh, *Tetrahedron*, 2012, **68**, 3605–3610.
- 320 Z. A. Page, Y. Liu, V. V. Duzhko, T. P. Russell and T. Emrick, *Science*, 2014, **346**, 441–444.
- 321 C.-Z. Li, C.-Y. Chang, Y. Zang, H.-X. Ju, C.-C. Chueh, P.-W. Liang, N. Cho, D. S. Ginger and A. K.-Y. Jen, *Advanced Materials*, 2014, **26**, 6262–6267.
- 322 S. Karak, Z. A. Page, J. S. Tinkham, P. M. Lahti, T. Emrick and V. V. Duzhko, *Applied Physics Letters*, 2015, **106**, 103303.
- 323 L.-M. Chen, Z. Xu, Z. Hong and Y. Yang, *Journal of Materials Chemistry*, 2010, **20**, 2575.
- 324 H.-L. Yip and A. K.-Y. Jen, *Energy & Environmental Science*, 2012, **5**, 5994.
- 325 J. You, L. Dou, K. Yoshimura, T. Kato, K. Ohya, T. Moriarty, K. Emery, C.-C. Chen, J. Gao, G. Li and Y. Yang, *Nature Communications*, 2013, **4**, 1446.
- 326 F. Verbakel, S. C. J. Meskers and R. A. J. Janssen, *Applied Physics Letters*, 2006, **89**, 102103.
- 327 T. Kuwabara, Y. Kawahara, T. Yamaguchi and K. Takahashi, *ACS Applied Materials & Interfaces*, 2009, **1**, 2107–2110.
- 328 H. Cheun, C. Fuentes-Hernandez, Y. Zhou, W. J. Potscavage, S.-J. Kim, J. Shim, A. Dindar and B. Kippelen, *The Journal of Physical Chemistry C*, 2010, **114**, 20713–20718.
- 329 J. Huang, Z. Yin and Q. Zheng, *Energy & Environmental Science*, 2011, **4**, 3861.
- 330 M. T. Dang, L. Hirsch, G. Wantz and J. D. Wuest, *Chemical Reviews*, 2013, **113**, 3734–3765.
- 331 E. Verploegen, R. Mondal, C. J. Bettinger, S. Sok, M. F. Toney and Z. Bao, *Advanced Functional Materials*, 2010, **20**, 3519–3529.

- 332 L. Derue, O. Dautel, A. Tournebize, M. Drees, H. Pan, S. Berthumeyrie, B. Pavageau, E. Cloutet, S. Chambon, L. Hirsch, A. Rivaton, P. Hudhomme, A. Facchetti and G. Wantz, *Advanced Materials*, 2014, **26**, 5831–5838.
- 333 M. Jørgensen, K. Norrman, S. A. Gevorgyan, T. Tromholt, B. Andreasen and F. C. Krebs, *Advanced Materials*, 2012, **24**, 580–612.
- 334 B. Watts, W. J. Belcher, L. Thomsen, H. Ade and P. C. Dastoor, *Macromolecules*, 2009, **42**, 8392–8397.
- 335 G. Griffini, J. D. Douglas, C. Piliago, T. W. Holcombe, S. Turri, J. M. J. Fréchet and J. L. Mynar, *Advanced Materials*, 2011, **23**, 1660–1664.
- 336 S. Khiev, L. Derue, G. Ayenew, H. Medlej, R. Brown, L. Rubatat, R. C. Hiorns, G. Wantz and C. Dagron-Lartigau, *Polymer Chemistry*, 2013, **4**, 4145.
- 337 J. W. Rumer and I. McCulloch, *Materials Today*, 2015.
- 338 H.-W. Liu, D.-Y. Chang, W.-Y. Chiu, S.-P. Rwei and L. Wang, *Journal of Materials Chemistry*, 2012, **22**, 15586.
- 339 O. Oklobia and T. S. Shafai, *Solar Energy Materials and Solar Cells*, 2013, **117**, 1–8.
- 340 L. Derue, O. Dautel, A. Tournebize, M. Drees, H. Pan, S. Berthumeyrie, B. Pavageau, E. Cloutet, S. Chambon, L. Hirsch, A. Rivaton, P. Hudhomme, A. Facchetti and G. Wantz, *Advanced Materials*, 2014, **26**, 5831–5838.
- 341 J. Kesters, S. Kudret, S. Bertho, N. Van den Brande, M. Defour, B. Van Mele, H. Penxten, L. Lutsen, J. Manca, D. Vanderzande and W. Maes, *Organic Electronics*, 2014, **15**, 549–562.
- 342 F. Neese, F. Wennmohs, A. Hansen and U. Becker, *Chemical Physics*, 2009, **356**, 98–109.
- 343 R. Sustmann, *Pure and Applied Chemistry*, 1974, **40**, 569–593.

